RELATIONSHIPS BETWEEN THE GEOMECHANICS AND PETROGRAPHY OF IGNIMBRITE.

A thesis
submitted in fulfillment
of the requirements for the degree of
Doctor of Philosophy in Earth Sciences
at the
University of Waikato

by

Vicki Glenys Moon

Department of Earth Sciences
University of Waikato
Hamilton, New Zealand

December, 1989

ABSTRACT

Fundamental petrographic controls on ignimbrite strength are examined, and those aspects of the texture and fabric of the rocks which are primarily responsible for the strength of ignimbrite identified. The range of strength exhibited by ignimbrite is quantifed, and the value of common, non-destructive indices as predictors of ignimbrite strength assessed, with predictive equations presented where appropriate. Models for the strength, jointing, and geomorphic development of an ignimbrite sheet are derived.

Compressive, shear, and tensile strengths, measured by using standard techniques, provide the basic geomechanical data; strength indices (density, porosity, rebound hardness, slake durability, and ultrasonic wave velocity) and petrographic measurements (bulk rock chemistry, mineralogy, texture, fabric, and the extent of post-depositional alteration) are compared with these data using regression analysis. Textural and fabric parameters are determined using image analysis, optical microscopy, and scanning electron microscopy to quantify the size, shape, and three-dimensional arrangement of the components making up the ignimbrite.

Ignimbrites have highly variable strength, but in all forms of loading are classified as weak rocks. The strength variation ranges over at least two orders of magnitude for the compressive strength, and one order of magnitude for the tensile strength. Such variation may occur within a single vertical section through an ignimbrite sheet. Marked softening upon saturation occurs for all forms of strength, and ignimbrites show considerable plastic deformation prior to failure - rarely is a brittle failure mechanism exhibited.

Bulk rock properties and index measurements reflect the low strength values; ignimbrites have low bulk densities, high porosities, low rebound hardnesses, and low velocities of ultrasonic wave transmission. They display a highly variable response to slaking, with some being almost completely broken down by gentle agitation, and others remaining unaffected.

The porosity provides the best indicator of compressive strength, and predictive equations relating dry and saturated compressive strength to porosity are presented. Dry bulk density can also be used as a predictor of compressive strength, but the relationship is not as strong as that for porosity. Predictive equations relating the compressive and tensile strength to the Schmidt hammer rebound provide good indicators of major variations in rock strength, but are insensitive to subtle strength changes.

Ultrasonic wave velocity is a useful laboratory indicator of the tensile strength of ignimbrite. Unlike those for other index properties, the relationship between ultrasonic wave velocity and tensile strength is insensitive to changes in the moisture content of the rock. This means it should also, with appropriate calibration, be applicable under field conditions.

The groundmass fabric exerts the primary control over the compressive and tensile strengths of ignimbrite. The influence of groundmass fabric is modified by the size of the crystals and clasts included within the ignimbrite, but these two components are of less significance than the groundmass fabric. Shear strength is not readily related to petrographic parameters.

Compressive strength is controlled by the packing of the groundmass shards (their alignment and the density of pore filling), and the extent to which the shards are welded at their points of contact. These factors control the distribution of stresses in the material, and the ease with which microfractures can propagate through the groundmass. The size of crystals and pumice clasts controls the concentration of stresses around such inhomogeneities, and hence the initiation of microfractures. However, the proportion of such clasts is not important, so long as a sufficient number are present to initiate microfractures. Tensile strength is controlled by the degree of alignment of the shards, and the hardness of the pumice clasts; aligned shards and hard pumice clasts result in an ignimbrite with high tensile strength. Only a small anisotropy exists in terms of the direction of shard alignment with respect to the direction of principal stress.

Idealised models of joint development, hillslope form, and geomorphic development are based upon predictable variations in the primary petrographic features recognised as influencing the strength of the ignimbrites - the groundmass fabric and the nature of shard welding. Variations in these properties caused by emplacement conditions result in predictable strength variations, and in characteristic jointing patterns associated with each strength zone. It is these strength and jointing patterns which dictate the means by which erosion can affect an ignimbrite, and hence the resulting landform patterns.

ACKNOWLEDGEMENTS

First and foremost, I am indebted to my supervisor, Professor M.J. Selby, for initiation of the topic, guidance through the research, and critical comments on the manuscript. I also wish to thank Dr. R.M. Briggs for advice and comments on the petrographic aspects of the study. Drs. A.P.W. Hodder, W.E. Bardsley, and W.P. de Lange assisted with general discussions, and specific advice on chemical, statistical, and computer-related problems respectively.

Mr. K. Palmer of Victoria University of Wellington is thanked for undertaking the geochemical analyses, and the University Grants Committee for providing funds for such analyses. Mr. S. Stokes is thanked for his assistance in operating the scanning electron microscope. The management of the Hinuera Stone Quarry kindly allowed access to their quarry, and provided specimens, and the Ministry of Energy (now Electricorp) allowed specimens to be collected from the Maraetai site.

Without the assistance of Mr. S. Bergin, who helped with specimen preparation, and maintained the equipment in working order throughout the study, this project could not have been completed. His help, plus that of the other technicians in the Earth Sciences Department, University of Waikato, is gratefully acknowledged.

TABLE OF CONTENTS

ABSTRACT i
ACKNOWLEDGEMENTS iii
TABLE OF CONTENTS iv
LIST OF FIGURES xi
LIST OF PLATES xii
LIST OF TABLES xiii
NOTATION xv

PART 1 - INTRODUCTION AND SAMPLE COLLECTION

CHAPTER 1 - INTRODUCTION 1

1.1 Aims of the study 1
1.2 Background 1
1.2.1 Variability 2
1.2.2 Previous geomechanical studies 3
1.3 Methods used in this study 4
1.4 Layout of this report 5

CHAPTER 2 - SITE SELECTION AND DESCRIPTION 6

2.1 Introduction 6
2.2 Site selection 6
2.2.1 Approaches to site selection 7
2.2.2 Selection of sites in this study 8
2.3 Site description 8
2.3.1 Petrological description 9
2.3.2 Induration 10
2.3.2.1 Welding 10
2.3.2.2 Field estimates of welding 11
2.3.2.3 Classification of induration 12
2.3.3 Jointing 13
2.3.3.1 Classification of jointing 14
2.4 Collection of specimens 14
2.5 Sites studied 15
2.5.1 Whakamaru Ignimbrite 15
2.5.2 Ongatiti Ignimbrite 17
2.5.3 Owharoa Ignimbrite 18
2.5.4 Site descriptions 18
2.6 Summary 20

PART 2 - GEOMECHANICS

CHAPTER 3 - STANDARD LABORATORY CONDITIONS 21

3.1 Introduction 21
3.2 Specimen preparation 21
3.2.1 Block usage 21
3.2.2 Specimen numbers 21
3.3 Laboratory procedures 22
3.3.1 Standard moisture contents 22
3.3.2 Estimation of true value and confidence limits 23
3.3.3 Required number of specimens 23
3.3.4 Data analysis 23

CHAPTER 4 - MECHANICAL STRENGTH 24

4.1 Introduction 24
4.2 Sample preparation 24
4.3 Testing equipment 25
4.4 Compressive strength 26
4.4.1 Test procedure 26
4.4.2 Results 26
4.5 Shear strength 27
4.5.1 Test procedure 27
4.5.2 Jig design 27
4.5.3 Soil shear box 28
4.5.4 Results 29
4.6 Tensile strength 29
4.6.1 Test procedure 29
4.6.2 Results 30
4.7 Comparison with other rocks 30
4.8 Nature of failure 31
4.8.1 Failure modes 32
4.8.2 Deformation 32
4.8.3 Crack surfaces 33
4.9 Summary 34

CHAPTER 5 - BULK ROCK PROPERTIES 36

5.1 Introduction 36
5.2 Definitions 36
5.3 Methods 36
5.3.1 Effect of specimen size 37
5.3.2 Errors in grain density determination 37
5.4 Grain density 38
5.5 Bulk density and porosity 38
5.6 Summary 39

CHAPTER 6 - HARDNESS AND DURABILITY 40

6.1 Introduction 40
6.2 Hardness 40
6.2.1 Types of hardness 40
6.2.2 Hardness measurement 41
6.3 Schmidt hammer 42
6.3.1 Instruments 42
6.3.2 Test procedure 42
6.3.3 Calibration 44
6.3.4 Results 45
6.4 Shore scleroscope 45
6.4.1 Instrument 45
6.4.2 Test procedure 46
6.4.3 Calibration 47
6.4.4 Results 47
6.5 Slake durability 48
6.5.1 Methods 48
6.5.2 Results 48
6.6 Summary 49

CHAPTER 7 - ELASTIC WAVE RESPONSE 50

7.1 Introduction 50
7.2 Wave propagation in rocks 50
7.3 Instrument 52
7.4 Notation 53
7.5 Ultrasonic waves 53
7.5.1 Results 53
7.5.2 Changes in ultrasonic velocity on draining 54
7.5.2.1 Previous draining experiments 55
7.5.2.2 Pore shape effects 56
7.5.2.3 Observed variations 57
7.5.2.4 Effects on $v_{pu,sat}$ and $v_{pu,dry}$ measurements 58
7.6 Seismic waves 58
7.6.1 Equations for elastic moduli 59
7.6.2 Attenuation 60
7.6.3 Procedure 60
7.6.4 Seismic wave velocity 61
7.6.4.1 Viability of experimental technique 61
7.6.4.2 Normalisation 62
7.6.4.3 Comparison of v_{ps} and v_{pu} 62
7.6.5 Variations in v_{ps} with applied stress 63
7.6.5.1 General trends 63
7.6.5.2 Effect of saturation 63
7.6.5.3 Effect of orientation 64
7.6.5.4 Loading and unloading cycles 64
7.6.6 Variations in v_{ss} with applied stress 65
7.6.7 Ratio of v_{ps} and v_{ss} 65
7.6.8 Elastic moduli 66
7.7 Summary 67

CHAPTER 8 - VALUE OF INDEX PROPERTIES AS PREDICTORS OF STRENGTH 69

8.1 Introduction 69
8.2 Methods 69
8.2.1 Linear regression 69
8.2.2 Control data 70
8.3 Bulk rock properties 70
8.3.1 Density 71
8.3.1.1 Compressive strength 71
8.3.1.2 Cohesion 72
8.3.2 Porosity 72
8.3.2.1 Compressive strength 72
8.3.2.2 Tensile strength 73
8.3.3 Physical interpretation 74
8.4 Hardness 75
8.4.1 Schmidt hammer rebound 75
8.4.1.1 Compressive strength 76
8.4.1.2 Tensile strength 77
8.4.1.3 Physical interpretation 77
8.4.2 Shore scleroscope rebound 78
8.4.2.1 Compressive strength 78
8.4.2.2 Tensile strength 79
8.4.2.3 Cohesion 79
8.5 Durability 80
8.6 Ultrasonic wave velocity 80
8.7 Summary 81

PART 3 - PETROGRAPHY

CHAPTER 9 - METHODS OF PETROGRAPHIC EXAMINATION 83

9.1 Introduction 83
9.2 X-Ray fluorescence 83
9.3 Image analysis 83
9.4 Optical microscopy 85
9.5 Scanning electron microscopy 85

CHAPTER 10 - CHEMISTRY AND MINERALOGY 87

10.1 Introduction 87
10.2 Bulk rock chemistry 87
10.3 Mineralogy 87
10.4 Crystal proportions from image analysis 88
10.5 Summary 89

CHAPTER 11 - TEXTURE 90

11.1. Introduction 90
11.2 Whakamaru Ignimbrite 90
11.2.1 Shards 90
11.2.2 Crystals 90
11.2.3 Pumice 92
11.3 Ongatiti Ignimbrite 92
11.3.1 Shards 93
11.3.2 Crystals 93
11.3.3 Pumice 96
11.4 Owharoa Ignimbrite 96
11.4.1 Shards 96
11.4.2 Crystals 98
11.4.3 Pumice 98
11.5 Component proportions 99
11.6 Summary 99

CHAPTER 12 - FABRIC 101

12.1 Introduction 101
12.2 Previous studies of microfabric 101
12.2.1 Terminology 101
12.3 Whakamaru Ignimbrite 102
12.3.1 Groundmass 102
12.3.2 Crystals 104
12.3.3 Pumice 104
12.4 Ongatiti Ignimbrite 104
12.4.1 Groundmass 104
12.4.2 Crystals 108
12.4.3 Pumice 108
12.4.3.1 Pumice clasts in thin-section 108
12.4.3.2 Pumice clasts under the electron microscope 110
12.4.3.3 Pumice / groundmass contact 110
12.5 Owharoa Ignimbrite 112
12.5.1 Groundmass 112
12.5.2 Crystals 112
12.5.3 Pumice 114
12.5.3.1 Pumice / groundmass contact 116
12.6 Summary of fabric parameters 116

CHAPTER 13 - POST-DEPOSITIONAL ALTERATION PROCESSES 117

13.1 Introduction 117
13.2 Whakamaru Ignimbrite 117
13.2.1 Welding 117
13.2.2 Devitrification 117
13.2.3 Vapour phase alteration 118
13.3 Ongatiti Ignimbrite 118
13.3.1 Welding 118
13.3.2 Devitrification 119
13.3.3 Vapour phase alteration 119
13.4 Owharoa Ignimbrite 119
13.4.1 Welding 119
13.4.2 Devitrification 119
13.4.3 Vapour phase alteration 120
13.5 Summary 120

CHAPTER 14 - JOINTING 121

14.1 Introduction 121
14.2 Joint development 121
14.2.1 Mechanisms of joint development 121
14.2.2 Columnar jointing 122
14.3 Jointing at study sites 122
14.3.1 Whakamaru Ignimbrite 123
14.3.2 Ongatiti Ignimbrite 126
14.3.3 Owharoa Ignimbrite 128
14.4 Summary 128

PART 4 - MODELS FOR STRENGTH, JOINTING, AND GEOMORPHIC DEVELOPMENT

CHAPTER 15 - RELATIONSHIPS BETWEEN PETROGRAPHIC AND GEOMECHANICAL PROPERTIES 129

15.1 Introduction 129
15.2 Methods 129
15.2.1 Regression 129
15.2.2 Ranking 130
15.2.3 Control data 130
15.2.4 Multiple regression 130
15.3 Petrographic controls on strength 131
15.3.1 Compressive strength 131
15.3.2 Cohesion 132
15.3.3 Angle of internal friction 134
15.3.4 Tensile strength 135
15.3.5 Index properties 136
15.4 Models for strength 138
15.4.1 Summary of significant parameters 138
15.4.2 Compressive strength 138
15.4.3 Cohesion 140
15.4.4 Angle of internal friction 141
15.4.5 Tensile strength 141
15.4.6 Slake durability 142
15.5 Volcanological context 143
15.5.1 Variations in eruption conditions 143
15.5.2 Vertical variations 144
15.5.3 Lateral variations 145
15.6 Summary 145

CHAPTER 16 - MODELS FOR JOINTING AND GEOMORPHIC DEVELOPMENT 147

16.1 Introduction 147
16.2 Model for jointing 147
16.2.1 Summary of main features 147
16.2.2 Controls on joint development 148
16.2.3 The model 149
16.2.4 Ongatiti and Owharoa Ignimbrites 151
16.3 Model for geomorphic development 152
16.3.1 Hillslope development 152
16.3.2 Landform development 153
16.4 Summary 154

CHAPTER 17 - CONCLUSIONS 158

17.1 Geomechanical variability of ignimbrite 158
17.1.1 Measured strengths 158
17.1.2 Wider variation 159
17.1.3 Value of "ignimbrite" as an engineering term 159
17.2 Strength indices 160
17.2.1 Bulk density and porosity 160
17.2.2 Schmidt hammer rebound 160
17.2.3 Ultrasonic wave velocity 160
17.3 Relationships between petrography and geomechanics 161
17.3.1 Compressive strength 161
17.3.2 Tensile strength 162
17.3.3 Shear strength 163
17.4 Models for jointing and geomorphic development 163
17.5 Further research 164

REFERENCES 166

APPENDICES

APPENDIX 1 - FORMATION OF IGNIMBRITE 175

A1.1 Introduction 175
A1.2 Vesiculation and fragmentation of the magma 175
A1.2.1 Magma vesiculation 176
A1.2.2 Magma fragmentation 176
A1.3 Pyroclastic fragments 177
A1.3.1 Pumice 177
A1.3.2 Glass shards 177
A1.3.3 Crystals 178
A1.3.4 Lithic fragments 178
A1.4 Eruption and deposition 178
A1.4.1 Plinian eruption columns 178
A1.4.2 Pyroclastic flows 179
A1.4.3 End-member models 180
A1.4.3.1 Model A 180
A1.4.3.2 Model B 180
A1.4.3.3 Spectrum of ignimbrite types 181
A1.5 Post-depositional alteration 182
A1.5.1 Welding 182
A1.5.2 Crystallisation 182
A1.5.3 Compaction 183
A1.5.4 Controls on alteration processes 183
A1.5.5 Effects of alteration processes 184
A1.6 Summary 185

LIST OF FIGURES

		opposite page
Figure 1.1:	Location map.	2
Figure 3.1:	Sequence of specimen preparation.	22
Figure 4.1:	Derivation of c and ϕ (c' and ϕ') for WHAKA/up specimens.	28
Figure 4.2:	Sketches of failed uniaxial compressive strength specimens from the Whakamaru Ignimbrite.	32
Figure 4.3:	Sketches of failed uniaxial compressive strength specimens from the Ongatiti Ignimbrite.	33
Figure 6.1:	Graphs of mass retained (%) versus slaking time for slake durability tests on each ignimbrites	50
Figure 7.1:	Variation in ultrasonic wave velocity on draining of specimens.	55
Figure 7.2:	Effect of an air / water interface within a pore on acoustic wave transmission.	56
Figure 7.3:	Variation in v_{ps} with axial stress.	63
Figure 7.4:	Variation in v_{ss} with axial stress.	65
Figure 7.5:	Variation in v_{ps}/v_{ss} with axial stress.	66
Figure 16.1:	Development of joints in the Whakamaru Ignimbrite exposed at Maraetai.	150
Figure 16.2:	Model for hillslope development.	153
Figure 16.3:	Stages in landscape development on an ignimbrite sheet.	154
Figure A1.1:	Models for the initiation of pyroclastic flows.	180

LIST OF PLATES

		page
Plate 2.1:	Field sites for (a) Whakamaru and (b) Ongatiti Ignimbrites.	16
Plate 2.1 (cont.):	Field sites for (c) Owharoa Ignimbrite.	19
Plate 11.1:	Photomicrographs of the Whakamaru Ignimbrite specimens.	91
Plate 11.2:	Photomicrographs of the Ongatiti Ignimbrite specimens. (a) ONG/1. (b) ONG/2.	94
Plate 11.2 (cont.):	Photomicrographs of the Ongatiti Ignimbrite specimens. (c) ONG/3.	95
Plate 11.3:	Photomicrographs of the Owharoa Ignimbrite specimens.	97
Plate 12.1:	Groundmass fabrics for the Whakamaru Ignimbrite.	103
Plate 12.2:	Groundmass fabrics for the Ongatiti Ignimbrite.	105
Plate 12.3:	Groundmass detail for the Ongatiti Ignimbrite.	107
Plate 12.4:	Groundmass and pumice detail for the Ongatiti Ignimbrite.	109
Plate 12.5:	Groundmass fabrics for the Owharoa Ignimbrite.	111
Plate 12.6:	Crystal / groundmass contacts in the Owharoa Ignimbrite.	113
Plate 12.7:	Pumice clasts from the Owharoa Ignimbrite.	115
Plate 14.1:	Jointing in the Whakamaru Ignimbrite profile at Maraetai. (a) unjointed zone. (b) columnar jointed zone.	124
Plate 14.1(cont.):	Jointing in the Whakamaru Ignimbrite profile at Maraetai. (c) blocky zone. (d) complex zone.	125
Plate 14.2:	Jointing in the Ongatiti Ignimbrite.	127
Plate 14.3:	Jointing in the Owharoa Ignimbrite.	127
Plate 16.1:	Early stages of landform development in ignimbrite.	155
Plate 16.2:	Middle stages of landform development in ignimbrite.	156
Plate 16.3:	Final stages of landform development in ignimbrite.	157

LIST OF TABLES

		opposite page
Table 2.1:	Field descriptions for Whakamaru Ignimbrite.	15
Table2.1 (cont.):	Field descriptions for Ongatiti Ignimbrite.	17
Table2.1 (cont.):	Field descriptions for Owharoa Ignimbrite.	18
Table 4.1:	Measured geomechanical properties for ignimbrites studied.	26
Table 4.2:	Regression coefficients for shear strength tests on the soft Whakamaru (WHAKA/up) Ignimbrite.	29
Table 4.3:	Representative strength values for a variety of lithologies.	30
Table 5.1:	Bulk rock properties of ignimbrites studied.	37
Table 5.2:	Dry bulk density data for cores from ONG/1-1.	38
Table 5.3:	Grain density of materials typically making up a volcanic rock of silicic composition.	38
Table 5.4:	Dry bulk density and porosity data for a variety of lithologies.	39
Table 6.1:	Derivation of calibration equation for two Schmidt hammers.	44
Table 6.2:	Schmidt hammer data for each site studied.	44
Table 6.3:	Shore hardness values for separate crystals of the types found in the ignimbrites studied.	46
Table 6.4:	Shore scleroscope rebound hardness values for the Whakamaru and Ongatiti Ignimbrites.	47
Table 6.4 (cont.):	Shore scleroscope rebound hardness values for the Owharoa Ignimbrite.	48
Table 6.5:	Second cycle slake durability index for each site studied.	49
Table 7.1:	Saturated and oven-dry ultrasonic wave velocities for ignimbrite cores at atmospheric pressure.	53
Table 7.2:	Mean ultrasonic wave velocities, and associated moist bulk densities, for five-core samples during draining experiment.	54
Table 7.3:	Seismic wave velocity data for each site.	61
Table 8.1:	Regression coefficients for density against mechanical strength parameters.	71
Table 8.2:	Regression coefficients for porosity against mechanical strength parameters.	73
Table 8.3:	Regression coefficients for Schmidt hammer rebound against mechanical strength parameters.	76
Table 8.4:	Regression coefficients for Shore scleroscope rebound against mechanical strength parameters.	78
Table 8.4 (cont.):	Regression coefficients for Shore scleroscope rebound against mechanical strength parameters.	79
Table 8.5:	Regression coefficients for slake durability index (I_{d2}) against mechanical strength parameters.	80
Table 8.6:	Regression coefficients for ultrasonic wave velocity against mechanical strength parameters.	81

Table 9.1:	Definitions of parameters measured using image analysis.	85
Table 10.1:	Chemical composition of ignimbrite specimens.	87
Table 10.2:	Modal mineralogical analysis of ignimbrite specimens.	88
Table 10.3:	Comparison of total crystal area measurements from image analysis and modal analysis.	89
Table 11.1:	Whakamaru Ignimbrite shard sizes.	92
Table 11.2:	Whakamaru Ignimbrite crystal form data.	92
Table 11.3:	Ongatiti Ignimbrite shard sizes.	93
Table 11.4:	Ongatiti Ignimbrite crystal form data.	93
Table 11.5:	Ongatiti Ignimbrite pumice form data.	96
Table 11.6:	Owharoa Ignimbrite shard sizes.	98
Table 11.7:	Owharoa Ignimbrite pumice form data.	98
Table 11.8:	Proportions of each component for the specimens studied.	99
Table 12.1:	Terminology used for fabric description.	101
Table 12.1 (cont.):	Terminology used for fabric description.	102
Table 12.2:	Summary of fabric parameters for each ignimbrite.	117
Table 13.1:	Summary of post-depostional alteration parameters for each ignimbrite.	120
Table 13.2:	Terminology used for describing post-depostional alteration.	120
Table 15.1:	Ranking classifications for fabric and alteration parameters.	130
Table 15.2:	Assignment of ranking numbers to each ignimbrite.	131
Table 15.3:	Regression coefficients for compressive strength.	132
Table 15.4:	Regression coefficients for cohesion.	133
Table 15.5:	Regression coefficients for angle of internal friction.	134
Table 15.6:	Regression coefficients for tensile strength.	135
Table 15.7:	Parameters which show relationships with strength.	138

NOTATION

$\Delta\eta$	unconnected pore space (%)
ϕ	angle of internal friction (dry) (°)
ϕ'	effective angle of internal friction (°)
ϕ_{tot}	angle of internal friction for combined saturated and dry data sets (°)
η	porosity (%)
η_{eff}	effective porosity (%)
η_{true}	true porosity (%)
μ	Poisson's ratio
μ_{dyn}	dynamic Poisson's ratio
$\mu_{dyn,sat}$	saturated dynamic Poisson's ratio
ρ	bulk density (kg m^{-3})
ρ_{dry}	oven-dry bulk density (kg m^{-3})
ρ_g	grain density (kg m^{-3})
ρ_{sat}	saturated bulk density (kg m^{-3})
ρ_{tot}	density for combined saturated and dry data sets (kg m^{-3})
θ	angle between the centre of a pore and the water/air interface (°)
σ_c	uniaxial compressive strength (Pa)
$\sigma_{c,dry}$	oven-dry uniaxial compressive strength (Pa)
$\sigma_{c,dry,pred}$	predicted oven-dry uniaxial compressive strength (Pa)
$\sigma_{c,sat}$	saturated uniaxial compressive strength (Pa)
$\sigma_{c,sat,pred}$	predicted saturated uniaxial compressive strength (Pa)
$\sigma_{c,soft}$	softening factor for uniaxial compressive strength (Pa)
$\sigma_{c,tot}$	uniaxial compressive strength for combined saturated and dry data sets (Pa)
$\sigma_{c,tot,pred}$	predicted uniaxial compressive strength for combined saturated and dry data sets (Pa)
σ_n	normal stress (Pa)
σ_t	unconfined tensile strength (Pa)
$\sigma_{t,dry}$	oven-dry unconfined tensile strength (Pa)
$\sigma_{t,sat}$	saturated unconfined tensile strength (Pa)
$\sigma_{t,soft}$	softening factor for unconfined tensile strength (Pa)
$\sigma_{t,tot}$	unconfined tensile strength for combined saturated and dry data sets (Pa)
τ	shear stress (Pa)
BC	Brazilian core (length:diameter ratio = 0.5:1)
CU	cubic specimen (60 mm cubic block)
c	cohesion (oven-dry) (Pa)
c'	effective cohesion (saturated) (Pa)
c_{soft}	softening factor for cohesion (Pa)
c_{tot}	cohesion for combined saturated and dry data sets (Pa)
E	Young's modulus (Pa)

E_{dyn}	dynamic Young's modulus (Pa)
$E_{dyn,sat}$	saturated dynamic Young's modulus (Pa)
G	shear modulus (Pa)
H	horizontal block orientation
I_{d2}	second cycle Slake Durability index (%)
K	bulk modulus (Pa)
LC	long core (length:diameter ratio = 2.5:1)
LOI	Loss on ignition (%)
ONG	Ongatiti Ignimbrite
OWH	Owharoa Ignimbrite
R	Schmidt hammer rebound value
R_L	L-type Schmidt hammer rebound value
R_P	P-type Schmidt hammer rebound value
r	pore radius (m)
r^2	regression coefficient
r^2_{adj}	regression coefficient adjusted for the degrees of freedom
SC	short core (length:diameter ratio = 1:1)
sd	standard deviation
TS	thin-section
V	vertical block orientation
v_p	velocity of compressional waves (m s^{-1})
$v_{p,air}$	velocity of compressional waves in air (m s^{-1})
$v_{p,water}$	velocity of compressional waves in water (m s^{-1})
$v_{ps,dry}$	oven-dry velocity of 1 MHz compressional waves (m s^{-1})
$v_{ps,sat}$	saturated velocity of 1 MHz compressional waves (m s^{-1})
$v_{pu,dry}$	oven-dry velocity of 54 kHz compressional waves (m s^{-1})
$v_{pu,sat}$	saturated velocity of 54 kHz compressional waves (m s^{-1})
v_s	velocity of shear waves (m s^{-1})
$v_{ss,dry}$	oven-dry velocity of 1 MHz shear waves (m s^{-1})
$v_{ss,sat}$	saturated velocity of 1 MHz shear waves (m s^{-1})
WHAKA	Whakamaru Ignimbrite
y	distance over which the wave passage is blocked (m)

PART 1 - INTRODUCTION AND SAMPLE COLLECTION

CHAPTER 1 - INTRODUCTION

1.1 Aims of the study

In the past, ignimbrites have caused considerable problems as foundation materials for engineering purposes. Most of the problems experienced can be linked to an incomplete knowledge of the behaviour of these materials under stress, and a lack of understanding of the variability of jointing in the rock mass. This study aims to fill this gap by gaining an understanding of the range of geomechanical properties of ignimbrite, and the relationship of these properties to the petrography of the material.

More specifically, the aims of the study are to:

(1) examine the geomechanical properties of ignimbrites in order to identify the variability of these materials in terms of their strength,

(2) identify a number of simple index properties which can be used as predictors of geotechnical behaviour,

(3) relate the geomechanical properties of these rocks to their petrographical properties, such as the composition and fabric, in order to identify those properties which control the behaviour of the material under stress, and

(4) develop predictive models of the strength, jointing, and geomorphic development.

1.2 Background

The initial impetus for this study came from the failure of two engineering projects which were founded on ignimbrite. The Ruahihi and Whaeo hydro-electric schemes are both located in the Bay of Plenty, New Zealand (figure 1.1). On September 20 1981, a section of the canal supplying water to the newly commissioned Ruahihi Power Station collapsed. Resulting erosion destroyed some 600 m of the canal and spilt more than 1 Mm^3 of debris over adjacent farmland and into the nearby Wairoa River (Report of the Committee to Inquire into the Failure of the Ruahihi Canal, 1982). Soon after this, the headrace canal for the Whaeo Power Scheme failed, on 30 December 1982, seriously damaging the partially completed power-house (Report of the Committee to Inquire into the Canal Failure on the Whaeo Power Scheme, 1983). Examination of the literature revealed that a similar

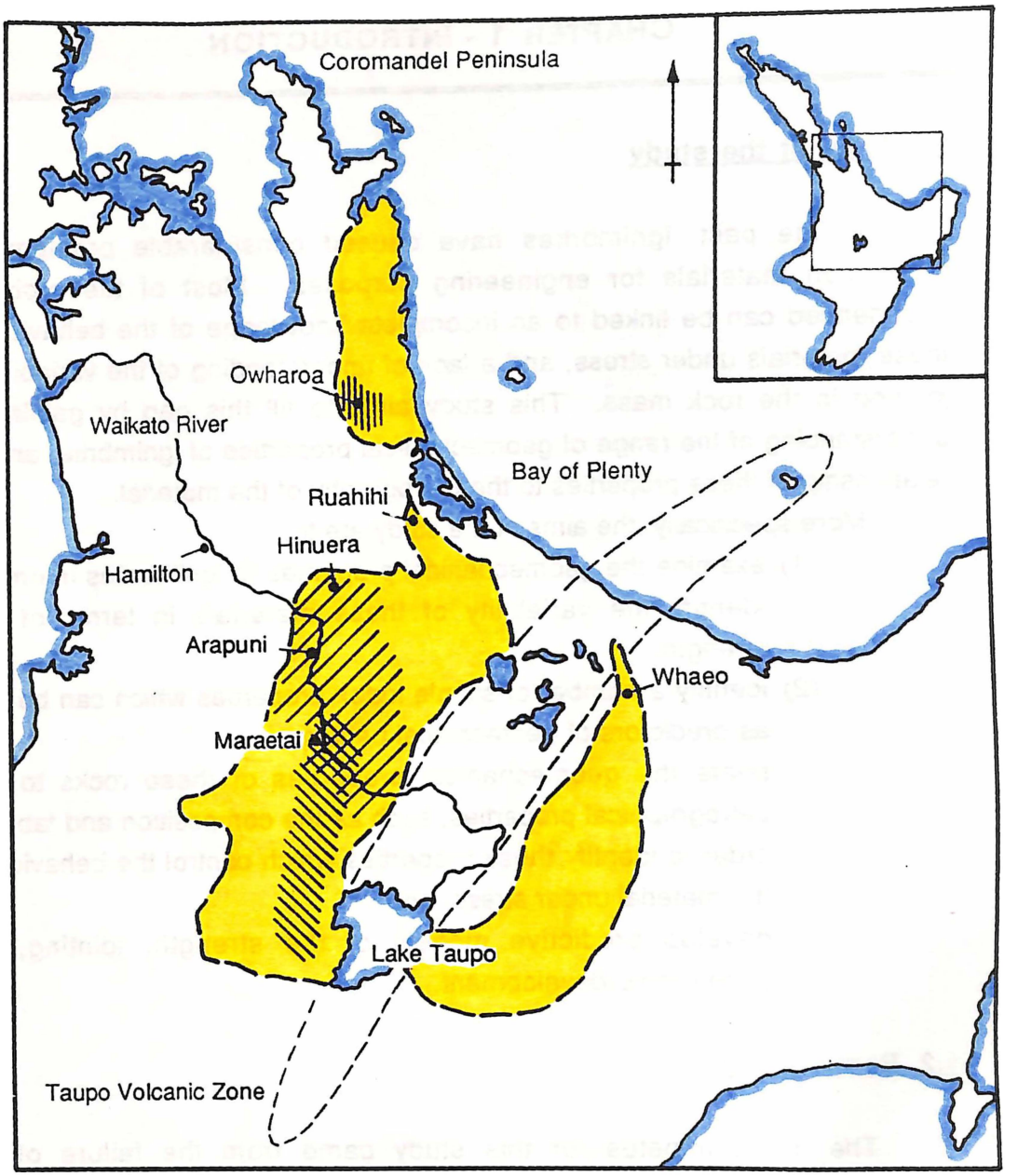

Figure 1.1: Location map showing the extent of ignimbrite in the Central North Island, approximate distributions of the ignimbrite sheets studied, and the sites referred to in the text. After Challis (1978).

problem had been experienced some 50 years previously when commissioning the Arapuni Dam; in this case the near failure of a large section of river bank threatened to tip the power-house into the Waikato River (Furkert, 1935).

Each of these failures can be attributed, in part, to the properties of the ignimbrite foundation material. They highlight a lack of knowledge of the behaviour of these materials under stress, and point to a lack of progress towards understanding the engineering behaviour of these materials over the past 50 years. Obviously, site-specific investigations, although essential, have not proved sufficient to produce a true insight into the geotechnical properties of ignimbrite. Therefore, some fundamental research is required into the properties of these materials, and the way in which their strength is developed.

The need for such research becomes particularly acute when the extent of ignimbrites is taken into consideration. In the Central North Island of New Zealand they cover large areas surrounding the Taupo Volcanic Zone (figure 1.1). Increased development in these areas has led to a need for more, and larger, engineering works, such as roading to facilitate harvesting of mature exotic forests, and the development of geothermal power stations. More such developments can be envisaged in the future, hence the need for a good understanding of the geomechanical behaviour of ignimbrites becomes crucial.

1.2.1 Variability

Exacerbating the problems discussed above is a difficulty in understanding and communicating what is meant by the term "ignimbrite". Until comparatively recently, even the geological community could not agree on a definition. However, recent work by volcanologists has led to the acceptance of a definition of the term "ignimbrite" which includes all of those pumiceous materials deposited from a pyroclastic flow (Walker, 1983). Such a definition encompasses materials with a huge variety of geomechanical properties, ranging from loose pumice deposits which are sufficiently weak to be classed as a non-cohesive engineering soil, through to dense materials which are strong enough as to be treated as a typical rock in an engineering sense.

Consequently, geological maps which simply group all of these materials as "ignimbrites" do not provide engineers with sufficient forewarning of the likely material properties, and the variations which may be encountered

in the materials. Due to experience on the Whakamaru, Maraetai, and Waipapa Dams, for which ignimbrite proved to be an admirable foundation material, the engineering community tends to think of these hard ignimbrites as typical. This has led to developments, such as the Ruahihi scheme, on materials that are not well suited to the problem, and for which insufficient site investigation has taken place. To quantify the strength variability of ignimbrites, and to identify index properties which will allow field and basic laboratory data to predict the strength of the material, is an important first step in understanding their engineering properties.

1.2.2 Previous geomechanical studies.

To date very little basic study of the geomechanical properties of ignimbrites has been undertaken. Most studies have been specific to the sites of engineering projects, and have therefore concentrated on a limited range of properties. In the 1930's the site investigation for the Arapuni Dam was undertaken, plus a further investigation following the development of problems with the dam (Marshall, 1930; Hornell and Werner, 1930; Furkert, 1935). These studies noted the very high porosity and low Young's modulus of the material. Site investigation for the Maraetai and Whakamaru Dams (Maloy and Lowe, 1945; Evison, 1956), and monitoring during filling of Lake Maraetai (James, 1955) showed a remarkable variation in the geomechanical properties of the material, and very high plastic deformation of the rock mass on load application. More recently, the Reports of the Committees of Inquiry into the Ruahihi (1982) and Whaeo (1983) canal failures noted the influence of elevated water pressures in soft, sensitive ignimbrites, and the tendency for tunnelling in dispersive materials.

More fundamental research has been undertaken by Rippa and Vinale (1983) and Nappi and Ottaviani (1986), who related the stress-strain characteristics of Italian pyroclastic rocks (including ignimbrites) to their eruptive mechanism and zeolite content. They have shown that the geomechanical properties of the rocks are strongly influenced by the eruptive mechanism, which controls the nature and degree of adherence of individual clasts. Research related to a site investigation for an underground nuclear waste storage dump in Nevada has shown that porosity is a good indicator of the compressive strength of ignimbrites, and that their loss on strength during saturation can be very significant (Price, 1983; Price *et al.*, 1985). Projects at the University of Waikato have measured the geomechanical properties of a

variety of ignimbrites, with the aim of quantifying the range of properties encountered in New Zealand ignimbrites (Hind, 1986; Idral, 1986).

These studies have measured many of the properties of the rocks, and identified a number of the important aspects of the material which must be taken into account when contemplating engineering developments on ignimbrite. However, no research has attempted to systematically investigate the nature of the material in terms of its petrography (chemistry, mineralogy, texture, and fabric) and the means by which this controls the strength of the material. Such work is required to give a fundamental understanding of the causes of strength in ignimbrites, and hence to develop predictive models of the strength and the variation within an ignimbrite sheet.

1.3 Methods used in this study

Samples from three ignimbrites, the Whakamaru, Ongatiti and Owharoa Ignimbrites, were chosen to represent a wide range of ignimbrite properties. Standard geomechanical methods were used, where possible, to determine the uniaxial compressive strength, shear strength, and tensile strength of the materials. Due to the low strength of some samples the standard techniques for measuring rock and soil strength had to be adapted to overcome the problems of dealing with materials which fall between the strength ranges of engineering rocks and soils.

Index and classification properties were measured in the field and laboratory. Bulk density and porosity were determined on specimens prepared for geomechanical testing. Rebound and penetration tests were used in the laboratory in order to examine, in detail, the hardness of the individual components of the samples; field versions of these tests were also employed in order to test their sensitivity and value in assessing ignimbrite strength in the field. Elastic wave velocity measurements on intact rock specimens were undertaken in the laboratory to assess their value as index properties, and to investigate their use in determining the elastic properties of the material.

Petrographical properties were examined using standard thin-section descriptive methods, and scanning electron microscopy was used to examine the structure of the material and the nature of the pore space within the rock. A computer-based image analysis system was used to measure the size, shape and proportion of the components within the material for both hand-specimen and thin-section samples. Bulk rock chemistry was determined by X-Ray

Fluorescence, and mineralogy was estimated from modal analysis (point-counting) of thin-sections.

Regression analysis was used to investigate the relationships between the petrographical properties and the geomechanical properties, and to determine predictive relationships between the index properties and the geomechanical properties. Standard statistical software packages (Minitab and Wingz) were used for this analysis (Ryan *et al.*, 1982; Informix Software, 1988).

1.4 Layout of this report

This thesis is divided into four parts. Part 1 (chapters 1 and 2) introduces the study, and discusses the selection of sites and collection of specimens for laboratory analysis. Part 2 (chapters 3 to 8) concentrates on the geomechanical aspects of the study. In chapter 3 the methods of geomechanical testing are discussed, and chapter 4 presents the geomechanical data which provides the basis for later analysis. In chapters 5 to 7 the index test data are presented, and in chapter 8 the relationships between the index properties and the geomechanical data are investigated, and predictive equations derived. Part 3 (chapters 9 to 14) examines the petrography and jointing of the specimens; chapter 9 discusses the methods used in petrographic analysis; chapters 10 to 13 discuss the chemistry, mineralogy, texture, fabric, and post-depositional alteration processes; and chapter 14 describes the jointing at the study sites. In part 4 (chapters 15 to 17) the relationships between the petrography and geomechanics are investigated, and models for the causes of strength discussed (chapter 15). Chapter 16 uses these strength models to derive a model for the development of jointing within an ignimbrite profile and, from this, a model of geomorphic development is derived. Chapter 17 summarises the main conclusions, and discusses areas for further research. In appendix 1 a review of the mechanisms of ignimbrite formation is given.

CHAPTER 2 - SITE SELECTION AND DESCRIPTION

2.1 Introduction

Three ignimbrites from the Central North Island, the Ongatiti, Owharoa, and Whakamaru Ignimbrites, were selected for detailed study. From each of these ignimbrites several sites were chosen to provide specimens for laboratory analysis. These sites were selected so that the specimens collected displayed a wide range of geomechanical and petrological properties. For each site studied, a field description of the rock mass and intact rock properties was made.

This chapter describes the procedures of site selection, the choice of parameters used in site description, and the methods of sample collection. Details of the location of each site and an outline of previous work undertaken on these sites are presented; field descriptions and photographs of each site are given in table 2.1 and plate 2.1 respectively.

2.2 Site selection

As a volcanic rock, ignimbrite is remarkable for the very large volumes produced by a single eruptive event or an eruptive sequence. Smith (1979) suggested that volumes of 10^2 to 10^3 km^3 are characteristic of silicic volcanic eruptions such as these. Lipman (1986) stated that many ignimbrite sheets may extend up to 100 km from source, and McPhie (1986) gave examples of ignimbrites for which the thickness is thought to be in excess of 1000 m. Within these deposits, the texture of the material tends to be remarkably homogeneous over large areas. However, extreme changes in the nature of the material can occur over surprisingly short distances (both vertically and laterally), initiated perhaps by relief in the underlying topography (as described by Briggs (1976b), for example), by changes in the vent or magmatic conditions at the time of the eruption (as described by Wright (1981), for example), or by changes in the mechanisms of eruption, transport, and deposition.

The design of a sampling plan for this study involved taking the above characteristics of ignimbrite into account. Added to these considerations were the additional constraints imposed by a lack of exposure within many New Zealand ignimbrites, due to their young age and consequently minimal erosion, and by the abundant vegetation which is found on many of the

ignimbrites. A number of approaches to site selection were considered, but most proved inappropriate for this study due mainly to the features noted above.

2.2.1 Approaches to site selection

A favoured approach would be to establish a sampling programme based entirely on statistical considerations. In order to draw statistically meaningful inferences sampling should be done on a truly random basis. This is the tenet upon which all traditional statistical analysis is based. Edgington (1980) however, noted the rarity of truly random samples; seldom can an entire population of interest be identified, let alone sampled without bias. This is certainly the case in many geological contexts because sampling is, of necessity, restricted to accessible outcrop, which may or may not reflect the range of properties of the rock mass. Unless features of the outcrop make up the population under consideration, the assumption of random sampling is automatically breached. For this study, the amount of accessible outcrop is so limited that attempting to produce random samples was not feasible.

Two common geological approaches are to sample either on the basis of the stratigraphy of the material, or by defining a regular grid on the outcrop. In an ignimbrite the first of these involves selecting sites from specific points within each flow unit identified. However, in many of the New Zealand ignimbrites the stratigraphy is unknown or disputed, and individual flow units are often not identifiable (as was shown by Martin (1965), and Briggs (1976b), for example). In these cases, sampling on inferred stratigraphy would result in spurious correlations being made. A regular grid could be applied to the outcrop, but this technique is only appropriate when information regarding changes with distance is required, which was not the aim of this study.

In order to establish the range of geomechanical properties expressed by ignimbrites, there is a case for sampling the material purely on the basis of established extreme properties. This would involve using a simple field instrument, such as a Schmidt hammer, to locate areas in which the strength reached extreme values and then sampling only these areas. Sampling on this basis would tend to favour the selection of localised examples of unusual materials, such as the extremely hard, glassy ignimbrites sometimes seen at the base of welded flows, or the exceptionally weak, altered materials found around gas escape zones. Although interesting, these extremes are volumetrically insignificant.

2.2.2 Selection of sites in this study

As none of these more rigorous approaches was appropriate, sites were selected on an essentially subjective basis by choosing areas which displayed a wide range of geomechanical and petrological properties. From literature review and field observation the three ignimbrites studied were chosen. The Whakamaru Ignimbrite is a crystal-rich, pumice-poor ignimbrite which shows extremes of very hard ignimbrite to soft ignimbrite in a single profile (Briggs, 1973, 1976a). The Ongatiti Ignimbrite, in contrast, is rich in large, rounded pumice clasts as well as crystals, and varies over a relatively narrow range of hardnesses (Olissoff, 1981). The Owharoa Ignimbrite is poor in crystals and has a well-developed foliate structure produced by lenticular, black pumice clasts (Ewart and Healy, 1966).

Within each of these ignimbrites a site was chosen which had suitable exposure and expressed the characteristic properties described above. Field testing using a Schmidt hammer, together with petrological descriptions, identified the normal ranges of materials within the profile, plus any extreme zones, such as highly jointed areas, or unusually weak or strong zones. These extremes were avoided and final field testing and sampling undertaken on sites which exhibited "typical" ignimbrite properties for each area identified.

This approach had limitations, as it relied on essentially subjective assessments of the range of properties present and the "typical" materials. However, it was considered the only possible one, given the large volume but poor exposure of the ignimbrites. Providing that statistical analyses were confined to the variations within and between the specimens collected, and not extended to the stratigraphy, this approach provided suitable data to fulfill the aims of this study.

2.3 Site description

A number of authors have set out general approaches to the field description of rock masses. Deere and Miller (1966), Bieniawski (1976, 1988), The Geological Society Engineering Group Working Party (1977), Brown (1981), Matula (1981), and Kirkaldie *et al.* (1987) have all identified a number of descriptive parameters and index tests which can be used to describe and classify rock masses. Although the details vary between these studies, the basic parameters of interest are the same. Initial description of the rock mass, involving a petrological description plus an assessment of the joint spacing

and joint block form, is inherent in all field descriptions. A more quantitative level of description involves the measurement of index properties of the rock, such as Schmidt hammer hardness for the intact rock, or mean joint spacing for the rock mass. Finally, detailed information on the stratigraphy, intact rock properties, and discontinuity spacing can be obtained using borehole logging and sophisticated geophysical techniques such as seismic surveys.

The aim of the site description in this study was to broadly classify the materials and ensure that a wide range of ignimbrite properties was sampled. Therefore, only the simplest level of petrological and jointing pattern description was considered. More detailed and quantitative information on the material properties was obtained through laboratory analysis, and is presented in later chapters.

The various standard procedures discussed in the references above do not always apply directly to ignimbrite; the lithological classifications of all of these works, for example, do not include pyroclastic flow deposits in their subdivisions. Consequently, the essential ideas embodied in these standard geotechnical approaches were adhered to, but the techniques were modified to incorporate much of the petrographic and stratigraphic terminology derived from volcanological studies of ignimbrites.

The field descriptions made at each site included:

(1) a general petrological description of the intact rock,
(2) the degree of induration of the ignimbrite, and
(3) the nature of the jointing.

2.3.1 Petrological description

Included in petrological descriptions of the materials were the following details: matrix colour; colour, size, shape and abundance of pumice clasts; type, size, shape and abundance of both lithic clasts and crystals; fabric of the rock; and state of weathering. Component sizes were expressed as a maximum observed, together with an estimate of the most common size. An estimate-by-eye was made of the abundance of the various components using the scheme of Fieldes (1968):

very abundant = >50%
abundant = 30-50%
very common = 10-29%
common = 5-9%
scarce = 1-4%
rare = <1%

The state of weathering was assessed using Dearman's (1974) scheme. The ignimbrites were chosen for their lack of weathering, thus only two categories were significant:

fresh = no visible sign of rock material weathering, perhaps slight discolouration on major discontinuity surfaces; and

slightly weathered = discolouration indicates weathering of rock material and discontinuity surfaces.

2.3.2 Induration

The induration of ignimbrites occurs primarily by compaction in conjunction with the welding which the glassy components undergo during cooling of the mass. Therefore, the degree of welding of the ignimbrites is commonly assessed on the basis of the hardness or density of the material in outcrop. This has led to a proliferation of poorly-defined and ill-applied terms which only serve to create confusion.

2.3.2.1 Welding

Welding itself, as defined by Smith (1960a), is the specific process which "promotes the union or cohesion of glassy fragments in a viscous state". He stated that the degree of welding may range from,

> "incipient stages marked by the sticking together or cohesion of glassy fragments at their points of contact to complete welding of the surfaces of the glassy fragments accompanied by their deformation and the elimination of pore space".

Three zones are recognised within a single cooling unit (Smith, 1960b): zone of no welding, zone of partial welding, and zone of dense welding. The boundary between the zone of no welding and the zone of partial welding is recognised by the detection of deformation of pumiceous fragments or shards. The zone of dense welding is recognised as being that zone where, "the rock is pore free,... were it not for entrapped gas". In this latter case the loss of pore

space which accompanies welding is used as an indicator of the extent to which welding has occurred. However, Smith (1960b) clearly pointed out the confusion which may arise when considering ignimbrites, especially older ones, which have undergone crystallisation processes. In these materials the elimination of pore space and induration of the rock may occur through secondary crystal growth rather than welding. Consequently, the deformation and coalescence of glassy components are, "the only positive criteria of welding in the tuffs which have crystallised" (Smith, 1960b).

2.3.2.2 Field estimates of welding

Petersen (1979) used the flattening ratios of megascopic pumice clasts as a field measure of the degree of welding. Flattening ratios (major / minor axes of the strained pumice clasts) of ≤2 indicate non-welded or incipiently welded ignimbrite, partly welded ignimbrites have flattening ratios of 2-6, and densely welded ignimbrites are recognised by ratios >6.

However, the recognition of the deformation of glassy components is often not such a simple task, and may involve the preparation of thin-sections for microscopic analysis. Under these circumstances subjective estimates of the porosity and hardness of the material are frequently used as indicators of the degree of welding. Unfortunately, this has resulted in a number of descriptive terms being used to describe welding, many of which appear to have no precise definition. Martin (1965), for example, referred to poorly welded, lightly welded, slightly welded and moderately welded ignimbrites, among others. These terms were not defined in his paper. Similarly, Briggs (1973) used these same terms very loosely, and in this case the use of many of them seems to contradict the original definitions of Smith (1960b). For example, she stated that, "...shards are slightly compressed in...the densely welded upper portion of sheet 1." For welding to be truly dense the shards would have to show considerable deformation. Again, no precise definitions of the welding terms were given. Numerous instances exist, especially in the New Zealand literature, in which "welding" seems to have become synonymous with "induration" and has been applied very subjectively to refer to the density and hardness of the material as it appears in the field, with no index tests used to quantify this.

In some cases classification systems based on the measured porosity of the material have been developed. Sheridan (1970), for example, divides the Bishop Tuff into three zones: the non-welded material, a zone of partial

welding for which the porosity ranges from 10 % to 45 %, and a densely welded zone for which the porosity is less than 10 %. In all of the above studies, with the exception of that of Petersen (1979), an inherent flaw is that one or two macroscopic properties (porosity and / or hardness) are being used to classify a microscopic property (welding). This approach is not always appropriate for the reasons pointed out by Smith (1960b). In particular, the porosity and hardness are controlled by many other factors in conjunction with the welding. In general what these authors were assessing was the degree of induration of the material, and "welding" applied in this sense is a misnomer.

2.3.2.3 Classification of induration

In order to avoid confusion and develop a classification system which could be readily applied in the field, and could be applied on a repeatable basis, the term "welding" was dispensed with altogether for field description in this study. In a later section, welding of the samples will be estimated from thin-section examination, where welding is defined in the strict sense of Smith (1960b). In the field, the degree of induration of the material was assessed, which meant that the effects of welding, compaction, and crystallisation did not have to be separated.

The basis for the field classification is the system of The Geological Society Engineering Group Working Party (1977), in which the ease with which a rock can be broken with a geological hammer is used as an estimate of its strength. Unfortunately, this system has actual compressive strength values associated with its categories. For an initial classification in a study such as this, to use field terms which imply a certain strength range is premature, thus a new system was defined for describing the hardness of ignimbrites which avoids either using a surrogate measure of welding, or classifying the strength before laboratory strength measurements were undertaken. The hardness of the material was estimated by a simple measure of the ease with which the material could be dug with a spade or broken with a geological hammer. This simple method was chosen rather than the Schmidt hammer index for two reasons: the value of the Schmidt hammer as an index test is to be assessed in detail in a later chapter; and the material covered such a range as to require two different instruments, making comparisons more difficult. The following categories were defined:

soft = material which can readily be dug with a spade or pick-axe,
firm = material into which the point of a geological hammer will be deeply imbedded with a sharp blow,
hard = material easily broken with a geological hammer, and
very hard = material harder than "hard".

A "soft" ignimbrite in this classification would generally fall within the zone of no welding in the classification of Smith (1960b); "firm" and "hard" materials would generally fall in the zone of partial welding; and "very hard" materials would generally be in the zone of dense welding.

2.3.3 Jointing

The primary jointing features formed in ignimbrites are tension fractures formed during cooling and compaction of the mass. Such jointing patterns are common in igneous rock bodies of various composition, and are characterised by columns with large aspect ratios (length / diameter) and polygonal cross-section (DeGraff and Aydin, 1987). Ignimbrites are often characterised in outcrop by very widely spaced columnar joints (Marshall, 1935). As they form perpendicular to the cooling surface, which is usually horizontal in ignimbrites which tend to pool in valleys, these joints are generally vertical.

However, simple columnar jointing does not fully account for the joint patterns seen in ignimbrites. Columnar jointing as developed in basalts typically consists of sharp, unique joints with distinct angular changes at the intersections of the joint planes (DeGraff and Aydin, 1987). In ignimbrites the columns are generally bounded by zones of several closely spaced joints, rather than a single, clearly defined joint plane. These joints tend to define wide, curved columns with domed tops.

Variations to this pattern are common. Many ignimbrites which have undergone significant compaction have an extensive system of horizontal joints superimposed on the columnar jointing pattern. A more complex form of jointing is also very common, especially in the very thick deposits, in which the vertical joints are distorted and relatively closely spaced. They tend to have variable strike directions and thus form complex joint blocks. In the case of many soft ignimbrites, the joints are so widely spaced that the rock masses are best described as unjointed (although occasional, generally vertical, joints do exist).

2.3.3.1 Classification of jointing

Numerous classifications exist to describe the jointing of rock masses. Most authors recognise a variety of joint properties which are needed to fully describe the jointing. These include the joint orientation, spacing, and persistence; the joint wall roughness and strength; the aperture, nature of filling, and amount of seepage; the number of joint sets; and the block size and shape. For field descriptions in this study, two parameters, the joint spacing and the shape of the joint blocks, were used to describe the jointing. The following descriptive terms were used to describe the joint block form:

unjointed = ignimbrite for which the length of the exposure is too small to determine the joint spacing, generally >10 m spacing;

columnar = material with regularly spaced columnar joint blocks, these vertical columns are separated by a series of joints with very close to close spacings, yet the columns themselves have very wide to extremely wide joint spacings;

blocky = horizontal compaction joints split the material into approximately cubic blocks; and

complex = curved joint blocks with no simple form apparent.

These descriptive terms were, where applicable, prefixed with terms describing the joint spacing, following the classification of Brown (1981):

extremely close = <20 mm,
very close = 20-60 mm,
close = 60-200 mm,
moderate = 200-600 mm,
wide = 600-2000 mm,
very wide = 2000-6000 mm, and
extremely wide = >6000 mm.

The width was defined as a modal width of the wide columns, rather than a mean width, in order to ignore the effects of the very closely spaced joints at the boundaries of the columns.

2.4 Collection of specimens

From each site large blocks of rock were collected. Generally one block with dimensions of approximately 0.5 x 0.5 x 0.2 m was sufficient, but in some cases such blocks were not available so several smaller blocks were collected.

	WHAKA/up	WHAKA/low
matrix:		
colour	pale reddish grey (2.5YR 7/2)	grey (N 6/0)
pumice:		
types	pale reddish orange (2.5YR 7/4), very soft, highly vesicular clasts	pale grey (2.5Y 8/1) to greyish yellow (2.5Y 6/2) in colour, very soft
size	maximum 50 mm, typically <10 mm	maximum 30 mm, typically <10 mm
shape	rounded	rounded
abundance	scarce	rare
crystals:		
types	quartz, feldspar, and biotite	quartz, feldspar, and biotite
size	<4 mm	<4 mm
abundance	common	abundant
lithics:		
types	not identifiable	rhyolite, ignimbrite, greywacke
size	<10 mm	<15 mm
abundance	rare	scarce
fabric	none	none
weathering	slight	unweathered
induration	soft	very hard
jointing	unjointed	moderate to wide spacing, complex

Table 2.1: Field descriptions for each of the sites studied. Numerical colour codes follow the notation of the Standard Munsell Colour Chart; other terms are defined in the text.

The orientation of each block was recorded. This was defined in terms of the actual physical orientation of the materials in the field and recorded as "vertical" or "horizontal". Due to the emplacement mechanisms of ignimbrites this corresponded, in all cases, to the alignment of any clasts in the material where apparent. This was ensured by avoiding sites which showed obviously unusual clast orientations, such as the sides of valleys in the pre-existing topography, which are not common in the voluminous ignimbrites under consideration. As clasts within an ignimbrite become aligned through compaction during cooling of the mass, the vertical direction corresponds to the direction of the principal stress at this time, and the horizontal direction corresponds to the major axis of the strain ellipse as expressed by the compressed pumice clasts.

This means of specimen collection automatically places a lower limit on the strength, as for blocks to be collected and transported, and specimens to be prepared for testing, the material must be sufficiently strong to remain coherent throughout sampling. This means that the loose, incoherent material which comprises many of the soft ignimbrites could not be sampled, or tested using rock mechanics techniques. These materials are commonly produced by very high-energy eruptions (model A, section A1.4.3.1), and are volumetrically quite significant portions of ignimbrites. In an engineering context they would be classed as soils, and treated as such. These materials were beyond the scope of this study, which is confined to ignimbrites which display the properties of rocks (or soft rocks in many cases) in an engineering sense.

2.5 Sites studied

2.5.1 Whakamaru Ignimbrite

The Whakamaru Ignimbrite as discussed in this study follows the original definition of Healy (1954). It consists of a series of pyroclastic flow deposits extending along the western margin of the Taupo Volcanic Zone (figure 1.1), where it is typically exposed as steep, jointed cliffs, both along the western side of Lake Taupo and further northwards in the valley of the Waikato River. Fission-track dating, by Kohn in 1973, indicates that its age is approximately 330,000 years (Briggs, 1976a). On the basis of petrographic variations within this ignimbrite, Briggs (1973, 1976a) concluded that the most likely source area is the Western Bays of Lake Taupo. However, from a more

(a) Whakamaru Ignimbrite (top)

The Whakamaru Ignimbrite at Maraetai is exposed as steep cliff faces approximately 100 m high along the Waikato River Valley. At the base the material is a hard, complexly jointed ignimbrite; the density decreases upwards to a soft, unjointed ignimbrite at the skyline.

Specimens were collected near the Maraetai 2 powerhouse at the lower left of this plate (WHAKA/low, NZMS 260 T16 496134), and from the soft material on the access road off this photo to the right (WHAKA/up, NZMS 260 T16 488136). This material is equivalent to that forming the artificial cuttings above the head-race canal at the top of the profile seen here.

(b) Ongatiti Ignimbrite (bottom)

Specimens were obtained from the Hinuera Stone Quarry (NZMS 260 T15 461614) shown in this plate. Here the material is quarried from an exposure ~50 m high, which shows very widely spaced columnar jointing.

Plate 2.1: Field sites.

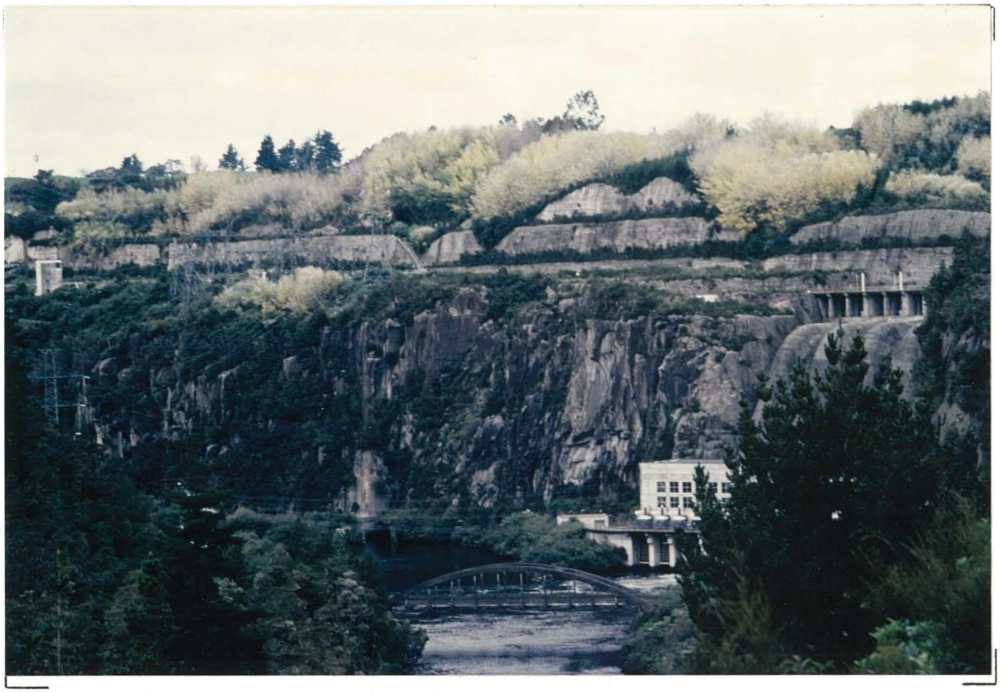


FIRTH

	ONG/1	ONG/2	ONG/3
matrix:			
colour	pale yellow (5YR 7/4)	grey (N 6/0)	pale yellow (5Y 7/3)
pumice:			
types	vary from pale yellow (5Y 8/3), highly vesicular clasts with common crystal inclusions, to grey (5Y 6/1), moderately dense, fine textured clasts	vary from pale yellow (5Y 8/3), highly vesicular clasts with common crystal inclusions, to pale grey (5Y 7/2), (5Y 7/2), medium density clasts; many grey clasts show extensive brown colouration	pale yellow (7.5Y 8/3), vesicular clasts with numerous crystal inclusions, and streaky pale grey (7.5Y 8/1) clasts
size	maximum 100 mm, typically 2-30 mm	maximum 70 mm, typically 15-30 mm	maximum 60 mm, typically <20 mm
shape	rounded	rounded	slightly elliptical
abundance	very abundant	abundant	very common
crystals:			
types	quartz and feldspar	quartz and feldspar	quartz and feldspar
size	<2 mm	<2 mm	<2 mm
abundance	common	common	common
lithics:			
types	rhyolite and greywacke	rhyolite and greywacke	rhyolite and greywacke
size	maximum 20 mm, typically <10 mm	maximum 20 mm, typically <10 mm	maximum 15 mm, typically <10 mm
abundance	rare	rare	rare
fabric	none	none	slight alignment
weathering	slight	unweathered	unweathered
induration	firm	hard	hard
jointing	very wide, columnar	very wide, columnar	very wide, columnar

Table 2.1 (cont.): Field descriptions for each of the sites studied. Numerical colour codes follow the notation of the Standard Munsell Colour Chart; other terms are defined in the text.

recent study of the stratigraphy of the deposit, Wilson *et al.* (1986) have suggested that the source is in an older volcanic centre near Maroa. This work by Wilson *et al.* (1986) uses the term "Whakamaru Ignimbrites" to refer to a large sequence of deposits of approximately 300,000 years B.P. which are found to both the west and east of Lake Taupo. The precise definition used is not central to this study, hence the original definition will be adhered to.

The Whakamaru Ignimbrite is generally a hard, pale grey, crystal-rich rock (Martin, 1965; Briggs, 1976b). However, the deposit varies considerably in thickness in response to the topography at the time of emplacement (Briggs, 1975), and thus the detailed lithologic properties vary considerably with vertical and lateral position within the sheet (Blank, 1965). This results in a range of properties from localised examples of dense, black, glassy rock to loose, pink, soft material.

Laboratory specimens of this ignimbrite were taken from along the Waikato River valley near the Maraetai Dam (plate 2.1a). Here the material forms steep cliff faces approximately 100 m high. At the base it is a very hard, complexly jointed ignimbrite. The density decreases upwards in the profile, with the top consisting of soft, unjointed ignimbrite. It is suggested that at least 3, and maybe up to 7, flow units are represented in this section (Hatherton, 1954; Briggs, 1976a,b).

One block (WHAKA/low, grid reference NZMS 260 T16 496134) was extracted from the level of the power-house at the base of the dam, in the zone of complex jointing, and a second block (WHAKA/up, grid reference NZMS 260 T16 488136) was taken from the access road through the upper, soft ignimbrite. The wide joint spacing, and hence massive nature, of the intermediate material made sampling impossible.

2.5.2 Ongatiti Ignimbrite

The Ongatiti Ignimbrite is an extremely widespread deposit which has been traced from Ngaruawahia in the north to Taumarunui in the south (Wilson, 1986), as shown in figure 1.1. Fission-track dating, by Kohn in 1973, gives an age of approximately 0.75 million years B.P. for this ignimbrite (Wilson, 1986). The source is currently believed to be a caldera volcano centred on the Mangakino area (Wilson, 1986). This caldera is now largely filled with later deposits, but has been reccgnised from geophysical evidence (Stern, 1979; Rogan, 1982) and pyroclastic stratigraphy (Wilson *et al.,* 1984).

	OWH/up	OWH/low
matrix:		
colour	pale grey (5Y 7/2)	pale grey (7.5Y 7/1)
pumice:		
types	pale grey (5Y 8/2), moderately vesicular clasts, and dark grey (N 3/0), glassy clasts	dark grey (N 3/0), dense, glassy pumices, and rounded, pale grey (5Y 8/2), moderately dense clasts
size	maximum 40 mm, typically 5-10 mm	maximum 60 mm, typically 15 mm
shape	glassy clasts flattened pale coloured clasts rounded	glassy clasts extremely flattened pale coloured clasts rounded
abundance	abundant	abundant
crystals:		
types	not identifiable	not identifiable
size	<1 mm	<1 mm
abundance	rare	rare
lithics:		
types	not identifiable	not identifiable
size	<10 mm	<10 mm
abundance	rare	rare
fabric	slight alignment	foliate
weathering	slight	slight
induration	hard	very hard
jointing	indeterminate	moderate spacing, columnar

Table 2.1 (cont.): Field descriptions for each of the sites studied. Numerical colour codes follow the notation of the Standard Munsell Colour Chart; other terms are defined in the text.

The Ongatiti Ignimbrite is characteristically white to yellow in colour, with abundant pumice clasts and crystals (Olissoff, 1981).

Approximately 60 km south of Hamilton, the Ongatiti Ignimbrite is exposed along a former course of the Waikato River (the Hinuera Gap) where it forms vertical cliffs approximately 50 m high. Within this exposure is the Hinuera Stone Quarry (grid reference NZMS 260 T15 461614), where the ignimbrite is quarried for use as a decorative building material (plate 2.1b). Because of the ease of obtaining cut blocks of an appropriate size from an otherwise massive material, laboratory specimens were taken from the quarry. As pre-cut blocks were used, no control on the stratigraphic position or block orientation was possible for this material. Three specimens were taken which represented a range of available materials; these are referred to as ONG/1, ONG/2, and ONG/3.

2.5.3 Owharoa Ignimbrite

The Owharoa Ignimbrite is only identified in a small outcrop area near Waihi, at the southern end of the Coromandel Peninsula (figure 1.1). The rock is associated with the Whitianga Group; a series of undifferentiated ignimbrites which, together with a number of rhyolites (Minden Rhyolites), form a band of silicic volcanism along the eastern side of the Coromandel Peninsula (Schofield, 1967; Skinner, 1986). This volcanism pre-dates the present Taupo Volcanic Zone, being active during the late Miocene and early Pliocene; the Owharoa Ignimbrite has been fission-track dated at 2.89 my (Skinner, 1986). The Owharoa Ignimbrite is characterised by a pale grey colour and abundant flattened lenticles of dark grey pumice (Ewart and Healy, 1966).

Laboratory specimens were taken from two sites, both of which were along Owharoa Road to the south of Karangahake Road. The lower site (OWH/low, grid reference NZMS 260 T13 549167) is a disused quarry approximately 200 m south of Karangahake Road (plate 2.1c). The upper site (OWH/up, grid reference NZMS 260 T13 549166) is approximately 50 m further south.

2.5.4 Site descriptions

Field descriptions of each site are presented in table 2.1. The fabric as given in this table refers to the degree of alignment of the macroscopic pumice clasts. Numerical colour designations given follow the notation of the

(a) Owharoa Ignimbrite

Field exposure of the Owharoa Ignimbrite is limited. A small, disused quarry (NZMS 260 T13 549167) was chosen for one site (OWH/low). The ignimbrite here is pale grey, and shows a moderately spaced columnar jointing pattern which is approaching a complex form.

Plate 2.1 (cont.): Field sites.

Standard Munsell Colour Chart, determined on wet samples; in the associated descriptions the term "light" has been amended to "pale" to avoid any possible confusion with the density of the rock.

2.6 Summary

Three ignimbrite sheets were sampled in order to provide material with a wide range of physical properties for laboratory testing. The specimens taken range from examples of very hard to soft material, from specimens of crystal-rich, pumice-poor ignimbrite to pumice-rich, crystal-poor material, and includes one ignimbrite which shows considerable flattening of the pumice clasts. The jointing varies from essentially unjointed material, through a simple, widely spaced, columnar jointing pattern, which is often quoted as being characteristic of ignimbrites, to a complex jointing pattern with large, broadly curved joint planes.

PART 2 - GEOMECHANICS

CHAPTER 3 - STANDARD LABORATORY CONDITIONS

3.1 Introduction

The preparation of laboratory specimens from the blocks collected in the field followed a standard pattern which was designed to ensure the maximum use of available material. Standard laboratory procedures for controlling the moisture content and required number of specimens for each test were defined; this chapter outlines these procedures.

3.2 Specimen preparation

3.2.1 Block usage

Large blocks collected from the field were used to provide material for all of the laboratory tests. Figure 3.1 shows schematically the sequence in which samples were prepared. Firstly, NX size (54 mm diameter) cores were cut for mechanical testing and image analysis. Material from the "skeleton" of the block left after removing the cores was used for hand specimens and slake durability samples, and offcuts from core ends were used to prepare thin-sections for petrographic analysis. Remnants of failed cores used in compressive strength tests provided powder samples for geochemical analysis, and further thin-sections were made of the failed samples to examine the crack development.

3.2.2 Specimen numbers

Code numbers were assigned to all specimens. These consisted of three components:

(1) the site designation,
(2) the number of the individual block collected, and
(3) a letter code and number describing the type of specimen prepared and its sequential number.

The site designations used were:

WHAKA = Whakamaru Ignimbrite,
ONG = Ongatiti Ignimbrite, and
OWH = Owharoa Ignimbrite.

These were qualified by the addition of /up, /mid. or /low to designate the

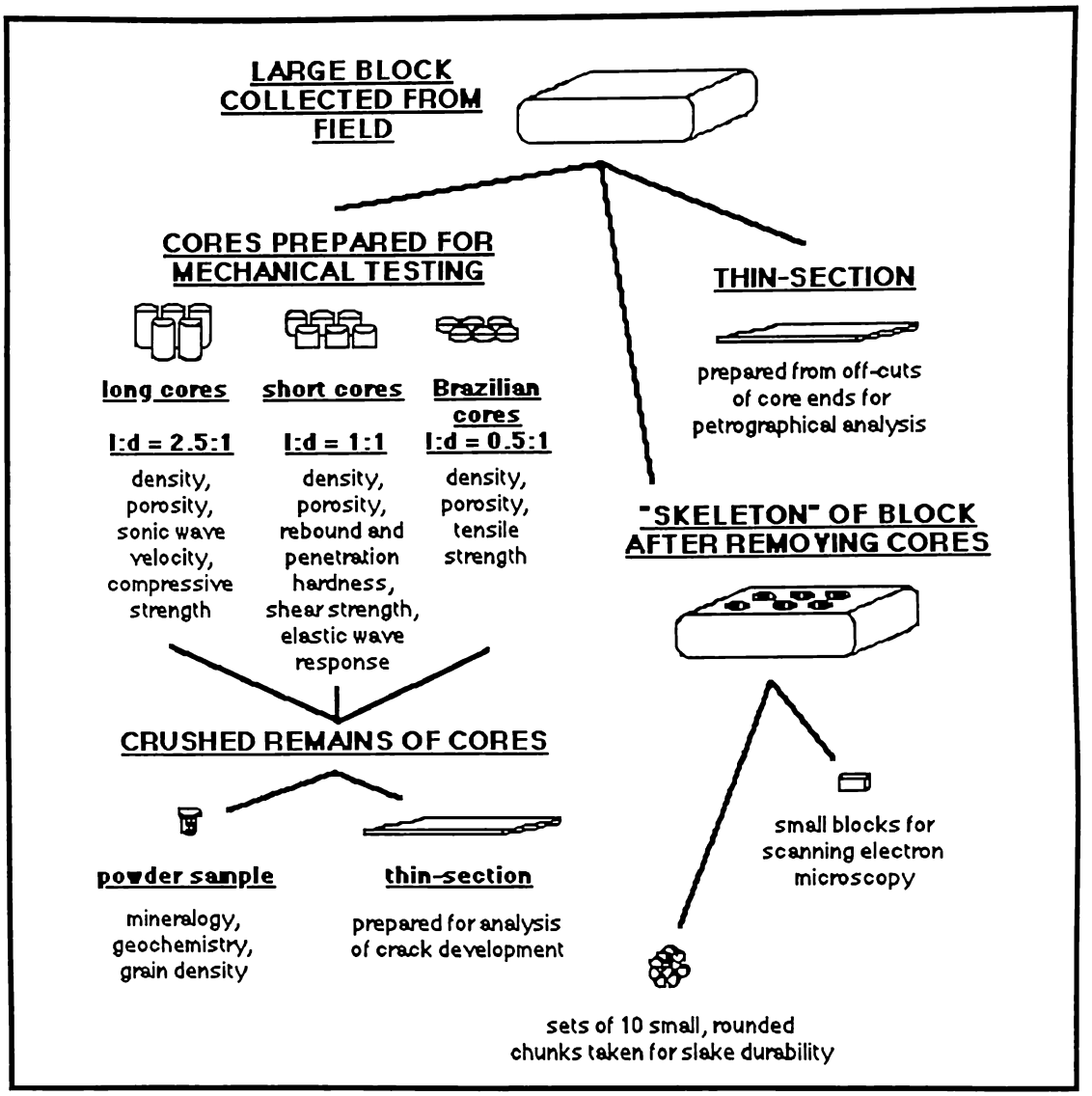

Figure 3.1: Sequence of specimen preparation. Image analysis was undertaken on cores prepared for mechanical testing and thin-sections prepared for petrographical analysis.

relative position in the sheet (or /1, /2, and /3 for the Ongatiti specimens, which did not have any stratigraphic control).

Specific test procedures required specimens of particular shapes and sizes. Letter codes defining the specimen type were:

LC = long core (length : diameter ratio = 2.5 : 1),
SC = short core (length : diameter ratio = 1 : 1),
BC = Brazilian core (length : diameter ratio = 0.5 : 1),
CU = cubic specimen (60 mm cubic block), and
TS = thin-section.

In many cases these were refined by the addition of a qualifier at the start of this code. These were:

V = vertical, and
H = horizontal

where vertical and horizontal refer to the actual orientation of the block in the field. This corresponded to the visible alignment of compressed clasts in the rock in all cases; "vertical" was perpendicular to the major axis of the lenticular pumice clasts and "horizontal" was parallel to the major strain axis.

An example of a specimen code number is:

WHAKA/low-1-VTS5

which translates as, the lower specimen of the Whakamaru Ignimbrite, block number 1, vertical thin-section number 5.

3.3 Laboratory procedures

3.3.1 Standard moisture contents

Many previous studies of rock mechanics have shown that the strength is, in many cases, strongly dependent upon the degree of saturation of the specimen (Hawkes and Mellor, 1970). To examine the extremes of strength, all tests were undertaken at one of two standard moisture conditions; oven-dry for which the specimens were dried overnight in an oven at 105 °C, and saturated for which the specimens were kept under water in a vacuum chamber until bubbles were no longer coming from the core (usually 24 to 36 hours). A check on the suitability of these times showed that constant weight conditions were achieved in the oven between 12 and 24 hours, and likewise, the cessation of bubbling under vacuum represented a constant weight condition.

3.3.2 Estimation of true value and confidence limits

For each parameter measured a number of replicate readings were taken. In most cases the mean value of these readings was taken to be the best estimate of the true value. Exceptions to this rule are discussed where appropriate. Quoted error estimates represent the 95 % confidence limits calculated using Student's t-distribution (assuming small sample sizes), and rounded to one significant figure.

3.3.3 Required number of specimens

The number of specimens used for each test was determined from two considerations: the desired accuracy of the test, and the volume of material available. In general, 95 % confidence limits within 5 % of the mean value were considered to be of sufficient accuracy. Where possible, replicate tests were undertaken until this requirement was satisfied. Unfortunately, many of the parameters being measured were so inherently variable, due to the heterogeneity of the material being investigated, that very large sample sizes (>200 cores) would have been required. Under these circumstances the volume of material which it was possible to collect and test controlled the number of replicate readings made.

3.3.4 Data analysis

Statistical analysis was performed using a standard computer analysis package (Wingz) on a Macintosh SE personal computer. Most analyses involved using linear regression, for which regression coefficients adjusted for the degrees of freedom (r^2_{adj}) are quoted. On occasion these coefficients can be negative, this is because the adjustment subtracts a value from the original r^2 value between 0 and 1. Errors in the intercept and slope for lines obtained by this analysis are based on the statistical standard errors in these values.

CHAPTER 4 - MECHANICAL STRENGTH

4.1 Introduction.

The strength of a rock refers to the peak stress which can be applied to a sample of rock before failure occurs. Measurement of the rock strength under various types of applied stresses (compressive, tensile, and shear) are extremely common geomechanical tests, and provide the standard engineering indices of rock behaviour. The techniques are standardised to provide comparable data from different laboratories.

For this study, the compressive (σ_c), shear (c,ϕ), and tensile (σ_t) strengths of rock cores were chosen as the basic geomechanical properties of the materials. Strength indices and petrographical properties presented in later chapters were measured with the intention of assessing their influence on, and value as predictors of, these three strength values.

This chapter:

(1) presents the results of a series of rock strength measurements carried out using standard procedures,

(2) examines the variability in the strength data compared with other rocks, and

(3) discusses the mechanisms of failure in these materials.

4.2 Sample Preparation.

Brown (1981) laid out detailed core sample requirements for strength testing. These were adhered to as closely as possible for all core preparation. Unfortunately, equipment constraints meant that cores could not be cut to a greater diameter than 54 mm. In almost every case this breached the requirement that the "diameter of the specimen should be related to the size of the largest grain in the rock by the ratio of at least 10 : 1" (Brown, 1981, p113). Each ignimbrite studied contained pumice clasts up to at least 30 mm in length (table 2.1) and the Ongatiti Ignimbrite contained abundant clasts up to 100 mm long. To properly fulfill the requirements, cores with diameters of 1000 mm (and lengths of >2 m) would have been necessary. This was not feasible, so the smaller core size (54 mm diameter) was chosen which allowed many replicate tests to be carried out.

The prepared cores also departed from the standard in that perfectly smooth cores were difficult to obtain from the softer material. This was due to

many of the crystals being, apparently, only weakly cemented in the matrix. Any form of sample preparation involving cutting or grinding of the material invariably resulted in such crystals being plucked from the surface. Being harder than the matrix they then gouged paths across the surface, leaving grooves along the core sides and across the ends. Samples where this was very pronounced were discarded, but, particularly in the softest Ongatiti Ignimbrite, core surfaces could not be prepared to the rigid specifications of Brown (1981).

For very soft materials coring was impossible, so block samples were cut using a diamond saw. However, this material was found to break down very readily when exposed to the cooling water of the saw, and therefore had to be cut very quickly by pushing the sample through by hand. This meant that the sides were not always perfectly perpendicular. Many other methods of core preparation were tried, such as dry coring and using hand and power saws, but each proved less successful than the diamond saw. Because of the volumetric significance of these soft rocks within ignimbrites, obtaining some measure of their strength was considered essential. Hence the imperfections in sample preparation were accepted.

4.3 Testing Equipment.

The primary compression machine used was a Soil-Test Concrete Testing Machine (model CT-710M, manufactured by Soil-Test Inc, Illinois, USA). The compression was applied by a hydraulic ram and the rate of stress application controlled by means of a valve on the motor assembly. Two gauges measured the applied load; one for weaker materials which ranged from 0 - 9000 kg and one for stronger materials calibrated from 0 - 120000 kg (although the equipment could only feasibly apply a load up to approximately 80000 kg).

For many weak ignimbrite samples the rate of load application could not be slowed sufficiently to allow a test of 10-15 minutes duration before failure, and the low peak load values were at the very lowest range of the equipment, which did not allow a sensitive enough reading of the strength to be obtained. For these samples an instrument with a much lower load range was used. This was a Wykeham-Farrance triaxial soil-testing compression machine, modified by the addition of large platens. In this equipment the load was applied by a ram from the base of the sample. Variable motor speeds and gearing allowed the ram to move at a very slow rate for weak materials.

	moisture	σ_c (MPa)	$\frac{\sigma_{cdry}}{\sigma_{csat}}$	c', c (MPa)	$\frac{c}{c'}$	ϕ', ϕ (°)	r^2_{adj} for τ/σ_n	σ_t (MPa)	$\frac{\sigma_{tdry}}{\sigma_{tsat}}$
WHAKA/up	saturated	0.23 ± 0.01	3.2	0.06 ± 0.01	2.3	35 ± 3	0.79		
	oven-dry	0.73 ± 0.07		0.14 ± 0.06		43 ± 5	0.87		
WHAKA/low	saturated	26 ± 3	1.7	9.0 ± 0.5	1.4	34 ± 1	1.00	1.9 ± 0.1	1.6
	oven-dry	44 ± 5		13 ± 2		35 ± 2	0.99	3.1 ± 0.2	
ONG /1-1	saturated	0.8 ± 0.1	5.9	0.19 ± 0.09	8.4	38 ± 4	0.94	0.12 ± 0.03	10.8
	oven-dry	4.7 ± 0.7		1.6 ± 0.5		33 ± 8	0.69	1.3 ± 0.4	
ONG /1-2	saturated			0.4 ± 0.1	6.8	33 ± 4	0.91		
	oven-dry			2.7 ± 0.5		27 ± 5	0.86		
ONG /2-1	saturated	3.5 ± 0.2	4.0						
	oven-dry	14 ± 2							
ONG /2-2	saturated			2.1 ± 0.8	3.3	31 ± 8	0.65	1.0 ± 0.1	3.4
	oven-dry			7 ± 2		32 ± 8	0.73	3.4 ± 0.2	
ONG /3-1	saturated	19 ± 3	2.2						
	oven-dry	42 ± 4							
ONG /3-2	saturated			3.4 ± 0.4	2.3	33 ± 2	0.98	2.1 ± 0.7	2.0
	oven-dry			7.8 ± 0.7		33 ± 3	0.97	4.2 ± 0.4	
OWH/up-V	saturated	17 ± 1	1.5	0.35 ± 0.06	2.3	33 ± 3	0.95	2.5 ± 0.3	1.5
	oven-dry	26 ± 3		0.8 ± 0.1		27 ± 4	0.85	3.8 ± 0.2	
OWH/up-H	saturated	12 ± 1	2.0	0.42 ± 0.07	1.8	33 ± 2	0.96	2.7 ± 0.2	1.6
	oven-dry	25 ± 3		0.74 ± 0.07		29 ± 2	0.96	4.4 ± 0.2	
OWH/low-V	saturated	36 ± 5	1.3	1.1 ± 0.2	1.2	31 ± 4	0.86	5.4 ± 0.5	1.3
	oven-dry	45 ± 6		1.3 ± 0.6		34 ± 7	0.70	7.1 ± 0.7	
OWH/low-H	saturated	27 ± 5	2.0	0.8 ± 0.2	1.8	34 ± 3	0.93	7 ± 2	1.0
	oven-dry	54 ± 4		1.4 ± 0.3		33 ± 3	0.94	6.8 ± 0.5	

Table 4.1: Measured geomechanical properties for ignimbrites studied. All values represent the mean for tests on a number of samples.

The narrow, flexible posts on this machine meant it had the capacity to store considerable amounts of energy during a test. This was released on sample failure with an alarming leap of the entire instrument. To avoid inaccuracies involved with this "soft" (Attewell and Farmer, 1976) machine response the tests were run very slowly. Occasionally this meant that samples took longer to fail than the 10 to 15 mins of Brown (1981), but it was felt that this was preferable to the sudden release of stored energy. A simple rod and dial-gauge mechanism was attached to the platens to give an axial strain measurement.

The standard test machine is referred to as the "UCS", and the soft rock testing machine is referred to as the "SRCM" throughout this thesis.

Prior to embarking on the laboratory work the calibrations of the dials on both instruments were checked by the local Ministry of Works laboratory. However, the ranges of the two devices (UCS and SRCM) were so different that it was impossible to obtain a direct calibration between them.

4.4 Compressive strength

4.4.1 Test procedure

For compressive strength testing, specimens of Ongatiti, Owharoa and lower Whakamaru (WHAKA/low) Ignimbrites were cut into 54 mm cores with a length : diameter ratio of 2.5 : 1 (135 mm long). The soft Whakamaru Ignimbrite (WHAKA/up) was cut into 60 mm cubic blocks. For all samples each dimension was measured in three different places and averaged. Before testing, sketches of the samples were made noting any large clasts, zones of staining and so forth. Cores were tested in both oven-dry and saturated conditions.

4.4.2 Results

Test results are summarised in table 4.1. The ignimbrites tested span a range of two orders of magnitude from 0.23 MPa (WHAKA/up) to 44 MPa (WHAKA/low). This ranges from a very low strength rock to a low strength rock in the classification of Deere and Miller (1966). Also of note in these values is that it is very common for one ignimbrite sheet to have units for which the strength varies by one order of magnitude (Ongatiti Ignimbrite) or even two orders of magnitude (Whakamaru Ignimbrite). Likewise, the ignimbrites show

marked variations in strength between oven-dry and saturated samples. A softening factor ($\sigma_{c,dry} / \sigma_{c,sat}$) of approximately 2 is typical, and in very porous samples the values reach 5 or even 6. This suggests that effective stresses due to water filled pores are very significant. Softening is most marked in the Ongatiti Ignimbrite specimens.

4.5 Shear strength

4.5.1 Test Procedure

The shear strength of intact rock samples was measured using the technique described by Protod'yakonov *et al.* (1969), in which rock cores were sheared by using angled jigs to impose a known shear angle from an initial compressive stress. A combination of different shear angles for samples from the same block allowed the Mohr-Coulomb equation to be calculated. These different angles were obtained by a combination of dies and wedges (Vutukuri *et al.*, 1974).

For each imposed angle, the peak applied load was resolved into components of shear and normal loads. From this, values of the shear strength (τ) and normal stress (σ_n) at failure were calculated. Plotting these on a graph of τ versus σ_n gave the cohesion (c,c') as the y-intercept and the angle of internal friction (ϕ, ϕ') as the slope of the best-fit straight line. The primed symbols (c',ϕ') refer to effective values measured when the pores were filled with water, the unprimed values (c,ϕ) were measured on dry cores.

4.5.2 Jig design

Protod'yakonov *et al.* (1969) discussed various different orientations of shear stress and jig designs. They recommended that cores with a length : diameter ratio of 1 : 1, which were sheared so that the failure plane was parallel to the ends of the core, gave the most reproducible results. This was the design used for the bulk of the samples in this study, with the jigs being made of hardened steel. As the ignimbrites used in this study tended to deform considerably before failure, they were often compressed firmly into the jigs, making their removal very difficult. Thus the original jig design was altered by the addition of a large grub screw and base plate in the ends which allowed the failed material to be forcibly removed.

For the softer ignimbrite material (ONG/1) the hardened steel jigs were

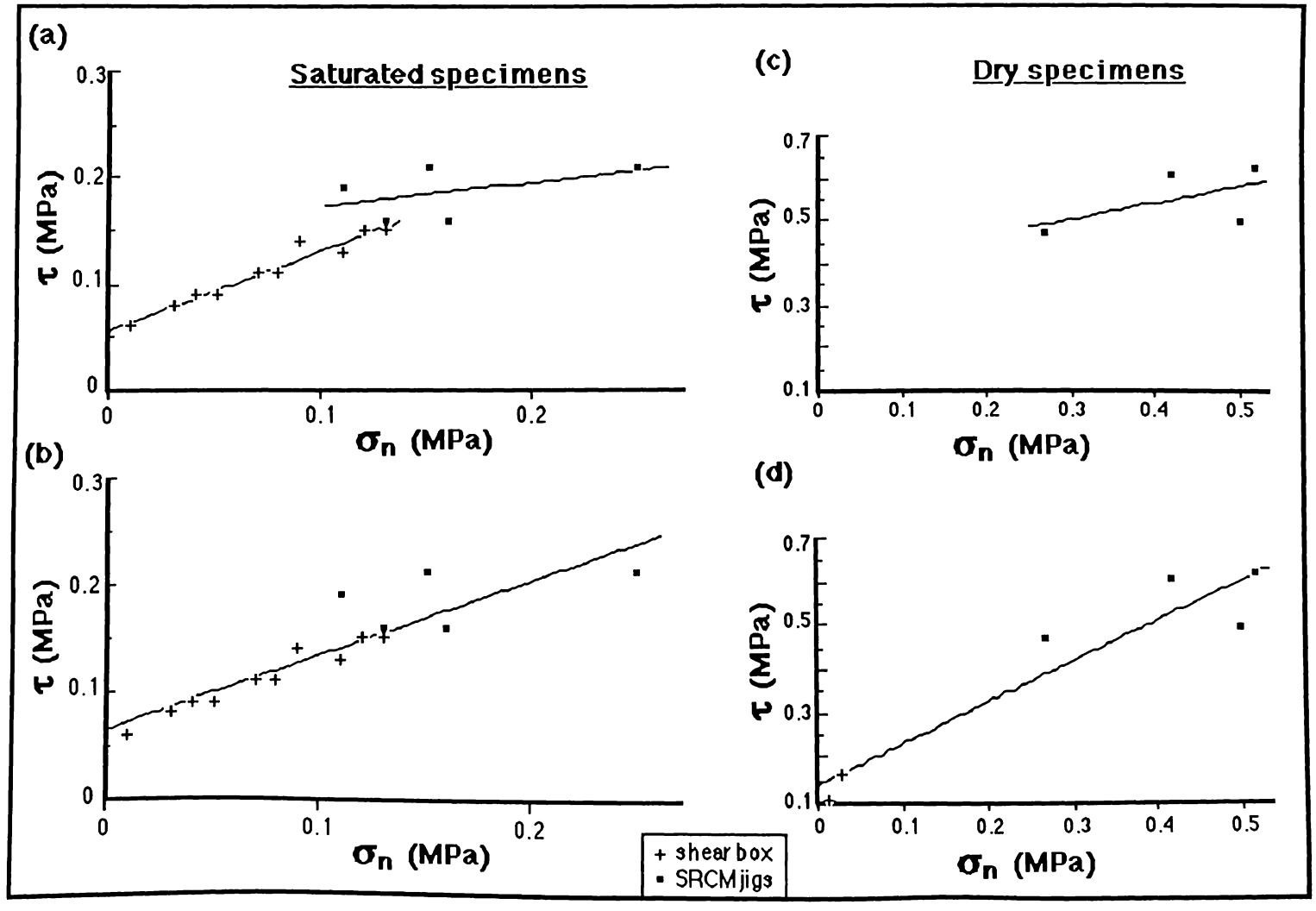

Figure 4.1: Derivation of c and ϕ (c' and ϕ') for WHAKAIup specimens.

calculated to apply a significant normal load to the cores by virtue of their weight. Thus aluminium jigs of the same design were built for these cores. However, their use was restricted to the weakest materials as the aluminium would deform at the stresses required to fail the stronger materials. Similarly, for the very softest material (WHAKA/up) which could not be cored, aluminium dies were made to take cubic specimens. In this case the ends of the specimens were exposed, and thus tensile failure of the ends prior to shear failure could not be entirely avoided. This may have slightly reduced the measured maximum strength as the tensile failure reduced the area of the shear failure plane. However, observations of the tested cubes suggested that this was not significant.

4.5.3 Soil shear box

For the very weak Whakamaru Ignimbrite (WHAKA/up) the range of normal loads achievable with the above technique was restricted to relatively high values. In order to extend this range a series of unconsolidated, undrained shear tests were carried out on a 60 mm x 25 mm Wykeham-Farrance direct soil shear box. For this test small blocks were cut, and tested following the standard soil shear test methods described by Vickers (1983).

In figure 4.1 the two sets of data obtained for the WHAKA/up specimen (those from the aluminium jigs and the direct soil shear box) are plotted for both saturated and dry specimens, and regression coefficients (r^2_{adj}) for linear regression lines are given in table 4.2. Figure 4.1a is for saturated specimens, and shows separate regression lines for each measurement technique; figure 4.1b shows the same data points with a single regression line for the combined data. Likewise, figure 4.1 c shows the regression line for the oven-dry specimens derived from the SRCM jigs, whereas figure 4.1d shows the regression line for the combined data set from the two techniques. It is apparent that the two pieces of equipment do not give exactly the same regression lines. In fact, the regressions obtained from the SRCM jigs alone are very poor in both the saturated and oven-dry cases, suggesting that this technique is not really suitable for these weak materials. For the saturated specimens, the soil shear box alone gives a very good regression coefficient, and this may therefore be the most appropriate means of testing these materials in shear. Unfortunately however, their oven-dry counterparts are too strong to obtain more than two data points from the soil shear box.

In order to treat both saturated and dry specimens in the same manner,

	c', c (MPa)	ϕ', ϕ (°)	r^2_{adj}
saturated specimens:			
shear box	0.06 ± 0.005	35 ± 2	0.95
SRCM jigs	0.15 ± 0.04	12 ± 12	0.00
combined	0.06 ± 0.01	35 ± 3	0.79
dry specimens:			
shear box	----	----	----
SRCM jigs	0.38 ± 0.17	21 ± 21	0.00
combined	0.14 ± 0.06	43 ± 5	0.87

Table 4.2: Regression coefficients for shear strength tests on the soft Whakamaru (WHAKA/up) Ignimbrite.

combined equations which treated the data from both devices together were calculated. These allowed a reasonable regression in each case. However, this combined regression was slightly suspect for the dry specimens, as the two devices gave separate clusters of data points, allowing a good regression to be drawn between the clusters. As it provided the best estimate obtainable of the shear strength of this material it was accepted as the data for this thesis.

4.5.4 Results

The values given in table 4.1 show a range of friction angle values of 27 - 43 °, but most are strongly clustered around 33 ± 2 °; this does not appear to be significantly affected by the moisture content of the rock. The value of cohesion varies from 0.06 MPa (WHAKA/up) to 13 MPa (WHAKA/low). The cohesion increases with increased induration, and the saturated effective cohesion is considerably less than the dry cohesion (average softening factor = 4.5). In general, the least indurated specimens within any one ignimbrite have the highest softening factors, and the Ongatiti Ignimbrite specimens show considerably more softening on saturation than the other ignimbrites.

It is interesting that the cohesion values do not follow the same trends as the compressive strength. The WHAKA/up and OWH/low specimens, for example, have very similar compressive strengths (both saturated and oven-dry), yet the WHAKA/up cohesion values are almost an order of magnitude greater than those for OWH/low. Overall the Owharoa Ignimbrite appears to have surprisingly low values of cohesion, given the relatively high compressive strength. This applies to both upper and lower specimens in each of horizontal and vertical orientations.

4.6 Tensile strength

4.6.1 Test Procedure

Tensile strength was assessed using the indirect Brazilian test method described by Brown (1981). For this test a jig was used to convert a vertical stress into a tensile load on a short core with a length : diameter ratio of O.5 : 1. The ISRM standards required a strip of masking tape to be applied around the perimeter of the sample in order to ensure proper loading of the specimen. However, for many ignimbrites it was found that this tape significantly

material	σ_c (MPa)	c (MPa)	ϕ (°)	σ_t (MPa)
granite	100-250	35-55	45-60	4-25
gabbro	150-300		10-30	5-30
basalt	80-300	35-55	48-50	6-30
sandstone	20-170	1-30	25-35	4-25
limestone	4-250	10-30	35-50	1-25
shale	5-160	1-20	15-30	2-10
dolomite	30-250	10-30	22	2-25
gneiss	50-200		31-35	4-20
marble	50-250	20-40	32-50	5-20
quartzite	85-300	20-40	26-60	3-30
slate	25-200	20-40	25-62	7-20

Table 4.3: Representative strength values for a variety of lithologies (compiled from Attewell and Farmer, 1976; Jumikis, 1979; Selby, 1982; Farmer, 1983).

increased the tensile strength of the samples. Thus it was not applied as this seemed a greater source of error than slight variations in the loading frame.

No tensile strength measurements could be obtained for the soft WHAKA/up ignimbrite for which coring was impossible.

4.6.2 Results

Each ignimbrite shows an increase in tensile strength with induration, and the measured values show considerable variation, spanning one order of magnitude within the Ongatiti Ignimbrite. In contrast with the cohesion values, the WHAKA/low specimen shows remarkably low values of tensile strength compared with the other ignimbrites. The WHAKA/low material is weaker in tension than both the OWH/up and ONG/3 specimens; it is considerably stronger than these in compression.

Softening factors for the Whakamaru and Owharoa Ignimbrites are consistently approximately 1.5, but the Ongatiti Ignimbrite undergoes considerably more softening upon saturation. The ONG/3 and ONG/2 specimens have softening factors of 2.0 and 3.4 respectively, whereas the ONG/1 specimen appears to have a softening factor of 10.8. This is thought to be exaggerated by the presence of large pumice clasts in some of the cores. Because of the small core size, large clasts completely dominate the specimen; these are the cause of the high errors associated with the tensile strength determinations. As these pumice clasts are very abundant (table 2.1) in this material, increasing the number of specimens does not improve the accuracy of the determination significantly. Softening of the pumice clasts upon saturation is thought to be much greater than that of the groundmass, hence the softening factor for the ONG/1 is believed to represent this pumice softening more than the true softening of the intact rock.

4.7 Comparison with other rocks

Table 4.3 lists mechanical strength properties for a selection of other rock types (compiled from Attewell and Farmer, 1976; Jumikis, 1979; Selby, 1982; and Farmer, 1983). It is apparent that, compared with these other lithologies, ignimbrites are weak materials under compressional stresses. Only soft sedimentary rocks, such as shale and some sandstones and limestones, reach comparably low values. Hind (1986) reported a dry compressive strength of 79 MPa for an ignimbrite from Ruahihi in New

Zealand; other published values fall within the same range of strengths as those measured in this thesis (Maloy and Lowe, 1945 (σ_c = 8 - 47 MPa); Rippa and Vinale,1983 (σ_c = 1 - 8 MPa); Price, 1983; Price *et al.*, 1985 (σ_c = 16 ± 5 MPa)).

In contrast, under tensile stresses the ignimbrites appear weak, but not remarkably so. Values of 2 - 7 MPa, which are typical of these ignimbrites, are similar to the values for limestone, considerably above those for sandstone and chalk, and reach close to the lowest value quoted for granite (9 MPa). No other published values of the tensile strength of ignimbrites are available for comparison.

Cohesion values are again comparable with those of soft sedimentary rocks such as sandstone, chalk, and shale, and the friction angle measurements are within the upper portion of the range quoted for these soft sedimentary rocks. Data quoted by Maloy and Lowe (1945) for ignimbrite show cohesion values of 3 - 14 MPa, and Hind (1986) measured cohesion values of 1- 35 MPa, and associated friction angles of 10 - 36 °. Again, these results are comparable with those obtained for the ignimbrites in this study, with one specimen of Hind's reaching a somewhat greater strength.

4.8 Nature of failure

All specimens, in each of compressive, shear, and tensile strength tests, underwent considerable deformation before reaching their measured peak strength; macroscopic cracks developed and extended through the specimens, and flakes broke away. In no instance was there a sudden, brittle failure. Such irreversible deformation is the result of the soft, porous nature of ignimbrites in general, and is evidence of pore closure and fracture development. However, differences between the specimens were apparent, with varying amounts of deformation prior to failure being displayed.

Most information regarding the nature of the failure was obtained for uniaxial compressive strength cores for two reasons: they are the largest cores, and hence failure modes are most easily observed; and they are not confined within jigs and so can be directly observed during loading. Consequently, the following discussion relates to the compressive strength measurements, but is believed, from the observations available, to apply equally well to the other types of stress application.

A simple rod and dial gauge mechanism for measuring the axial deformation undergone by the specimen during loading was designed, and

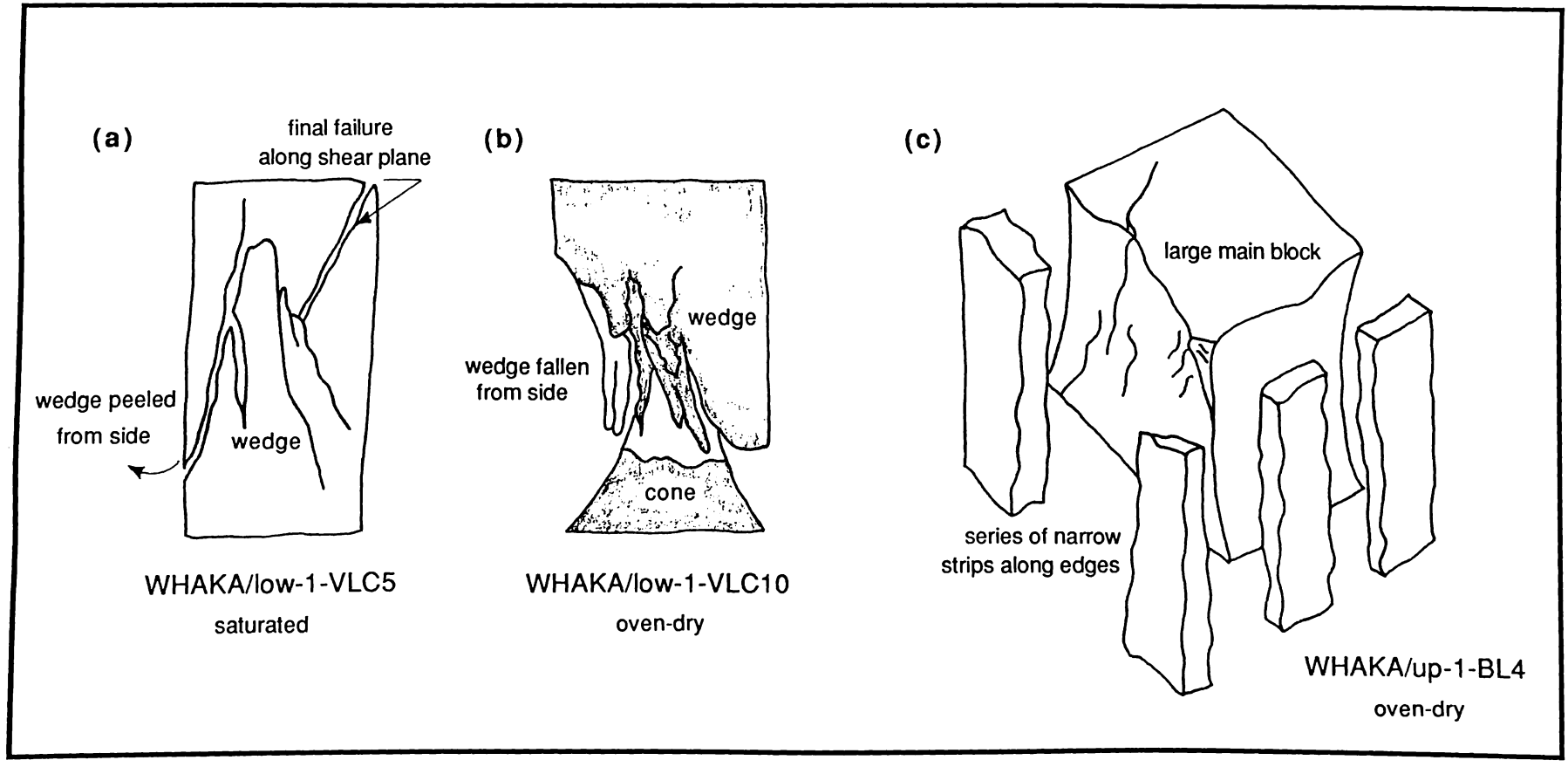

Figure 4.2: Sketches of failed uniaxial compressive strength specimens from the Whakamaru Ignimbrite. Each specimen displays a cataclastic failure mode, with a shear plane developed by coalescence of tension cracks causing final rupture for specimen (a).

fitted to the SRCM. This was not considered to have been adequately installed and calibrated to obtain reliable measurements of the static Young's modulus, but did give a general indication of the stages of deformation exhibited by the materials. No such device was available for the UCS.

4.8.1 Failure modes

Representative sketches of failed cores are given in figures 4.2 and 4.3. Most specimens displayed a failure mode classified as cataclastic in the scheme of Hawkes and Mellor (1970); cones representing the area of compression related to the frictional end effects were left at each end of the specimens, and flakes peeled away from the core sides in tensile failure (figure 4.2a,b; figure 4.3a). This failure mode was most pronounced in the strongest ignimbrites (WHAKA/low, ONG/3, and OWH/low).

Other specimens failed by means of approximately vertical cracks extending through the cores (figure 4.3b,c); the axial cleavage failure mode of Hawkes and Mellor (1970). This mode was really only displayed by the Ongatiti Ignimbrite, particularly for the oven-dry specimens, and generally the vestiges of a compressional cone could be seen in the failed remnants (figure 4.3c). Saturated Ongatiti Ignimbrite specimens sometimes showed a similar failure (figure 4.3b). In these cases it appeared to be the presence of pumice clasts which determined the path over which cracks propagated; in general the cracks were concentrated in pumice clasts.

The cubic specimens tested for the WHAKA/low generally retained a main intact block, whilst a number of broken, narrow strips peeled away from the edges (figure 4.2c). The intact blocks always had curved faces, and the strips peeled away in tension. This is also a cataclastic type failure, but is poorly developed. This is probably a result of the inability to carefully machine the materials, resulting in high frictional effects along the faces in contact with the platens.

4.8.2 Deformation

The release of the stress by tensile failure was very slow in most cases. During loading circumferential flakes could be seen to develop slowly by crack extension from one end towards the other. These flakes then slowly peeled away from the body of the core. Often the final rupture was along a shear plane developed by coalescence of the cracks defining several of these

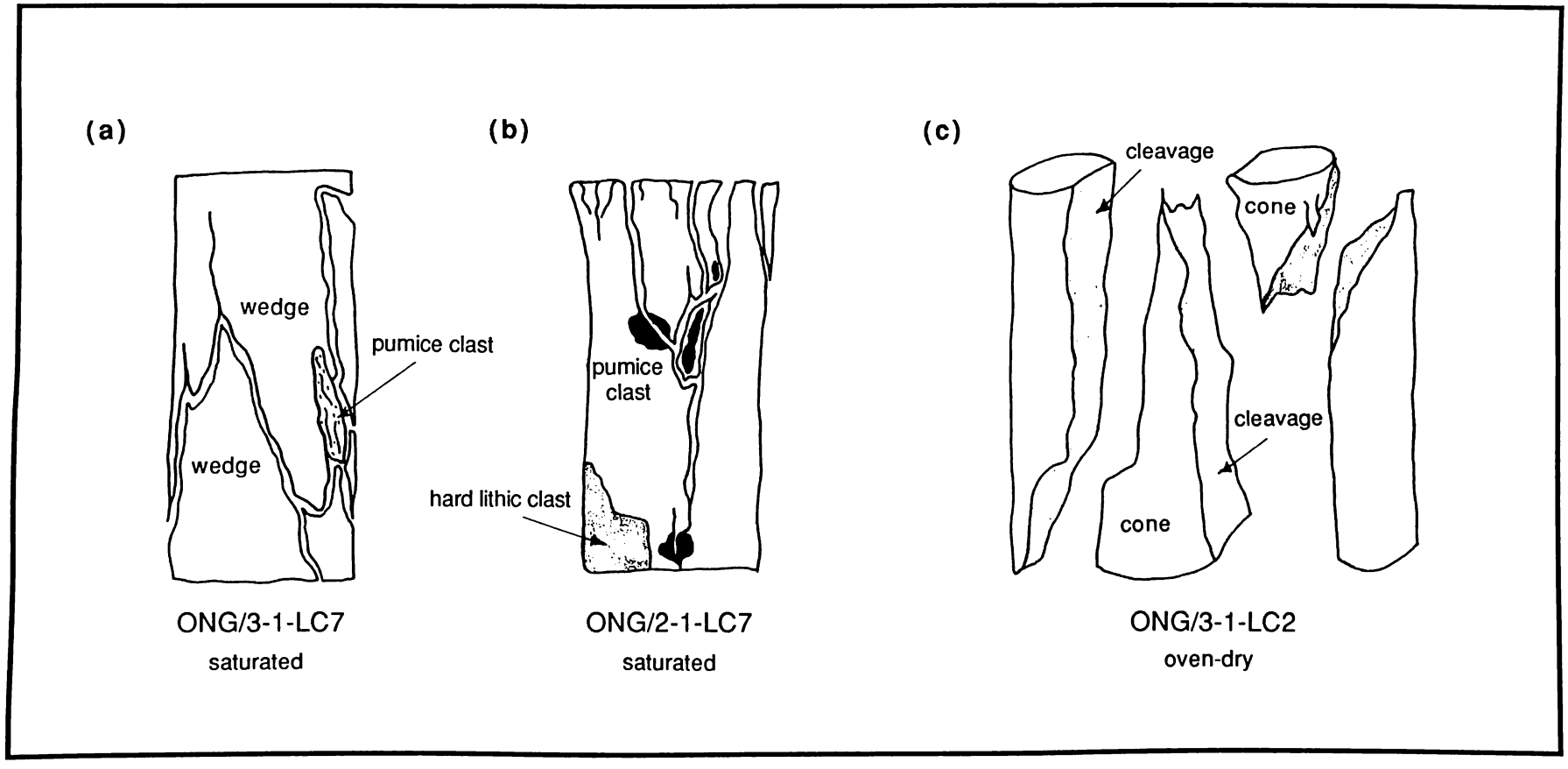

Figure 4.3: Sketches of failed uniaxial compressive strength specimens from the Ongatiti Ignimbrite. Specimen (a) displays a cataclastic failure mode, specimens (b) and (c) show axial cleavage as their primary mode of failure.

wedges (figure 4.2a).

Generally a reasonably coherent core could be retrieved after the peak strength had been exceeded; if the loading ceased at this point, the deformation was halted, if continued loading was applied the specimen continued to deform. This behaviour is characteristic of weaker materials, (σ_c = 50-100 MPa; Attewell and Farmer, 1976), and conforms to the description of "class 1" rocks of Attewell and Farmer (1976).

Audible cracking could generally be heard throughout the test. Stress versus strain curves, where available for weak materials tested on the SRCM, showed all of the components of a "typical" curve as described by Farmer (1983) and Attewell and Farmer (1976). Initial irrecoverable deformation representing pore closure and specimen compaction was followed by a zone of approximately elastic deformation extending to about 80 % of the peak stress. Beyond this point macroscopic cracks became visible, and the cores underwent considerable deformation; this continued until after the peak stress was exceeded.

The failure process as a whole was best observed in the lower Whakamaru Ignimbrite (WHAKA/low) specimen. For the Owharoa Ignimbrite the failure was more discrete, and most closely approached a brittle failure. The failure in the Ongatiti Ignimbrite specimens, even the strongest one, tended to be very long and slow, suggesting the greatest amount of compaction. This is thought to be due to the abundant pumice clasts in this material, which, as mentioned above, tended to have cracks concentrated in them. These pumices appeared to undergo considerable compaction, thus providing zones through which cracks extended.

4.8.3 Crack surfaces

The cracked surfaces of the failed specimens were examined under a binocular microscope (18x magnification) to observe the nature of the crack development. As well, large thin-sections were prepared of the failed specimens after uniaxial compressive strength testing. These included a complete slice across the cores in the direction perpendicular to the compressive load, and allowed the nature of the cracking to be examined in detail.

It was apparent that crack development was primarily through the groundmass of the ignimbrites, leaving crystals protruding from the crack surfaces. Rarely did the cracks extend through crystals, and in all cases where

cracks were seen to pass through crystals they exploited cleavage planes or pre-existing fractures within the crystals. However, thin-section examination showed a tendency for the cracks to seek out the crystal / groundmass contacts; a very large number of crystals were evident along fracture planes compared with the total number of crystals in the specimens. In this way the cracks exhibited a very rough, curved surface with crystals either protruding from the face, or leaving "pluck holes" from which crystals had been removed.

Crystals are believed to represent hard, relatively non-deformable (high elastic modulus) zones within ignimbrites, thus providing regions in which stresses can concentrate along their boundaries (Farmer, 1983). Cracks will tend to be initiated at, and propagate away from, areas of such stress concentration (Pollard and Aydin, 1988). It is thus believed that much of the crack initiation occurs at crystal / groundmass contacts, and that the cracks propagate from these areas through the matrix, to join with neighbouring crystals.

Pumice clasts were also conspicuous along the failed surfaces. Cracks often extended both around and through the pumice clasts. Examination of these pumices showed them to be extremely compressed, much more so than the nearby groundmass. The compressed nature of the pumice clasts suggests that they had experienced much more plastic deformation than the groundmass.

These clasts are also thought to provide regions of crack initiation, but in this case it is because of their relative softness (low elastic modulus), rather than hardness as for the crystals. The plastic deformation must be accompanied by a concentration of stresses, allowing crack initiation. In this case however, the soft nature of the pumices allows the cracks to extend through them, as well as around their boundaries.

4.9 Summary

Measured strength values show ignimbrites to be weak materials in comparison with other lithologies, particularly for compressive and shear strengths, but less so for tensile strengths. Compressive and tensile strengths, and cohesion values, can be highly variable, commonly ranging over one, and sometimes even two, orders of magnitude within a single ignimbrite deposit. On saturation the strength of ignimbrite is considerably reduced from that of the oven-dry equivalent, with softening factors as high as 6 being quite common. In contrast, the angle of internal friction is remarkably consistent

between all of the ignimbrites studied, and is relatively unaffected by moisture content.

Some surprising comparisons between the ignimbrites studied are evident: the lower Whakamaru Ignimbrite specimen is strong in compression and shear, yet relatively weak in tension. In contrast, the Owharoa Ignimbrite specimens have similar compressive strengths to the lower Whakamaru Ignimbrite, yet are much weaker in shear, and stronger in tension. The Ongatiti Ignimbrite specimens all show medium strength values for all tests, and the upper Whakamaru Ignimbrite is the weakest in every case.

All of the ignimbrites tested underwent considerable deformation prior to reaching their peak strength, and macroscopic fractures could be seen to develop and propagate through the cores, accompanied by audible cracking. This was particularly true for the weaker specimens, and is believed to represent considerable compaction and closure of pore space prior to failure. Fracture surfaces showed evidence of crack initiation at inhomogeneities in the rock (crystals and pumice clasts), and propagation through the groundmass between these inhomogeneities.

CHAPTER 5 - BULK ROCK PROPERTIES

5.1 Introduction

The density and porosity of rock materials have been interpreted as exerting a significant control over the strength of the material (Attewell and Farmer, 1976). Deere and Miller (1966) have shown that the density is not, by itself, a good predictor of the rock strength for a variety of lithologies, but does provide a useful strength indicator in combination with other properties. To examine the relationship between density, porosity, and strength, and to test the validity of using these properties as strength indices for ignimbrites, the bulk density (saturated and dry), porosity (true and effective), and grain density of each of the ignimbrite specimens were measured.

This chapter presents the results of these measurements. Chapter 8 considers their relationships to the geomechanical base data established in chapter 4.

5.2 Definitions

Bulk density (ρ) is simply defined as the mass per unit volume of the material. The saturated bulk density (ρ_{sat}) is that obtained when the pore space is filled with water, and hence the total mass includes the mass of water; the dry bulk density (ρ_{dry}) is that obtained when the pore space is filled with air. The grain density (ρ_g) is the density of the components making up the rock, obtained from a powdered rock sample. It does not include the pore space, and is therefore independent of the structure of the material.

Porosity (η) is the proportion of the rock volume (as a percentage) which is occupied by pore space. The effective (η_{eff}) porosity refers to the volume of the rock occupied by pores which are interconnected and become filled with water during saturation, whereas the true porosity (η_{true}) includes all of the pore space within the rock.

5.3 Methods

The standard methods described by Brown (1981) for determining the bulk density and effective porosity of regularly shaped specimens from saturation and caliper measurements were used to measure these properties for each prepared core prior to destructive testing. The grain density of the

	ρ_{sat} (kg m^{-3})	ρ_{dry} (kg m^{-3})	ρ_g (kg m^{-3})	η_{eff} (%)	η_{true} (%)	$\Delta\eta$ (%)
WHAKA/up-1	1644 ± 10	1212 ± 10	2520 ± 50	42 ± 2	51 ± 2	18 ± 6
WHAKA/low-1	2290 ± 2	2124 ± 2	2600 ± 30	16.6 ± 0.1	18 ± 1	8 ± 3
ONG/1-1	1730 ± 20	1300 ± 30	2490 ± 30	43 ± 1	48 ± 1	10 ± 1
*ONG/1-2	1750 ± 20	1340 ± 30		42 ± 1		
ONG/2-1	1920 ± 20	1580 ± 20	2540 ± 40	34 ± 1	38 ± 1	11 ± 3
*ONG/2-2	1950 ± 20	1620 ± 40		32 ± 2		
ONG/3-1	2112 ± 8	1911 ± 8	2470 ± 60	20 ± 1	23 ± 1	13 ± 4
*ONG/3-2	2050 ± 20	1790 ± 40		27 ± 1		
OWH/mid-1	1822 ± 8	1580 ± 10	2380 ± 60	23.8 ± 0.6	34 ± 1	29 ± 3
OWH/mid-2	1824 ± 5	1580 ± 6		24.5 ± 0.4		
OWH/low-1	2067 ± 6	1928 ± 8	2320 ± 80	13.9 ± 0.6	17 ± 1	18 ± 6
OWH/low-2	2021 ± 6	1880 ± 20		14 ± 1		

Table 5.1: Bulk rock properties of ignimbrites studied. $\Delta\eta$ represents the unconnected pore space as a percentage of the true porosity. Errors in density and effective porosity are calculated from 95% confidence limits; errors in true porosity and $\Delta\eta$ are calculated from error analysis on contributing values. An asterisk denotes those blocks for which the bulk density and porosity values are from measurements on short cores only.

specimens was measured using a standard density bottle determination on small samples of ground rock (as described by Vickers (1983)). From knowledge of the dry bulk density and grain density, the true porosity of the material was calculated. These data are summarised in table 5.1 for each ignimbrite studied.

5.3.1 Effect of specimen size

As many of these ignimbrites contain large, porous pumice clasts, the bulk density and porosity values for small cores are often dominated by a single clast within the core. From the data in table 5.2 it is apparent that there is much more variation in the dry bulk density measured from the short cores than in that from the long cores, even though an analysis of variance suggests that the two sets of data are from the same population. Likewise, the long core measurements give a higher average bulk density than the short cores.

The data from long cores are thought to better represent the rock body as a whole, as they give a more representative sample with less influence from single clasts. Consequently, the bulk density and effective porosity values given in table 5.1 represent means of the values measured for long cores only. For those blocks from which no long cores could be obtained, short core results are used to estimate the bulk density and effective porosity. These blocks are marked with an asterisk in table 5.1.

5.3.2 Errors in grain density determination

The grain density values are the means of several determinations from each block. Relatively high errors are associated with these values. This is a limitation of the technique, which relies upon calculating small masses from the differences between two very similar masses; this results in the errors becoming quite significant. Increasing the number of readings does not produce a significant increase in the accuracy of the measurement.

The true porosity values are calculated from the mean values of dry bulk density and grain density. Errors are assessed from the percentage errors in the density determinations, and hence incorporate the errors involved in determining the grain density.

	number in sample	mean	sd	95 % confidence limit
ONG/1-1-long cores	20	1297	58	± 57
ONG/1-1-short cores	20	1242	136	± 64
ONG/1-1-total	40	1270	107	± 35
Analysis of variance		$F_{0.05} = 4.08 > F_{sample} = 2.77$ samples from same population		

Table 5.2: Dry bulk density data for cores from block ONG/1-1. The mean and standard deviation are shown for sets of data collected from long and short cores, plus from the combined data set. An analysis of variance comparing the data from the long and short cores suggests that the two sets are from the same population, yet the standard deviation for the short cores is larger than for the long cores, reflecting the greater variability in these cores.

	density (kg m^{-3})
volcanic glass	2330 - 2413
felsic minerals	
quartz	2650
feldspar	2560 - 2760
mafic minerals	
biotite	3000
pyroxene (augite)	3400
amphibole (hornblende)	3200

Table 5.3: Grain density of materials typically making up a volcanic rock of silicic composition. The density of volcanic glass varies with its chemical composition. The wide variation in density for the feldspars is because this group of minerals forms a system with solid solution relations, with each mineral in the solid solution having a slightly different density from the others. In any one material only a limited range of minerals, and hence densities, within this range is likely to be present. Data from Carmichael (1984).

5.4 Grain density

The grain densities of the materials likely to make up a volcanic rock of silicic composition are given in table 5.3. All of the measured grain density values presented in table 5.1 are consistent with the ignimbrites being a mixture of predominantly felsic minerals and glass. However, there are distinct variations between the ignimbrites: the Whakamaru Ignimbrite has the highest grain density of between 2500 and 2600 kg m^{-3}, the Ongatiti Ignimbrite has a grain density of approximately 2500 kg m^{-3}, and the Owharoa Ignimbrite has a somewhat lower grain density of between 2300 and 2400 kg m^{-3}.

Two possible explanations exist for this variation; either the glass content, or the chemical composition (and hence density) of the glass, varies between the ignimbrites. Simple chemical variations in the glass are not sufficient to account for the differences observed, hence it would appear that the Owharoa Ignimbrite has the highest glass content, and the Whakamaru Ignimbrite the lowest. This agrees with the field observations presented in table 2.1, in which it was noted that the Owharoa Ignimbrite is the poorest in crystals, and the Whakamaru Ignimbrite has the highest crystal content.

5.5 Bulk density and porosity

Compared with crystalline rocks, the ignimbrites studied have a very high porosity, and hence low bulk density, and span a wide range of porosities. The densely welded Whakamaru Ignimbrite (WHAKA/low), for example, has an effective porosity of 16.6 %, whereas its poorly welded counterpart (WHAKA/up) has an effective porosity as high as 43.3 %. Table 5.4 presents dry bulk density and porosity values from a variety of rocks and engineering soils. It is apparent that the ignimbrites in this study extend across an enormous range of porosity and density values. They range from values typical for a granular soil, to those typical of porous sedimentary rocks such as some varieties of sandstone and limestone. Such a wide range of porosities is not uncommon for ignimbrites (Marshall, 1935; Maloy and Lowe, 1945; Rippa and Vinale, 1983; Price, 1983; Price *et al.*, 1985; Hind, 1986).

The differences between the true and effective porosities are also noteworthy. In all cases there is a proportion of the pore space within the rock which is taken up by pores which are not connected to the pore system, or are too small to be filled with water during saturation under normal laboratory conditions. The final column of table 5.1 lists $\Delta\eta$, the percentage of the true

material	dry bulk density (kg m-3)	porosity (%)
granite	2600 - 2900	0.5 - 2.9
gabbro	2800 - 3100	0.1 - 3.6
basalt	2800 - 2900	0.1 - 22
rhyolite	2400 - 2600	4 - 6
sandstone	2000 - 2600	5 - 25
limestone	2200 - 2600	5 - 27
shale	2000 - 2400	10 - 30
dolomite	2500 - 2600	0.2 - 5
gneiss	2800 - 3000	0.5 - 1.5
marble	2600 - 2700	0.5 - 2
quartzite	2600 - 2700	0.1 - 0.5
slate	2600 - 2700	0.1 - 0.5
granular sand	1300 - 1850	29 - 50
granular silt	1260 - 1850	29 - 52

Table 5.4: Dry bulk density and porosity data for a variety of lithologies (compiled from Attewell and Farmer, 1976; Jumikis, 1979; Farmer, 1983). The values for granular sand and silt represent the extremes of close and loose packing for well-sorted samples of the stated grain size.

porosity not accounted for by the effective porosity, and hence due to unconnected pore space. This value was obtained from:

$$\Delta\eta = \frac{\eta_{true}-\eta_{eff}}{\eta_{true}} \times 100$$

Two trends can be seen in the $\Delta\eta$ data: for the Whakamaru and Owharoa Ignimbrites the most indurated specimens (lower sites) have a smaller proportion of unconnected pores than their softer counterparts (the same trend is apparent for the Ongatiti Ignimbrite, but there is such a small variation in the $\Delta\eta$ values that it is not significant given the errors in the calculation); and the Owharoa Ignimbrite has a very much greater proportion of unconnected pores than the other ignimbrites. This high proportion of unconnected pores in the Owharoa Ignimbrite may be associated with the considerable alignment of the pumice clasts in this material, suggesting that the flattening of the clasts results in a closing off of the pore spaces. However, the high proportion of unconnected pores in the more indurated specimens is a surprising result, as induration related to compaction and cohesion of the components would be expected to close off pore connections. That this is not the case suggests that the unconnected pores close preferentially on induration.

5.5 Summary

The rocks display a wide range of density and porosity values. Their porosities are very high compared with crystalline rocks, and they span a much wider range of porosity and density values, even within one single ignimbrite deposit, than most other rocks. The grain density values show a high variability due to the measurement procedure, but suggest that the Owharoa Ignimbrite has a higher glass content than the Whakamaru and Ongatiti Ignimbrites. The Owharoa Ignimbrite also appears to have a higher proportion of unconnected pores than the other two ignimbrites, which is presumably related to the flattening of the pumice clasts, and the less indurated materials of all of the ignimbrites have a higher proportion of unconnected pores than their harder counterparts.

6.1 Introduction

Hardness and durability tests were undertaken in order to address two aims:

(1) to determine index properties in order to ascertain the value of index tests as predictive measures of ignimbrite strength, and
(2) to measure the hardness of the clasts making up the ignimbrites in order to assess their contribution to the total ignimbrite strength.

To achieve these aims several field and laboratory instruments were used. Hardness was assessed using rebound (Schmidt hammer and Shore scleroscope) techniques, and the slake durability index was used to measure the durability of the samples.

6.2 Hardness

Hardness is an extremely complex property which is difficult to understand and interpret in terms of physical units (Deere and Miller, 1966). Hardness always contains components of both material strength and elasticity, and is dependent upon the strength of the individual grains, the strength of any cementing material, and the strength of grain-to-grain and grain-to-cement contacts (Deere and Miller, 1966). There is no single definition of hardness; the definition and means of measurement depend upon the use to which the data will be put. Due to this complexity, all measures of hardness are made on a relative scale. Despite these drawbacks, the hardness is commonly used as an indicator of material strength, due to the ease with which simple, index measurements can be made.

6.2.1 Types of hardness

Deere and Miller (1966) described two distinct types of hardness measurement: indent hardness, for which permanent, plastic deformation of the material occurs; and dynamic hardness, for which the elastic properties of the material may be as important as the plastic properties. The first of these includes both the abrasion resistance, or the ability of the surface of the material to resist scratching by a tangential applied force, and the resistance to

a normal, penetrating force. The latter includes only the resistance to a normal, penetrating force which is acting over a short time span.

Abrasion resistance is commonly used in mining and tunnelling applications, where the ability of the rocks to be cut and ground is of importance (for example, Jenni and Balissat, 1979; Farmer *et al.,* 1979; Janach and Merminod, 1982). The resistance to static indentation is most often used in soil mechanics, and provides the basis for many engineering classifications of soils (for example, Sanglerat, 1972; Durnunoglu and Mitchell, 1975a,b). It has also been applied to rocks, but, due to the strength of many rock materials, either a very small sample (cone indentor (Mining Research and Development Establishment, 1977), for example), or a high-powered device (as described by Kidybinski (1979), for example) is required. Dynamic hardness testing has recently become a very common means of assessing rock strength, and many correlations between dynamic (or rebound) hardness, and compressive strength or elastic moduli have been attempted (for example, Deere and Miller, 1966; Irfan and Dearman, 1978).

For this study dynamic hardness was examined using both field and laboratory techniques for the entire range of materials encountered.

6.2.2 Hardness measurement

Measurement of dynamic hardness involved measuring the amount of elastic rebound of a mass fired with a known force against a surface. Two instruments were used for this purpose: a Shore scleroscope and a Schmidt hammer. In the Shore scleroscope the mass is a small, diamond-tipped hammer which falls vertically under the influence of gravity onto a smooth rock surface. The mass is small and falls a relatively short distance. It is, therefore, a delicate laboratory instrument designed for measuring the hardness of very small areas on carefully prepared surfaces. It was thus used to address the second aim of this chapter; to measure the hardness of individual components of the ignimbrites. In contrast, the Schmidt hammer is a robust field instrument which measures the rebound of a relatively large mass fired, using a spring, against a relatively large surface area. It was used to assess its value as a field index test and predictor of rock strength.

6.3 Schmidt hammer

Originally the Schmidt hammer was designed to measure the strength of concrete (Proceq S.A., 1977). However, its use in geomorphology and engineering as a means of assessing the hardness of earth materials has been established for some time (for example, Day and Goudie, 1977; Irfan and Dearman, 1978). Many studies have been undertaken in order to assess the validity of the instrument for this use, and to attempt to establish relationships between the Schmidt rebound hardness and a variety of geomechanical properties.

6.3.1 Instruments

The Schmidt hammer relies upon a spring mechanism to fire a known mass with a constant force against the surface being tested. The distance to which the mass rebounds is measured on a relative scale, giving a rebound value (R) in non-dimensional units. There are two main types (Proceq S.A., 1960, 1977): one in which the mass and spring mechanisms are enclosed in a steel barrel, and one in which the mass is on the end of a rotating arm. The first of these is intended for harder materials and has two different mass and spring combinations: an "N" type (impact energy = 2.207 N m), and a "L" type (impact energy = 0.735 N m) with a lighter mass and weaker spring. The "P", or pendulum, type (impact energy = 0.883 N m) is intended for use on the very softest materials. Although the impact energy of the P-type hammer is greater than that of the L-type, it is applied over a much larger hammer head surface, thus making it more appropriate for weaker materials.

For most previous work on earth materials the N-type hammer has been favoured (Day and Goudie, 1977; Irfan and Dearman, 1978; Sheorey *et al.*, 1984), and some use has been made of the L-type hammer (Deere and Miller, 1966; Williams and Robinson, 1983). The P-type hammer has been put to only limited use on weak rocks (Taylor and Spears, 1981). For the ignimbrites in this study, a combination of an L-type and a P-type hammer was found to best suit the range of materials.

6.3.2 Test procedure

In choosing the testing procedure for the Schmidt hammers a number of factors discussed in the literature were considered:

(1) statistical validity of the data,
(2) operator and machine variance,
(3) any destructive effects of the test on the material,
(4) the effect of material conditions on the test result, and
(5) the required number of readings.

Poole and Farmer (1980) showed that, provided a realistic lower cut-off point is used to eliminate artificially low values (a cut-off of R=30 for an N-type hammer was suggested), the data approximates to a normal distribution. They also showed that the variability in the hammer is less than that in the rock. The data are thus statistically valid.

Operator variance was shown to be insignificant by Day and Goudie (1977), however, McCarroll (1987) showed that machine variance can become significant, especially as a hammer ages. Careful, and frequent, calibration against known standards (steel and aluminium anvils) is thus essential, as is regular maintenance and cleaning (McCarroll, 1987).

Two quite different approaches to testing have been taken in the past (Poole and Farmer, 1980): repeated testing on a single site, and single-impact testing on separate sites. Poole and Farmer (1980) showed that rebound values tend to rise during the first 3-4 continuous impacts at a point. They advised that, to achieve minimum variability, the peak value of at least five continuous impacts at a point be selected. In contrast, Day and Goudie (1977) also noted this rise with repeated measurements at one site, and attributed it to local partial crushing of the rock and concluded that, for greatest accuracy, the hammer must be moved to a new site for each test. For the ignimbrites considered in this study, the high porosity of the materials means that local crushing may be expected to be very significant. Hence only single-impact readings were taken.

Day and Goudie (1977) showed that cracks, voids and joints beneath the impact site significantly reduce the rebound reading, as does proximity to the edge of the rock mass. The moisture content of the rock also affects the readings, with values reduced on saturation, yet the rock temperature has no significant effect. Rough, dirty, or flaky surfaces also result in lowered values (Proceq S.A., 1977; Day and Goudie, 1977; Williams and Robinson, 1983). A carborundum stone is provided with each hammer to smooth and clean the surface before testing. However, Williams and Robinson (1983) considered that the surface texture may have such a significant effect that, "the use of the Schmidt hammer to measure the relative hardness of different rock types ... seems particularly doubtful". They went on to conclude that Schmidt hammer

material	R_P	R_L
concrete	131 ± 1	33 ± 1
timber	50 ± 3	21 ± 1
ignimbrite	55 ± 3	23 ± 1
ignimbrite	105 ± 3	38 ± 1
sandstone	59 ± 6	18 ± 1
grit	48 ± 6	16 ± 1
WHAKA/up	51 ± 6	20 ± 1
ONG/2	93 ± 2	23.7± 0.8
ONG/3	104 ± 5	36.4± 0.7
linear regression	$R_L = 0.23R_P + 7.96$	$r^2_{adj} = 0.70$

Table 6.1: Derivation of calibration equation for two Schmidt hammers.

	R_P	R_L
WHAKA/up	51 ± 6	20 ± 1
WHAKA/low	(87)	28 ± 1
ONG/1	41 ± 4	(17)
ONG/2	93 ± 2	23.7 ± 0.8
ONG/3	104 ± 5	36.4 ± 0.7
OWH/up		
OWH/low	(122)	36 ± 1

Table 6.2: Schmidt hammer data for each site studied. Values in brackets are calculated values based upon the calibration equation derived in section 6.3.3.

values can only be considered representative of a, "given rock and a given surface texture of that rock".

The required number of readings was determined for this study by the same considerations as for the laboratory work, that is, the error in the mean value calculated from 95 % confidence limits should be less than 5 % of the mean.

For this study, the procedure of Brown (1981) was adhered to; at least 20 readings from individual points, separated by at least the plunger diameter, were taken, and the mean value calculated. Careful surface preparation to remove alteration products and smooth the surface was undertaken prior to testing, and all visible defects in the material were avoided for sample sites. Where abnormally low readings occurred they were ignored, although no strict cut-off point was defined, this being determined by the values and their variation for each site.

6.3.3 Calibration

The P-type and L-type hammers are calibrated to different scales. Hence, a calibration equation was defined for the two hammers used in this study so as to make the data from the two different devices comparable. A variety of materials, including some from the study sites where feasible, was tested using both hammers (see table 6.1), and a linear regression undertaken on the data to give a best-fit calibration equation. As the two instruments were designed to measure over different hardness ranges, only a limited variety of materials were available which gave reliable readings using both hammers.

Given the dependence of rebound hardness on a variety of material properties, including strength and elasticity, the scatter in the data in table 6.1 is not surprising, as each material could be expected to have a different response. However, a regression coefficient of $r^2_{adj} = 0.70$ is thought to give an adequate calibration for these purposes. This may actually be a somewhat better regression than truly exists, as the data form two separate clusters; no materials could be found which fell in between these two extremes. As the two ignimbrite samples fell one within each cluster, and their values were adequately described by the regression equation, it was accepted as a suitable calibration for this study.

6.3.4 Results

Table 6.2 presents the Schmidt hammer data for each of the ignimbrites studied.

6.4 Shore scleroscope

Deere and Miller (1966) reviewed the use of the Shore scleroscope prior to 1966, until which time it appears to have been a commonly used instrument for determining the hardness of rocks and minerals. Deere and Miller (1966) saw it as a useful index of rock hardness, although they noted that it proved less versatile than the Schmidt hammer. Since this time the use of the Shore scleroscope has declined markedly; Martin (1986) stated, "In view of the simplicity and convenience of the Schmidt hammer, it is surprising that other simple rebound tests such as the Shore scleroscope ... do not seem to have been widely used as a rock index". This may be the result of several somewhat disappointing experiences with the Shore scleroscope (Singh, 1981; Taylor and Spears, 1981) for which the instrument proved unsuitable as an indicator of material strength.

This apparently poor performance of the Shore scleroscope when compared with that of the Schmidt hammer may be attributed to differences in the equipment; the Shore hardness measures the rebound on a very small area, giving a surface reading, whereas the Schmidt hammer measures a more macroscopic, mass-hardness property of the material (Deere and Miller, 1966). Bearing this in mind, it is not surprising that the Schmidt hammer provides a better indicator of strength parameters which are measured as bulk properties of the intact rock. However, in order to assess the contribution of individual components within the material to the overall strength, an instrument which can measure the hardness of very small areas is required. This is the use to which the Shore scleroscope was put in this study.

6.4.1 Instrument

A model C-2 Shore scleroscope, as described by Brown (1981), was used in this study. A diamond tipped hammer with a tip diameter of 0.1-0.4 mm and a mass of 2.3 ± 0.5 g falls, under the influence of gravity, through a distance of 251.2 +0.13 - 0.38 mm (Brown, 1981) to impact on the test

mineral type	Shore hardness
feldspar (plagioclase)	92 ± 3
quartz	65 ± 1
biotite	32 ± 2
amphiboles (hornblende)	60 ± 4
pyroxenes (augite)	51 ± 1
opaques (magnetite)	21 ± 3

Table 6.3: Shore hardness values for separate crystals of the types found in the ignimbrites studied.

surface. The distance of rebound is measured on a relative scale calibrated from 0-140.

6.4.2 Test procedure

Unlike the Schmidt hammer, there has not been a large amount of information published regarding the testing procedure for the Shore scleroscope. However, due to the similarity of the two tests, the same considerations as discussed for the Schmidt hammer were taken into account for the Shore scleroscope. In particular, the point of impact was shifted to a new position for each reading, and an average of at least 20 readings was taken wherever possible. This is in accordance with the methods suggested by Brown (1981).

Short cores prepared for mechanical testing were used as specimens for Shore scleroscope testing; these had sufficient mass to be unmoved by the impact. The ends of the cores were flat and polished, thus providing ideal surfaces for rebound testing. Both saturated and oven-dry cores were tested.

For each block the various components making up the material (groundmass, pumice, and lithics) were tested separately. Although crystals were often present in the core ends, the impact of the hammer frequently caused them to shatter, or to move, as their cementing to the matrix was weak in many cases. Therefore, instead of obtaining crystal hardnesses directly from the specimens, examples of large, single crystals of the types found within the ignimbrites (as determined in chapter 10) were used to obtain representative hardnesses for these components. As many of the mineral identifications cannot be precise, feldspars, for example, form a series of solid solutions from which a variety of types may be present amongst the crystals in the ignimbrite, representative crystals were chosen to represent each mineral type. Table 6.3 gives the Shore scleroscope rebound values for each mineral type.

Twenty hardness readings were taken for each component within each core, except in the cases of some pumice and lithic clasts where there was insufficient surface area exposed to obtain 20 readings. Under these circumstances as many values as was feasible were obtained. Mean values were calculated for each core, and the means of the means used as representative values for the block.

	WHAKA/up		WHAKA/low	
	dry	sat	dry	sat
groundmass	7.1 ± 0.8	2.1 ± 0.3	70 ± 2	59 ± 1
softening factors	3.4		1.2	

	ONG/1-1		ONG/1-2		ONG/2-2		ONG/3-2	
	dry	sat	dry	sat	dry	sat	dry	sat
groundmass	7.6±0.2	2.5±0.1	7.4±0.1	3.0±0.1	17.0± 0.7	7.7± 0.3	25.8±0.7	15.3± 0.7
pumice	2.7±0.4	1.1±0.1	2.3±0.3	1.2±0.2	5.8± 0.7	2.7± 0.4	7.9±0.8	6.5± 0.9
lithic		14 ±6		20 ±6	50 ±30	40 ±10	67 ±?	40 ±10
groundmass / pumice	2.8	2.3	3.2	2.5	2.9	2.9	3.3	2.3
groundmass / lithic		0.2		0.2	0.3	0.2	0.4	0.4
softening factors:								
groundmass		3.0		2.5		2.2		1.7
pumice		2.5		1.9		2.2		0.8
lithic						1.3		1.6

Table 6.4: Shore scleroscope rebound hardness values for Whakamaru and Ongatiti Ignimbrites.
? = insufficient data available to calculate an error value.

6.4.3 Calibration

Calibration bars of known hardness were provided with the instrument; the rebound of these bars was checked before each period of testing. Two bars were provided with nominal rebound values of 23-25 units, and 90-92 units. Throughout the period of testing the instrument read slightly low on the hardest of these (86-88 units). Cleaning and adjusting the instrument made no change. Calibration readings on the softer bar fell within the stated range. As most of the specimens tested were near the lower range of the instrument, this discrepancy was ignored and the values were not corrected at all. A simple correction based on the calibration data points suggests that for readings below 30 no correction is required, for readings between 30 and 80 one unit could be added, and for readings above 80 two units could be added. This would make the data more comparable with published data, but all values within this study are internally consistent.

6.4.4 Results

Shore scleroscope data collected from all specimens are summarised in table 6.4. This table includes mean rebound values for each component of the ignimbrites, together with softening factors, and the ratios of the hardnesses of the components. No pumice clasts of sufficient size were available for testing in the Whakamaru Ignimbrite.

Each ignimbrite can be seen to show an increase in both groundmass and pumice clast hardness with induration, whereas the lithic clast hardness is unrelated to the hardness of the groundmass. In all cases there is considerable softening of the groundmass and pumice clasts on saturation; this is least significant in the hardest, least porous specimens, and greatest in the most porous ignimbrites. In general, the softening factors of the pumice clasts are very similar to those of the groundmass in which they are enclosed. Lithic clasts also show similar softening factors where sufficient data are available.

Ratios of groundmass to pumice hardnesses are presented for the Ongatiti and Owharoa Ignimbrites. For the Ongatiti Ignimbrite the groundmass is consistently 2 - 3 times harder than the pumice clasts in both oven-dry and saturated conditions. In the Owharoa Ignimbrite, the groundmass is generally approximately 1.4 - 2 times harder than the pumice clasts for the upper specimen, and the groundmass and pumice clasts are of approximately the

	OWH/up-V		OWH/up-H		OWH/low-V		OWH/low-H	
	dry	sat	dry	sat	dry	sat	dry	sat
groundmass	23 ± 2	14 ± 1	21 ± 3	13 ± 5	58 ± 3	35 ± 9	47 ± 11	29 ± 5
pumice	16 ± 9	10 ± 2	11 ± 4	6 ± 4	54 ± 7	36 ± 9	38 ± 20	29 ± 9
lithic	52 ±27	34 ±42	55 ±14	28 ±17	72 ±64	36 ±26	50 ± 14	45
groundmass / pumice	1.44	1.40	1.91	2.17	1.07	0.97	1.24	1.00
groundmass / lithic	0.44	0.41	0.38	0.46	0.81	0.97	0.89	0.64
softening factors								
groundmass	1.64		1.62		1.66		1.62	
pumice	1.60		1.83		1.50		1.31	
lithic	1.53		1.96		2.00		1.11	

Table 6.4 (cont.): Shore scleroscope rebound hardness values for the Owharoa Ignimbrite.

same hardness in the lower specimen (where considerable clast flattening was observed (table 2.1). No consistent trends are apparent between the vertical and horizontal measurements. For both the Ongatiti and Owharoa Ignimbrites the lithic clasts are considerably harder than the groundmass.

6.5 Slake durability

Hind (1986) noted a remarkable tendency for ignimbrites to behave in an extreme fashion in the slake durability test. Many of his samples exhibited virtually no loss in mass on slaking, whereas a number broke down almost completely, leaving virtually no material retained in the test drum. Similar tests were undertaken on the ignimbrites in this study.

6.5.1 Methods

The slake durability procedure described by Brown (1981) was followed for this study; the slaking fluid was de-ionised water. Three slaking cycles were undertaken, and the percentage of the original material remaining determined after each cycle. The second cycle (I_{d2}) slake durability index is the most commonly used comparative index, and it is this which is reported in this study.

6.5.2 Results

Table 6.5 gives the mean I_{d2} for each ignimbrite block, together with the verbal classification of the durability following the scheme of Gamble, 1971 (after Goodman, 1980). In figure 6.1 a graph of loss in weight versus slaking time is given for each specimen.

In this case the extremes of behaviour noted by Hind (1986) can be seen, but of interest is the fact that some of the Ongatiti Ignimbrite specimens fall between these two extremes.

Beavis (1985) noted that difficulty often arises in interpreting slake durability data, as they contain components of both simple slaking through wetting and drying, and mechanical abrasion which occurs during rotation of the cage of the slake durability apparatus. The behaviour exhibited by these ignimbrites is thought to include both of these aspects, but mechanical abrasion may well be dominating the results. Certainly the WHAKA/up specimens showed a tendency to break down in water during saturation in the

	I_{d2}	classification
WHAKA/up	30 ± 5	very low
WHAKA/low	98.8 ± 0.4	very high
ONG/1	73 ± 2	medium
ONG/2	90 ± 1	medium high
ONG/3	98 ± 1	very high
OWH/up	97.9 ± 0.8	high
OWH/low	99.3 ± 0.4	very high

Table 6.5: Second cycle slake durability index for each site studied. Classifications are based on the scheme of Gamble, 1971 (after Goodman, 1980).

vacuum bath. However, measurements of the loss of weight by this mechanism showed an approximately 5 % loss in one period of saturation, or an expected 10 % loss over two slaking cycles. This contrasts with the $I_{d2} \approx 70$ % loss measured in the slake durability test, suggesting that as much as 60 % of the initial mass was lost through mechanical abrasion. It is suggested that this proportion also applies to the other specimens for which loss of material on saturation alone was insignificant.

Assuming that mechanical breakdown is of greater importance than slaking, this means that the slake durability test provides a ready index of the degree of induration of firm to soft ignimbrites; well indurated specimens remain virtually intact when subjected to this weak slaking force, poorly indurated specimens undergo almost complete breakdown. It also has implications in terms of the geomorphic development on such ignimbrites; their ability to be broken down very readily under a weak abrasive force, especially in conjunction with water, means that rapid stream erosion and entrenchment may be expected. From an engineering point of view, any mechanical disruption of such material may result in a rapid deterioration of the material strength.

6.6 Summary

Rebound hardness values were measured using Schmidt hammers (L-type and P-type) in the field, and a Shore scleroscope in the laboratory. The Schmidt hammers gave field measurements of the rebound of a relatively large area of rock; the Shore scleroscope gave readings of the rebound of individual components over a very small area. An adequate, but not highly correlated, calibration equation was derived between the two Schmidt hammers using a variety of materials.

The Shore scleroscope values span a wide range. The hardness of all components tends to increase with induration; lithic clasts are generally the strongest components, with the groundmass spanning a range of hardnesses, and the pumice clasts being the weakest. All components show considerable softening upon saturation.

The slake durability index shows a range of values from extremes of virtually no loss on slaking, to almost complete breakdown. Unlike the results of Hind (1986), ignimbrites showing intermediate behaviours were observed.

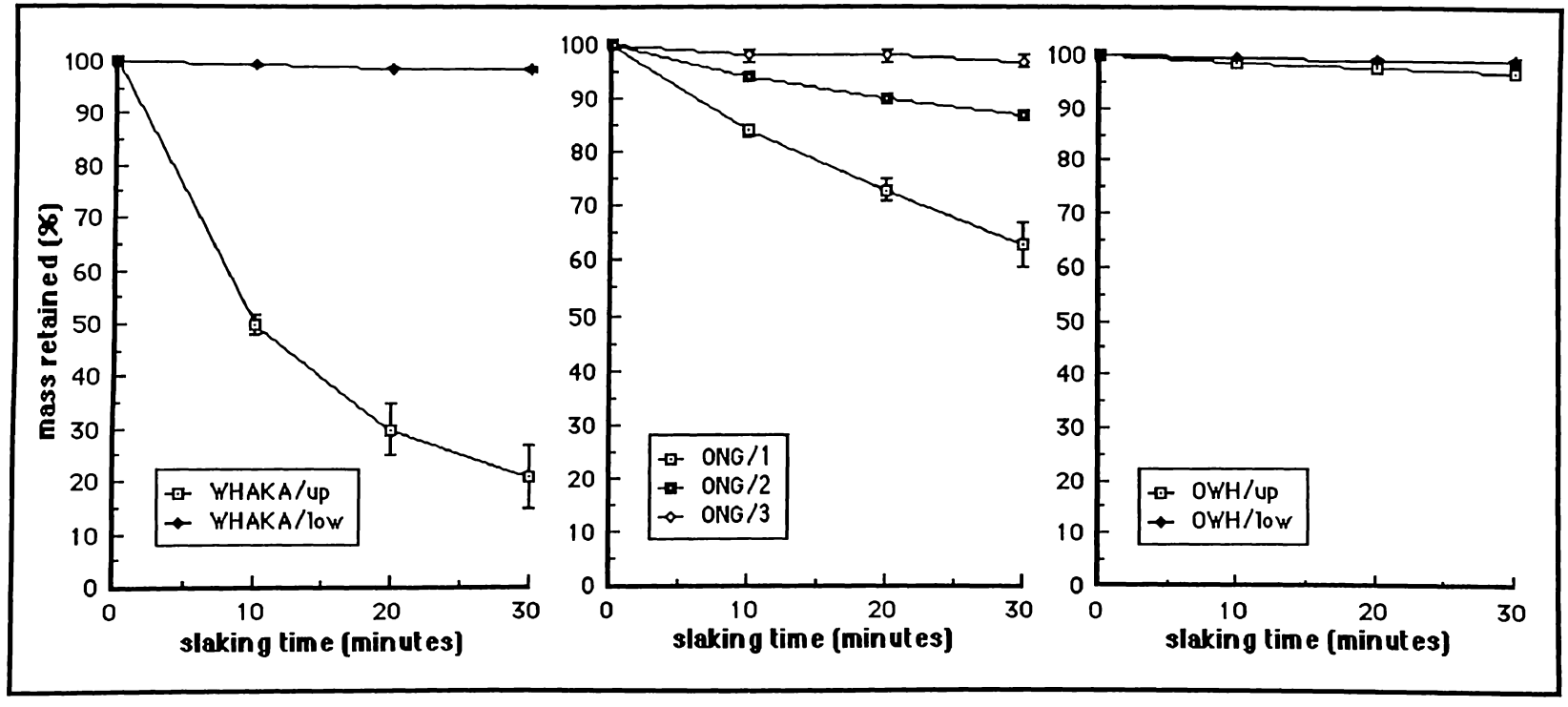

Figure 6.1: Graphs of mass retained (%) versus slaking time for slake durability tests on each ignimbrite.

CHAPTER 7 - ELASTIC WAVE RESPONSE

7.1 Introduction

Monitoring of rock properties by measuring the velocities of elastic waves has become a common, non-destructive means for both field and laboratory characterisation of rock properties. Paulsson and King (1980) and King (1983) each reviewed a wide variety of field applications of elastic waves; and seismic methods are a standard geophysical exploration technique for assessing mineral prospects, rock physical properties, and hydrological parameters (The Geological Society Engineering Geology Working Party, 1988).

Numerous field and theoretical studies have been undertaken concerning the propagation of elastic waves in rocks. It was not an aim of this study to extensively review this literature, or to provide an analysis of the propagation of elastic waves in ignimbrite. Rather, the value of measuring elastic wave velocities in ignimbrite for predicting other geomechanical properties was investigated. To this end, elastic waves were used under laboratory conditions only, in order to fulfill two aims:

(1) to use the compressional (P-type) wave velocity as an index of rock quality, and to investigate its value as a predictor of rock strength, and

(2) to attempt to measure dynamic elastic constants using both compressional and shear (S-type) waves.

7.2 Wave propagation in rocks

Several important conclusions drawn from the literature regarding the propagation of elastic waves in porous media such as rocks are summarised below.

(1) Two compressional waves and one shear wave co-exist, and propagate independently. One of the compressional waves is a diffusive wave which can be ignored in real terms (Biot, 1956a,b).

(2) Theoretically, the primary dependencies of the wave velocities are upon the density and elastic properties of the material. In a perfectly elastic substance the velocities are given by (Alonso and Finn, 1975):

$$v_p = \sqrt{\frac{E}{\rho}} \quad \text{and} \quad v_s = \sqrt{\frac{G}{\rho}} \qquad \ldots (7.1)$$

where: v_p = velocity of compressional waves (m s^{-1}),
v_s = velocity of shear waves (m s^{-1}),
ρ = bulk density (kg m^{-3}),
E = Young's modulus (Pa), and
G = shear modulus (Pa).

The addition of pore space containing a fluid phase means that the velocity becomes a much more complex function of effective elastic moduli and density coefficients of the combined medium, together with the frequency of the waves. However, the form of the equations remains the same (Biot, 1956a,b). Pore size and shape distributions, together with other inhomogeneities in the rock sample complicate the relationships even further (Goodman, 1980), as does the inclusion of a fine phase, such as clay minerals, within the pores (Wilkins *et al.,* 1986).

Likewise, the size and shape of the sample through which the waves move, with respect to wave frequency and amplitude, also introduce a number of additional parameters into the relationship (Alonso and Finn, 1975).

(3) Experimentally, the wave velocity also varies with the degree of saturation of the rock; the velocities of compressional waves are higher when the rock is saturated with water than when it is dry or gas-saturated. Yang and King (1986) showed that for a regularly jointed rock mass v_p is a function of the joint porosity and the bulk modulus of the saturating fluid, whereas v_s remains essentially independent of the presence of water in the pores. At high joint porosities the ratio of v_p / v_s is greater for the saturated rock than for the intact rock, and is less than the intact rock value for dry samples (Yang and King, 1986).

These effects can be relatively easily explained intuitively by comparing the propagation velocities of elastic waves in different media: $v_{p,water} > v_{p,air}$, and shear waves are unable to propagate through a fluid phase. Consequently, if the path length through pores is a significant proportion of the total path length, then compressional waves travelling through a water-saturated sample show an overall higher velocity than those through the same sample when dry. Shear waves are unaffected as they are unable to propagate through the pores in either case.

However, in some instances v_s has been reported as being lowered by fluid saturation compared with dry values (Toksoz *et al.,* 1976; Winkler, 1985).

Winkler (1985) attributed this to additional wave dispersion, and hence energy attenuation, not accounted for by Biot (1956a,b) theory.

(4) The shape of the pores in typical crystalline rocks plays an important role: Nur and Simmons (1969) stated that an increase in compressional wave velocity due to saturation occurs when the pores are in the form of cracks, but not when they are in the form of round holes. However, it is notable in the literature, that most works assume the pore space to be either in the form of wide, narrow cracks, or long, rounded tubes (for example, Biot, 1956b; Nur and Simmons, 1969; O'Connell and Budiansky, 1974,1977; Yang and King, 1986). Very few studies (for example, Toksoz *et al.*, 1976) assume that the pores can be spherical holes, or attempt to relate measured velocities to the observed pore size and shape distributions, as in Murphy (1982) and Wilkins *et al.* (1986).

(5) Significant wave attenuation (energy dispersion and loss) occurs within rocks. Attenuation decreases as a function of confining pressure, and increases with increased saturation. In dry samples attenuation of P- and S-waves is approximately the same, in saturated samples S-waves are attenuated more than P-waves (Johnston and Toksoz, 1980).

Attenuation is believed to occur through a number of mechanisms, including friction (Johnston and Toksoz, 1980), and fluid flow within and between cracks and pores (O'Connell and Budiansky, 1977). These mechanisms assume varying importances with different frequencies, and consequently the amount of attenuation is frequency dependent, and depends on the rock type, and pore size and shape distribution (Johnston and Toksoz, 1980).

7.3 Instrument

A "Pundit" (Portable Ultrasonic Non-destructive Digital Indicating Tester), supplied by C.N.S. Electronics, London (Anon., 1983), was used to produce and monitor the acoustic waves used in this study. This unit produced elastic waves using piezoelectric transducers; a range of such transducers meant that a variety of frequencies could be produced. In this study two different frequencies were used: 54 kHz and 1 MHz. At 54 kHz only compressional (or P-type) waves were available; at 1 MHz both compressional and shear (or S-type) waves were produced. By measuring the time delay between transmitted and received pulses, the Pundit produced a display of the travel time through the specimen.

	$v_{pu,sat}$ (m s^{-1})	$v_{pu,dry}$ (m s^{-1})
WHAKA/up-1	1620 ± 10	600 ± 30
WHAKA/low-1	2140 ± 60	2070 ± 20
ONG/1-1	1390 ± 70	2250 ± 40
ONG/2-1	2440 ± 60	2900 ± 40
ONG/3-1	3370 ± 30	3640 ± 20
OWH/mid-1-V	2370 ± 50	2850 ± 50
OWH/mid-2-H	2780 ± 40	3350 ± 60
OWH/low-2-V	3400 ± 70	3800 ±100
OWH/low-1-H	3930 ± 70	4180 ± 60

Table 7.1: Saturated and oven-dry ultrasonic wave velocities for ignimbrite cores at atmospheric pressure.

To ensure a good acoustic coupling, a couplant was used between the core and the transducer faces. Liquid soap was used as the couplant for the 54 kHz waves, and thin aluminium foil plates were inserted between the transducer and core faces to provide a couplant for the 1 MHz waves.

7.4 Notation

Throughout this thesis, waves at the 54 kHz frequency are referred to as "ultrasonic waves", whereas those at the 1 MHz frequency are referred to as "seismic waves". In order to distinguish between these frequencies the following notation is employed (see notation list):

v_{pu} = velocity of compressional waves of 54 kHz frequency,

v_{ps} = velocity of compressional waves of 1 MHz frequency, and

v_{ss} = velocity of shear waves of 1 MHz frequency.

These conventions are adhered to for all of the laboratory data. When the frequency is not significant, such as in theoretical equations, the additional subscripts are ignored and the velocities of compressional and shear waves simply referred to as v_p and v_s respectively.

7.5 Ultrasonic waves (54 kHz)

Ultrasonic waves were measured on long cores at atmospheric pressure and room temperature. Some measurements were made on short cores of Ongatiti Ignimbrite, and there was found to be a small, but significant, difference in the data from the long and short cores. Having longer path lengths, the long cores were thought to provide a better average velocity than the short cores, and to be less affected by large clasts. Thus only long core data are reported and used for comparison. Initially, all long cores from each block were tested in both oven-dry and saturated conditions.

7.5.1 Results

Ultrasonic wave velocity data are presented in table 7.1; values quoted in this table represent means from all available long cores from each block. From table 7.1 it can be seen that:

(1) within each ignimbrite there is an increase in ultrasonic wave velocity with increased induration (from table 2.1), or increased dry bulk density (table 5.1);

WHAKA/low density (kg m^{-3})	WHAKA/low velocity ($m\,s^{-1}$)	OWH/up density (kg m^{-3})	OWH/up velocity ($m\,s^{-1}$)	OWH/low density (kg m^{-3})	OWH/low velocity ($m\,s^{-1}$)
2120 ± 7	2040 ± 30	**horizontal**		**horizontal**	
2231 ± 4	1620 ± 20				
2246 ± 5	1610 ± 20	1580 ± 20	3500 ± 100	1911 ± 4	4420 ± 80
2252 ± 5	1600 ± 20	1590 ± 20	3300 ± 100	1918 ± 5	4260 ± 60
2260 ± 5	1640 ± 10	1650 ± 20	3200 ± 100	1937 ± 5	4200 ± 100
2267 ± 5	1690 ± 20	1720 ± 30	3000 ± 100	1963 ± 7	4250 ± 90
2284 ± 4	1880 ± 30	1790 ± 20	2950 ± 90	2030 ± 10	4100 ± 100
2286 ± 4	1940 ± 50	1815 ± 7	3000 ± 100	2030 ± 20	4200 ± 100
2286 ± 4	2080 ± 70				
2286 ± 4	2060 ± 80	**vertical**		**vertical**	
2284 ± 4	2010 ± 40				
2280 ± 4	1920 ± 30	1570 ± 20	3000 ± 100	1880 ± 40	3800 ± 200
2274 ± 5	1820 ± 20	1590 ± 20	2900 ± 100	1890 ± 40	3700 ± 200
2259 ± 5	1710 ± 20	1662 ± 9	2700 ± 200	1940 ± 40	3600 ± 300
2238 ± 5	1620 ± 20	1740 ± 20	2500 ± 300	1950 ± 10	3700 ± 300
2177 ± 8	1540 ± 20	1790 ± 10	2500 ± 100	2020 ± 30	3400 ± 200
2135 ± 7	1770 ± 20	1810 ± 10	2500 ± 100	2020 ± 20	3400 ± 200
2127 ± 7	1860 ± 20				
2127 ± 7	1860 ± 20				

ONG/1 density (kg m^{-3})	ONG/1 velocity ($m\,s^{-1}$)	ONG/2 density (kg m^{-3})	ONG/2 velocity ($m\,s^{-1}$)	ONG/3 density (kg m^{-3})	ONG/3 velocity ($m\,s^{-1}$)
1320 ± 70	2180 ± 60	1550 ± 70	2810 ± 50	1920 ± 20	3540 ± 40
1390 ± 70	2000 ± 100	1580 ± 70	2650 ± 80	1920 ± 20	3440 ± 60
1600 ± 80	1010 ± 60	1650 ± 70	2470 ± 80	1960 ± 20	3500 ± 50
1610 ± 80	1000 ± 60	1720 ± 70	2000 ± 100	1970 ± 20	3330 ± 80
1610 ± 80	1010 ± 70	1770 ± 70	2100 ± 100	1990 ± 20	3330 ± 90
1620 ± 70	1000 ± 60	1830 ± 20	2060 ± 90	2080 ± 20	3230 ± 60
1730 ± 50	1110 ± 60	1870 ± 40	2090 ± 60	2110 ± 20	3240 ± 40
1740 ± 50	1170 ± 50	1870 ± 40	2110 ± 70	2110 ± 20	3280 ± 50
1740 ± 50	1160 ± 70	1860 ± 30	2010 ± 90	2100 ± 20	3230 ± 80
1740 ± 50	1240 ± 90	1880 ± 40	2110 ± 70	2110 ± 20	3200 ± 20
1740 ± 50	1190 ± 60	1870 ± 40	2040 ± 60	2110 ± 20	3140 ± 60
1730 ± 50	1160 ± 60	1860 ± 40	2020 ± 70	2100 ± 20	3140 ± 70
1710 ± 50	1190 ± 70	1840 ± 40	2020 ± 70	2080 ± 20	3140 ± 50
1640 ± 50	1000 ± 100	1770 ± 40	2000 ± 80	2020 ± 20	3100 ± 70
1510 ± 50	1000 ± 70	1660 ± 60	2000 ± 100		
1400 ± 70	1220 ± 70	1610 ± 70	2120 ± 90		

Table 7.2: Mean ultrasonic wave velocities, and associated moist bulk densities, for five-core samples during draining experiment.

(2) between the ignimbrites there is not a direct increase in ultrasonic wave velocity with increased bulk density - the WHAKA/low specimen, for example, has a higher density yet lower velocity than the ONG/3 and OWH/low specimens; and

(3) the v_{pu} for saturated cores is, in most cases, less than the v_{pu} for oven-dry cores.

From equation 7.1 it is expected that the ultrasonic wave velocity will decrease with increased density. However, in practice the increase in elastic modulus which usually accompanies an increase in density will generally override this and result in an apparent increase in velocity with density (Smith, 1977). This is obviously the case within each ignimbrite, and variations in the elastic moduli between the ignimbrites appear to have a more significant influence than variations in density.

It is expected that the velocity of compressional waves should increase upon saturation, as water filled pores allow faster propagation of waves than air filled pores (section 7.2). This is only the case for the Whakamaru Ignimbrite in this study; all of the Ongatiti and Owharoa Ignimbrite specimens show a decrease in velocity at the higher moisture content. Hind (1986) noted similar trends for many of his ignimbrite samples, which he explained in terms of the high porosity of many of the ignimbrites.

7.5.2 Changes in ultrasonic velocity on draining

In order to investigate this decrease in velocity upon saturation further, the following section considers in detail the change in v_{pu} with moisture content for a subset of each group of cores on draining from the saturated state. A sub-sample of 5 cores was chosen from each block and saturated. These were then allowed to drain under gravity, and tested periodically during draining, then oven-dried. At each testing interval the mass of the sample was also measured, and the moist bulk density at the time determined. The WHAKA/up specimen could not be included in this test as the material could not withstand the extra cycle of saturation and draining.

In table 7.2 mean v_{pu} values of the five-core samples and the associated moist bulk densities are presented. Comparison of saturated and oven-dry end-members from these sub-samples and the complete data sets shows that the densities agree within error limits in all cases, but the velocities do not, with the exception of those for the most indurated specimens (WHAKA/low, OWH/low). This may mean that the sub-samples are too small to truly

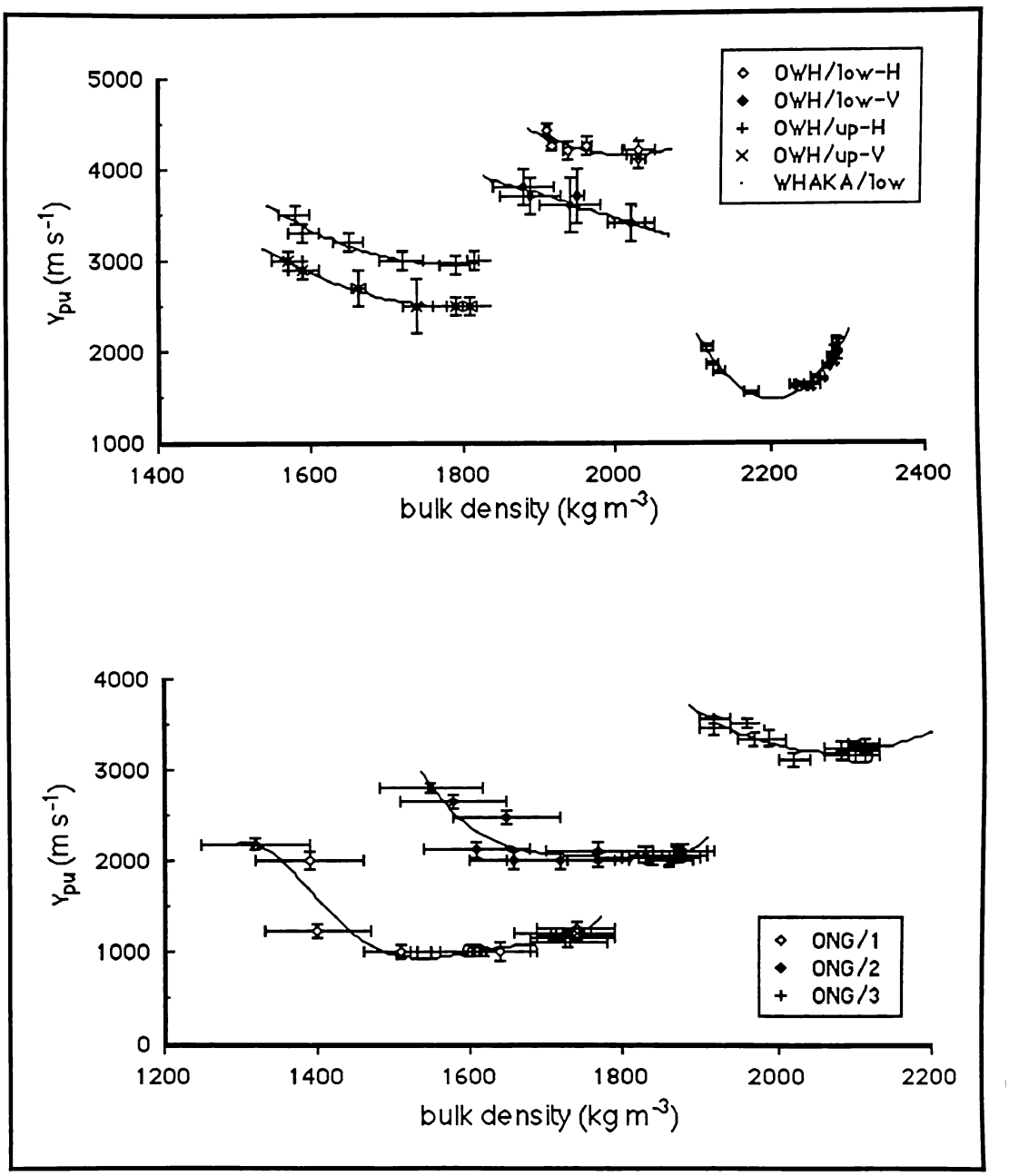

Figure 7.1: Variation in ultrasonic wave velocity on draining of specimens.

represent the full data sets. However, the agreement of the densities suggests that this is not entirely so, and it is thought that this represents a high sensitivity of the ultrasonic wave velocity to slight changes in moisture content, as will be discussed below.

Curves of v_{pu} versus bulk density for these cores are presented in figure 7.1. These show two different trends:

(1) for the Owharoa Ignimbrite the velocities generally rise steadily from a low value at saturation to a higher value at the oven-dry condition, and

(2) for the Whakamaru Ignimbrite the ultrasonic wave velocity falls rapidly from the saturated value, describes a deep "U" shape, and rises back to the $v_{pu,dry}$ value.

The values for the Ongatiti Ignimbrite show a less marked effect - the ONG/1 and ONG/2 specimens show a similar, but somewhat more subdued, curve to the WHAKA/low specimen, and the ONG/3 specimen shows a curve similar to those of the Owharoa Ignimbrite. Again $v_{pu,sat}$ is less than $v_{pu,dry}$ in all cases.

7.5.2.1 Previous draining experiments

Similar experiments have been carried out on various lithologies in the past. Nur and Simmons (1969), Toksoz *et al.* (1976), and Frisillo and Stewart (1980) all described curves for which an initial very sudden drop in v_p occurs as draining first begins, followed by a much flatter, but steadily decreasing, curve falling to the $v_{p,dry}$ value. These curves did not fall below the $v_{p,dry}$ value. Toksoz *et al.* (1976) examined the question theoretically, and found that theoretical curves of this form could be fitted to experimental data previously published. In their derivation the gas and liquid phases of the pore fluid were seen as being either a miscible mix, a mixture of gas bubbles within the liquid, or different phases occupying different pores. In each of these cases effective values of the elastic moduli of the fluid could be calculated, and hence the v_p predicted theoretically.

Other workers however, have measured curves which fall markedly from saturation to a value below the dry value, then increase again as the rocks become dry (Inoue and Ohomi, 1981; Murphy, 1982). Inoue and Ohomi (1981) noted that this was common in a variety of soft rocks. Murphy (1982) ascribed the initial drop in velocity on draining as a purely modulus effect as the addition of a significant amount of gas into the pores reduced the pore fluid bulk modulus effectively to zero. At the other end of the curve Murphy (1982)

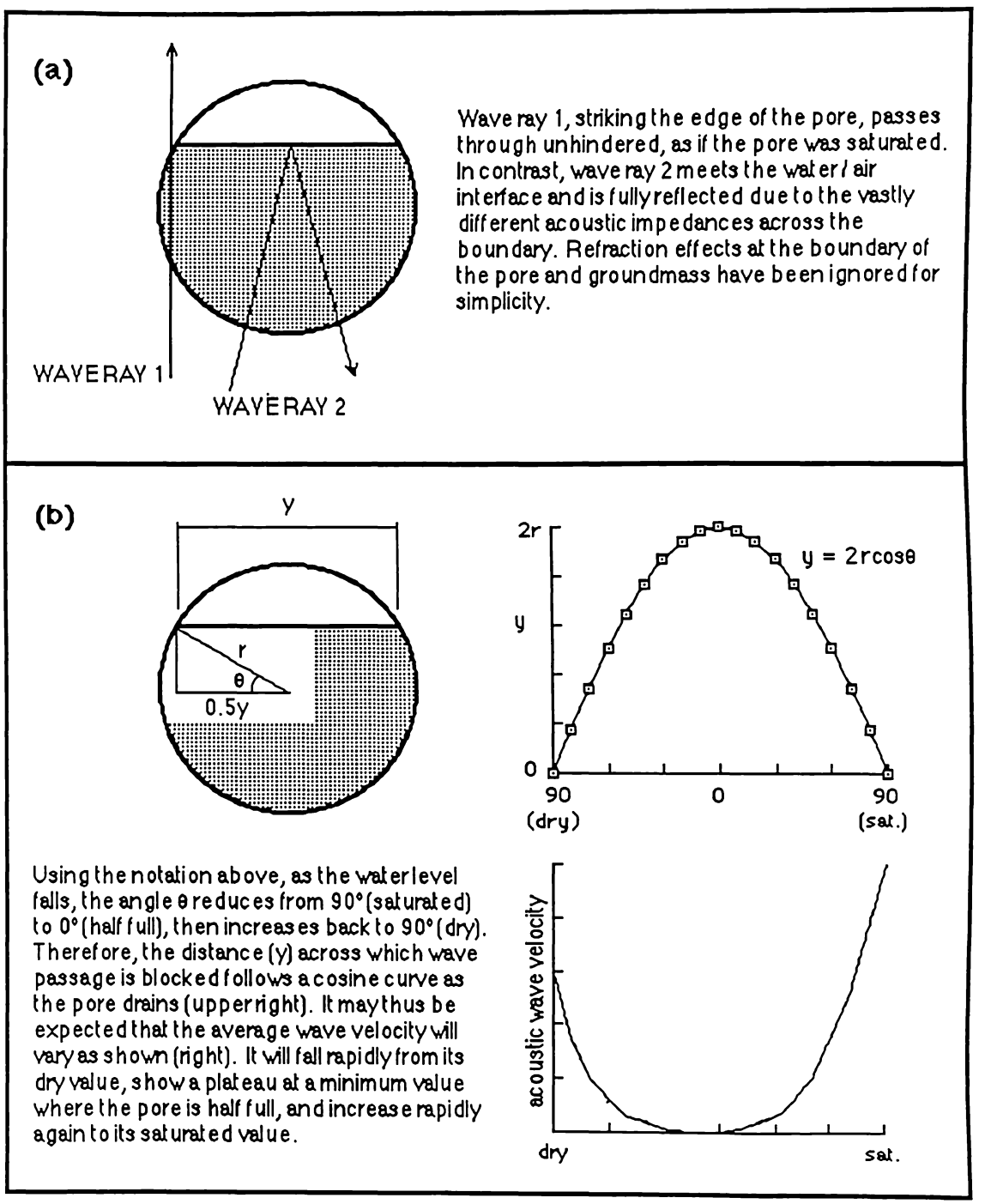

Figure 7.2: Effect of an air / water interface within a pore on acoustic wave transmission.
(a) Influence upon single wave rays.
(b) Influence upon average wave velocity.

observed a sudden increase in v_p near the dry state. This he explained as a capillary effect.

It is of note that in many of these studies particular emphasis was placed upon the fact that this effect occurs predominantly in rocks with crack-shaped pores rather than rounded pores (Nur and Simmons, 1969; Toksoz *et al.,* 1976), and the explanations given above assume that this is the case (Murphy, 1982). Toksoz *et al.* (1976) stated that the velocity of both compressional and shear waves is higher when the medium is saturated with gas than when saturated with water for spherical pores, whereas both compressional and shear wave velocities are lower for the gas-saturated case when the pores are crack-shaped.

7.5.2.2 Pore shape effects

As discussed above, theoretical considerations have generally assumed the pores to be crack-like, for which a steadily decreasing type of curve may be expected. However, the pores in ignimbrite are frequently rounded (as seen from fabric studies, chapter 12), and may consist of approximately spherical voids in some cases (note that this agrees with the observation of Toksoz *et al.* (1976) that the wave velocity may be higher for gas-saturated than for water-saturated specimens when the pores are spherical).

It is apparent that if the pores have a rounded cross-section, then, as they drain, there will be an air-water interface within the pores (compare this with the three mixing models discussed earlier (Toksoz *et al.,* 1976), in which no such interface exists). Due to the vastly different acoustic impedances of air and water, waves striking such an interface will be fully internally reflected (Pain, 1983), and will thus not be capable of passing through the pore space (figure 7.2a). This is different from either the saturated or dry conditions when the impedance difference between the rock and water, or rock and air, allows the waves to travel through the pores. Thus under partially saturated conditions the average path length of the waves is much greater than for either saturated or dry conditions, and so the apparent velocity is lower.

Looking at this effect in more detail, it is apparent that the pores, as a pathway, will not be cut off immediately that draining begins. Considering a rounded pore, as shown in figure 7.2a, which is partially filled with water, waves impinging upon the edge of the pore can pass through unimpeded,

whereas those striking the centre of the pore are reflected by the interface. The distance, y (figure 7.2b) across which the waves are impeded is given by:

$$y = 2r\cos\theta \qquad \ldots (7.2).$$

As the water level falls (θ reduces), the distance (y) across which the wave passage is blocked becomes much greater. Consequently, the distance (y) may be expected to approximate to a cosine curve as the pore drains (figure 7.2b), reaching a maximum when the pore is half-filled, and minima when the pore is either fully saturated or completely dry. Following on from this, the velocity curve (figure 7.2b) may also be expected to follow a general cosine-type curve, with maxima at the oven-dry and saturated extremes, and falling to a minimum between these values. The actual curve is dependant upon many factors, such as the distribution of pore sizes, the total porosity, and the relative speeds in the rock framework and dry and saturated pores, thus the curve shown in figure 7.2b is schematic and idealised.

Obviously, in real rocks either of these two extremes (crack-like or rounded pores) is an approximation; all rocks will have a proportion of pores fitting each extreme and ranging between the two end-members, together with a distribution of actual pore sizes. This means that neither of the two extremes will fit the real situation entirely, but each rock may be expected to contain elements of each to a greater or lesser extent.

7.5.2.3 Observed variations

These trends observed above for the ignimbrite specimens give a qualitative indication of the shape of the pore space within the rocks. The Owharoa Ignimbrite, in which the velocity does not fall below the $v_{pu,dry}$ value, would appear to have the most crack-like pores of all (this is not surprising given the lenticular nature of the pumice clasts), whereas the Ongatiti and Whakamaru Ignimbrites appear to have much more rounded pores. In the case of the Ongatiti Ignimbrite, the pores are most rounded in the ONG/1 specimen, and least rounded in the ONG/3 specimen. This corresponds to the observed slight flattening of the pumice clasts in the ONG/3 specimen (table 2.1). Pore shape will be examined using scanning electron microscopy in chapter 12.

Of particular interest is the apparent roundness of the pores in the Whakamaru Ignimbrite sample. This sample was extracted from a very

indurated position in the lower portions of a very deep flow. Under normal conditions this would be expected to be a very compressed rock, with extensive lenticularity. However, the occasional pumice clasts which are found also tend to be rounded (table 2.1) rather than elongated.

7.5.2.4 Effects on $v_{pu,sat}$ and $v_{pu,dry}$ measurements

The $v_{pu,sat}$ values shown on the draining curves presented in figure 7.1 remain consistently lower than the $v_{pu,dry}$ values, even for the Whakamaru Ignimbrite. This agrees with the observations of Toksoz *et al.* (1976) for spherical pores, but is not well explained by any of the theoretical considerations discussed.

In this case it is thought that the effect may be attributed to incomplete saturation (or desiccation) of the cores. Despite vacuum saturation, there is inevitably some air which is not removed at the pressures obtained in the vacuum, and, likewise, oven-drying leaves some water within the material. Assuming that this air (or water) is creating an interface, as described above, the ultrasonic waves are impeded, and the measured velocity reduced. It is notable that repeated measurements near saturation (or the oven-dry condition) do not give reproducible results (section 7.5.2). This is thought to be the result of slight differences in the degree of saturation (or dryness), as approaching complete saturation (or desiccation) the curves may be expected to rise very sharply (figure 7.2), making determinations at these extremes highly variable. This is shown by the curve for the Whakamaru Ignimbrite in figure 7.1. Consequently, measurements at these extremes may be expected to show a relatively high degree of scatter and thus large confidence limits, as seen in table 7.1.

7.6 Seismic waves

Higher frequency (1 MHz) seismic waves were studied with the intention of measuring the dynamic elastic moduli of the ignimbrites. Calculation of these moduli from elastic wave velocity data is a common technique in both the field and laboratory (for example, Evison 1956). In this study the procedure of King, outlined in Anon (1983) was followed.

7.6.1 Equations for elastic moduli

Calculations of the dynamic elastic moduli rely upon the fact that the velocities of elastic waves are controlled primarily by the density and elasticity of the medium (section 7.2). Toksoz *et al.* (1976) stated that the velocities of seismic waves in porous rocks can be expressed by:

$$v_p^* = \sqrt{\frac{K^* + \frac{4}{3G^*}}{\rho^*}} \qquad \text{... (7.3)}$$

$$v_s^* = \sqrt{\frac{G^*}{\rho^*}} \qquad \text{... (7.4)}$$

where: K = bulk modulus (Pa).

In these equations a star superscript is taken to mean an effective property for the composite medium, taking into account the properties of the rock matrix plus any pore-filling fluids. These effective properties vary considerably with pore size, shape and saturation (Toksoz *et al.,* 1976), and hence create the trends noted earlier in section 7.2. The star superscript will not be retained, but in this section all values can be assumed to be effective values for the composite media as measured directly. In deriving equations 7.3 and 7.4 the assumption was made that the wavelength is long compared with a length defining the pore size (equivalent diameter, width, or aspect ratio) (Toksoz *et al.*, 1976).

Well-defined relationships exist between elastic constants. In particular K and G can be expressed in terms of E and μ by the following equations (Farmer, 1968):

$$K = \frac{E}{3(1-2\mu)} \qquad \text{... (7.5)}$$

$$G = \frac{E}{2(1+\mu)} \qquad \text{... (7.6)}$$

Substituting these into equations 7.3 and 7.4, and rearranging gives the following relationships:

$$E_{dyn} = \rho v_s^2 \left(\frac{3v_p^2 - 4v_s^2}{v_p^2 - v_s^2} \right) \quad \ldots (7.7)$$

$$\mu_{dyn} = \frac{v_p^2 - 2v_s^2}{2(v_p^2 - v_s^2)} \quad \ldots (7.8)$$

where: E_{dyn} = dynamic Young's modulus (Pa), and
μ_{dyn} = dynamic Poisson's ratio.

which describe the dynamic elastic moduli in terms of wave velocity and bulk density alone. These equations are only strictly true for isotropic media (King, 1983).

7.6.2 Attenuation

As discussed in section 7.2, wave attenuation is strongly frequency dependent, with attenuation increasing as a power function of the wave frequency. Consequently, these high frequency seismic waves undergo considerably greater attenuation than their ultrasonic counterparts. This is sufficient in most rocks, and certainly in all of the ignimbrites examined in this study, to mean that the amount of energy reaching the Pundit receiver is below the detection level at atmospheric pressure.

However, attenuation decreases at increased pressure, so by placing the rock and transducers under compression in the UCS or SRCM machines, readings could be obtained at a range of pressures. Unfortunately, ignimbrites are not ideal for this due to their inhomogeneity and high porosity, and hence in the case of the softer samples, attenuation was so great that no readings could be obtained even under pressure. Likewise, attenuation of S-waves is greater than P-waves (Winkler, 1983), and hence for many of the samples v_{ss} values could not be obtained, or could only be obtained at pressures close to the failure point of the rock.

7.6.3 Procedure

The procedure attributed to King in Anon (1983) was adhered to. As the UCS machine has only a limited distance between the platens, and the seismic wave transducers are each 60 mm long, only short cores could be used for this test. This was also necessitated by the wave attenuation which meant that no signal could be received from long cores.

	moisture condition	v_{ps} (ms^{-1}) low stress	v_{ps} (ms^{-1}) peak	v_{ss} (ms^{-1}) low stress	v_{ss} (ms^{-1}) peak
WHAKA/up	saturated	-	-	-	-
	oven-dry	-	-	-	-
WHAKA/low	saturated	800 ± 300	3400 ± 100	590 ± 80	2100 ± 700
	oven-dry	2100 ± 100	3170 ± 60	1300 ± 200	3030 ± 30
ONG/1	saturated	-	300 ± 200	-	-
	oven-dry	114 ± ?	615 ± ?	-	-
ONG/2	saturated	500 ± 500	1000 ± 600	-	-
	oven-dry	200 ± 300	860 ± 60	-	-
ONG/3	saturated	525 ± ?	943 ± ?	-	-
	oven-dry	700 ± 400	1400 ± 700	-	-
OWH/up-vert	saturated	700 ± 400	1000 ± 300	199 ± ?	346 ± ?
	oven-dry	700 ± 600	2000 ± 2000	514 ± ?	1466 ± ?
OWH/up-hori	saturated	600 ± 500	1300 ± 400		
	oven-dry	1043 ± ?	3060 ± 90	907 ± ?	1500 ± 900
OWH/low-vert	saturated	759 ± ?	3330 ± 40	851 ± ?	2000 ± 1000
	oven-dry	1000 ± 200	3500 ± 200	1000 ± 1000	2000 ± 1000
OWH/low-hori	saturated	1240 ± ?	3570 ± 20	1300 ± 700	2000 ± 1000
	oven-dry	833 ± ?	3800 ± 200	1500 ± 700	2300 ± 500

Table 7.3: Seismic wave velocity data for each site.
- \- = attenuation of waves so great that no results could be obtained.
- ? = insufficient reliable data available from which to calculate a sensible error estimate (one or two data points only).

Acoustic coupling was achieved by thin aluminium foil plates which were imbedded into the specimens by the initial application of a low pressure. To remove the effects of these plates on the calculated wave velocities, a calibration run, in which the travel times of both P- and S-waves through the plates alone were measured at a range of pre-determined loads, was undertaken prior to each testing session. These calibration values were then subtracted from those measured for the specimen-plus-plates assembly at the same loads.

Stress levels at which readings were taken were determined from a knowledge of the compressive strength of the material (table 4.1). About 10 equal intervals were defined between 0 and the compressive strength, and these used as the reading levels.

To obtain readings the load was slowly increased to the desired value and held steady at that level until stable readings were obtained on the Pundit. This was repeated for each load level. In some instances an unloading curve was obtained in the same way after the maximum load was reached.

7.6.4 Seismic wave velocity

In table 7.3 seismic wave velocity data are presented for each site. Only two values of v_{ps} and v_{ss} are given in each case; those measured at the lowest stress at which a stable reading could be obtained, and the peak value of the velocity. Each value represents the mean measured on several cores.

7.6.4.1 Viability of experimental technique

From the stated confidence limits in table 7.3, it is apparent that very little confidence can be placed in the means obtained from these measurements. This is attributed to two causes: only a very limited number of specimens (3-5) was tested in each case, and the measurements obtained vary immensely between individual cores. Due to this high variability between cores, little value was seen in reproducing the measurements on a large number of cores, as this would have only a limited effect on the accuracy of the data.

Data from each individual core are consistent, that is, each core shows consistent trends with applied stress. However, cores from the same block frequently show vastly different velocities. This is believed to be due to the inherent inhomogeneity of ignimbrites. As discussed earlier, pore and crack

shape and distribution have a marked effect on wave velocity and attenuation, especially at the extremes of moisture content. Add to this the effects of a variable clast composition and distribution, and it becomes apparent that wave velocity may be expected to be highly variable. This is exacerbated by the fact that only short cores could be used, in which relatively small clasts can make up a significant portion of the path length.

For these reasons, data obtained from this procedure are not considered to give particularly precise estimates of the true wave velocities in ignimbrites. It is therefore recommended that the technique only be used in very specialised studies requiring seismic wave velocities under compression, such as when dynamic elastic moduli are required in particular.

7.6.4.2 Normalisation

In this study only limited reliance was placed upon the actual seismic wave velocity values; they were not analysed in detail, or considered as predictors of ignimbrite strength. However, the trends in the data are undoubtedly of significance. Hence in all further graphs in this chapter the axes have been normalised. This allowed the trends in the individual cores to be averaged and compared. The applied stress was normalised by dividing by the average compressive strength ($\sigma_{c,dry}$ or $\sigma_{c,sat}$ as appropriate) of the block under consideration (table 4.1), and the velocities, v_{ps} and v_{ss}, were normalised by dividing each value by the peak reading for that individual core. Many of the normalised axial stress values are greater than 1.0. This is because the normalisation was based upon the uniaxial compressive strength measured from long cores. Some of the short cores had slightly greater compressive strengths than their long counterparts, hence the high normalised values.

7.6.4.3 Comparison of v_{ps} with v_{pu}

Of particular note in table 7.3 is the fact that, even in spite of the large confidence limits, the compressional wave velocity at 1 MHz is considerably lower than that at 54 kHz. This is most obvious at the low stress values (closest to the atmospheric pressure at which v_{pu} was measured), but even the peak values are still lower than their v_{pu} counterparts. This shows that, for these rocks at least, v_p is strongly dependent upon wave frequency.

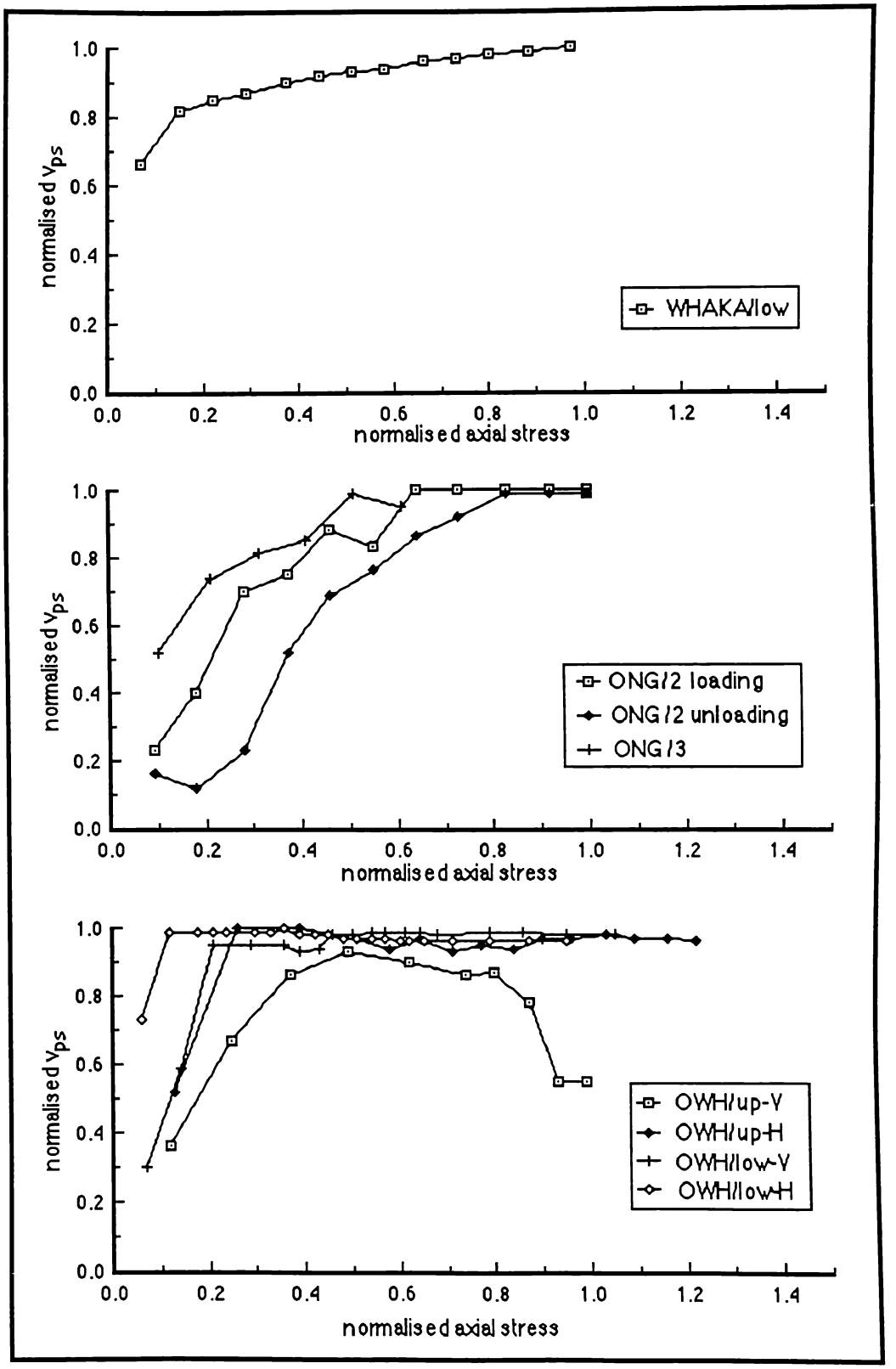

Figure 7.3: Variation in v_{ps} with axial stress for oven-dry specimens.

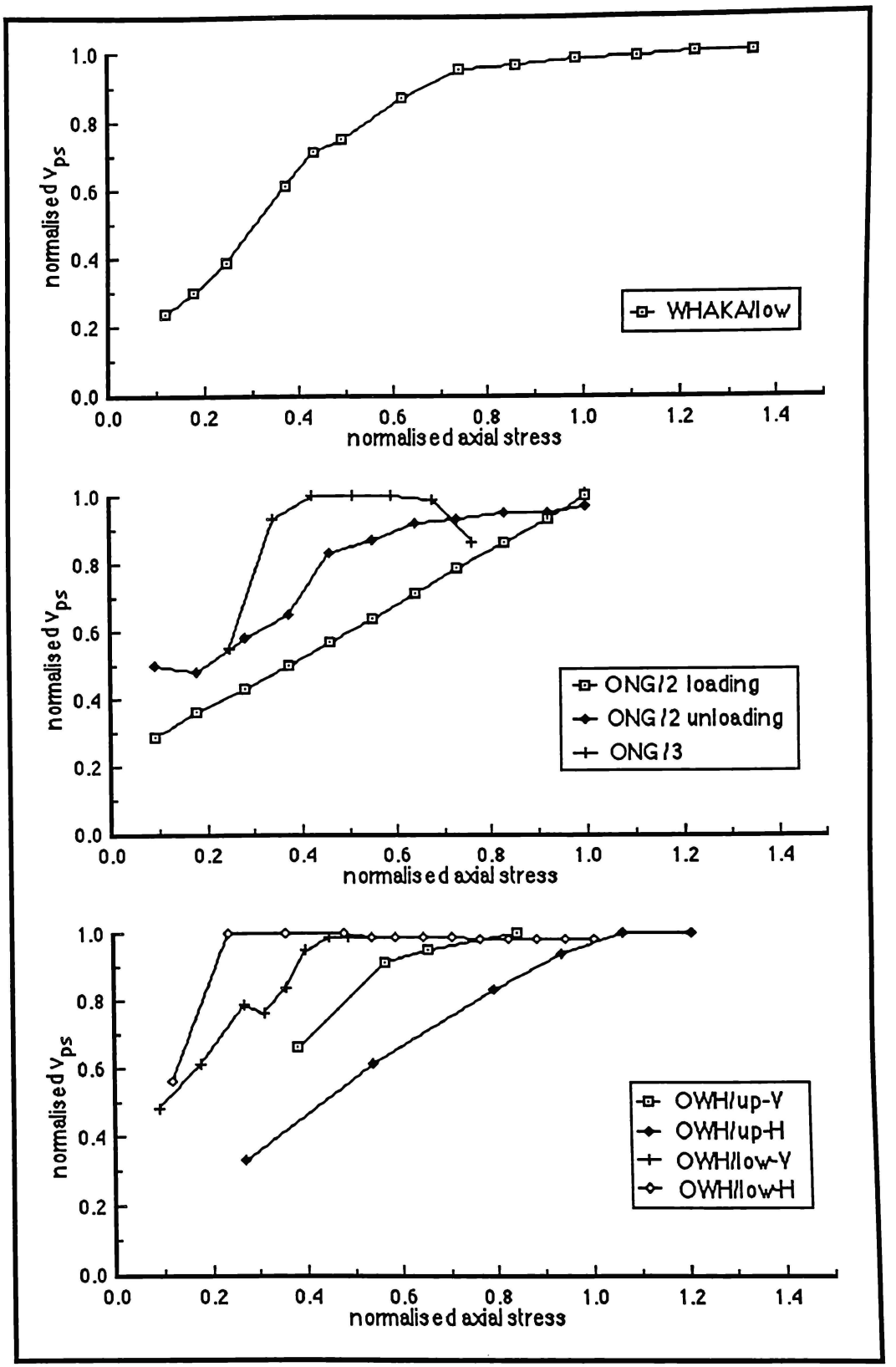

Figure 7.3 (overlay): Variation in v_{ps} with axial stress for saturated specimens.

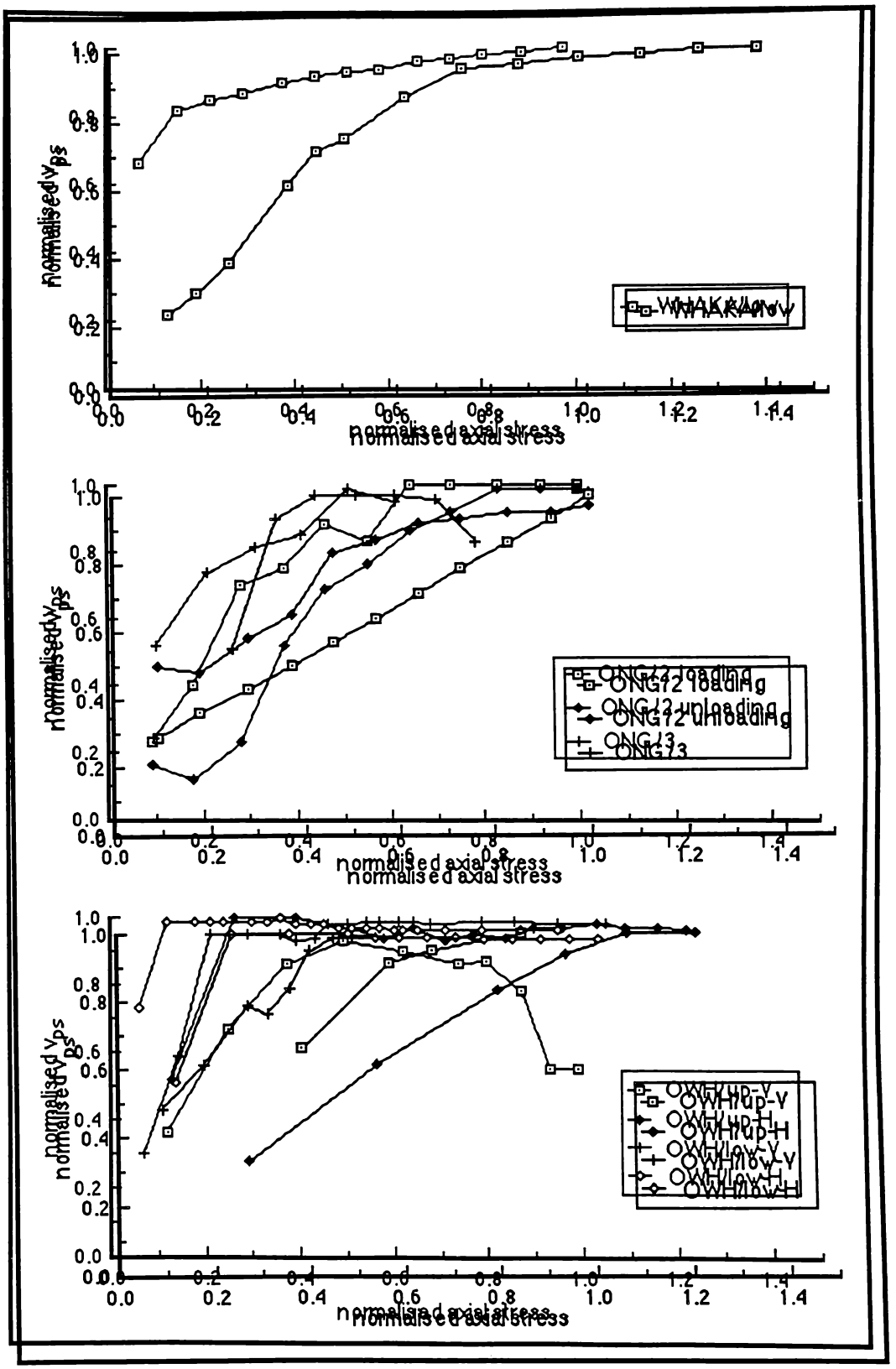

Figure 7.3: Variation in v_{ps} with axial stress for oven-dry specimens.

Figure 7.3 (overlay): Variation in v_{ps} with axial stress for saturated specimens.

As with v_{pu}, on taking nominal "saturated" and "oven-dry" values, there is an unexpected decrease in wave velocity upon saturation for most cores. This is true for both v_{ps} and v_{ss} measurements. From section 7.2, this lowering of v_{ss} with saturation is not uncommon, and the lowering of v_{ps} may be due to the same reasons as discussed in section 7.5. Without more accurate data these effects are impossible to interpret fully.

7.6.5 Variations in v_{ps} with applied stress

Figure 7.3 presents graphs of v_{ps} (normalised to peak) versus applied stress (normalised to compressive strength) for each of the ignimbrites studied; for the ONG/2 specimen both loading and unloading curves are given. Graphs for oven-dry specimens are overlain by those for saturated specimens.

7.6.5.1 General trends

In general, the curves can be seen to start at a low velocity when the stress is initially applied, they rise sharply to a peak value, and flatten-off at this level. The low initial value represents the rock in its natural state; pores and cracks will result in a low velocity as discussed in section 7.2. With a slight increase in pressure the void spaces begin to close, resulting in an increase in the measured wave velocity, until a point is reached where significant void closure no longer occurs and the velocity flattens off at this level. This variation is assumed to equate to the regions of initial plastic deformation followed by elastic deformation of a "typical" stress / strain curve as described by Farmer (1983).

In some cases however, the velocity drops off again after reaching its peak value. In these cases the point where rapid micro- and macro-fracture development occurs is reached. As a reverse of the trend described above, the opening of new fractures within the material results in the measured velocity falling.

7.6.5.2 Effect of saturation

In general the saturated curves start lower than the dry, and reach their peak much later; their rising limbs are flatter than those for their dry counterparts. The flatter curve is believed to represent the dissipation of pore water pressure within the saturated cores. Pore closure cannot occur as

readily when the pores are filled with water, and it takes a greater applied stress, together with a longer time (which is not allowed for in the testing procedure), for effective stresses to be overcome and the voids to close. Therefore, the velocity reaches a peak at a higher stress, and rises at a reduced rate with increased stress.

7.6.5.3 Effect of orientation

For the Owharoa Ignimbrite, the curves obtained from vertical cores generally show a much flatter curve than those obtained from the corresponding horizontal cores. This again is thought to be a pore closure effect, and related to a significant anisotropy in the pore shape. It is assumed that only those cracks and pores with a significant alignment in the direction perpendicular to the applied stress will be closed, those parallel to the applied stress will dilate if anything. Ultrasonic velocities suggest that a significant proportion of the pore space in the Owharoa Ignimbrite is comprised of crack-like openings rather than rounded pores (section 7.5.5.3), these seismic data confirm this, and provide evidence that the voids are oriented in the same direction as the lenticular pumice clasts. In a horizontal sample the compression is parallel to the crack axes, there is little compression of the voids, and the velocity will rises to its peak very rapidly. In contrast, in a vertical sample the compression is perpendicular to the crack axes, there is significant compression of the pores, and the velocities rise to their peak at a much slower rate.

7.6.5.4 Loading and unloading cycles

Both loading and unloading curves are shown for the ONG/2 specimens. The saturated and dry curves do not show consistent patterns, except that it is apparent in both cases that the velocities measured on unloading do not follow the same curves as those measured on loading of the cores. This is the result of permanent, irreversible damage occurring within the core prior to failure.

For the saturated curve, the specimens were not loaded beyond their peak velocities, and the unloading curve finish at a higher velocity than the initial low stress value. This is thought to result from the void space closure and sample compaction which produces the initial rise in velocity upon loading; this is not relieved upon unloading and the velocities at low stress are

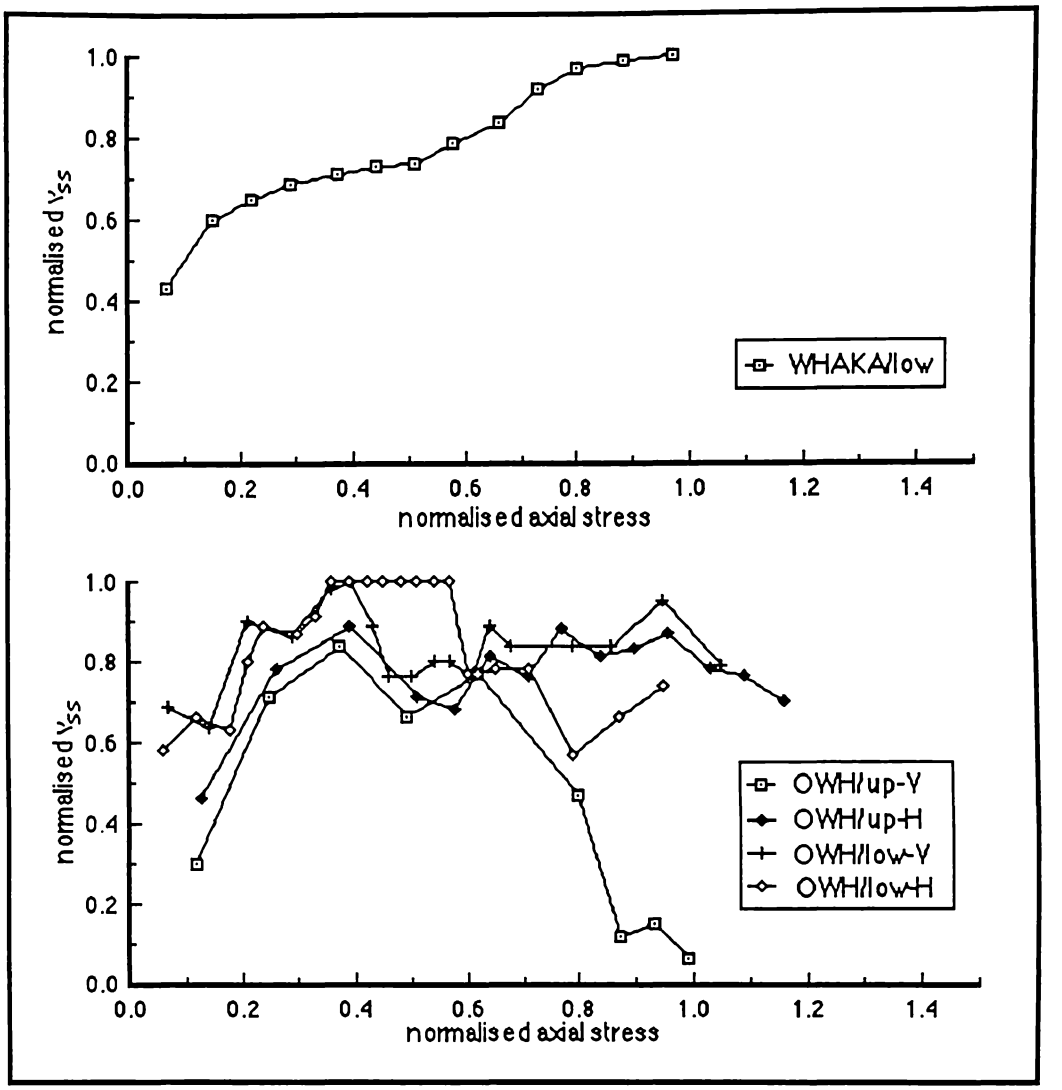

Figure 7.4: Variation in v_{ss} with axial stress for oven-dry specimens.

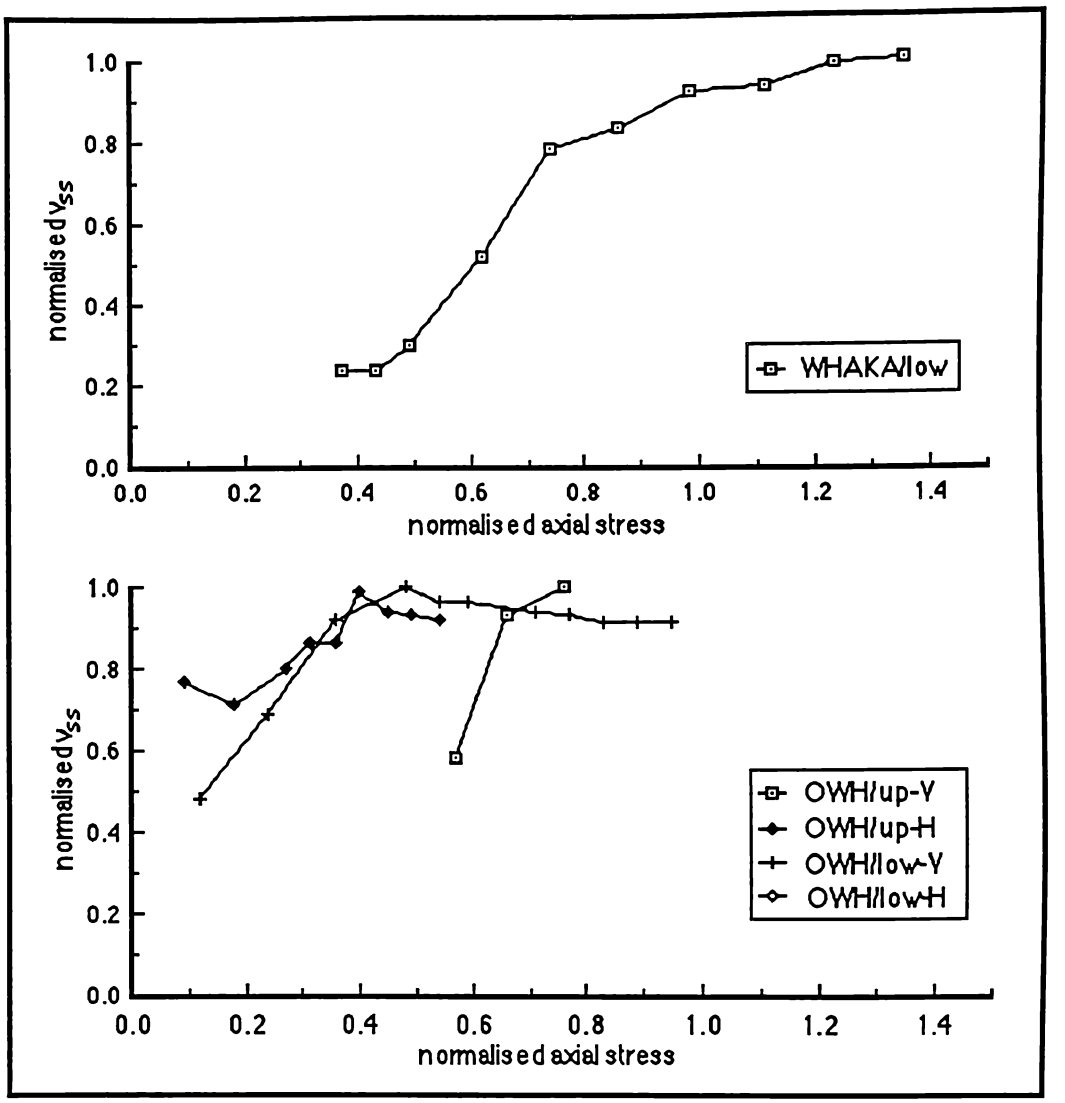

Figure 7.4 (overlay): Variation in v_{ss} with axial stress for saturated specimens.

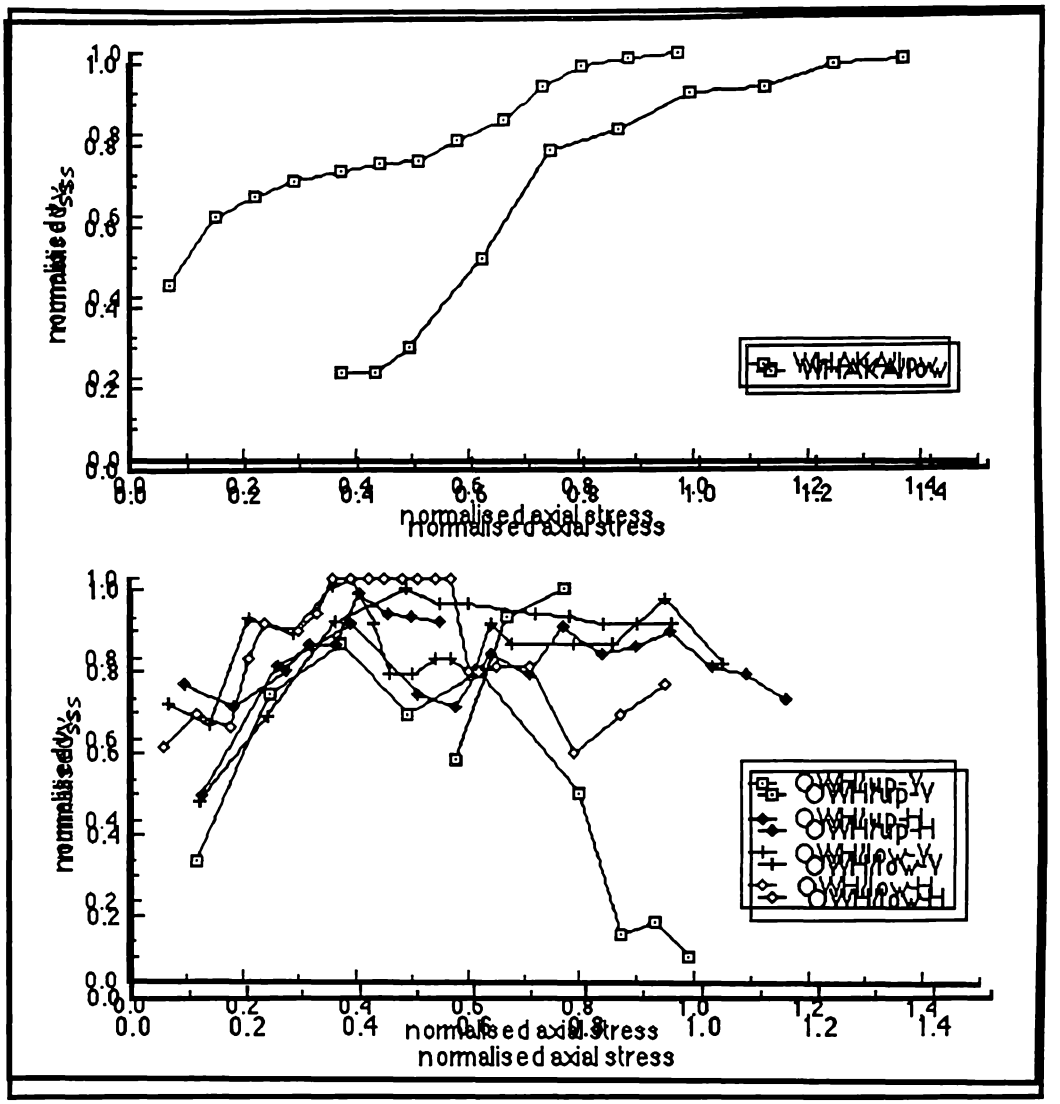

Figure 7.4: Variation in v_{ss} with axial stress for oven-dry specimens.

Figure 7.4 (overlay): Variation in v_{ss} with axial stress for saturated specimens.

consequently higher. In contrast, the dry specimens were loaded until just beyond their peak velocities, and the unloading curve shows velocities consistently below those measured on loading. In this case new fractures were presumably developed as the cores were loaded close to failure (in fact, macro-fractures could be seen along the core edges in some cases). Thus new fractures were initiated and opened, and therefore the velocities on unloading are less than those during loading.

Hence it is apparent that permanent, irreversible damage occurs during compression of the cores, and occurs at quite low values of the normalised applied stress. This results in a hysteresis in the seismic wave velocities on loading and unloading; the exact form of this hysteresis will be entirely dependent upon the stress history of the core, that is, how close to failure it has been loaded. This conclusion seems intuitive. It may also be expected that it will be most significant in these porous rocks.

7.6.6 Variations in v_{ss} with applied stress

Figure 7.4 shows the variations in shear wave velocity with applied stress for the Whakamaru and Owharoa Ignimbrites respectively; no shear wave measurements were obtainable for the Ongatiti Ignimbrite. The shear wave curves are much less predictable than those for the compressional waves, especially for the Owharoa Ignimbrite. This is believed to be due primarily to the means of measurement, which is insensitive given the high attenuation, and hence low received energy, of the signal in these porous rocks.

As for compressional waves, the velocity of shear waves tends to rise with increased applied stress from an initially low value. Void space compaction should not affect the shear wave velocity significantly (section 7.2), as S-waves do not propagate through a fluid phase. However, if the voids close to the extent that pathways are linked across them, then the measured shear wave velocity will increase. This would seem to be the case for these ignimbrites.

7.6.7 Ratio of v_{ps} and v_{ss}

In figure 7.5 graphs of the ratio of compressional and shear wave velocities versus normalised applied stress are plotted. Considerable variability is notable in these graphs; this is due to the variability noted

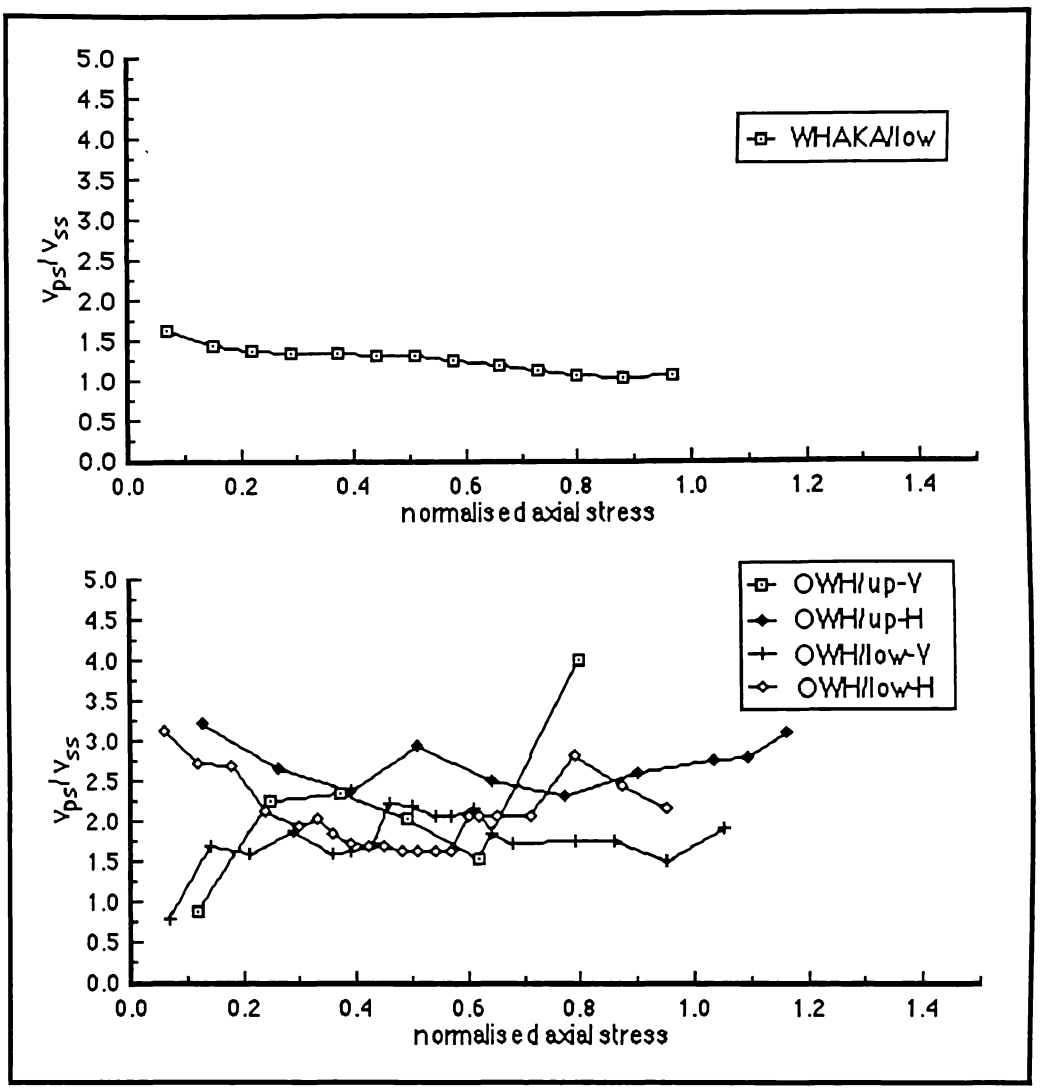

Figure 7.5: Variation in v_{ps}/v_{ss} with axial stress for oven-dry specimens.

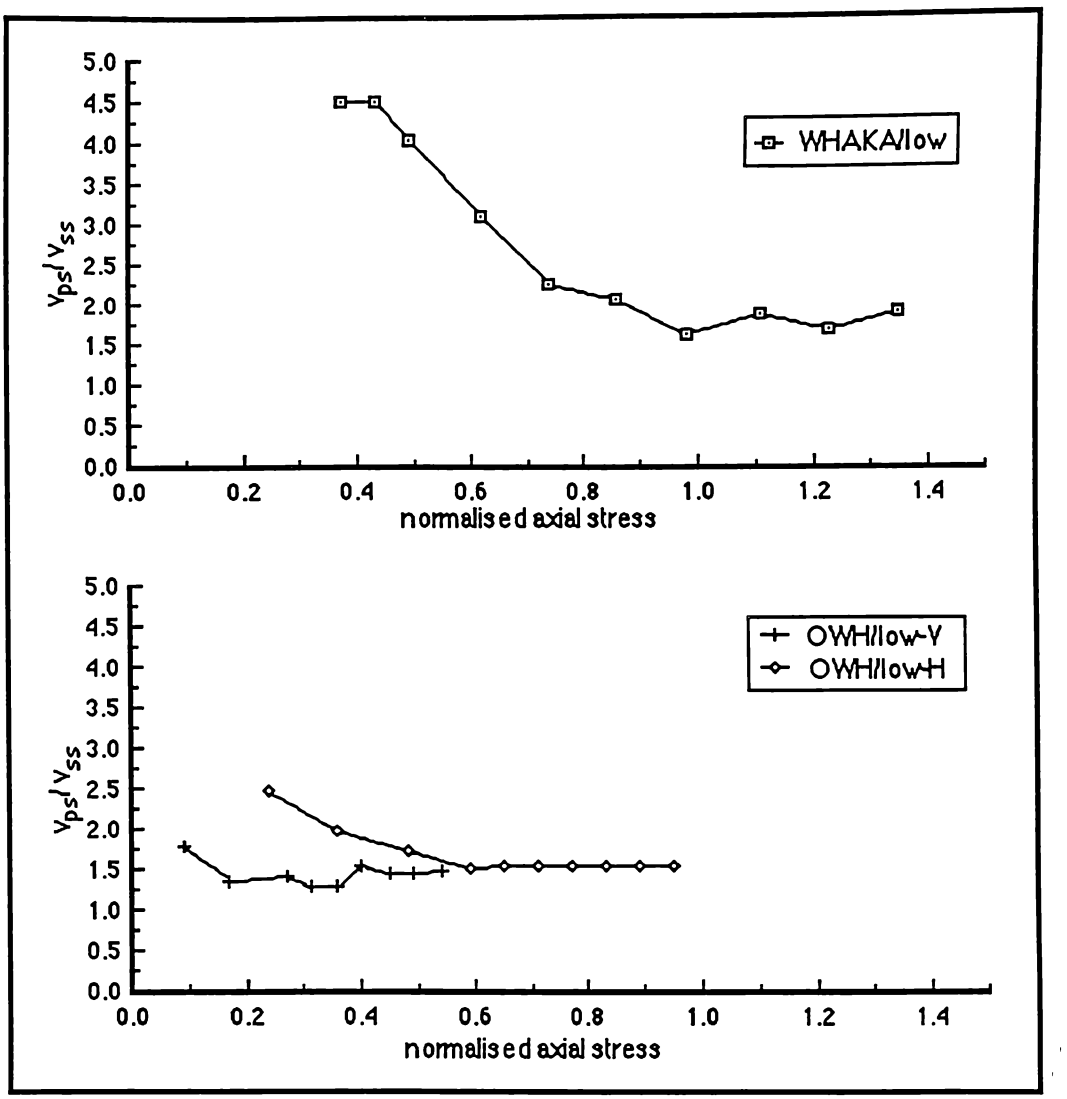

Figure 7.5 (overlay): Variation in v_{ps}/v_{ss} with axial stress for saturated specimens.

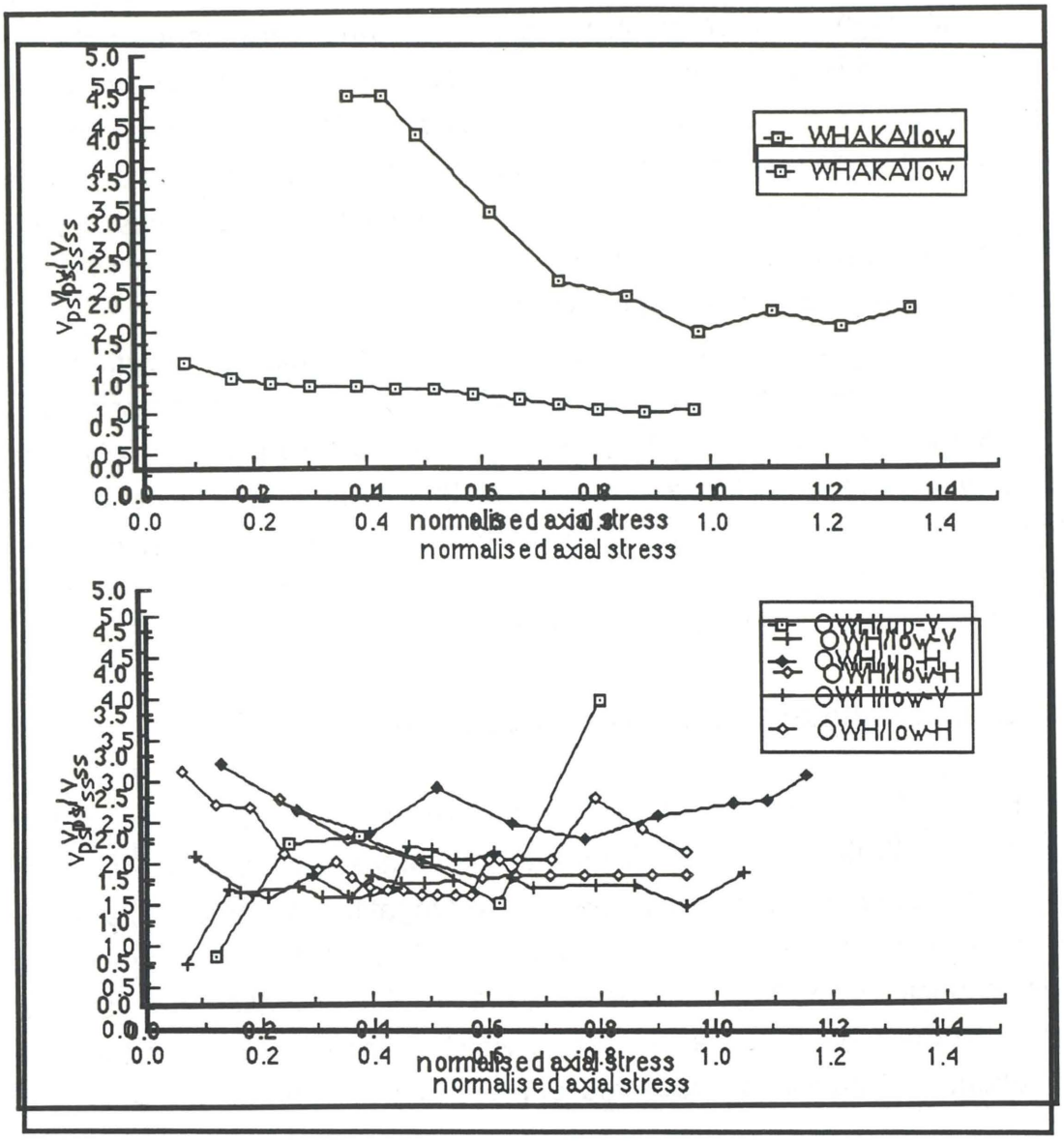

Figure 7.5 (overlay): Variation in v_{ps}/v_{ss} with axial stress for saturated specimens.

Figure 7.5: Variation in v_{ps}/v_{ss} with axial stress for oven-dry specimens.

previously in the shear wave velocity, and is therefore an artefact of the testing technique.

For most samples the ratio of the two velocities falls rapidly with the initial stress application, then flattens off to an essentially constant value. This means that with increasing stress the shear wave velocity is initially much more strongly affected (in real terms) than the compressional wave velocity - both velocities increase, but the shear wave velocity does so much more rapidly. This is a reflection of the closure of void space allowing a much shorter path length for the shear waves, whereas the effect is less for the compressional waves as they travel through the void space.

The flattening off of the graphs occurs at a value of v_{ps} / v_{ss} of approximately 1.5 for both the Whakamaru Ignimbrite and the saturated Owharoa Ignimbrite, and approximately 1.6 - 2.0 for the dry Owharoa Ignimbrite specimens. This is approximately the ratio of wave velocities in earth materials (Smith, 1977).

7.6.8 Dynamic elastic moduli

The difficulty in obtaining reliable values for seismic wave velocity (section 7.6.4), and especially for the S-wave velocity (section 7.6.7) meant that this technique of measuring dynamic elastic moduli was not successful. No S-wave data could be obtained for any of the Ongatiti Ignimbrite specimens, and no data (either P-wave or S-wave) could be obtained for the WHAKA/up specimen. Therefore, no dynamic elastic moduli could be calculated for any of these materials. Likewise, for all specimens, the wave velocity measurements were highly variable between cores (section 7.6.4.1) and the ratio of P- to S-wave velocities was variable (section 7.6.8). As the equations for dynamic elastic moduli are dependent upon these measurements (equations 7.7 and 7.8), these variations made estimates of the elastic moduli highly variable, and unreliable.

Those cores from which sufficient data could be obtained to calculate values of the dynamic elastic moduli suggest approximate values of:

WHAKA/low	$E_{dyn,sat} = 10^3$ MPa	$\mu_{dyn,sat} = 0.4 - 0.5$
	$E_{dyn,sat} = 10^4$ MPa	$\mu_{dyn,sat} = 0.3$
OWH/up	$E_{dyn,sat} = 10^2$ MPa	$\mu_{dyn,sat} = 0.5$
OWH/low	$E_{dyn,sat} = 10^4$ MPa	$\mu_{dyn,sat} = 0.4 - 0.5$

These values suggest that the materials are highly deformable, with a low Young's modulus and high Poisson's ratio compared with other rocks, but are comparable with other dynamic moduli measurements for ignimbrites (Yamanouchi *et al.*, 1981; Hind, 1986).

7.7 Summary

Overall, measurements of elastic wave velocity (at both ultrasonic and seismic frequencies) are not successful for these ignimbrites due to their inhomogeneity, high porosity, and high wave attenuation. This is especially true for the seismic waves for which attenuation is so great that reliable readings cannot be obtained for many of the specimens.

Ultrasonic wave velocity measurements at nominal saturation and oven-dry conditions show considerable variability. Draining experiments, for which velocity measurements were made at a variety of moisture contents as the cores dried out, show that the change in velocity with moisture content near the moisture extremes is very rapid. This makes the measurements highly sensitive to slight variations in the moisture content at these points, hence the variability in these values.

Both ultrasonic and seismic wave velocities show consistent reductions in wave velocity upon saturation of the specimens for most ignimbrites. This is unexpected from theoretical considerations, but has been reported in the literature for other soft and / or porous rocks. No suitable explanation is available, but the sensitivity of the velocities to moisture content at these moisture extremes may suggest that incomplete saturation or desiccation of the materials leads to imprecise measurements.

Between the moisture extremes the ultrasonic wave velocity responds to changes in the moisture content in different ways for each specimen. These responses are interpreted in terms of the shape of the void spaces within the specimens; the Whakamaru Ignimbrite appears to have rounded pores, as do the ONG/1 and ONG/2 specimens, whereas the Owharoa and ONG/3 specimens appear to have crack-like voids. These observations are in keeping with field observations of the lenticularity or otherwise of the pumice clasts; seismic wave data for the Owharoa Ignimbrite confirm that these cracks are aligned in the same orientation as the lenticular pumice clasts.

Variations in v_{ps} with applied stress suggest considerable void closure upon initial loading of the specimens, leading to significant, irreversible damage to the specimens at low stresses. Further deformation occurs with the

opening of fractures as the specimen approaches failure. These deformations lead to considerable hysteresis in the velocities upon loading and unloading, and confirm that repeated loading cycles cannot be used for these ignimbrites.

Estimates of dynamic elastic moduli, where possible, suggest that the ignimbrites are highly deformable materials, with low Young's moduli, and high Poisson's ratios compared with other materials.

CHAPTER 8 - VALUE OF INDEX PROPERTIES AS PREDICTORS OF STRENGTH

8.1 Introduction

Linear regression analysis was used to seek relationships between the mechanical properties (compressive strength, tensile strength, cohesion, and angle of internal friction) established in chapter 4, and the index measurements discussed in chapters 5 to 7 (bulk rock properties, hardness, durability, and ultrasonic wave velocity). This was undertaken in order to address two aims:

(1) to see if any of the measured properties of the rocks provide sensitive indices to the mechanical strength, and

(2) to search for possible causal relationships between the measured properties and the strength, so as to examine the causes of the rock strength.

8.2 Methods

8.2.1 Linear regression

Linear regression between two variables was the basic technique used to examine possible relationships between mechanical properties and index measurements. Multiple regressions and more complex mathematical relationships (such as higher order polynomials, or logarithmic relationships) were not considered justified at this initial stage of seeking general relationships.

In all cases the regression was performed using the mechanical strength property as the dependent variable and the index property as the independent variable. Values of the regression coefficient adjusted for the degrees of freedom were recorded. A cut-off of $r^2_{adj} \geq 0.50$ was applied. In order for relationships to be considered significant, groups of high regression coefficients were looked for (high coefficients between both saturated and dry values, for example); occasional "stray" high values were examined, but in no case did they prove to be anything other than a mathematical coincidence.

Where applicable, each parameter was regressed with values measured on the same block of ignimbrite (all cases except for the Schmidt hammer rebound and slake durability). Likewise, directionality for Owharoa

Ignimbrite measurements was maintained as appropriate. However, many of the index properties, such as bulk density, grain density, porosity, and matrix and pumice rebound, have no directionality - in these cases average values of the mechanical strength were calculated for the block, ignoring the core orientations.

For all properties, saturated and oven-dry data sets were treated separately, plus a combined data set was considered which included both saturated and oven-dry values. For these "total" data sets, the subscript "tot" was added to the standard notation for each variable.

8.2.2 Control data

The data presented by Hind (1986) were used as a control set. These were measured on several ignimbrites from the Ruahihi area of New Zealand, using the same equipment and techniques as in this study, thus ensuring comparability of the results. No other suitable data were available in the literature for control data. In most cases this was due to uncertainty regarding the precise test conditions (specimen size and shape, or moisture condition, for example).

Comparisons were made by calculating regression equations between the measured strength values of Hind (1986) and values predicted by the equations derived in this study. Ideally, if the predictions were perfect, a slope of 1.0 and intercept of 0 (together with a high regression coefficient) would be expected for these regression analyses.

8.3 Bulk rock properties

Table 8.1 presents regression coefficients for each strength property versus density (bulk density and grain density); ρ_{tot} refers to the total bulk density data set. Table 8.2 presents regression coefficients for each strength property versus porosity (effective and true), and the proportion of unconnected pore space. In the following discussion, only those parameters for which significant relationships are apparent are discussed.

	$\sigma_{c,tot}$	$\sigma_{c,dry}$	$\sigma_{c,sat}$	$\frac{\sigma_{cdry}}{\sigma_{csat}}$
ρ_{tot}		-	-	
ρ_{dry}	-	0.89	0.79	
ρ_{sat}	-	0.75	0.62	
ρ_g				

	$\sigma_{t,tot}$	$\sigma_{t,dry}$	$\sigma_{t,sat}$	$\frac{\sigma_{tdry}}{\sigma_{tsat}}$
ρ_{tot}		-	-	
ρ_{dry}	-			
ρ_{sat}	-			
ρ_g				

	c_{tot}	c	c'	$\frac{c}{c'}$
ρ_{tot}	0.55	-	-	
ρ_{dry}	-		0.54	
ρ_{sat}	-	0.61	0.69	
ρ_g				

	ϕ_{tot}	ϕ	ϕ'
ρ_{tot}		-	-
ρ_{dry}	-		
ρ_{sat}	-		
ρ_g			

Table 8.1: Regression coefficients for density against mechanical strength parameters.
- = regression not calculated as relationships non-physical

8.3.1 Density

8.3.1.1 Compressive strength

It is apparent that the compressive strength is quite strongly related to the bulk density of the material, with high regression coefficients for both saturated and dry bulk densities. However, for both the saturated and oven-dry cores, the dry bulk density gives a better indication of the compressive strength than does the saturated bulk density. This presumably represents the pore water pressures in the saturated specimens providing an additional influence on the strength, and resulting in more scatter in the values.

Of interest is the lack of a significant regression for the total bulk density data set. The saturated and oven-dry materials do not follow the same relationship with density, again presumably due to the influence of pore water pressures. Consequently, a general predictive relationship between compressive strength and bulk density is not feasible. This is confirmed by the lack of any significant relationships between the bulk density and the softening factor for compressive stresses.

Relationships between the compressive strength at the moisture extremes and the oven-dry bulk density (equations 8.1 and 8.2 below) are good, but to extend these to materials at an intermediate moisture content is unrealistic.

$$\sigma_{c,dry} = 0.06(\pm 0.01)\rho_{dry} - 67(\pm 13) \quad \text{... (8.1)}$$

$$\sigma_{c,sat} = 0.03(\pm 0.03)\rho_{dry} - 42(\pm 12) \quad \text{... (8.2)}$$

Regression equations between the measured compressive strength values of Hind (1986) and values predicted by the above equations using his dry bulk density values, give the following:

$$\sigma_{c,dry} = 1.0(\pm 0.2)\sigma_{c,dry,pred} + 3(\pm 8) \qquad r^2_{adj} = 0.79$$

$$\sigma_{c,sat} = 0.8(\pm 0.3)\sigma_{c,sat,pred} + 7(\pm 4) \qquad r^2_{adj} = 0.67$$

The dry equation, in particular, shows a significant agreement between the predicted and measured values - the agreement is not as good for the saturated equation. Taking into account the standard errors in these regressions, the derived predictive equations do adequately predict the strength of the control data, although a large error allowance exists. Dry bulk

density is, therefore, a good predictor of the compressive strength (both oven-dry and saturated) of ignimbrites.

8.3.1.2 Cohesion

Some significant regression coefficients exist for the cohesion related to the bulk density. Both saturated and dry densities are related to the cohesion; in this case it is the saturated bulk density which gives the best indication of the cohesion. There also exists some relationship between the total bulk density and cohesion data sets. The following regression equations describe these relationships:

$$c_{tot} = 0.010(\pm 0.002)\rho_{tot} - 14(\pm 4) \quad \text{... (8.3)}$$

$$c = 0.017(\pm 0.005)\rho_{sat} - 29(\pm 9) \quad \text{... (8.4)}$$

$$c' = 0.012(\pm 0.003)\rho_{sat} - 21(\pm 6) \quad \text{... (8.5)}$$

Unfortunately, Hind (1986) did not measure saturated bulk densities. Comparison of predicted and measured values using equation 8.3 (using dry bulk density as part of the total data set) shows a very poor regression, and suggests that these relationships are not generally applicable for ignimbrites. This is confirmed by there being no relationships between bulk density and softening factor, suggesting that a single, mathematical equation will not adequately describe the change in cohesion with density at all moisture contents.

8.3.2 Porosity

8.3.2.1 Compressive strength

High regression coefficients exist between compressive strength values and the effective and true porosities of the ignimbrites; these are considerably better than those for the bulk density, and apply to saturated, oven-dry, and total data sets. Some relationship also exists between porosity and the softening factor. Linear regression gives the following equations:

	$\sigma_{c,tot}$	$\sigma_{c,dry}$	$\sigma_{c,sat}$	$\frac{\sigma_{cdry}}{\sigma_{csat}}$
η_{eff}	0.77	0.96	0.93	0.68
η_{true}	0.78	0.98	0.91	
$\Delta\eta$				

	$\sigma_{t,tot}$	$\sigma_{t,dry}$	$\sigma_{t,sat}$	$\frac{\sigma_{tdry}}{\sigma_{tsat}}$
η_{eff}		0.50		0.72
η_{true}				0.58
$\Delta\eta$				

	c_{tot}	c	c'	$\frac{c}{c'}$
η_{eff}				0.50
η_{true}				
$\Delta\eta$				

	ϕ_{tot}	ϕ	ϕ'
η_{eff}			
η_{true}			
$\Delta\eta$			

Table 8.2: Regression coefficients for porosity against mechanical strength parameters.

$$\sigma_{c,tot} = -1.2(\pm0.2)\eta_{true} + 57(\pm6) \quad \text{... (8.6)}$$

$$\sigma_{c,dry} = -1.42(\pm0.08)\eta_{true} + 72(\pm3) \quad \text{... (8.7)}$$

$$\sigma_{c,sat} = -1.0(\pm0.1)\eta_{eff} + 42(\pm3) \quad \text{... (8.8)}$$

$$\frac{\sigma_{cdry}}{\sigma_{csat}} = 0.11(\pm0.02)\eta_{eff} - 0.2(\pm0.6) \quad \text{... (8.9)}$$

Comparison of values predicted using these equations and measured values of Hind (1986) gives the following regression equations:

$$\sigma_{c,tot} = 0.9(\pm0.3)\sigma_{c,tot,pred} + 7(\pm8) \qquad r^2_{adj} = 0.47$$

$$\sigma_{c,dry} = 1.1(\pm0.3)\sigma_{c,dry,pred} + 10(\pm10) \qquad r^2_{adj} = 0.71$$

$$\sigma_{c,sat} = 0.6(\pm0.2)\sigma_{c,sat,pred} + 6(\pm3) \qquad r^2_{adj} = 0.80$$

$$\frac{\sigma_{cdry}}{\sigma_{csat}} = 0.1(\pm0.3)\frac{\sigma_{cdry}}{\sigma_{csat}},_{pred} + 2(\pm1) \qquad r^2_{adj} = -0.26$$

The regression coefficient for the predicted and measured softening factors shows that the use of equation 8.9 as a predictive equation is non-sensical. Despite the relationship for the saturated values having the highest regression coefficient, the slope is significantly different from 1.0 (taking the standard error into account); the control data can be predicted from the data measured in this study, but the relationship is not direct. The other two give better values for the slope, however, the regression coefficient for the total data set is poor. The derived equation for the dry values appears to give a good prediction of the control data.

Consequently, the porosity (both true and effective), is a good indicator of the compressive strength. A predictive equation for the oven-dry compressive strength based upon the true porosity (equation 8.7) appears to apply generally to ignimbrites, and provides a more reliable prediction than the bulk density considered above.

8.3.2.2 Tensile strength

Some relationship appears to exist between the softening factor under tensile stresses and porosity, particularly the effective porosity. The following equation describes this relationship:

$$\frac{\sigma_{tdry}}{\sigma_{tsat}} = 0.29(\pm0.08)\eta_{eff} - 4(2) \quad \text{... (8.10)}$$

No control data are available with which to test the general applicability of this equation, and without a number of high regressions between tensile strength and porosity, no physical significance is attributed to this equation.

8.3.3 Physical Interpretation

From the foregoing discussion four conclusions can be drawn:

(1) compressive strength is related to dry bulk density,
(2) compressive strength is strongly related to porosity (both true and effective),
(3) a possible, weak, relationship exists between bulk density and cohesion, and
(4) tensile strength is not related to the bulk rock properties.

Physically, a relationship between the density or porosity of a rock and its compressive strength would seem intuitively reasonable (Attewell and Farmer, 1976), as the closeness of the packing of the individual grains making up the rock must influence the development and propagation of fractures. It is of some interest that the porosity gives a considerably better prediction than the density; rather than the amount of solid material contained within a unit volume of the rock, it appears to be the volume of pore space which has the greatest influence on compressive strength. As pores provide inhomogeneities, and weak zones, within the rock, stresses will concentrate around their margins. They are therefore regions around which fractures can be initiated. It is the initiation of such fractures which ultimately controls the rock strength.

Cohesion presumably arises through some form of chemical or physical bonding between individual components within the rock. Proximity of such components will no doubt enhance such bonding, hence a relationship between density and cohesion is intuitively reasonable. That such a relationship is not strongly evident suggests that other factors have a greater influence on the cohesion.

The lack of any relationships between the bulk rock properties and the tensile strength is also significant. Presumably, in tension, the density or porosity of the materials is not a significant control on the development of fractures. This implies that the fractures develop prior to the stress concentrations noted above becoming significant. This points to other factors, such as the tensile strength of individual bonds within the ignimbrites, or the

arrangement and contact relationships of individual components, having a greater influence on the tensile strength than the pore space.

These conclusions suggest lines of research for the following sections on petrography. The way in which the porosity of the ignimbrites is created (size and shape of the pores), appears to be significant for determining the controls on compressive strength. The cohesion and tensile strength appear to rely more upon other factors, possibly the arrangement of, and nature of the bonds between, individual components. These factors are examined in later chapters.

8.4 Hardness

8.4.1 Schmidt hammer rebound

For engineering purposes especially, a rapid field test which could be used as a predictor of intact ignimbrite strength would be invaluable. The Schmidt hammer has been used to some extent for this purpose in New Zealand, and has been investigated as an index test for other rock types for engineering purposes; Deere and Miller (1966) considered that the Schmidt hammer rebound, in conjunction with the unit weight of the material, provided a good index of rock strength and elastic moduli for the range of rocks they tested, and Irfan and Dearman (1978) stated that for $R \geq 40$ (N-type hammer), the Schmidt hammer was a suitable index of weathering grade in granitic rocks.

Many authors have attempted to empirically derive relationships between Schmidt rebound and other geomechanical properties, generally uniaxial compressive strength, Young's modulus, and point load strength. Most of these studies have found a curvilinear relationship between these properties (Deere and Miller, 1966; Irfan and Dearman, 1978; Sheorey *et al.,* 1984), whereas others, often considering a limited range of materials, have derived linear relationships (Al-Jassar and Hawkins, 1979; Pasamehmetoglu *et al.,* 1979). Of significance in these works is the fact that, with the exception of Deere and Miller (1966), each of these studies was dealing with a single lithology or closely related group of lithologies, and none of the derived equations were the same. This led Al-Jassar and Hawkins (1979) to conclude that, "... for each rock type there is a different correlation, ... and that the use of a single correlation chart for different lithologies could be dangerous".

	$\sigma_{c,tot}$	$\sigma_{c,dry}$	$\sigma_{c,sat}$	$\frac{\sigma_{cdry}}{\sigma_{csat}}$
R_L	0.63	0.80	0.67	0.58
R_P	0.54	0.67	0.56	

	$\sigma_{t,tot}$	$\sigma_{t,dry}$	$\sigma_{t,sat}$	$\frac{\sigma_{tdry}}{\sigma_{tsat}}$
R_L	0.50	0.62		0.61
R_P	0.59	0.81	0.52	0.81

	c_{tot}	c	c'	$\frac{c}{c'}$
R_L				
R_P				

	ϕ_{tot}	ϕ	ϕ'
R_L			
R_P			0.59

Table 8.3: Regression coefficients for Schmidt hammer rebound against mechanical strength parameters.

Obviously, the application of a previously published relationship directly to ignimbrite is inappropriate, yet it is apparent that within a lithology Schmidt hammer rebound may provide an indication of the material strength. However, each ignimbrite deposit is the product of an individual eruptive sequence, and thus chemical and textural differences between flows may result in significantly different responses for each ignimbrite. If this is the case, the use of the Schmidt hammer as a predictor of engineering properties would be limited.

8.4.1.1 Compressive strength

From table 8.3 it is apparent that strong relationships exist between the Schmidt hammer rebound and the compressive strength of the ignimbrites. Both L-type and P-type hammers give good regression coefficients, but the L-type coefficients are consistently higher for the compressive strength.

Derived predictive equations for the L-type hammer are:

$$\sigma_{c,tot} = 2.0(\pm 0.4)R_L - 30(\pm 10) \quad \text{... (8.11)}$$

$$\sigma_{c,dry} = 2.5(\pm 0.5)R_L - 40(\pm 10) \quad \text{... (8.12)}$$

$$\sigma_{c,sat} = 1.5(\pm 0.4)R_L - 30(\pm 10) \quad \text{... (8.13)}$$

$$\frac{\sigma_{cdry}}{\sigma_{csat}} = -0.17(\pm 0.06)R_L + 8(\pm 2) \quad \text{... (8.14)}$$

The equations for oven-dry and saturated specimens are very similar, with slightly different constants representing the range of compressive strength between moisture content extremes. Equation 8.11 for the total data set represents an average of these two curves. Unfortunately the data of Hind (1986) for the Schmidt hammer were not collected or presented with sufficient rigour to make them useful as a control data set.

The similarity of the equations for the extremes of moisture content, together with the good relationship with softening factor, suggest that the Schmidt hammer does provide a good field indicator of the compressive strength of ignimbrites. If estimates of the compressive strength at the moisture extremes are required then equations 8.12 and 8.13, as appropriate, should be used, otherwise equation 8.11 will give an average strength estimate. Data collected with a P-type hammer should be converted to L-type equivalent values using a calibration equation such as that presented in table 6.1.

8.4.1.2 Tensile strength

Like the compressive strength, very high regression coefficients exist for the tensile strength against Schmidt hammer rebound. However, in this case it is the P-type hammer which shows the highest regression coefficients. The following equations describe the relationships:

$$\sigma_{c,tot} = 0.06(\pm 0.02)R_P - 3(\pm 2) \quad \text{... (8.15)}$$

$$\sigma_{c,dry} = 0.06(\pm 0.02)R_P - 2(\pm 1) \quad \text{... (8.16)}$$

$$\sigma_{c,sat} = 0.06(\pm 0.03)R_P - 3(\pm 2) \quad \text{... (8.17)}$$

$$\frac{\sigma_{cdry}}{\sigma_{csat}} = -0.12(\pm 0.03)R_L + 15(\pm 3) \quad \text{... (8.18)}$$

In this case there is an even greater similarity between the equations for oven-dry and saturated conditions, with the same slopes in each case, and intercepts which agree within the standard error bounds. These two are both well described by the average equation derived for the total data set.

Again, no suitable control data exists with which to test the generality of these equations. However, the high regression coefficients, overall agreement between the relationships for saturated and dry conditions, and the existence of a good regression for the softening factor, together suggest that these are truly related, and that the results are not simply a mathematical coincidence.

8.4.1.3 Physical interpretation

As mentioned in section 6.2, hardness measurements contain a wide variety of contributing factors. This makes them difficult to interpret physically; dynamic hardness may be related to both the compressive strength and elasticity of the material (Deere and Miller, 1966).

It is of some interest that the Schmidt hammer rebound provides a good predictor of the tensile strength, as this relationship has not been examined previously. In this case, weak tensile strengths may be exerting a significant control on the Schmidt hammer rebound due to breakage of bonds or contacts within the material. Even hard ignimbrite specimens showed some indentation after a Schmidt hammer test, implying that crushing and breakage of the structure had occurred. This indentation may have resulted from the breakage of linkages in tension in the region immediately surrounding the impact site (compression must be most significant directly under the hammer

	$\sigma_{c,tot}$	$\sigma_{c,dry}$	$\sigma_{c,sat}$	$\frac{\sigma_{cdry}}{\sigma_{csat}}$
Groundmass tot	0.67	-	-	
Groundmass dry	-	0.66	0.75	
Groundmass sat	-	0.52	0.60	
Groundmass soft	-	-	-	
Pumice tot	0.57	-	-	
Pumice dry	-		0.68	
Pumice sat	-		0.74	
Pumice soft	-	-	-	0.58
Lithic tot	0.60	-	-	
Lithic dry	-		0.62	
Lithic sat	-			
Lithic soft	-	-	-	0.65

	$\sigma_{t,tot}$	$\sigma_{t,dry}$	$\sigma_{t,sat}$	$\frac{\sigma_{tdry}}{\sigma_{tsat}}$
Groundmass tot		-	-	
Groundmass dry	-			
Groundmass sat	-			
Groundmass soft	-	-	-	0.83
Pumice tot	0.58	-	-	
Pumice dry	-	0.74	0.93	
Pumice sat	-	0.76	0.94	
Pumice soft	-	-	-	
Lithic tot		-	-	
Lithic dry	-			
Lithic sat	-			0.69
Lithic soft				0.50

Table 8.4: Regression coefficients for Shore scleroscope rebound against mechanical strength parameters.
- = regression not calculated as relationships non-physical

head). Such crushing may strongly control the amount of elastic rebound of the hammer head.

8.4.2 Shore scleroscope rebound

Table 8.4 presents regression coefficients for Shore scleroscope rebound against compressive, tensile, and shear strength parameters. Groundmass, pumice, and lithic rebound hardnesses are treated separately. A large number of significant regressions can be seen in this table. Due to the relative infrequency with which the Shore scleroscope is used as an index of rock properties, a list of a large number of predictive equations describing these regression equations is seen as being of little value. Instead, areas in which significant regressions are apparent are discussed, and their ramifications in terms of the control of various components on ignimbrite strength considered. Relationships derived here are considered again in chapter 15 when the proportions of each component (measured in the petrographic examination) are included in the examination. If predictive equations are required, they can readily be derived from the data presented in earlier chapters.

8.4.2.1 Compressive strength

A number of high regression coefficients can be seen for compressive strength against both groundmass and pumice rebounds; some possible relationships also exist with the lithic rebound values. As the Schmidt hammer rebound shows a strong correlation with compressive strength, it is encouraging that the Shore scleroscope values reflect this relationship. In this case however, there is very little relationship between rebound and the softening factor under compressive stresses.

The high regression coefficients for the groundmass against compressive strength regressions suggest that the hardness of the groundmass exerts a considerable control on the compressive strength of the ignimbrite (or at least that the same factors control both properties). The oven-dry groundmass values give the highest regression coefficients for both the oven-dry and saturated compressive strengths. However, a relatively good regression still exists between the groundmass total data set, and the compressive strength total data set.

	c_{tot}	c	c'	$\frac{c}{c'}$
Groundmass tot		-	-	
Groundmass dry	-		0.55	
Groundmass sat	-		0.69	
Groundmass soft	-	-	-	
Pumice tot		-	-	
Pumice dry	-			
Pumice sat	-			
Pumice soft	-	-	-	
Lithic tot		-	-	0.53
Lithic dry	-			
Lithic sat	-			0.80
Lithic soft	-	-	-	

	ϕ_{tot}	ϕ	ϕ'
Groundmass tot		-	-
Groundmass dry	-		
Groundmass sat	-		
Groundmass soft	-	-	-
Pumice tot		-	-
Pumice dry	-		
Pumice sat	-		
Pumice soft	-	-	-
Lithic tot		-	-
Lithic dry	-		
Lithic sat	-		0.52
Lithic soft	-	-	-

Table 8.4 (cont): Regression coefficients for Shore scleroscope rebound against mechanical strength parameters.
- = regression not calculated as relationships non-physical

Interestingly, the pumice hardness also shows high regression coefficients with the saturated compressive strength. Softening of the pumice upon saturation was considerable for all specimens with significant amounts of pumice. This appears to be reflected by the pumice clasts exerting a control over the compressive strength when saturated, and may be compared with the observations in section 4.8.1 in which it was noted that many of the cracks observed in failed specimens tended to be concentrated around pumice clasts.

Some relatively high regression coefficients can be seen for the lithic clast hardness against compressive strength. However, there are only a few such coefficients; at this stage they are not considered significant.

Softening of the pumice and lithic clasts is related to the softening factor under compressive stresses.

8.4.2.2 Tensile strength

No high regression coefficients exist between the groundmass hardness and the tensile strength. However, very strong correlations are apparent between the pumice hardness and the tensile strength for both saturated and oven-dry specimens. This suggests that the hardness of the pumice clasts has a very strong influence upon the tensile strength of the ignimbrites (again, the concentration of cracks in failed specimens on the pumices was notable). This may partially be due to the small core size used for this test in which pumice clasts may account for a significant portion of the core volume, but nevertheless is believed to be an important conclusion in terms of the controls on the tensile strength of ignimbrites.

8.4.2.3 Cohesion

Few significant regression coefficients can be seen for the cohesion against component hardnesses. A possible relationship exists between the groundmass hardness and the saturated cohesion, but this is not reflected by high regression coefficients for the dry cohesion. Likewise, some relationships are seen between the lithic clast hardness and the softening factor for cohesion. Little physical justification can be seen for these regressions, given the lack of significant relationships between the lithic clast hardness and the overall cohesion values. These are interpreted as mathematical relics.

	$\sigma_{c,tot}$	$\sigma_{c,dry}$	$\sigma_{c,sat}$	$\frac{\sigma_{cdry}}{\sigma_{csat}}$
I_{d2}		0.53		

	$\sigma_{t,tot}$	$\sigma_{t,dry}$	$\sigma_{t,sat}$	$\frac{\sigma_{tdry}}{\sigma_{tsat}}$
I_{d2}				0.97

	c_{tot}	c	c'	$\frac{c}{c'}$
I_{d2}				

	ϕ_{tot}	ϕ	ϕ'
I_{d2}		0.62	

Table 8.5: Regression coefficients for slake durability index (I_{d2}) against mechanical strength parameters.

8.5 Slake durability

Regression coefficients for slake durability (I_{d2}) index against strength properties are presented in table 8.5. The absence of many significant regression coefficients is the most notable feature of this table. The only very high coefficient is that between I_{d2} and the softening factor under tensile stresses. This gives the following equation:

$$\frac{\sigma_{tdry}}{\sigma_{tsat}} = -0.36(\pm 0.03)I_{d2} + 36(\pm 2) \qquad \ldots (8.19)$$

Hind's (1986) data does not include tensile strength measurements so the general validity of this equation for ignimbrites cannot be tested. However, intuitively a relationship between softening on saturation, and the amount of breakdown during slaking cycles would seem realistic. That this only occurs for tensile stresses implies that the breakdown during slaking is due primarily to the breaking of bonds in tension. Mechanical attrition in such a test is likely to occur through chipping of small portions from the surface of the test specimens. Tensile fracture will be required for such chips to be removed. Equation 8.19 is therefore believed to have a physical basis.

Other possible relationships exist between slake durability index and dry compressive strength or angle of internal friction. These have relatively low regression coefficients, and in both cases comparison with the control data gives very poor correlations (r^2_{adj} = 0.27 and -0.50 respectively). These are not thought to be real relationships.

8.6 Ultrasonic wave velocity

As mentioned in section 7.6.4.1, seismic wave velocities measured using the equipment in this study were not used as predictors of ignimbrite strength due to the poor wave transmission, and hence high variability in the results. Only ultrasonic wave velocities were considered. Regression coefficients for ultrasonic wave velocities against strength parameters are presented in table 8.6. No significant regression coefficients exist for either of the shear strength parameters; one can be seen for the compressive strength, and a number of high coefficients occur for the tensile strength.

A sole regression coefficient of 0.66 between $v_{pu,sat}$ and $\sigma_{c,dry}$ is not considered to indicate a strong relationship between these variables. When

	$\sigma_{c,tot}$	$\sigma_{c,dry}$	$\sigma_{c,sat}$	$\frac{\sigma_{cdry}}{\sigma_{csat}}$
$v_{pu,tot}$		-	-	
$v_{pu,dry}$	-			
$v_{pu,sat}$	-	0.66		

	$\sigma_{t,tot}$	$\sigma_{t,dry}$	$\sigma_{t,sat}$	$\frac{\sigma_{tdry}}{\sigma_{tsat}}$
$v_{pu,tot}$		-	-	
$v_{pu,dry}$	-	0.73	0.59	
$v_{pu,sat}$	-	0.81	0.68	

	c_{tot}	c	c'	$\frac{c}{c'}$
$v_{pu,tot}$		-	-	
$v_{pu,dry}$	-			
$v_{pu,sat}$	-			

	ϕ_{tot}	ϕ	ϕ'
$v_{pu,tot}$		-	-
$v_{pu,dry}$	-		
$v_{pu,sat}$	-		

Table 8.6: Regression coefficients for ultrasonic wave velocity against mechanical strength parameters.
- = regression not calculated as relationships non-physical

the derived equation is used to compare predicted and measured values with the control data of Hind (1986), a poor regression results, suggesting that this relationship is not of value as a predictor of compressive strength.

In contrast, a number of high regression coefficients are seen for the tensile strength (both saturated and dry) against the ultrasonic wave velocity.

$$\sigma_{t,dry} = 0.0017(\pm 0.0004)v_{pu,sat} - 1(\pm 1)$$
$$\sigma_{t,dry} = 0.0017(\pm 0.0004)v_{pu,dry} - 1(\pm 2)$$

Obviously, within the error limits these two equations are the same. Consequently they can be combined to give a single relationship, as given in equation 8.20 below. Likewise, the equations for the saturated tensile strength can be combined into a single predictive equation, given in equation 8.21 below.

$$\sigma_{t,dry} = 0.0017(\pm 0.0004)v_{pu} - 1(\pm 2) \quad \ldots (8.20)$$
$$\sigma_{t,sat} = 0.0024(\pm 0.0007)v_{pu} - 4(\pm 2) \quad \ldots (8.21)$$

Again, no control data are available for tensile strength, but the large number of significant regression coefficients for tensile strength in table 8.6 suggests that these relationships will provide good predictive equations for ignimbrites.

It is of interest that the tensile strength appears to be well predicted by ultrasonic wave velocity whilst the compressive strength is not. A compressional wave travelling through a medium causes both compression and rarefaction, that is, both compressive and tensile stresses are applied to the rock. In the case of ignimbrites the tensile strength is considerably less than the compressive strength (chapter 4). From the results given above it would appear that this weaker tensile strength is exerting a greater influence on the wave velocity, perhaps by tensile breakage occurring at contacts between glass shards.

8.7 Summary

Linear regression analysis was used to search for relationships between geomechanical properties of the ignimbrites and a variety of index measurements. From this analysis it is apparent that a number of indices provide sufficiently good indicators of the compressive and tensile strengths of

ignimbrite to be used as predictive relationships. In particular, the Schmidt hammer rebound is a good field index of the compressive and tensile strengths of these ignimbrites, using either L-type or P-type hammers (or a combination of both). Bulk density and porosity both provide excellent predictions of the compressive strength of the material, and the ultrasonic wave velocity gives a good prediction of the tensile strength. These relationships are presented in terms of mathematical equations, with appropriate error allowances; they could be used to derive estimates of the strength parameters when laboratory measurements are impossible.

Strong relationships between compressive strength, bulk density, and porosity suggest causal relationships, with the closeness of the packing of the grains, and the size and shape of the pore spaces, having a significant control on the development of compressive strength within the materials. In contrast, these properties have very little influence upon the tensile strength.

Likewise, the Shore scleroscope rebound hardness of the groundmass and pumice components are strongly related to the compressive strength, suggesting that the strength of these components play a significant role in creating the compressive strength of the intact rock. Lithic clasts do not seem to be significant in this sense. The rebound hardness of the pumice clasts is the only Shore scleroscope rebound value to have a significant influence upon the tensile strength of the materials, suggesting that this weak component is a limiting factor in the total tensile strength of the intact rock. Shear strength parameters are unrelated to the rebound hardness of the individual components.

PART 3 - PETROGRAPHY

CHAPTER 9 - METHODS OF PETROGRAPHIC EXAMINATION

9.1 Introduction

In order to examine the nature of the petrographic control over ignimbrite strength, a petrographic examination of each block was undertaken. This aimed:

(1) to obtain quantitative data on component size, shape, and proportion (the texture of the rocks);
(2) to provide descriptive information regarding the structure of the rocks, and the contact relationships between various components (the fabric);
(3) to examine the nature of the jointing at each site; and
(4) to determine the chemical and mineralogical composition of the specimens.

This chapter discusses the methods used in the analysis.

9.2 X-Ray fluorescence

X-Ray Fluorescence (XRF) was used to determine the major element chemistry of each sample. The analysis was undertaken at Victoria University of Wellington.

The bulk rock composition of ignimbrites is not the most reliable indicator of the original melt chemistry, as sorting and alteration during transport and deposition may significantly alter the chemistry (Fisher and Schmincke, 1984). For this, the chemistry of individual pumice clasts is the only method of determining the original magmatic composition. In this study however, the bulk rock chemistry of the individual blocks was measured as it was assumed to provide a more direct association with strength on an intuitive basis, it being the composition of the actual material for which the strength was measured.

9.3 Image analysis.

A Dapple Systems ImagePlus automatic image analyser (Dapple, 1986) was used to determine component sizes for both hand specimen and thin-section samples. An object, such as a photograph or prepared sample, was

placed beneath a video camera. This was linked to an Apple IIe computer which scanned the image and recorded it as an array of 256 x 256 pixels. Each pixel was digitised with a brightness value ranging from 0 (black) to 63 (white). By manually setting discriminators for the upper and lower brightness levels a binary image could be produced in which pixels within the set brightness range were 'on' and those outside were 'off'. In this way components of interest could be selected. To assist this process a range of image enhancement software was available, together with a mouse for manual image discrimination. Having produced a binary image of the desired component, the system automatically calculated the proportion of the image included in the chosen area, and software was available which calculated and stored a variety of shape parameters for each feature within the image. A statistics package was also available which performed a range of statistical operations on the stored data.

Hand specimen samples could be analysed directly by this technique as long as a smooth surface was available. For thin-sections, a small table with diffusing glass was built to allow transmitted light to be used, and a standard bellows system attached to the lens for close-up work. The one requirement of the system was that the component of interest could be distinguished from its surroundings in terms of a grey, or brightness, scale. Pumice clasts within hand specimens were ideal for this, as were crystal grains in thin-section.

Pumice clasts in many of the ignimbrites reached lengths of up to 100 mm (table 2.1). Hence a number were greater than the 54 mm core diameter used for strength determinations. In order to derive meaningful measurements for relating to the measured strength, the total pumice population in the blocks was not considered appropriate, rather, the size and shape of the pumice clasts included within the prepared cores was thought to be the most sensible parameter. Hence, the smooth ends of prepared cores were used to provide images for analysis of the size and shape of pumice clasts.

For both crystals and pumice clasts, a standard set of measured parameters was chosen from those available. These are listed and defined in table 9.1. They were chosen as they:

Parameter	Definition
Feature area	The number of contiguous pixels which comprise the object, converted to the units of measurement according to the calibration (note, cut off minimum for counting = 5 pixels).
Length	The longest projected dimension of the feature.
Perimeter	The distance around the edges of the feature. This is summed as the pythagorean distance between the end points of each line of pixels.
Form-factor	A measure of the shape of the feature, calculated as $\frac{4\pi}{\text{perimeter}^2}$. The maximum value is 1.0 (a circle), and smaller values indicate increasing irregularity.
Fractal dimension	This describes the degree of roughness of the outline of the feature. Smooth Euclidean shapes have a dimension for the outline of 1.0, whereas outlines that are locally rough will have a larger value.

Table 9.1: Definitions of parameters measured using image analysis.

(1) describe the feature sizes (area, length),
(2) describe the actual length of contact of the feature and the matrix, and the roughness of this contact (perimeter, fractal), and
(3) describe the relative length of perimeter compared with the feature area (form-factor).

These parameters were expected intuitively to exert an influence on the strength.

Image analysis also proved a very rapid technique for obtaining a measure of the areal proportion of crystals and pumice clasts as a percentage of the total area examined. However, only the total crystal population was examined in this way as the different mineral species often showed only minimal differentiation in terms of the grey scale.

9.4 Optical microscopy.

Unfortunately, in thin-section the glass shards were not able to be distinguished from their surroundings in terms of their brightness using the image analyser. Sizes of these were measured directly from the micrometer scale in the optical microscope. The longest dimension (length) was measured, together with the shortest dimension at right angles to this length (width). From this an aspect ratio (length / width) was calculated. In order to ensure that a suitably large sample was measured the shards were measured in groups of ten. Following measurement of each sample of ten shards the mean length and standard error of the entire sample was calculated. Continued measurements were made until taking a further sample of ten shards made no difference to these statistics. This usually involved 30-50 measurements.

Modal analysis of crystal proportions was carried out from point-counting of thin-sections. For each slide 1000 points were counted; 95 % confidence limits on each proportion were calculated using a binomial distribution. For this analysis each crystal type was identified and counted separately, all other material (glass shards, pumice clasts, lithic clasts) was included together in a "non-crystal" count.

9.5 Scanning electron microscopy.

Small (~10 x 10 mm) blocks were used for scanning electron microscope study. Best results were obtained from specimens in which a

freshly broken surface was exposed, as this gave the best representation of the texture of the material. The specimens were cleaned in fresh water and dried prior to plating.

The electron microscope was used to study the fabric of the ignimbrite, looking in particular at the three dimensional arrangement of the glass shards, the nature of the porosity, and the contacts between different components. The small size of the sample studied, and the high magnifications involved in electron microscopy, resulted in exceptionally small areas being represented in each photograph. Thus detailed measurements were not taken from these photographs as the sizes were not thought to be representative of the entire sample.

	SiO_2	TiO_2	Al_2O_3	Fe_2O_3*	MnO	MgO	CaO	Na_2O	K_2O	P_2O_5	LOI	total
WHAKA/up	70.81	0.33	15.66	2.65	0.07	0.23	1.55	2.41	3.03	0.02	3.04	99.80
WHAKA/low	72.97	0.29	14.15	2.38	0.06	0.49	2.30	4.00	2.88	0.06	0.28	99.86
ONG/1	68.42	0.41	15.77	2.62	0.02	0.25	2.59	4.18	2.62	0.01	3.07	99.96
ONG/2	66.65	0.41	15.95	4.08	0.11	0.63	2.69	4.44	2.23	0.05	3.11	100.35
ONG/3	68.80	0.36	14.90	3.45	0.07	0.70	2.62	4.30	2.61	0.10	1.70	99.61
OWH/mid	73.63	0.12	12.96	1.50	0.02	0.13	1.10	2.68	3.93	0.02	4.19	100.28
OWH/low	73.67	0.11	13.00	1.56	0.02	0.14	1.13	2.81	3.89	0.02	3.94	100.29

Table 10.1: Chemical composition of ignimbrite specimens. Values are uncorrected weight percentages.
* Total Fe as Fe_2O_3
LOI = loss on ignition

CHAPTER 10 - CHEMISTRY AND MINERALOGY

10.1 Introduction

Bulk rock chemistry determined from X-Ray fluorescence, and modal crystal proportions estimated from point-counting are presented for each of the ignimbrite specimens. Modal crystal proportions are compared with areal percentages derived from image analysis to assess the quality of image analysis measurements.

10.2 Bulk rock chemistry

The data obtained from X-Ray fluorescence are presented in table 10.1. Comparison with the data of Wedepohl (1969) shows that these ignimbrites are rhyodacitic to rhyolitic in composition. The Owharoa Ignimbrite has the highest silica content of the three, and the Ongatiti Ignimbrite has the lowest. As the data here is for the bulk rocks, further geochemical interpretation is unwarranted.

10.3 Mineralogy

Modal crystal data are presented in table 10.2 for all of the ignimbrite specimens. The data for the Owharoa specimens were collected on thin-sections cut in the vertical direction. However, data from sections cut horizontally were comparable within error bounds.

For the Whakamaru Ignimbrite, a total crystal percentage of 34 ± 3 % for the lower specimen makes this the most crystal-rich ignimbrite of the three (as noted in hand specimen, table 2.1). Plagioclase feldspar is by far the most abundant mineral. Quartz is the next most abundant, with biotite, augite, hypersthene, and opaque minerals present in smaller quantities.

The Ongatiti Ignimbrite contains approximately 27 ± 3 % crystals. This does not vary significantly between the specimens (ranging from 26 ± 3 % for ONG/1 to 29 ± 3 % for ONG/3). Plagioclase feldspar is by far the most abundant mineral in all specimens, though its proportion is greatest in the ONG/3 specimen. Quartz is present in significant quantities in ONG/1, forming 2.6 % of the ignimbrite (or 10 % of the total crystal population); it is less abundant in the other two specimens. Small amounts of hornblende,

	feldspar	quartz	biotite	hornblende	augite	hypersthene	opaque	total crystal	non-crystal
WHAKA/up	19 ± 3	1.0 ± 0.8	0.5 ± 0.7		0.3 ± 0.6	0.5 ± 0.7	0.8 ± 0.8	22 ± 3	78 ± 3
WHAKA/low	29 ± 3	4 ± 1	tr		0.6 ± 0.7	tr	0.6 ± 0.7	34 ± 3	66 ± 3
ONG/1	23 ± 3	3 ± 1		0.1 ± 0.5		0.6 ± 0.7	0.1 ± 0.5	26 ± 3	74 ± 3
ONG/2	22 ± 3	1.5 ± 0.9		0.3 ± 0.6		2 ± 1	0.6 ± 0.7	27 ± 3	73 ± 3
ONG/3	27 ± 3	0.9 ± 0.8		0.1 ± 0.5		0.5 ± 0.7	0.7 ± 0.7	29 ± 3	71 ± 3
OWH/up	5 ± 1	0.7 ± 0.7	0.1 ± 0.5	0.3 ± 0.6				6 ± 1	94 ± 2
OWH/low	5 ± 1	0.3 ± 0.6	tr	tr				5 ± 2	95 ± 2

Table 10.2: Modal mineralogical analysis of ignimbrite specimens. Values are percentages, with errors representing 95 % confidence limits. All values are rounded to one significant figure.

hypersthene, and undifferentiated opaques are also seen, but no biotite or augite are present in these slides.

Crystals comprise only 5 ± 1 % of the Owharoa Ignimbrite. Of these, plagioclase feldspars comprise almost all of the crystals, with quartz the next most abundant. Small amounts of biotite and hornblende are present in the upper specimen.

10.4 Crystal proportions from image analysis

Total crystal proportions were also measured from image analysis. These data are given in table 10.3 (the equivalent values measured by modal analysis, as given in table 10.2, are included for comparison). No values are given for the Owharoa Ignimbrite, as too few crystals were present for image analysis (as will be discussed in section 11.4.2).

Errors in the image analysis values in table 10.3 are very difficult to estimate, as the machine simply counts the number of pixels which are 'on' (or white), and calculates this as a percentage of the total number of pixels. There is obviously no error involved in this calculation. However, there is an error associated with acquiring the image and accurately determining the outlines of the components. The magnitude of this error will depend upon the colour differentiation between the components of interest, and other external factors such as the quality of the lighting, and the focus of the camera. Experimental methods were designed to minimise these errors, however, they can never be totally removed, and will be different for every specimen and its particular colour characteristics. Therefore, although these percentage areas are quoted without error allowances, it should always be kept in mind that there will be a small error associated with them.

Comparison of the areal percentages measured using image analysis with the values measured using modal analysis, show the two techniques to give comparable results within error bounds. This agreement is taken as confirmation of the image analysis data. The image analysis software has been extensively tested to ensure that it measures and the feature size and shape correctly once the component of interest has been differentiated and the image acquired (Dapple, 1986). Consequently, if it can be demonstrated that the component is being adequately identified by the machine, reasonable confidence can be placed in the size and shape measurements. As the crystal area measured here is the same as that determined from modal analysis, it seems appropriate to assume that the crystals are being adequately

	image analysis	modal analysis
WHAKA/up	25	22 ± 3
WHAKA/low	31	34 ± 3
ONG /1	26	26 ± 3
ONG /2	27	27 ± 3
ONG /3	28	29 ± 3

Table 10.3: Comparison of total crystal area measurements from image analysis and modal analysis. Values are percentages of total viewed area.

recognised by the machine, and therefore that later measurements presented in chapter 11 are representative of the crystal sizes. Errors in these size measurements are derived from statistical considerations on the size distributions (95 % confidence limits). These errors are quite large, due to the variability in feature size, and hence outweigh the errors discussed above in discriminating the components.

10.5 Summary

Each of the ignimbrites is of rhyolitic to rhyodacitic composition, and shows characteristic minerals derived from a silicic magma. The Whakamaru Ignimbrite contains the greatest abundance of crystals, with the Ongatiti Ignimbrite containing only slightly fewer, and the Owharoa Ignimbrite containing virtually no large crystals. The relative abundances of each mineral varies between the ignimbrites, but in each case plagioclase feldspars are the most abundant crystals, with quartz the next most abundant, and small amounts of various other minerals.

CHAPTER 11 - TEXTURE

11.1 Introduction

In this study, the "texture" of the rocks is taken to refer to the size and shape of the individual components (the crystals, shards, pumice clasts, and lithic fragments) making up the ignimbrites. This was studied using both hand specimen (image analysis) and thin-section (image analysis and optical microscopy) samples.

Note that a complication arises with the terminology. In chapter 10, point-counting produced a "modal" analysis of the crystal proportions. This is a standard petrographic term for this type of analysis. For image analysis data, distributions of measured sizes are obtained, for which maximum, mean and modal sizes are presented. In this case, "mode" is used in the standard statistical sense of the most common size.

11.2 Whakamaru Ignimbrite

11.2.1 Shards

The groundmass of the Whakamaru Ignimbrite is very fine grained in thin-section, with shards difficult to distinguish, particularly in the lower specimen, due to minimal colour differentiation (plate 11.1). Cuspate or lunate shards representing broken bubble walls are the most common.

Shard sizes are summarised in table 11.1. The data show minimal distinction between the two specimens, with differences between the mean values all being within the quoted error allowances.

11.2.2 Crystals

In thin-section, plagioclase feldspar forms large, often zoned, tabular crystals, and small, shattered fragments. The quartz crystals are rounded, and generally show extensive resorption textures with deep embayments. The hypersthene, biotite, and hornblende crystals are small in comparison with the feldspar and quartz, and are often fractured with many pieces of the crystal missing from the section. This may be due to natural fracturing associated with eruption and transport, or may simply be the result of thin-section preparation.

(a) WHAKA/up (top) magnification 13x

A fine groundmass, with shards difficult to distinguish due to minimal colour differentiation, is typical of the Whakamaru Ignimbrite. Pale brown cuspate or lunate shards are apparent in this photomicrograph, surrounded by a darker brown background. The brown colours of the shards are indicative of extensive devitrification. The shards are randomly arranged, with no apparent alignment. Several large, white plagioclase crystals are apparent at the left of this view, and many shattered fragments can also be seen.

(c) WHAKA/low (bottom) magnification 13x

Differentiation of the shards from the background is even more difficult in the lower specimen. The ignimbrite is extensively devitrified, and the shards are cryptocrystalline, and often show a suture line along their axes when viewed under crossed polarisers. Those shards distinguishable show long,complex forms, and a general alignment.

Plate 11.1: Photomicrographs of the Whakamaru Ignimbrite specimens.

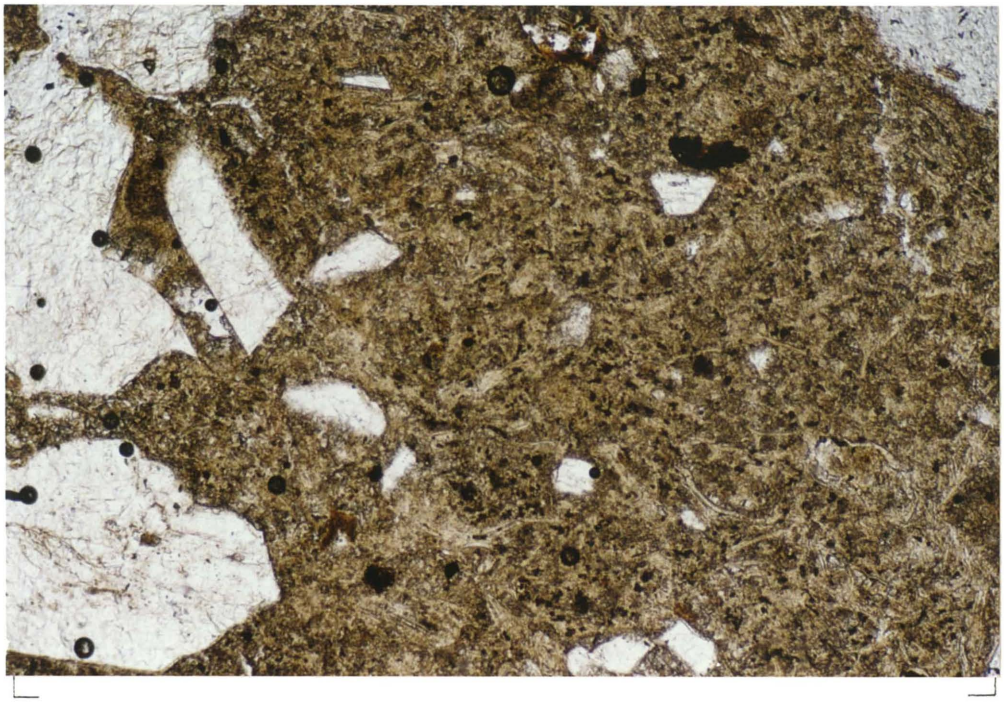

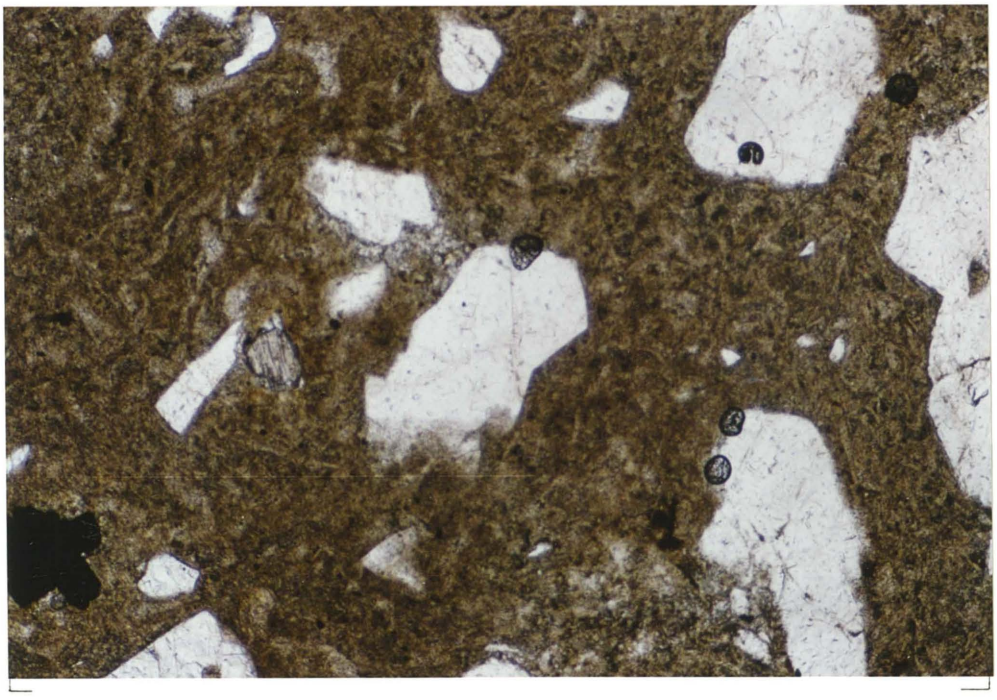

	maximum size (mm)	mean length (mm)	mean aspect ratio (length / width)
WHAKA/up	0.30 x 0.05	0.16 ± 0.01	11 ± 1
WHAKA/low	0.22 x 0.04	0.15 ± 0.01	10 ± 1

Table 11.1: Whakamaru Ignimbrite shard sizes.

specimen	parameter	minimum	maximum	mean	mode
WHAKA/up	area		1.44	0.045 ± 0.006	0.003
	length		1.74	0.23 ± 0.01	0.064
	perimeter		7.27	0.69 ± 0.04	0.30
	form-factor	0.13	1.00	0.72 ± 0.01	1.00
	fractal	1.00	2.23	1.27 ± 0.02	1.50
WHAKA/low	area		2.28	0.15 ± 0.01	0.010
	length		2.91	0.45 ± 0.02	0.17
	perimeter		10.75	1.34 ± 0.05	0.38
	form-factor	0.21	1.00	0.70 ± 0.01	0.99
	fractal	1.00	2.30	1.21 ± 0.02	1.45

	number of features	% of viewed area
WHAKA/up	521	25
WHAKA/low	683	31

Table 11.2: Whakamaru Ignimbrite crystal form data.
Units: area = mm^2, length = mm, perimeter = mm.

Opaque minerals form small crystals, often with alteration rims surrounding them.

In table 11.2 crystal form data for the Whakamaru Ignimbrite specimens are presented. For these, there is a distinct, and significant, reduction in all of the maximum, mean, and modal crystal sizes (area, length, and perimeter) in the upper specimen. This is a true variation, and, from observation of the thin-sections, appears to reflect a much greater degree of fragmentation of the crystals in the upper specimen.

The differences may be slightly exaggerated by the measurement technique, as the smaller overall population in the upper specimen required a lesser camera-to-specimen distance, and hence a greater magnification. This may slightly bias the results, as the larger crystals may not be adequately represented in the sample taken. Likewise, the lower magnification for the lower specimen means that the smaller crystals may not be included in the measured sample; in this way the differences in the true populations are exaggerated. However, this error exists for any measurement technique. It is hence accepted as unavoidable, and the results treated as the best estimates obtainable of the true measurements.

Modal form-factors of approximately 1.00 show that the bulk of the crystals are rounded in both specimens. However, the lower mean form-factors of approximately 0.70 show that the populations have a significant portion of non-rounded crystals - these are probably the common tabular forms of plagioclase feldspars. Fractal dimensions of 1.45 and 1.50 represent a degree of roughness along the outlines. This is believed to reflect the resorption features noted for many of the quartz crystals.

11.2.3 Pumice

Insufficient pumice clasts were available for any quantitative analysis. Estimates by eye of the proportion of pumice clasts suggest that they comprise less than 1 % (rare, table 2.1) of the lower specimen, and approximately 5 % (scarce, table 2.1) of the upper specimen. As noted in the site descriptions (table 2.1), they are generally rounded in both specimens.

11.3 Ongatiti Ignimbrite.

The shard texture of the Ongatiti Ignimbrite is readily distinguished in all specimens due to clear colour distinction between the shards and the

	maximum size (mm)	mean length (mm)	mean aspect ratio (length / width)
ONG/1	0.40 x 0.05	0.15 ± 0.02	7 ± 1
ONG/2	0.39 x 0.09	0.19 ± 0.02	10 ± 1
ONG/3	0.53 x 0.15	0.19 ± 0.02	13 ± 1

Table 11.3: Ongatiti Ignimbrite shard sizes

	parameter	minimum	maximum	mean	mode
ONG/1	area		1.78	0.11 ± 0.01	0.01
	length		3.31	0.42 ± 0.02	0.14
	perimeter		9.39	1.25 ± 0.06	0.38
	form-factor	0.17	1.00	0.69 ± 0.01	0.65, 0.99
	fractal	1.00	2.04	1.23 ± 0.03	1.45
ONG/2	area		1.48	0.09 ± 0.01	0.01
	length		2.12	0.39 ± 0.02	0.18
	perimeter		7.46	1.11 ± 0.06	0.40
	form-factor	0.17	1.00	0.67 ± 0.01	0.64, 0.98
	fractal	1.00	2.37	1.25 ± 0.03	1.40
ONG/3	area		1.62	0.12 ± 0.01	0.02
	length		2.31	0.42 ± 0.02	0.14
	perimeter		7.53	1.23 ± 0.06	0.40
	form-factor	0.19	1.00	0.72 ± 0.01	0.65, 0.98
	fractal	1.00	2.14	1.24 ± 0.02	1.45

	number of features	% of viewed area
ONG/1	353	26
ONG/2	329	27
ONG/3	444	28

Table 11.4: Ongatiti Ignimbrite crystal form data.
Units: area = mm^2, length = mm, perimeter = mm.

surrounding material (plate 11.2). Shards are platy or cuspate, with many complex forms, such as "Y-junctions" (Fisher and Schmincke, 1984), representing the junction of three or more bubbles

11.3.1 Shards

Shard size and aspect ratio data for the Ongatiti Ignimbrite are presented in table 11.3. The shards are slightly smaller (maximum size) in the ONG/1 and ONG/2 specimens than in the ONG/3 specimen; this is not marked. Accompanying this smaller overall shard size is a slightly smaller mean length, and a significantly smaller aspect ratio in the ONG/1 specimen. Again, these variations are measurable, but not marked.

11.3.2 Crystals

Plagioclase feldspar crystals occur as subhedral crystals with tabular forms, or small fragments broken during the eruption. The crystal margins are rounded due to resorption in all specimens, and in the ONG/3 specimen some deep embayments occur, together with frequent zoning of the crystals. A coarse fracturing is also apparent in some plagioclase crystals. This breaks the crystal into small units by seemingly exploiting the cleavage planes, yet the overall form of the crystal is preserved. Quartz exists as anhedral crystals with rounded outlines and deep embayments due to resorption. These resorption features are most apparent in the ONG/3 specimen, and least so in the ONG/1 specimen. Hornblende, hypersthene, and opaque minerals are all small compared with the quartz and feldspar crystals.

Table 11.4 presents crystal form data for the crystal population in each of the Ongatiti Ignimbrite specimens. Very little in the way of systematic changes can be seen between the specimens; differences in the mean values for area, length, and perimeter can be accounted for by the quoted error allowances. All specimens show similar form-factors and fractal dimensions, suggesting similar crystal shapes in all three. Each specimen shows a bimodal form-factor distribution, with one mode at approximately 0.98, representing almost circular features, and another mode at about 0.65 representing a group of less regular crystals. This lower mode is believed to represent the tabular plagioclase crystals. The fractal dimension shows that local roughness features exist , which, in many cases, are believed to represent the resorption features of the quartz crystals, as discussed above.

(a) ONG/1 (top) magnification 13x

The shard texture of the Ongatiti Ignimbrite is readily distinguished. The shards in this photomicrograph are crisp and white, and surrounded by an amber background; devitrification is only slight. These shards are platy or cuspate, and many "Y-junctions" are apparent. Shards are randomly arranged. Numerous large, white plagioclase crystals can be seen.

(b) ONG/2 (bottom) magnification 13x

In this view the shards are curved, and show a partial alignment. This alignment is apparent between the crystals, but the shards are randomly arranged in other areas. The shards remain crisp and white in this specimen, and the background is amber to pale brown, indicating only slight devitrification.

Plate 11.2: Photomicrographs of the Ongatiti Ignimbrite specimens.

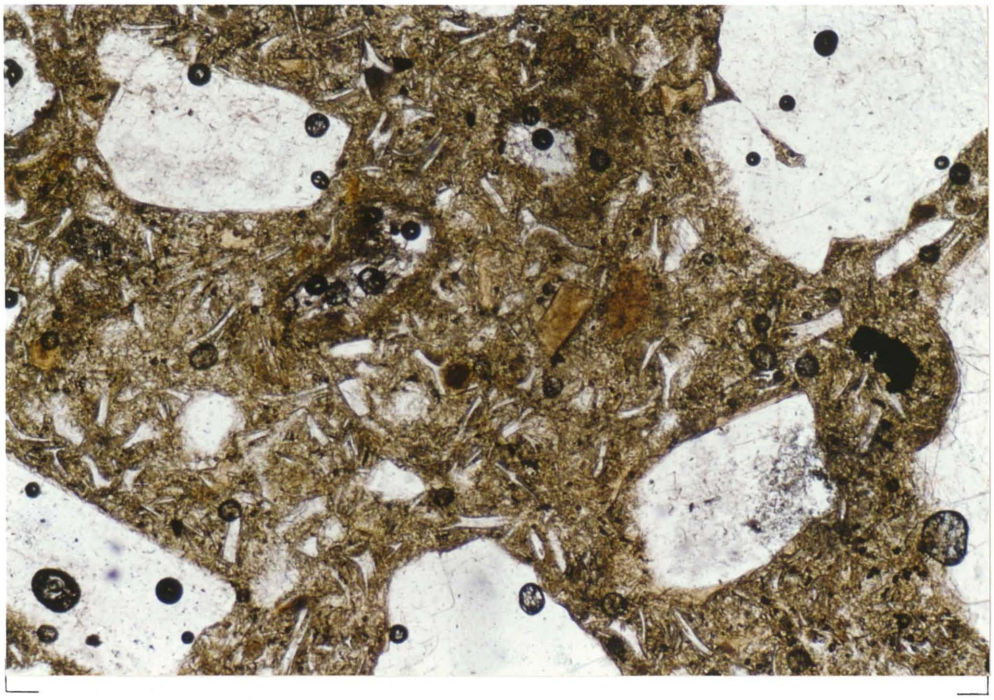

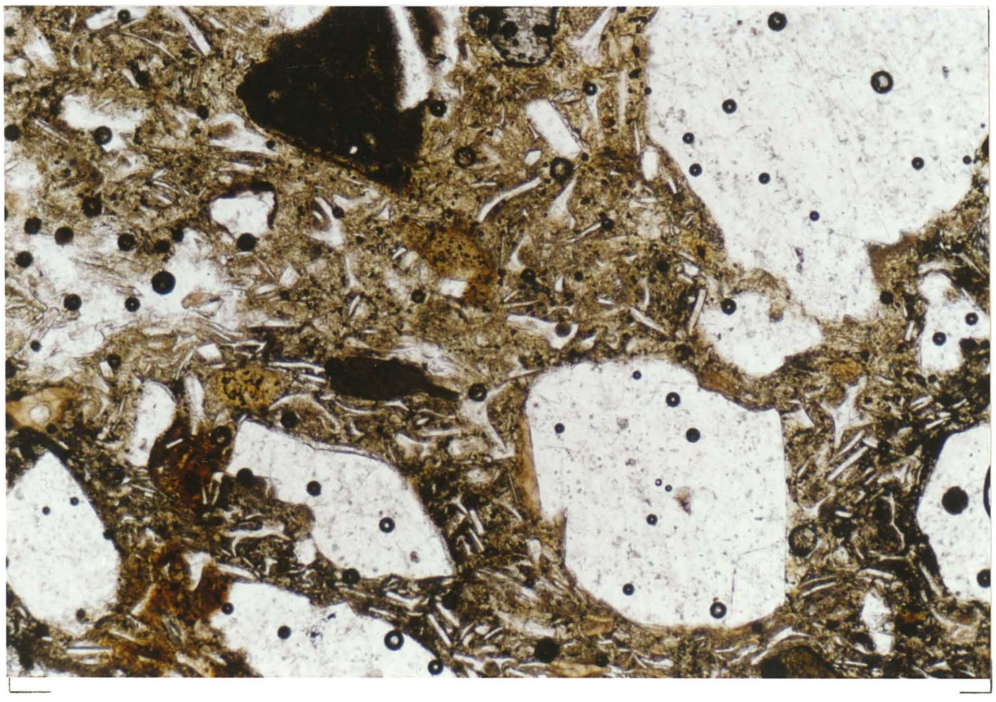

(c) ONG/3 magnification 13x

Pale brown, cuspate shards are apparent in this photomicrograph. They tend to be noticably elongated, and show a general alignment (occasional patches of non-aligned shards are seen). The pale shard colours and pale brown background suggest that devitrification is somewhat more extensive in this specimen than in the other Ongatiti Ignimbrite specimens, but the difference is not great.

Plate 11.2(cont.): Photomicrographs of the Ongatiti Ignimbrite specimens.

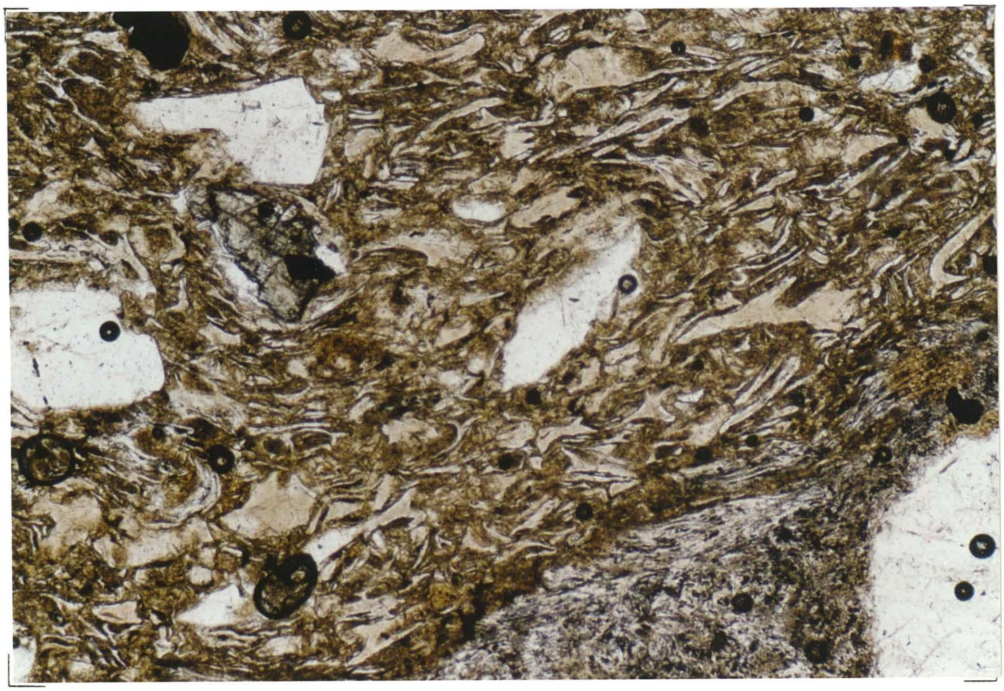

	parameter	minimum	maximum	mean	mode
ONG/1	area		878	8 ± 2	0.7
	length		50.4	2.5 ± 0.2	1.3
	perimeter		153.4	7.1 ± 0.5	2.6
	form-factor	0.17	1.00	0.75 ± 0.01	1.00
	fractal	1.00	2.31	1.15 ± 0.03	1.45
ONG/2	area		717	9 ± 2	0.6
	length		50.5	2.8 ± 0.2	1.3
	perimeter		190.5	8.1 ± 0.7	2.5
	form-factor	0.21	1.00	0.75 ± 0.01	1.00
	fractal	1.00	2.37	1.15 ± 0.03	1.45
ONG/3	area		174	5 ± 1	0.6
	length		25.4	2.5 ± 0.2	2.7
	perimeter		101.1	7.5 ± 0.6	1.3
	form-factor	0.17	1.00	0.70 ± 0.01	1.00
	fractal	1.00	2.44	1.16 ± 0.04	1.60

	number of features	% of viewed area
ONG/1	629	23
ONG/2	428	16
ONG/3	255	5

Table 11.5: Ongatiti Ignimbrite pumice form data.
Units: area = mm^2, length = mm, perimeter = mm.

11.3.3 Pumice

Measurements of the size and shape of the pumice clasts are presented in table 11.5. The maximum size (area, length and perimeter) of the pumice clasts in the ONG/3 specimen is considerably less than that in the ONG/1 and ONG/2 specimens. This is reflected by a slightly smaller mean area in this ONG/3 specimen, but the modal sizes are essentially the same in all three.

Mean form-factors are the same in the ONG/1 and ONG/2 specimens, but slightly less in the ONG/3 specimen, implying a greater degree of flattening of the clasts in the lower specimen. However, modal form-factors are the same in all three (1.00) - the small clasts are rounded in all cases.

The mean fractal measurements are the same (within error limits) in all specimens, but the modal value in the ONG/3 specimen is greater. This suggests that the pumice clasts in the ONG/3 specimen have a much rougher outline than those in the ONG/1 and ONG/2 specimens.

11.4 Owharoa Ignimbrite

A complex groundmass texture dominated by numerous small pumice clasts is characteristic of the Owharoa Ignimbrite in thin-section (plate 11.3). The distinction between pumice clasts and glass shards is somewhat subjective as material of all sizes ranging from individual shards, through small clasts of a few vesicles thick (pumice shards), to relatively large pumice clasts is present. This is particularly true for the upper specimen. The shards are difficult to distinguish from the background fine material due to only minimal colour differentiation. Those visible are cuspate, with occasional "Y-junctions" and similar complex forms.

11.4.1 Shards

Table 11.6 gives the size and aspect ratios for glass shards from both vertical and horizontal thin-sections of the Owharoa Ignimbrite. Two trends are apparent: the shards are somewhat longer in the lower specimen than in the upper one, and they are longer and have a greater aspect ratio in vertical sections than in horizontal ones. Individually these trends could merely represent sorting within the flow, or alignment with the flow direction respectively. However, together they are taken to be evidence of some

(a) OWH/up (top) magnification 13x

The groundmass texture of the Owharoa Ignimbrite is characteristically very complex, with numerous very small pumice clasts, including pumice shards being apparent. This makes the distinction between pumice clasts and glass shards difficult. In this photomicrograph white shards are enclosed in a pale brown background, indicating only minimal devitrification. The shards have complex forms: platy, curved, and cuspate shards are all present in the shard population. A partial to general alignment is apparent, particularly near pumice clasts.

(b) OWH/low (bottom) magnification 13x

Strong alignment of the glass shards exist in the lower specimen. The shards have a complex form, many "Y-junctions" and pumice shards are apparent. White to pale brown shards are surrounded by a pale brown background, indicating slight devitrification.

Plate 11.3: Photomicrographs of the Owharoa Ignimbrite specimens.

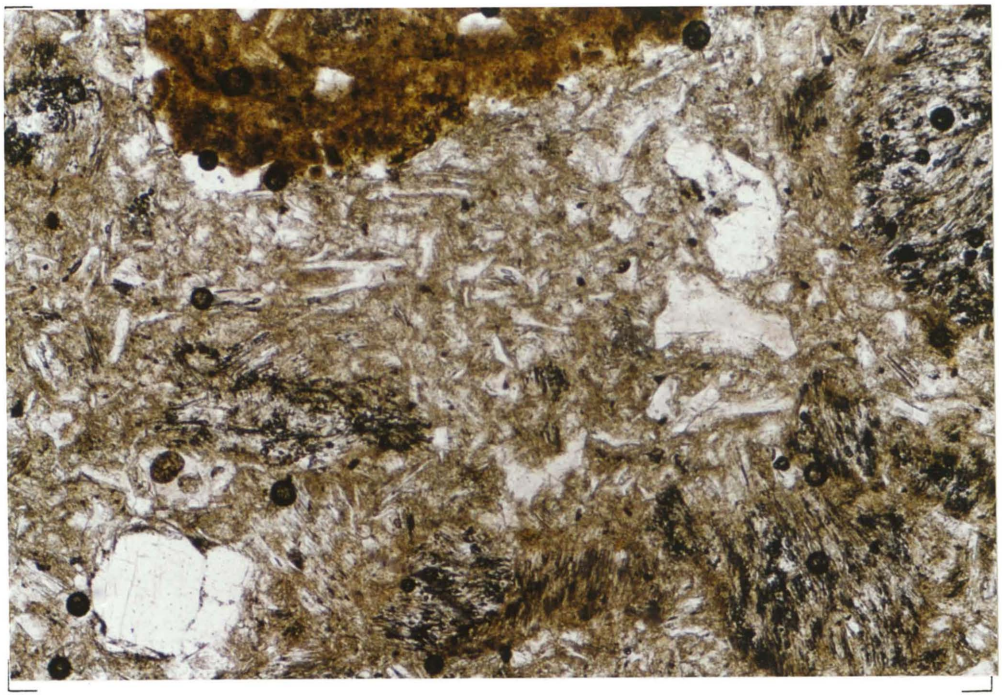

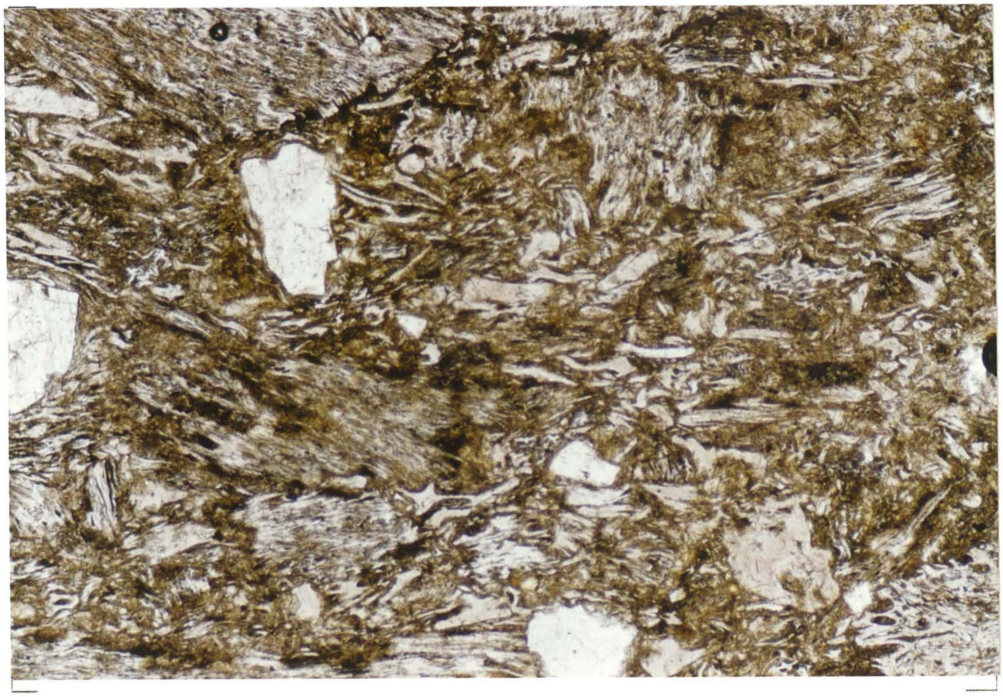

	orientation	maximum size (mm)	mean length (mm)	mean aspect ratio (length / width)
OWH/up	vertical	0.43 x 0.02	0.15 ± 0.02	10 ± 1
	horizontal	0.25 x 0.05	0.13 ± 0.01	7 ± 1
OWH/low	vertical	0.90 x 0.02	0.19 ± 0.02	10 ± 1
	horizontal	0.53 x 0.04	0.19 ± 0.02	8 ± 1

Table 11.6: Owharoa Ignimbrite shard sizes.

	parameter	minimum	maximum	mean	mode
OWH/up horizontal	area		949.8	4.4 ± 0.9	0.6
	length		49.34	2.32 ± 0.07	1.24
	perimeter		134.5	6.7 ± 0.2	2.5
	form-factor	0.13	1.00	0.74 ± 0.01	1.00
	fractal	1.00	2.89	1.25 ± 0.02	1.45
OWH/up vertical	area		142.8	3.1 ± 0.3	0.6
	length		18.52	2.26 ± 0.07	1.18
	perimeter		51.8	6.2 ± 0.2	2.5
	form-factor	0.21	1.00	0.78 ± 0.01	1.00
	fractal	1.00	2.14	1.15 ± 0.02	1.44
OWH/low horizontal	area		298.3	4.4 ± 0.5	0.6
	length		29.10	2.39 ± 0.07	1.26
	perimeter		104.1	6.9 ± 0.2	2.7
	form-factor	0.14	1.00	0.77 ± 0.01	1.00
	fractal	1.00	2.43	1.19 ± 0.02	1.40
OWH/low vertical	area		261.5	3.5 ± 0.3	0.8
	length		40.91	2.55 ± 0.07	1.28
	perimeter		118.9	6.9 ± 0.2	2.6
	form-factor	0.18	1.00	0.75 ± 0.01	1.00
	fractal	1.00	2.58	1.20 ± 0.01	1.49

	number of features	% of viewed area
OWH/up-vertical	1185	23
OWH/up-horizontal	976	11
OWH/low-vertical	1149	16
OWH/low-horizontal	1661	13

Table 11.7: Owharoa Ignimbrite pumice form data.
Units: area = mm^2, length = mm, perimeter = mm.

compaction and distortion of the shards during cooling of the ignimbrite. The differences are not large, suggesting that this distortion is not great.

11.4.2 Crystals

Most of the crystals present in the Owharoa Ignimbrite are small fragments - complete crystals are very rare. Plagioclase fragments are often zoned, and frequently show a combination of rounded and sharp edges on one fragment. The rounded edges are interpreted as original crystal margins showing rounding due to resorption, whereas the sharp edges are the broken faces of the fragmented crystals. Quartz crystals are also fragmented; resorption features similar to, but not as marked as, the ones noted for the Ongatiti and Whakamaru Ignimbrites are seen. Biotite and hornblende form small, tabular crystals.

The paucity of crystals in the Owharoa Ignimbrite meant that an insufficient number could be measured using image analysis to give a suitable statistical analysis of the sizes. From measurements using the optical microscope, they reach a maximum length of approximately 1 mm, with an estimated modal length of approximately 0.2 mm.

11.4.3 Pumice

Table 11.7 presents the pumice form data for the Owharoa Ignimbrite, with measurements undertaken for both horizontal and vertical planes. There is little difference between the two specimens, in that the clasts in the horizontal plane in both the upper and lower specimens have very similar mean and modal sizes, and likewise for the clasts in the vertical plane for each specimen. However, there is a significant difference in the mean areas measured for the vertical and horizontal planes; the clasts are significantly smaller in the vertical plane. As the mean lengths are similar in each plane, this smaller area represents the significant flattening of the clasts noted in table 2.1. This flattening is not reflected in the form-factor measurements. This implies that the smaller clasts, which, by virtue of their numbers, become very important in the total distribution, are generally rounded, and the flattening is largely confined to the larger clasts. This is in keeping with thin-section observations, in which clast flattening is not marked.

Fractal dimensions are similar in all cases, implying similar roughness for the outlines of each. These fractal dimensions are similar to those

	groundmass	crystals	pumice	lithics
WHAKA/up	69	25	<5	<1
WHAKA/low	67	31	<1	<1
ONG/1	50	26	23	<1
ONG/2	56	27	16	<1
ONG/3	76	28	5	<1
OWH/up	79	6	17	<1
OWH/low	80	5	14	<1

Table 11.8: Proportions of each component for the specimens studied. Values are areal percentages.

measured for the pumice clasts in the Ongatiti Ignimbrite, and considerably less than the fractal dimensions measured for the crystals in the Whakamaru and Ongatiti Ignimbrites. The pumice clasts in both cases, therefore, have smoother perimeters than the crystals.

11.5 Component proportions

In table 11.8 the areal proportions of each component are presented for all of the specimens. The crystal proportion was measured by both image analysis and point-counting, and gave comparable results within error bounds, as discussed in section 10.4. So that the data for each component are consistent, the image analysis proportions were chosen for further analysis. Pumice proportions were obtained from the image analysis data presented in tables 11.5 and 11.7. No independent check was available for these measurements. The lithic component of each ignimbrite, the crystals in the Owharoa Ignimbrite, and the pumice component of the Whakamaru Ignimbrite were too insignificant to be accurately determined using image analysis (sufficient volume of material could not be examined to give a representative sample). The crystal proportion of the Owharoa Ignimbrite was obtained from the point-counting data; the lithic proportions for each specimen, and the pumice proportions for the Whakamaru Ignimbrite were estimated (see table 2.1). The groundmass proportion was obtained by subtraction from 100 %.

11.6 Summary

Mean shard sizes are similar in all of the ignimbrites. Some variations exist between specimens from the Owharoa and Ongatiti Ignimbrites, with the lower Owharoa and ONG/3 specimens having slightly longer shards, with a greater aspect ratio, than their counterparts. Crystal sizes are variable, depending on the degree of fragmentation of the crystals.

Pumice clasts of a wide range of sizes are present; those in the Owharoa Ignimbrite are consistently smaller than those in the Ongatiti Ignimbrite on average, but their modal sizes are similar. Large pumice clasts in the Owharoa Ignimbrite are flattened when viewed in the vertical plane with respect to their form in the horizontal plane; small pumice clasts do not appear to show this flattening.

The Whakamaru Ignimbrite contains the highest proportion of crystals, and the least proportion of pumice clasts. The Ongatiti Ignimbrite is rich in

both crystals and pumice clasts, and consequently has the least proportion of groundmass in general (the lower specimen is an exception). The Owharoa Ignimbrite has a relatively high proportion of pumice clasts, but is relatively depleted in crystals compared with the other two ignimbrites.

The data measured in this chapter are used in chapter 15 to examine the influence of textural parameters on the geomechanical properties of the ignimbrites.

SHARD FORM:	the shape of individual glass shards derived from fragmentation of the vesiculated magma
platy:	shards are flat plates from the glass walls separating large flattened vesicles*
curved:	shards are platy, but show considerable curvature
cuspate:	cuspate or lunate shaped fragments of broken bubble walls that are commonly Y-shaped in cross-section representing remnants of three bubble junctions*
complex:	the shard population contains a mixture of platy, curved, and complex shards
SHARD ALIGNMENT:	the extent to which shard faces are parallel
random:	shards show no preferred orientation
partial:	shards are aligned in localised patches (generally between crystals or clasts), but show random orientations elsewhere
general:	considerable shard alignment (long axes aligned within about ± 10 °) occurs for most of the groundmass, but some areas exist of less regular alignment
parallel:	the bulk of the shards are aligned to be parallel
SHARD CONTACTS:	the angle at which the individual shards contact
none:	shards do not contact
point:	shards contact at a high angle (> 45 °), giving point contacts (in two dimensions) only
tangential:	shards contact at a low angle (< 45 °), giving a longer distance of contact
complete:	the shard edges are conformable with one another
PORE SHAPE:	the roundness or otherwise of pores
rounded:	pores are rounded
slightly elongated:	some degree of flattening of the pores is apparent
elongated:	pores are noticeably elliptical
strongly elongated:	pores are compressed to form ellipses with large aspect ratios
PORE FILLING:	the density of material infilling the pores created by the glass shards
vapour phase:	crystals formed by deposition from a vapour phase fill otherwise open pore spaces
open:	pore spaces have only small, amounts of fragmentary material in them; this is loosely packed
partial:	pore spaces are approximately half-filled with fragmentary material
dense:	the pore spaces have an extensive filling of fragmentary material which is densely packed

Table 12.1: Terminology used for fabric description.
* Definitions from Fisher and Schmincke (1984)

CHAPTER 12 - FABRIC

12.1 Introduction

In this study, the "fabric" of the rocks is taken to refer to the orientation and arrangement of the various components, and the contact relationships between them. The fabric was studied using thin-sections and scanning electron microscope images.

12.2 Previous studies of microfabric

Microfabric has been appreciated as an important factor in the strength of clay soils for some time, particularly those of marine origin. This has led to a number of classification schemes being erected to describe the microscopic structure of such materials (for example, Grabowska-Olszewska *et al.*, 1984). These were reviewed by Huppert (1986), who has recently demonstrated that the microfabric of soft, clay-rich sedimentary rocks from New Zealand can also exert a strong influence over the mechanical behaviour of these materials Huppert (1986, 1988) .

As a corollary to this, it may be expected that microfabric is an important property in determining the mechanical behaviour of soft pyroclastic materials such as ignimbrites. Preliminary studies of this have been undertaken by Rippa and Vinale (1983) and, for a specific lithophysal zone, by Price *et al.* (1985). These studies, particularly the former, suggested that microstructural control may be significant, but were of insufficient detail to be definitive.

12.2.1 Terminology

Heiken (1972) and Heiken and Wohletz (1985) have undertaken a very detailed electron microscope description of volcanic ash materials, and used this in the interpretation of eruption conditions. The study relied upon describing the form and surface features of individual pyroclasts, and many classification terms were developed for this purpose. Unfortunately, these do not apply directly to ignimbrites, where it is the contacts and aggregations of individual components which are of greatest interest. Likewise, the microstructural terms discussed by Huppert (1986) for clay materials are not directly applicable to ignimbrites.

CRYSTAL FORM: the extent of fragmentation and shattering of the crystals

whole:	crystals retain their form developed in the magma chamber
slight breakage:	some crystals show shattering, and occasional fragments occur
shattered:	most crystals are shattered, and fragments are common
fragments:	whole crystals are rare

CRYSTAL / GROUNDMASS CONTACT: the extent to which crystals are bound to the groundmass

plucked:	crystals are removed by specimen preparation techniques
loose:	crystals remain in the groundmass during specimen preparation, but are loose, with a physical separation between the two components
non-welded:	crystals are firmly bound within in the groundmass, but no actual welding occurs between the glass shards and the crystals
welded:	crystals are welded to the glassy components (commonly occurs for phenocrysts within pumice clasts)

PUMICE FORM: the extent of alteration and breakage of pumice clasts

spherulitic:	pumice clasts are devitrified, and have lost their pumiceous texture
open, glassy:	clasts are not devitrified, they have open vesicles
fragmented, glassy:	clasts are not devitrified, breakage of some vesicle walls has occurred
dense, glassy:	clasts are not devitrified, vesicle breakage has partially infilled the vesicles with broken fragments

PUMICE / GROUNDMASS CONTACT: the extent to which pumice clasts are bound to the groundmass

lapping:	the groundmass shards lap against the pumice clasts with no welding; this is the only type of contact observed

Table 12.1 (cont.): Terminology used for fabric description.

The terminology of Carr (1981), who undertook a scanning electron microscope study of the post-depositional changes in the Matahina Ignimbrite, is appropriate, but is only applicable to the post-depostional alteration features. Consequently, for this study, the terms applied are specific to the problem being addressed. They are defined in table 12.1, and were chosen to incorporate, where possible, appropriate aspects of previous schemes, and not to contradict them.

12.3 Whakamaru Ignimbrite

12.3.1 Groundmass

Shard alignment is marked in the lower Whakamaru Ignimbrite specimen, the shards are generally within approximately ± 10 ° alignment (plate 11.1a). This is referred to as "general" alignment (table 12.1). The shards are randomly arranged in the upper specimen (plate 11.1b).

Under the scanning electron microscope, the lower Whakamaru Ignimbrite specimen appears as a very densely packed material, with little definition between the components (plate 12.1b). Some large, apparently glassy, curved shards can be identified as bright ridges. The shards lie very close together, leaving narrow spaces between them, but their curvature results in essentially rounded spaces. These gaps between the shards are densely infilled with broken, glassy fragments, giving the low porosity noted in table 5.1.

In contrast, the upper specimen has a very open structure, with large void spaces (plate 12.1a). The shards are completely devitrified, having become coarsely crystalline throughout their entire thickness, yet they retain a platy form. Very rarely are they in direct contact with other shards, except at their corners or over very limited surface areas of contact. Surrounding the shards is an extensive network of coarsely crystalline material which is attributed to vapour phase alteration. This has produced a loose infilling of crystals throughout the void spaces, however, the crystals do not interlock but still leave an open structure. Photography of the WHAKA/up specimen under the scanning electron microscope was unsuccessful due to the very high contrast of the vapour-phase component. Plate 12.1a is the best photograph obtained.

(a) WHAKA/up (top) magnification 430x

Several large "glass shards" are apparent surrounding a pore in the centre of this view. These shards have undergone complete devitrification, and now appear as "carpets" of coarsely crystalline material. They define a large, rounded pore. Surrounding the shards (top right) is a background of coarse, crystalline material representing deposition from a vapour phase.

(b) WHAKA/low (middle) magnification 500x

The groundmass of this specimen is densely packed, with little definition of individual components. Bright ridges believed to represent glass shards can be seen. These are long and curved, with complex forms. They describe rounded pore spaces (lower right) which are densely infilled with fine, fragmentary material.

(c) WHAKA/low (bottom) magnification 270x

A "pluck hole" representing the former site of a crystal is seen in the centre of this view. These are very common in the Whakamaru Ignimbrite, and attest to a weak bonding between the crystals and the groundmass. Chemical analysis of the surface of this pluck hole shows an enrichment of iron compared with the surrounding matrix. This is believed to be the result of weathering.

Plate 12.1: Groundmass fabrics for the Whakamaru Ignimbrite.

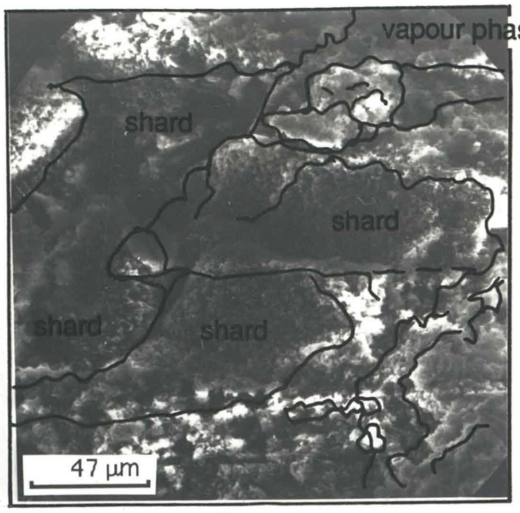
vapour phase material
shard
shard
shard
shard
47 µm

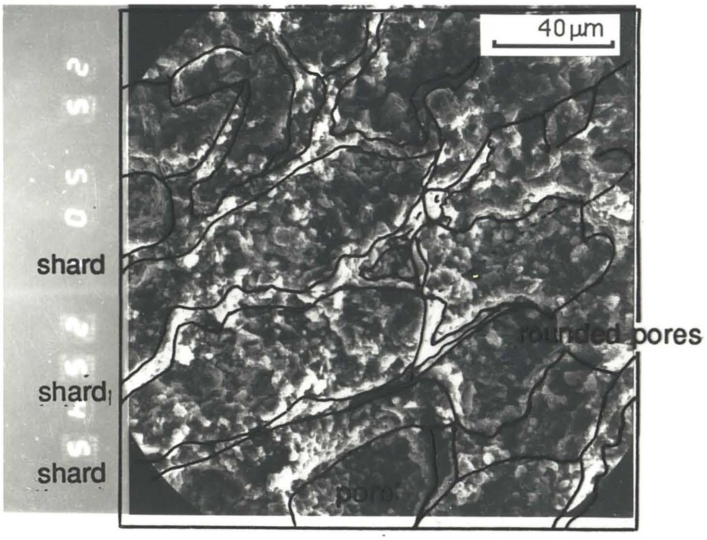
40 µm
shard
shard
shard
rounded pores
pore

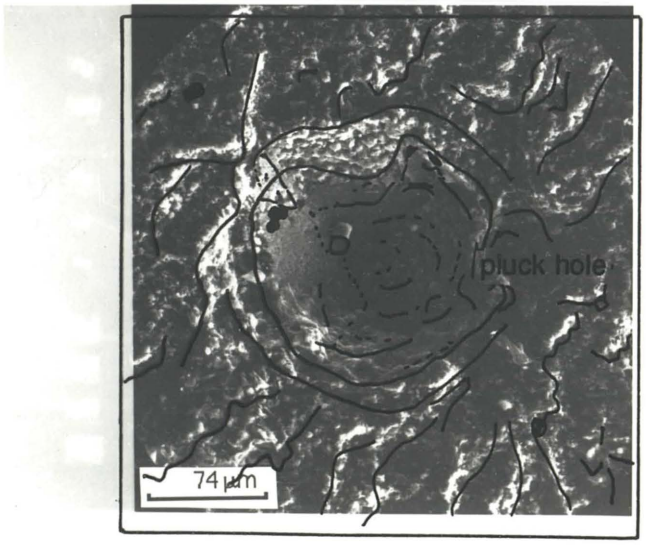
pluck hole
74 µm

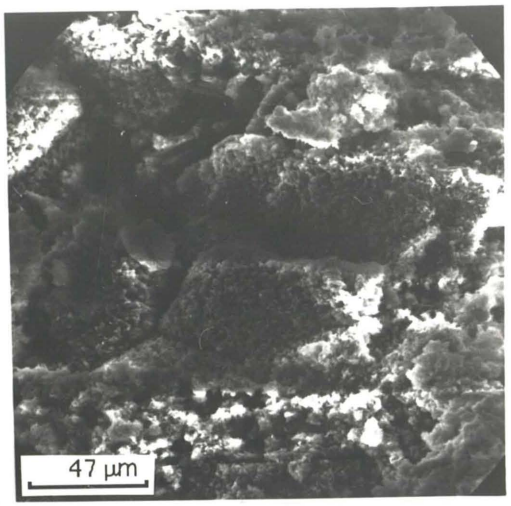
47 µm

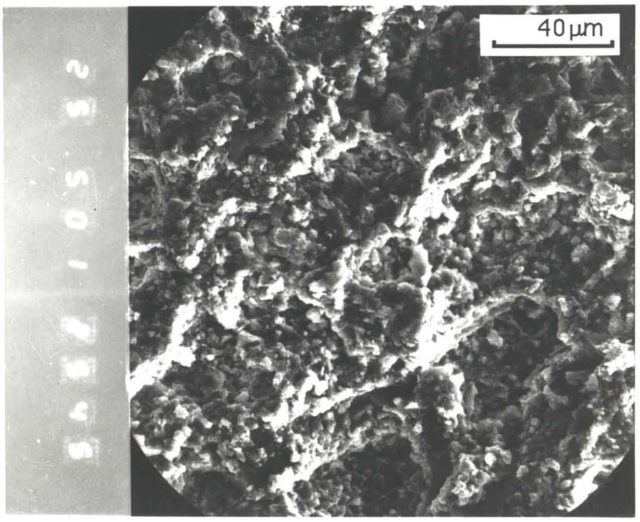
40 µm

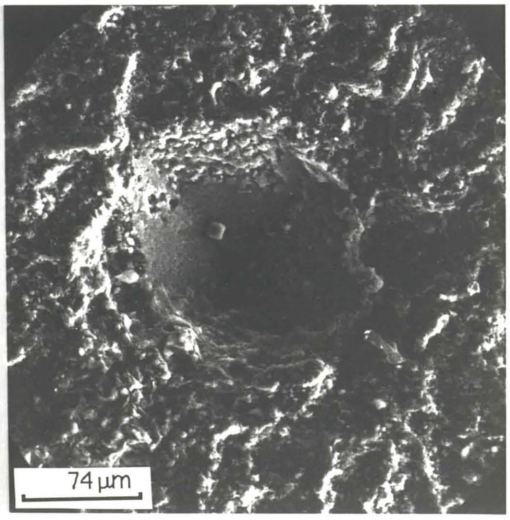
74 µm

12.3.2 Crystals

Contacts between the crystals and the groundmass are apparently very weak, as evidenced by a large number of "pluck holes" (plate 12.1c) seen in this ignimbrite. These represent the space in which crystals sat prior to specimen preparation; their removal by preparation techniques suggests a very weak contact.

12.3.3 Pumice

As noted in section 11.2.3, pumice clasts are very rare in this ignimbrite. None were able to be identified from scanning electron microscopy. All pumice clasts identified from thin-section examination show cryptocrystalline textures, often with extensive spherulite development. None of the original pumiceous textures are apparent in either specimen.

12.4 Ongatiti Ignimbrite

12.4.1 Groundmass

The differences in shard aspect ratio noted for the Ongatiti Ignimbrite in section 11.3.1 is associated with variations in the degree of alignment of the shards. In the ONG/1 specimen they tend to be randomly arranged, with no apparent alignment. In the ONG/2 specimen they have a partial alignment which shows up as the long axes of the shards being essentially parallel in localised areas, particularly between crystals, but randomly arranged in other areas. In the ONG/3 specimen they show general alignment, with the shards having the same overall orientation to within ± 10 °.

From the scanning electron micrographs in plate 12.2 it can be seen that this increased shard size and alignment is accompanied by a change in the contact relationships between the shards. In the ONG/1 specimen (plate 12.2a), randomly arranged shards tend to contact only at localised points, with a large angle described by the contacting shards (generally > 45 °). In the ONG/2 specimen (plate 12.2b), the shards are somewhat aligned, yet still only tend to contact at localised points where the curvature of the shards results in them touching tangentially - the angle between the shards is small (generally < 45 °). In the ONG/3 specimen (plate 12.2c) tangential contacts are the norm, however, the area of contact is greater, as the shards are now almost

(a) ONG/1 (top) magnification 180x

A number of large, platy glass shards are apparent; they are randomly arranged, with very limited contact points between the shards. This results in large, open, rounded pore spaces. A pervasive coating of fine, fuzzy material is apparent throughout this plate.

(b) ONG/2 (middle) magnification 330x

Packing is denser in this specimen, but individual glass shards can be seen with a variety of orientations; two small, platy shards in the centre have their large surfaces aligned parallel to the page, one large shard near the lower right (seen in section) is aligned perpendicular to these. However, a partial alignment means that the open structure of (a) above is lost. Pore space between the shards has a significant infilling of fine, fragmentary material, but this is not densely packed. The shard seen in section shows a clean, glassy face with no evidence of crystallisation. All other surfaces in the view are coated in the same fuzz as in (a) above.

(c) ONG/3 (bottom) magnification 330x

The shards in this specimen have much more complex, curved forms than those above. A rounded "bubble" feature representing the walls of a vesicle in the original melt is seen in the upper centre of the plate. To the immediate left of this is a long, curved glass shard which extends right to the bottom of the plate. Approximately parallel to this are a number of others, giving the groundmass an overall direction of alignment. At points where the ends of these long, curved shards contact, there is no evidence of a suture line or break; they are believed to have welded at these points. However, where the large, flat, glassy surfaces are in close proximity no contact or welding is apparent. Apart from sectioned surfaces, this groundmass is also coated in fine fuzz.

Plate 12.2: Groundmass fabrics for the Ongatiti Ignimbrite.

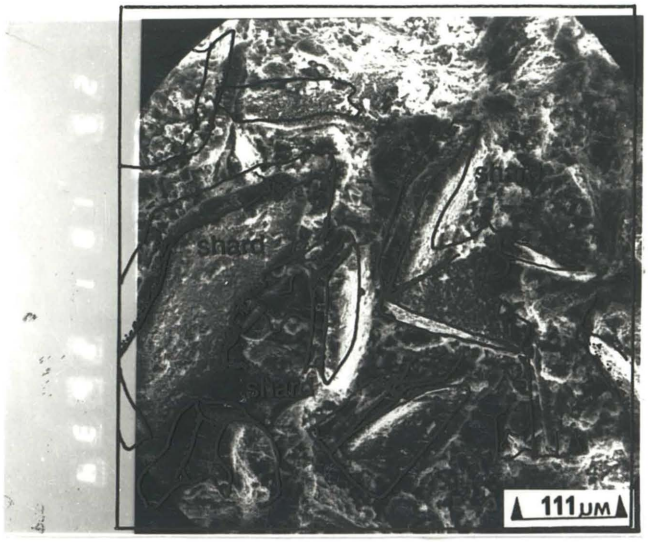
111µm

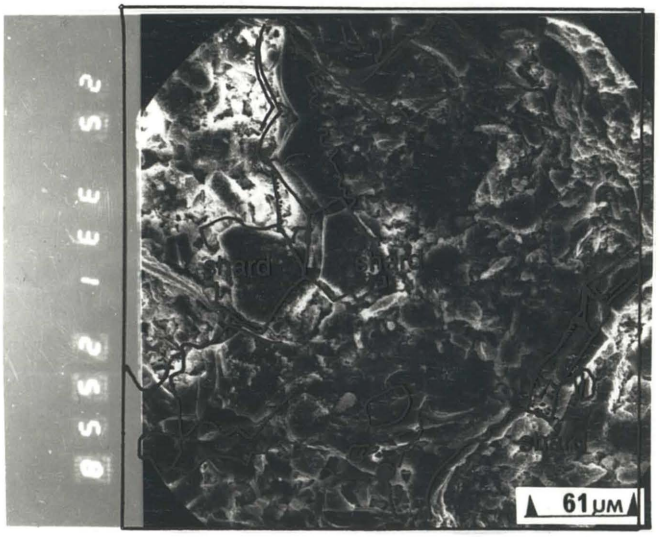
61µm

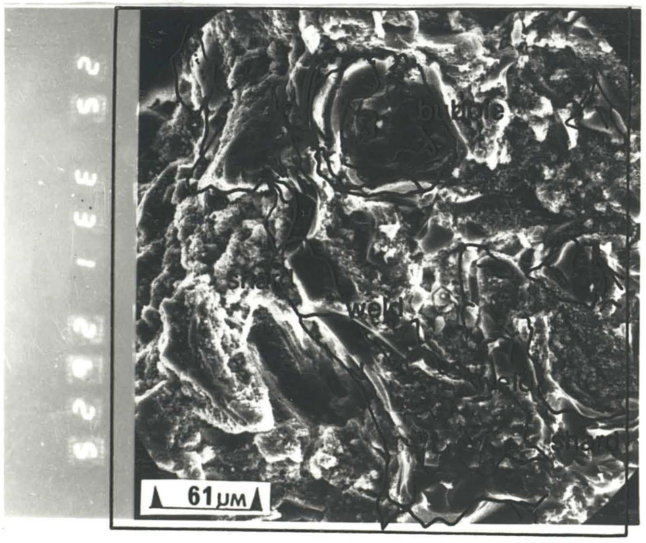
61µm

111µm

61µm

61µm

conformable. These contact relationships can be seen to influence the shape of the void spaces. The ONG/1 specimen has very large, open, interconnected pores, whereas the pores in the ONG/3 specimen are much smaller, more elongated, and are loosely filled with fragments of broken shards. The ONG/2 specimen falls between these two extremes.

An interesting feature of the scanning electron micrographs in plate 12.2 is the pervasive coating of fine material which gives all of the surfaces a fuzzy, web-like texture. Scanning electron micrographs with a greater magnification were taken in order to examine this material in greater detail (plates 12.3 and 12.4a).

In each of these plates, shards can be seen which are thickly coated in this fine material; this shows no evidence of a crystalline structure at the magnifications obtainable (though this does not rule out the possibility of such a structure existing beyond the limits of the microscope used). Of particular significance is that glass surfaces within pumice clasts do not have this cohering material, but the outer surfaces of the pumice clasts are coated. For this reason, the material is thought to represent finely fragmented material which adhered to the shard surfaces during transport in the pyroclastic flow. In particular, it is thought to attest to a relatively energetic eruption and flow in which the vesiculated magma was broken into shards, small shard fragments, and much very fine, glassy material. This appears to have adhered to the shard surfaces, but was unable to penetrate into large pumice clasts. Were this material due to vapour phase deposition, vesicular pumice clasts would be a prime site for deposition.

However, without detailed chemical analysis, the nature of this material cannot be conclusively identified. Such analysis is beyond the scope of this study. For this study, the fine material will be referred to as "dust", this being a general term for fine ash material.

The particular significance of this material is displayed in plate 12.3b, in which four glass shards which have been sectioned by sample preparation procedures are apparent. Clean, fresh shard surfaces can be seen surrounded by a thin layer of the dust. Of note is the fact that the dust provides the contact between the shards in all cases; at no time can true cohesion, or welding, of the glassy shards be seen in this electron micrograph. Comparison with plate 12.2 shows this to be the general case for each of the Ongatiti Ignimbrite specimens, though in the ONG/3 specimen occasional true glass welding does occur. The dust thus appears to be the medium by which welding has occurred for the bulk of the Ongatiti Ignimbrite.

(a) ONG/2 (top) magnification 650x

A large, platy shard can be seen in the centre of this plate, with a smaller, parallel shard adhering to its flat face. These are thickly coated in a very fine, fuzzy material which has no apparent crystalline structure (see plate 12.4a).

(b) ONG/2 (bottom) magnification 900x

Four approximately parallel shards are seen in the centre of this view. Like those in (a) above, these have a coating of fine, fuzzy material (although it is not as thick in this case). These shards have been sectioned by specimen preparation procedures, and have a clean, glassy nature between the fuzzy outer surfaces. This fuzz is interpreted as dusty material which has coated the shards during eruption and transport in the pyroclastic flow. No welding of the glassy surfaces is apparent; contact between the shards only occurs across the dust, suggesting that this provides the primary medium for welding in this ignimbrite.

Plate 12.3: Groundmass detail for the Ongatiti Ignimbrite.

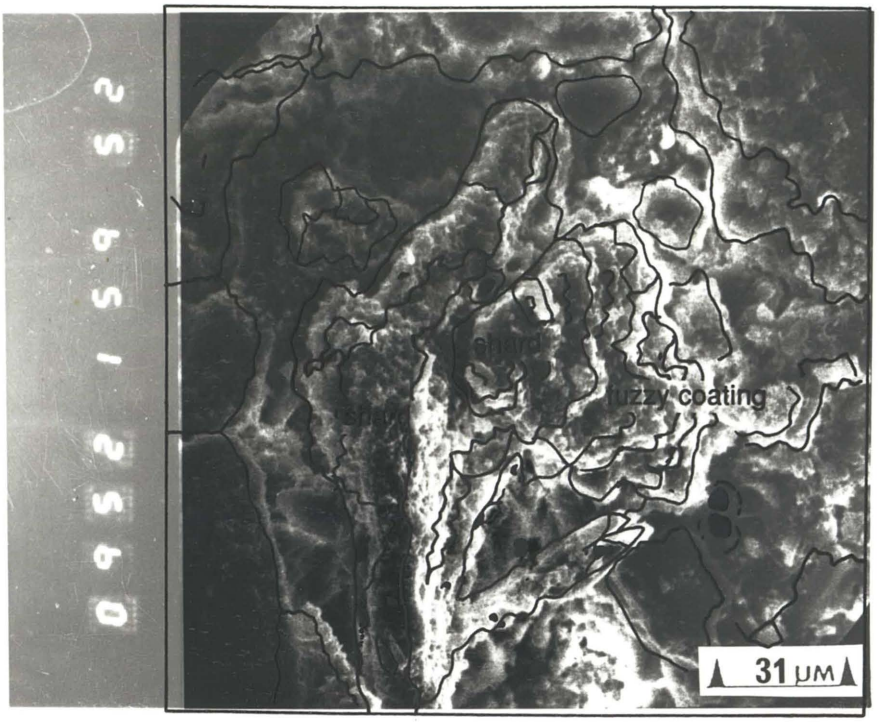
shard
fuzzy coating
31 µm

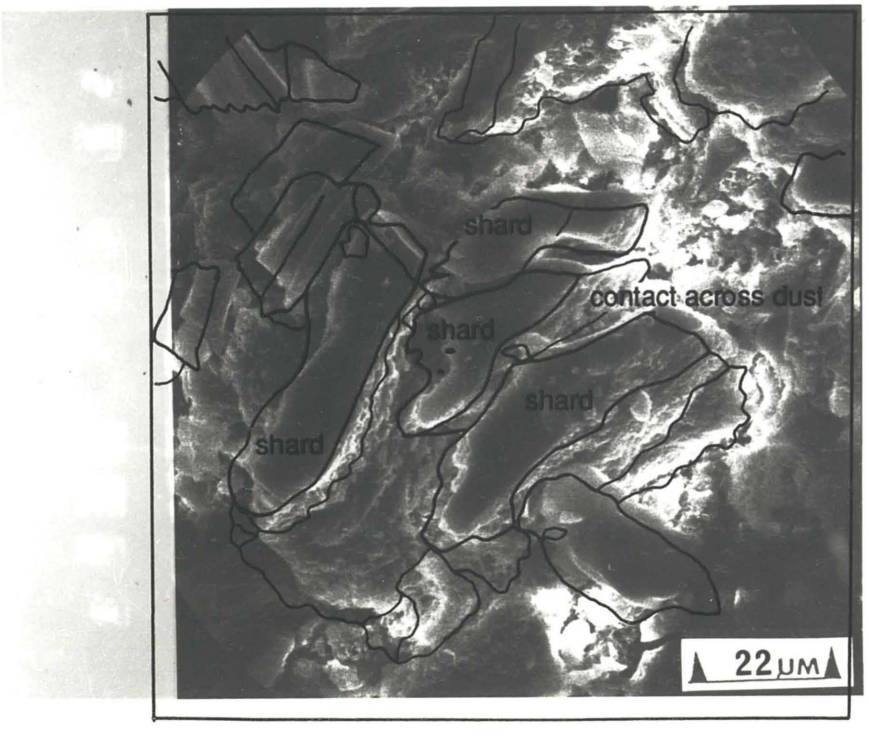
shard
contact across dust
shard
shard
shard
22 µm

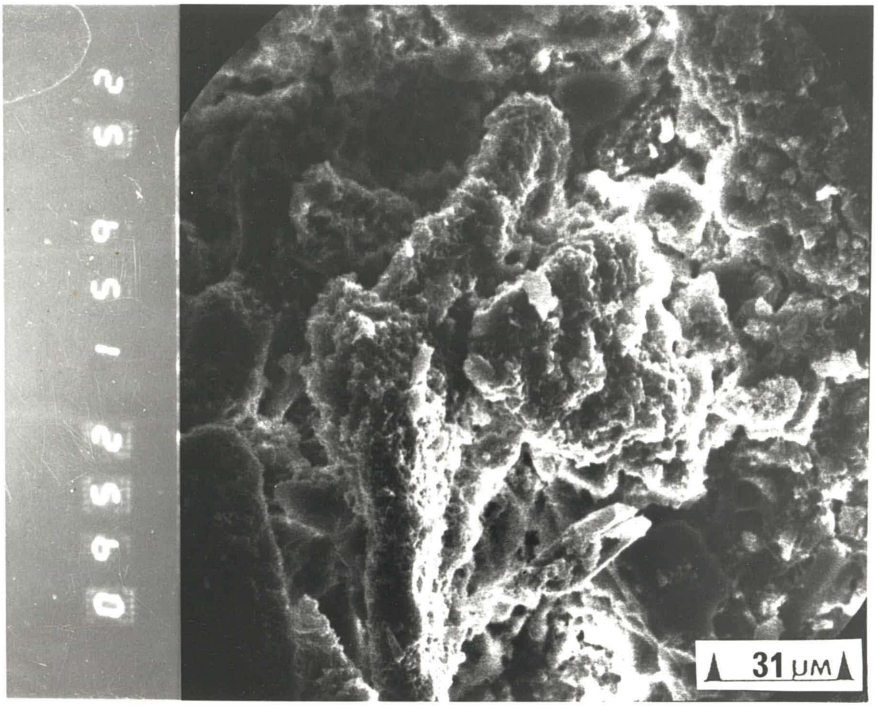
31 µm

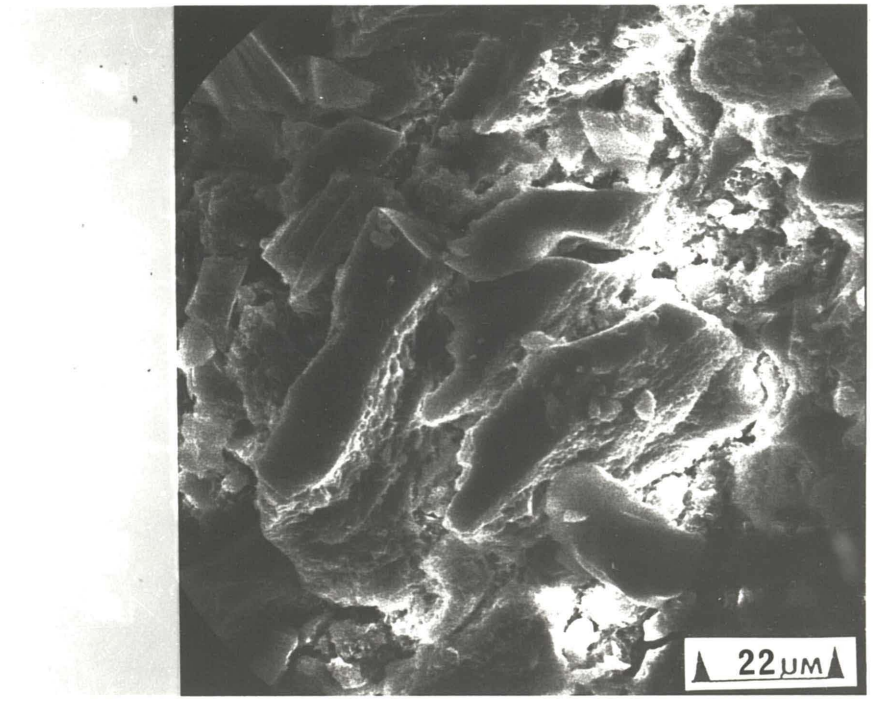
22 µm

12.4.2 Crystals

In thin-section, large crystals almost invariably show a fine network of fractures across the entire crystal area; these commonly exploit the cleavage planes. This fine fracturing is believed to be the result of transport processes, and is thought to be further evidence of an energetic eruption and pyroclastic flow. Fracturing also occurs on a much larger scale whereby original crystals have been split apart along cleavage planes. Such fracturing cannot have occurred during transport, as the crystal would not have remained intact. It is thus interpreted as a post-depositional feature caused either by chemical processes, or by tensile stresses in the cooling mass causing fracturing of the crystal.

The contact between the crystals and groundmass is non-welded, with a band of fine material between the "normal" groundmass and the crystal. This type of contact is the same as occurs in the Owharoa Ignimbrite, as shown in plate 12.6b.

12.4.3 Pumice

12.4.3.1 Pumice clasts in thin-section

In thin-section, pumice clasts with two different morphologies are apparent. Type 1 pumice clasts are characterised by large, expanded vesicles separated by thick vesicle walls. Zones of large vesicles tend to be surrounded by zones of much smaller vesicles which are distorted to be conformable with the walls of the larger vesicles. In many cases coalescence of several vesicles has occurred to give very large vesicles with broken walls protruding into them.

In the ONG/1 specimen the vesicles show no favoured orientation, in the ONG/3 specimen the vesicle elongation is generally parallel to the direction of shard alignment. Likewise, intricate fiamme are present along the edges of the pumice clasts in the ONG/3 specimen, but are absent in the ONG/1 specimen. These also align with the general shard orientation. These effects are all believed to be due to compaction of the material after deposition, which has caused the large vesicles to become elongated in the direction parallel to the major strain axis, and for the vesicle walls to break away from the edge of the clasts, producing the fiamme.

(a) ONG/3 (top) magnification 2200x

Closer examination of the dust at higher magnification shows a lack of an apparent crystalline structure; no obvious structure could be seen at the highest magnifications obtainable. This does not rule out a crystalline structure, it could simply not be determined within the resolution of the machine. The material is believed to have undergone some alteration (possibly devitrification), to give the forms seen in this view, but a crystalline structure is not clearly developed.

(b) ONG/3 (bottom) magnification 600x

Pumice clasts in the Ongatiti Ignimbrite are composed of long, tubular, open vesicles. The pore spaces within the pumice clasts are open, and free from any shattered, infilling material. Of particular note in the pumice clasts is the clean, unaltered nature of the glass; no dust coating is seen. The coating is present, however, along the outer surfaces of the pumice clasts and is ubiquitous on the shards of the groundmass.

Plate 12.4: Groundmass and pumice detail for the Ongatiti Ignimbrite.

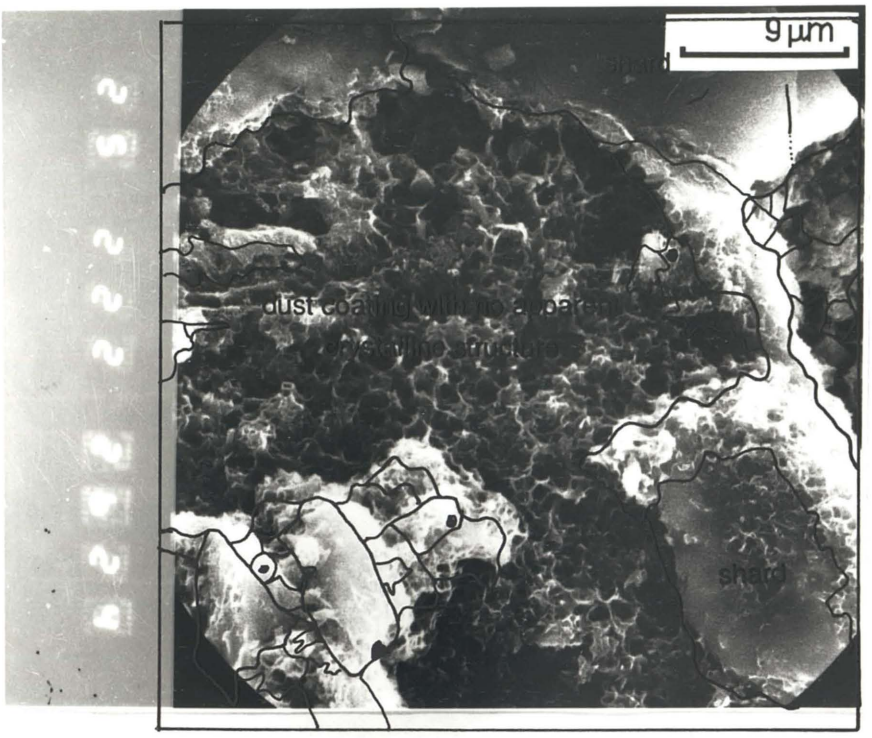
9 µm
shard
dust coating with no apparent
crystalline structure
shard

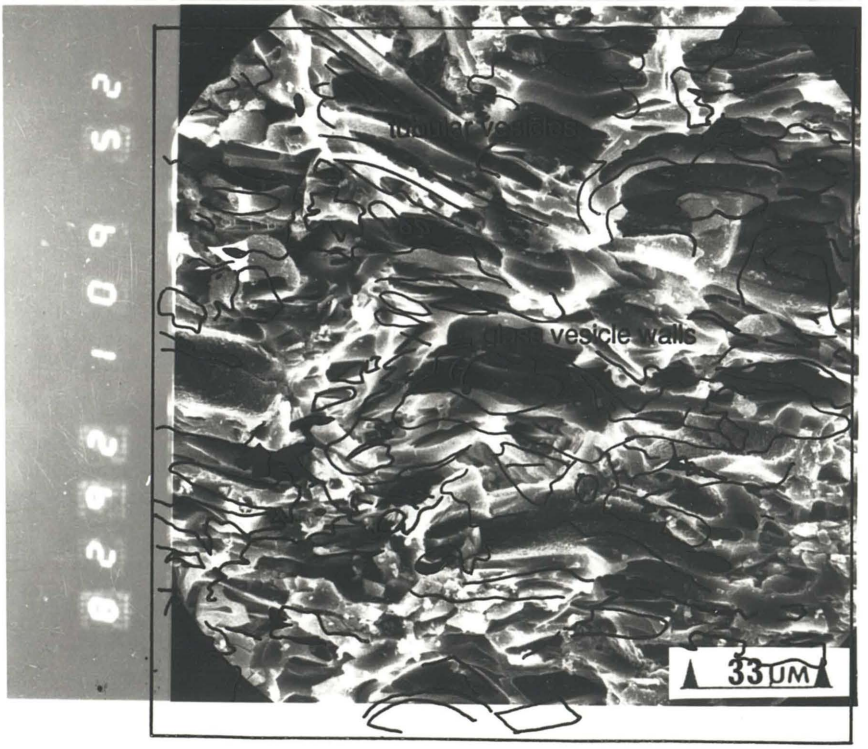
tubular vesicles
glass vesicle walls
33µM

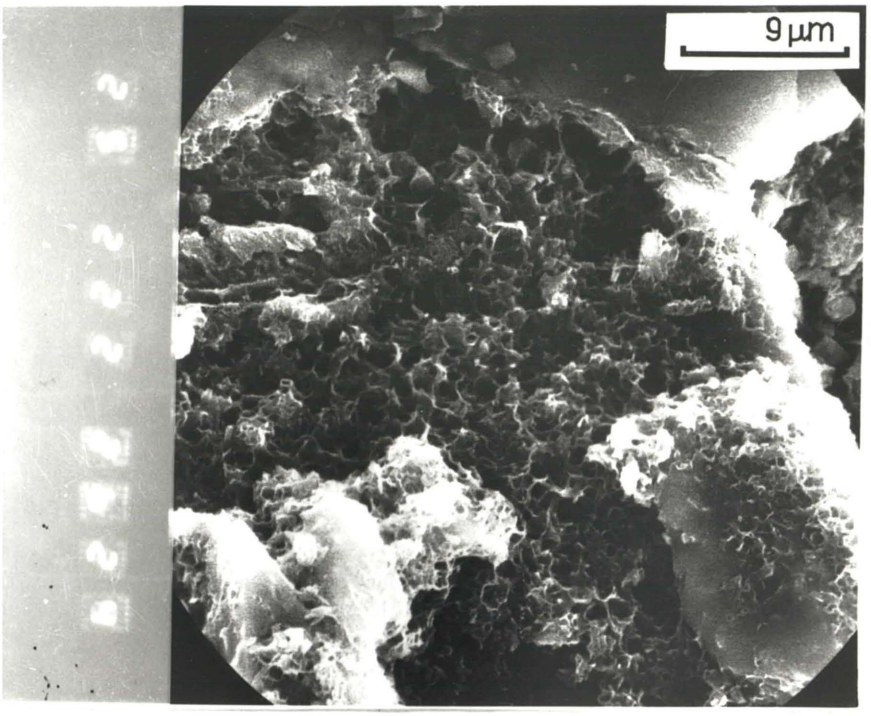
9 µm

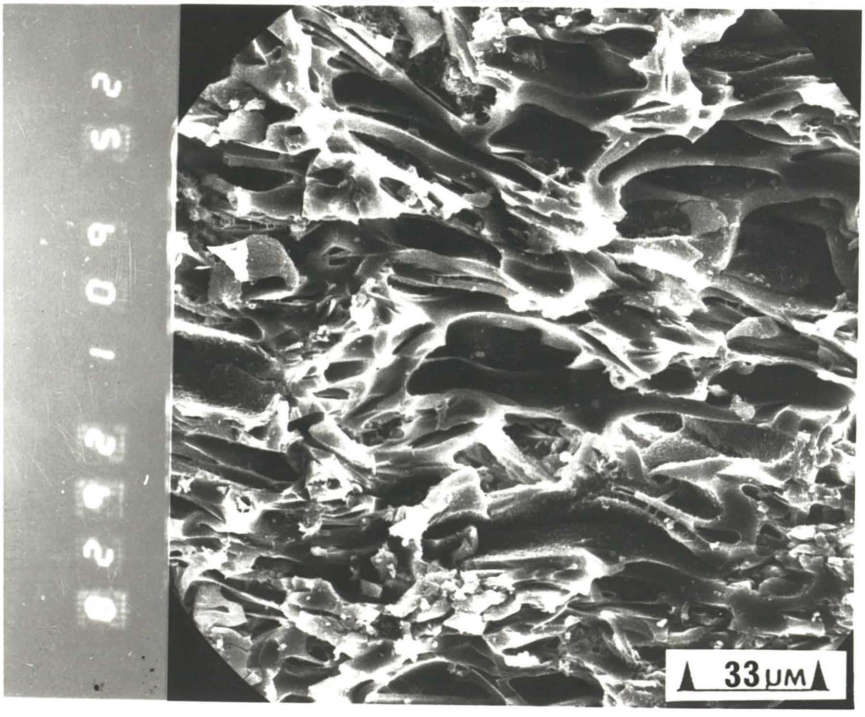
33 µm

Type 2 pumice clasts are readily distinguished from type 1 by extremely distorted vesicles, and very narrow vesicle walls. This gives the clasts an exceptionally streaky appearance in thin-section. In all of the specimens the orientation of the vesicles in these clasts is highly variable, ranging through all 360 ° in the thin-sections. There is also a notable lack of fiamme developed on the edges of these clasts; they tend either to have smooth edges parallel to the long axis of the vesicles, or ragged boundaries at right angles to this which represent fracture of the clasts. These clasts therefore show no real evidence of compaction.

The differences in the form of the vesicles in the two types of pumice clast are attributed to variations in the style of vesiculation in the magma chamber; temporal and spatial variations in the nature of vesiculation in an erupting chamber are common (Sparks, 1978a). The type 2 pumice clasts appear to have a more rigid structure, as they show no evidence of compaction under the same overburden stresses as the type 1 pumice clasts.

12.4.3.2 Pumice clasts under the electron microscope

Under the electron microscope, the different pumice clasts are not able to be distinguished. Compared with the matrix, the pumices in all specimens are highly porous zones (plate 12.4b). They are made up of many open vesicles separated by zones of clean, fresh glass.

Of particular note in plate 12.4b is the exceptionally clean nature of the glass surfaces compared with those of the matrix. Unlike the matrix glass, there is only a very minimal amount of dust within the pumice clasts. Occasionally very large, open pores within pumices are infilled with shattered fragments, but this is uncommon.

12.4.3.3 Pumice / groundmass contact

The groundmass laps against the pumice clasts, with no welding apparent under the scanning electron microscope. In thin-section, some favoured alignment of the shards, making them parallel to the edges of the pumice clasts, is seen, particularly in the ONG/1 specimen. Where present, the fiamme give the pumice clasts a very long, complex contact.

(a) OWH/up (top) magnification 650x

Large, blocky shards are apparent in this view. These show a general direction of alignment across the plate. No welding of the shards is apparent; their boundaries are marked by narrow breaks or non-welded contacts. Some pitting of the glass is apparent in the form of small holes; and furry coatings, believed to be devitrification products, are seen lining some of the shard surfaces. However, the shards are generally glassy, and have not undergone extensive devitrification. Pore spaces between the shards are elongated due to the overall shard alignment. They tend to be relatively wide and open, with some broken material loosely infilling them.

(b) OWH/low (bottom) magnification 1000x

The alignment of shards in this view is marked, running from the lower left to upper right of the electron micrograph. Large, glassy shards make up the groundmass, with mainly fresh surfaces exposed. Some furry devitrification material is apparent on many surfaces, but this does not extend into the centre of the shards. The distinction between individual shards is not apparent, suggesting that true welding has occurred at the points of contact. The pore space is narrow and elongated due to the shard alignment, and in most cases is densely infilled with broken, fragmentary material.

Plate 12.5: Groundmass fabrics for the Owharoa Ignimbrite.


non-welded contact
shard
blocky shard
elongated pore
shard
31µм


20 µm
shard
weld
shard
weld


31μм

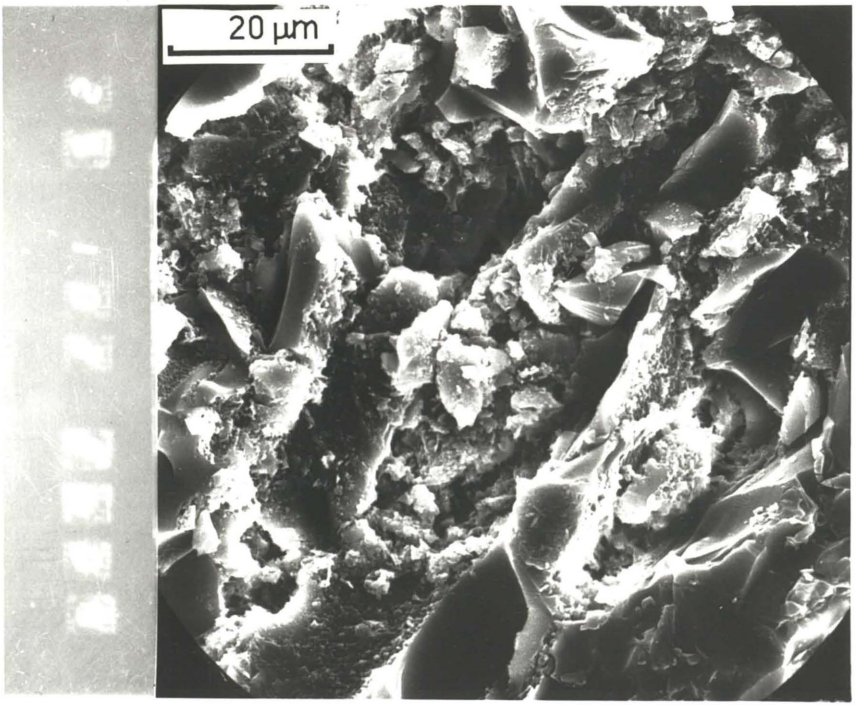
20 μm

12.5 Owharoa Ignimbrite

12.5.1 Groundmass

In thin-section (plate 11.3), the shards of the upper specimen show a general alignment, particularly in vertical sections. This is particularly notable for the long shards, the short ones tend to be randomly arranged, or show a partial alignment in localised areas. In the lower specimen the alignment is more marked, with close, parallel shards in some zones, particularly between crystals or pumice clasts.

Scanning electron micrographs show shards of very complex form, which are difficult to trace (plate 12.5). The shards in both lower and upper specimens are curved, and coalesce (or weld) across the glass at points of contact. Due to the curvature of the shards, these contact points make up only a small proportion of the total shard surface area.

In the lower specimen the spaces between these complex shards are largely filled with tightly packed fragments of glass (plate 12.5b). This results in the pore spaces in this material consisting of narrow, tortuous channels between neighbouring shards. In contrast, the upper specimen shows a much more open fabric between the shards (plate 12.5a); the spaces are partially filled with fragmental material, but some open spaces remain to give more rounded pore shapes. It is striking that the shard surfaces in this ignimbrite are comparatively clean, and free of the dust noted for the Ongatiti Ignimbrite.

12.5.2 Crystals

Few crystals are apparent in the Owharoa Ignimbrite (section 11.4.2), and those present are mainly broken fragments. In scanning electron microscope views (plate 12.6a), they often show some surface fracturing suggestive of breakage during transport.

Scanning electron micrographs of the contact between crystals and the groundmass are shown in plate 12.6. There appears to be no firm, welded contact between these two components, rather, the groundmass appears to lap against the crystal faces. In general there is a very narrow, physical separation between the two. In detail (plate 12.6b), there is apparently a glassy "selvedge" running parallel to the crystal face, but not quite in contact with the face. Between this selvedge and the "normal" groundmass is a zone of fine groundmass material.

(a) OWH/low (top) magnification 180x

Several crystals can be seen within this plate: one each at the upper left and lower right, and a smaller one in the upper right. These are surrounded by the dense groundmass. The groundmass appears to merely lap against the crystals, with no firm contact. A separation can be seen along many of the boundaries.

(b) OWH/low (bottom) magnification 1000x

This shows in more detail at the contact between the groundmass and the crystal in the lower right corner of (a) above. The smooth, dark area in the lower part of the view is the crystal, the true groundmass is seen at the upper left. It can be seen that there is a glassy "selvedge" along the boundary, with no welding or other form of adhesion of the components along this boundary (a physical separation is apparent). Between this glassy selvedge and the true groundmass is a zone of material which is more fragmented than the rest of the groundmass. This sequence is typical of the crystal / groundmass contacts in the Owharoa and Ongatiti Ignimbrites.

Plate 12.6: Crystal / groundmass contacts in the Owharoa Ignimbrite.

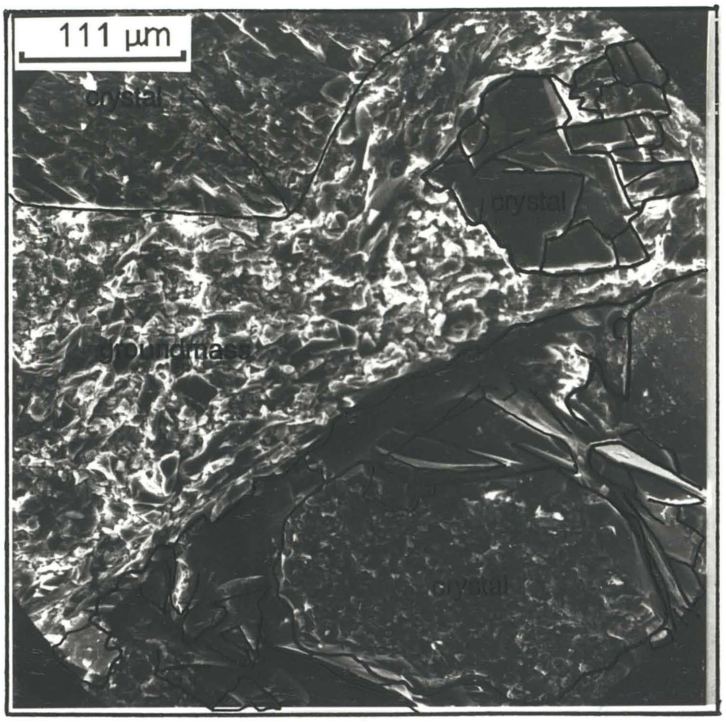
111 µm
crystal
crystal
groundmass
crystal

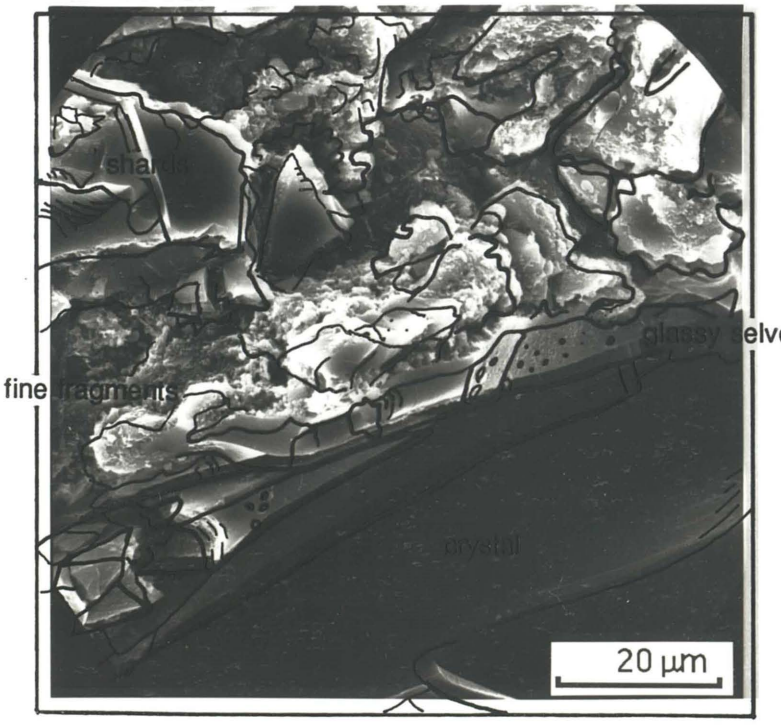
shards
glassy selvedge
fine fragments
crystal
20 µm

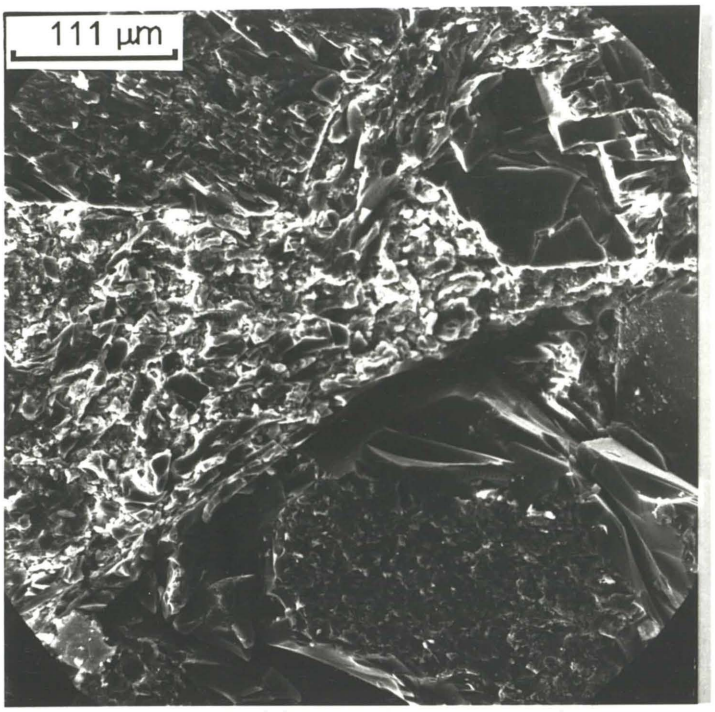
111 µm

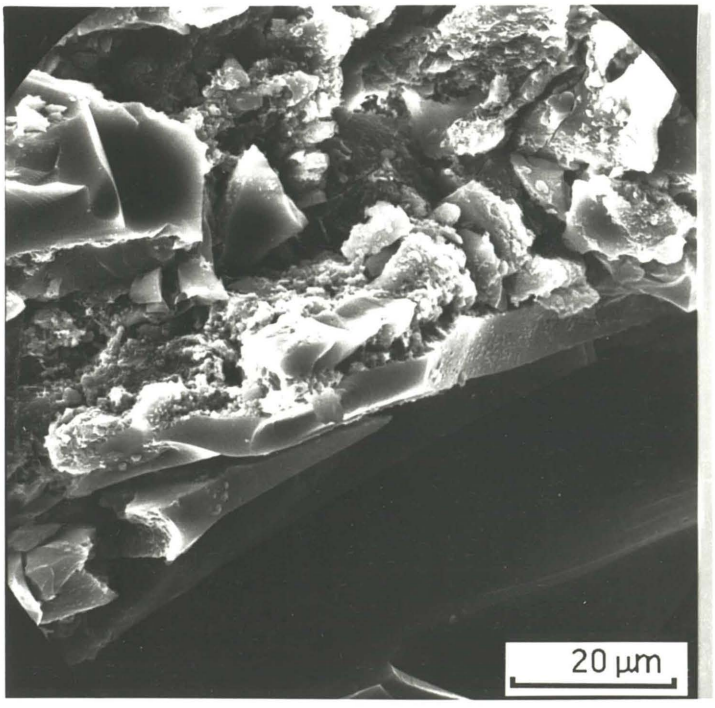
20 µm

12.5.3 Pumice

In thin-section two distinctive types of pumice clasts are apparent in the lower specimen. Type 1 pumice clasts, which are believed to correspond to the black clasts of hand-specimen, are pale pinky brown in thin-section, with thin black streaks representing the original bubble walls. The type 2 pumice clasts (yellow clasts of hand specimen) have a more open structure than the type 1 clasts.

Under the electron microscope, the type 1 pumice clasts from the lower specimen are almost indistinguishable from the groundmass. They are very glassy, with wide,clean glass surfaces which show a strong alignment. The porosity is in the form of narrow, tortuous channels, and they differ from the groundmass primarily by the relative paucity of shattered glass fragments between the vesicle walls. The extreme streakiness of these clasts is evident in thin-section. This is much more apparent in vertical than horizontal specimens; in vertical sections the streaks are long and continuous, in horizontal sections the streaks are shorter and often discontinuous. In general, the streakiness lies parallel to the long dimension of the clast.

Under the electron microscope, type 2 pumice clasts can be seen to have a much greater porosity than the surrounding groundmass. They show large, open vesicles separated by wide glassy walls (plate 12.7b). This results in the pore spaces in these clasts being much larger, and more open than those in the surrounding groundmass. In thin-section, they appear the same in both horizontal and vertical sections, suggesting that they are randomly arranged in the specimen.

In thin-section, pumice clasts in the upper specimen are highly variable: some are extremely streaky and show as very dark clasts; others are dark brown to black with streaky but wide, open vesicles; and a few light brown to pink clasts with an open, twisty structure occur. These clasts do not readily fall into categories. Under the electron microscope, open, rounded pumice clasts are seen (plate 12.7a). These show a marked direction of elongation. The pumice clasts have clean glass surfaces, and a relatively large porosity compared with the groundmass.

The glass walls of the pumice clasts in both the lower and upper specimen are characteristically pitted with numerous, small, round pits (plate 12.7c). These are believed to represent etching by acidic fluids associated with the eruption.

(a) OWH/up (top) magnification 240x

Pumice clasts are a distinctive feature of the Owharoa Ignimbrite under the electron microscope. Long, narrow tubes separated by thin vesicle walls can be seen in this view. The glass surfaces show no evidence of alteration products on their surfaces, and the vesicles are open, with no significant amounts of infilling material. The alignment of the vesicles is not consistent throughout the specimen - clasts with vesicles aligned in all directions were observed.

(b) OWH/low (middle) magnification 800x

The pumice clasts of the lower specimen often have less open structures, with narrow, elongated vesicles separated by relatively thick, clean glass walls. In this clast some fragmentation is apparent, which has resulted in some fractured material settling into the vesicles. This is common, but is by no means the case in all of the pumice clasts. Again, the vesicle alignment is not consistent through the specimen. At the top left of the view the contact with the groundmass is seen. The groundmass simply laps against the pumice clast, with no welding or coherence of any sort. Often this zone is finer than the bulk of the groundmass, with some alignment of the fragments parallel to the pumice clast. This contact is typical of those seen in all of the ignimbrites.

(c) OWH/low (bottom) magnification 1800x

The glass within the pumice clasts of the Owharoa Ignimbrite shows a large number of small, circular pits. These are believed to represent etching of the glass by acid solutions, probably by vapours associated with the eruption.

Plate 12.7: Pumice clasts from the Owharoa Ignimbrite.

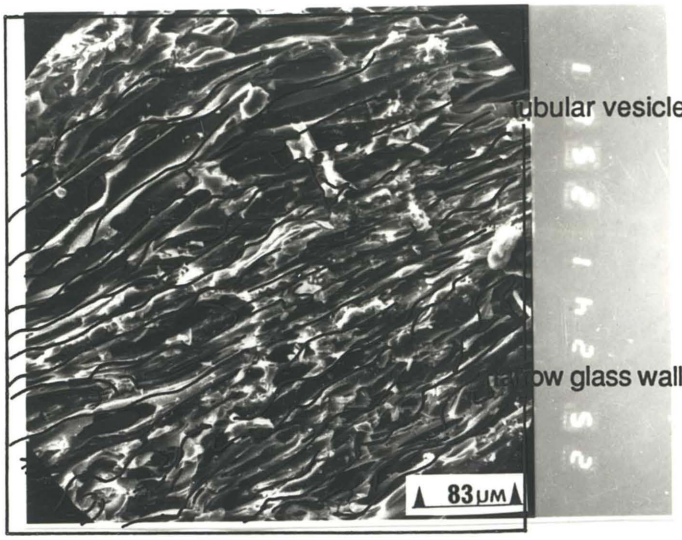
tubular vesicles
ow glass walls
83µm


25µm
vesicles
tubular ves
glass walls

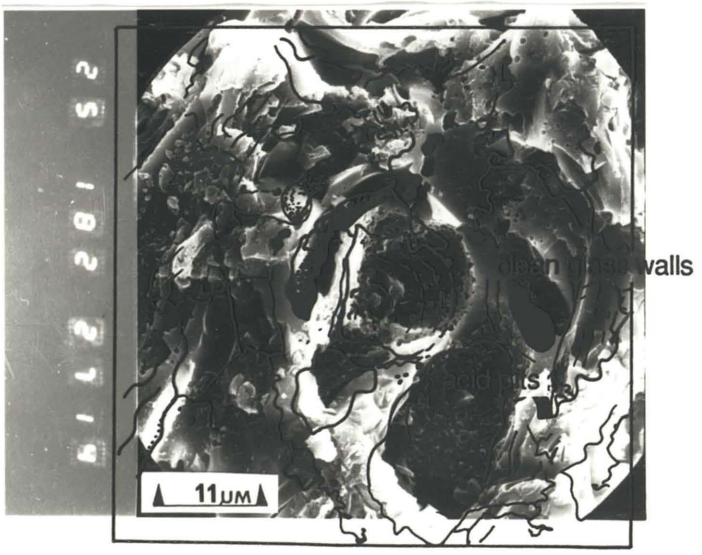
walls
11µm

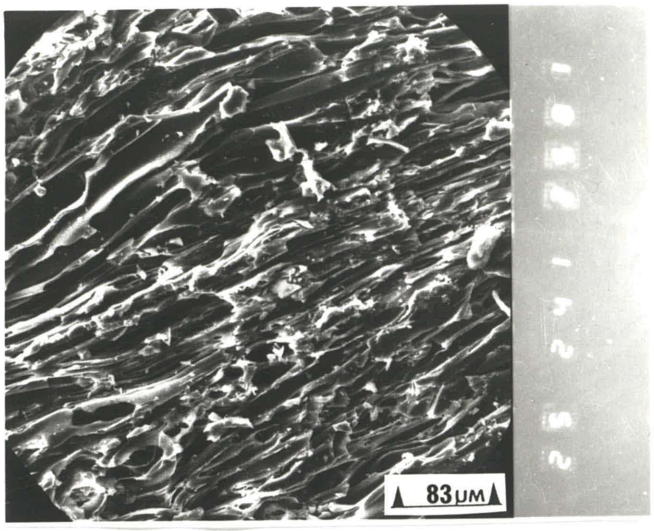
83µm

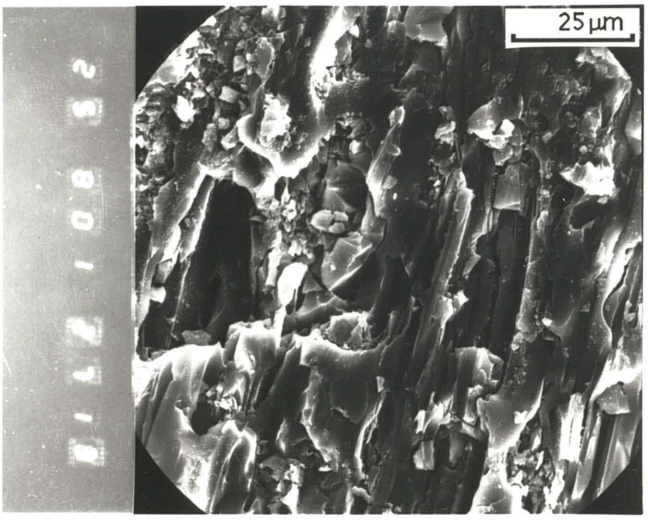
25µm

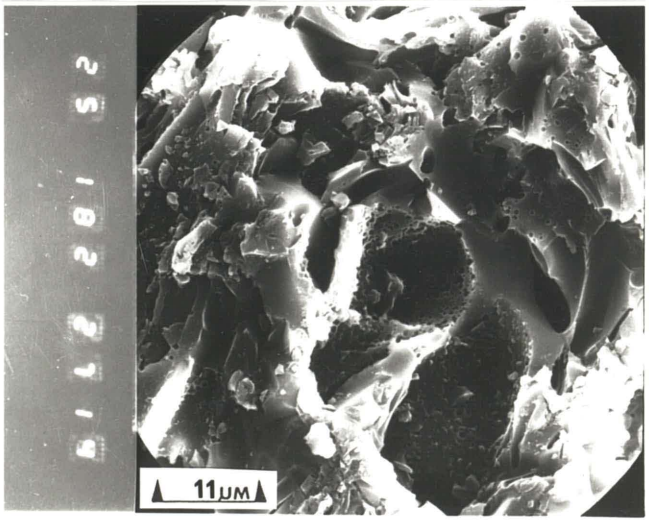
11µm

12.5.3.1 Pumice / groundmass contact

Many of these pumices have well developed fiamme, giving an exceptionally long, complex boundary. The groundmass appears to lap against the pumice clasts with no welding along the contact.

12.6 Summary table of fabric parameters

Table 12.2 summarises the main features of the fabric for each specimen, using the terminology defined in table 12.1. Table 12.2 provides the basis for the ranking of fabric parameters in chapter 15.

	shard form	shard alignment	shard contacts	pore shape	pore filling
WHAKA/up	platy	random	point	rounded	vapour phase
WHAKA/low	complex	general	tangential	rounded	dense
ONG /1	platy	random	point	rounded	open
ONG /2	curved	partial	tangential	slightly elongated	partial
ONG /3	cuspate	general	tangential	slightly elongated	dense
OWH/up	complex	general	tangential	elongated	dense
OWH/low	complex	parallel	tangential	strongly elongated	dense

	crystals	crystal /gm contact	pumice	pumice / gm contact
WHAKA/up	whole	plucked	spherulitic	lapping
WHAKA/low	whole	plucked	spherulitic	lapping
ONG /1	shattered	non-welded	open, glassy	lapping
ONG /2	shattered	non-welded	open, glassy	lapping
ONG /3	shattered	non-welded	open, glassy	lapping
OWH/up	fragments	non-welded	open, glassy	lapping
OWH/low	fragments	non-welded	dense, glassy	lapping

Table 12.2: Summary of fabric parameters for each ignimbrite.
gm = groundmass

CHAPTER 13 - POST-DEPOSITIONAL ALTERATION PROCESSES

13.1 Introduction

Many of the products of post-depositional alteration processes could be identified from the petrographic analysis. These are discussed for each ignimbrite in turn.

The distinction between devitrification and vapour phase alteration is defined by the position of the crystalline products; alteration which is confined within shard margins is attributed to devitrification, alteration on the outer surfaces of shards is attributed to deposition from a vapour phase.

13.2 Whakamaru Ignimbrite

13.2.1 Welding

Evidence of the nature of the welding in the Whakamaru Ignimbrite is obscured by the products of other alteration processes. However, the complexity of the large, curved glassy ridges observed in the lower specimen (section 12.3.1) suggests that they are not individual shards, but rather a number of shards which have coalesced at their points of contact. Such coalescence is always at the ends of shards; no cases are seen where flat shard faces have welded.

For the upper specimen, no coherence of the individual shard components is apparent at all, suggesting that welding plays no part in controlling the strength of this material.

13.2.2 Devitrification

Devitrification is intense throughout the Whakamaru Ignimbrite profile. In thin-section (plate 11.1), both specimens show medium to dark brown colours typical of devitrified glass; individual shards are difficult to distinguish. Under crossed polarisers the shards and pumice clasts are obvious bright zones with a cryptocrystalline texture, and "suture" lines along the axis of many shards. Under the scanning electron microscope, complete devitrification of the shards in the upper specimen is ubiquitous. This is especially apparent

when shards are seen in section, when they appear as a crystalline "carpet" which retains its original platy shard form.

Devitrification of pumice clasts is also apparent in that they are cryptocrystalline under crossed polarisers, and usually display a spherulitic texture.

13.2.3 Vapour phase alteration

Accompanying the extensive devitrification of the Whakamaru Ignimbrite is extreme vapour phase alteration of the upper specimen. Scanning electron microscope examination shows the pore spaces to be largely infilled with long crystals which have obviously grown *in situ.* These show typical growth patterns associated with crystals precipitating from a fluid phase. Such crystallisation is not as marked in the lower specimen, but some alteration products are apparent on shard surfaces under the electron microscope.

The greater degree of vapour phase alteration in the upper specimen is believed to simply represent the passage of great quantities of rising vapours, derived from lower in the profile, through this material. Such a process would favour deposition in the upper portions of the ignimbrite.

13.3 Ongatiti Ignimbrite

13.3.1 Welding

The dust in the Ongatiti Ignimbrite is thought to provide the medium for welding. Rather than the glass shards being hot enough to weld together, the dust which adheres to the shards bridges the gap by welding onto each shard. This, especially for the ONG/1 specimen, may well have been sufficient to allow welding by means of this dust in a deposit which was otherwise too cool for welding to occur. This explains why material which otherwise shows many characteristics of a very cool deposit, which would normally be expected to be non-welded, is actually soft to firmly welded. Some true welding of the glass shards is also observed in the lower specimen.

From a geomechanical viewpoint, welding across the dust may be expected to be weak compared with true welding of the glass shards. In the ONG/1 specimen the shards are widely spaced and contact only at limited points, thus the welding occurs only at limited points and is across wide bands of the dust. With greater shard alignment and packing in the ONG/2 specimen,

the length of contact increases and the thickness of the dust decreases, resulting in much stronger bonding.

13.3.2 Devitrification

In thin section, the groundmass of the Ongatiti Ignimbrite consists of white to light brown glass shards within an amber to medium brown background (plate 11.2). The colour of both the shards and the background is most intense in the ONG/3 specimen (pale brown shards in a medium to dark brown background), and least intense in the ONG/1 specimen (predominantly crisp, white shards in an amber to pale brown background).

These brown hues are generally taken to indicate some degree of devitrification of the glassy material (Smith, 1960a), and the darkening represents an increase in the intensity of devitrification. However, the devitrification is relatively weak in all of these specimens, as the colours remain brown, no spherulitic or granophyric textures are apparent, and the shards invariably remain isotropic. It is of note however, that immediately surrounding many of the shards in all specimens is a narrow, black strip. This is thought to represent the dust.

13.3.3 Vapour phase alteration

No obvious evidence of vapour-phase alteration is apparent under the scanning electron microscope for the Ongatiti Ignimbrite. Consequently, vapour-phase alteration is assumed to be minimal in these specimens.

13.4 Owharoa Ignimbrite

13.4.1 Welding

In both specimens, welding appears to occur at the limited points of contact of individual shards, at which points the glassy material of the shards has completely coalesced to make the suture indistinguishable.

13.4.2 Devitrification

The shards in this material tend to be relatively crisp and pale in colour, and are surrounded by an amber background (plate 11.3). As for the Ongatiti

	shard welding	devitrification	vapour phase alteration
WHAKA/up	none	extensive	extensive
WHAKA/low	glass	considerable	considerable
ONG /1	dust	slight	slight
ONG /2	dust	slight	slight
ONG /3	dust, some glass	slight	slight
OWH/up	glass	slight	slight
OWH/low	glass	slight	slight

Table 13.1: Summary of post-depositional alteration parameters for each ignimbrite.

SHARD WELDING: whether or not the glass has coalesced at the shard contacts

none:	no glass coalescence has occurred
dust:	dust provides the medium for shard welding
tips:	small areas of glass coalescence occur at points of contact
glass:	extensive areas of glass coalescence occur where the shards are in contact (will only occur for "tangential" or "complete" shard contacts)

DEVITRIFICATION: the extent to which glassy components have crystallised

none:	no crystallisation is apparent
slight:	amber colours in thin-section indicate some devitrification, but the shards remain isotropic
considerable:	shards are no longer isotropic, colours in thin-section are dark brown, and shards are difficult to distinguish
extensive:	shards are cryptocrystalline in thin-section, and completely crystalline in scanning electron microscope views

VAPOUR-PHASE ALTERATION: the extent of crystallisation from a vapour-phase

none:	no vapour-phase deposits are apparent
slight:	small amounts of vapour-phase crystallisation are seen
considerable:	pore spaces and glass surfaces are lined with vapour-phase deposits
extensive:	pores are closely infilled with material grown *in situ.* from a vapour-phase

Table 13.2: Terminology used for describing post-depositional alteration.

Ignimbrite, this suggests that devitrification has only occurred to a limited extent in this ignimbrite. Some pink to orange coloured shards suggest that devitrification is slightly greater than for the Ongatiti Ignimbrite, but the differences are subtle, and not able to be quantified.

13.4.3 Vapour phase alteration

Vapour phase alteration is assumed to be minimal in the Owharoa Ignimbrite, as no obvious evidence of this process is apparent under the scanning electron microscope. Some alteration material can be seen on glass shards and within pumice clasts, but this is minimal.

13.5 Summary

Table 13.1 summarises the post-depositional alteration processes for each ignimbrite, and table 13.2 presents the terminology used for describing the extent to which these processes have occurred.

Each ignimbrite shows different styles and extents of welding, devitrification, and vapour phase alteration. The Whakamaru Ignimbrite has welded shards at the base of the profile, and is non-welded at the top, plus has extensive devitrification, and intense vapour phase alteration throughout the profile.

The Ongatiti Ignimbrite shows welding across a dusty material throughout the profile, with only limited true glassy welding in the lower specimen. This ignimbrite shows evidence of only limited devitrification and vapour phase alteration.

The Owharoa Ignimbrite has welded shards in both the upper and lower specimens. Devitrification and vapour-phase alteration appear to have been of relatively minor extent in this ignimbrite.

CHAPTER 14 - JOINTING

14.1 Introduction

Jointing in ignimbrites may develop either through cooling, stress release on weathering, or tectonic processes, but as the ignimbrites under consideration in this study are generally unweathered and very young in geological terms (Quaternary), cooling is considered the most significant process for joint formation. As mentioned in appendix 1, the literature generally classifies ignimbrites as displaying simple, widely-spaced columnar jointing. From the field descriptions in chapter 2, this would appear to be an oversimplification. Hence this chapter will:

(1) review the mechanisms for cooling joint development, and

(2) examine the range of jointing patterns (block size and shape) expressed at the study sites.

14.2 Joint development

14.2.1 Mechanisms of joint development

Pollard and Aydin (1988) have recently presented a review of the pattern, surface morphology, and development of jointing in rocks. The main points of relevance to this study are outlined below.

(1) Joints develop due to the local tensile stress exceeding the tensile strength of the intact rock material.

(2) Regions of high stress concentration develop at inhomogeneities in the rock, such as large grains, inclusions, or void spaces; such areas may concentrate stress by 3 times the regional stress, and regional compressive stresses can be converted into local tensile stresses by the geometry of the inhomogeneity.

(3) Fractures will be initiated at zones of high stress concentration, and will propagate away from such points, developing perpendicular to the direction of maximum tensile stress. The direction of joint propagation can be inferred from the surface morphology of the joint plane (Kylander and Dean, 1985).

(4) A fracture will terminate either by striking another discontinuity, or by releasing sufficient tensile stress through plastic strain that further joint development is unnecessary.

14.2.2 Columnar jointing

Materials which undergo cooling or desiccation commonly show a regular geometric pattern of joints; in igneous rocks these are referred to as columnar joints. They are characterized by quadrangular to hexagonal cross-sections, and large aspect ratios (length / diameter). Their long axis develops perpendicular to the cooling surface, and their size may vary over an enormous range (Aydin and DeGraff, 1988). Recent papers by DeGraff and Aydin (1987), and Aydin and DeGraff (1988) have summarised the development of columnar joints in basalt flows, as shown by the joint surface morphology. Their main points are summarised below.

(1) Columnar joints develop in response to contraction (hence tensile stresses) which accompanies cooling of a rock mass.

(2) They grow inwards from a chilled upper and lower surface towards the hotter central area. Growth from the top is generally much faster than that from the bottom.

(3) Each joint grows in segments, starting at a nucleation point and propagating along the joint plane until an area is reached where the temperature is still high and therefore tensile stresses are low. Consequently growth increments are expressed on the surface of the joint.

(4) Joints terminate at a triple-junction; the orientation of this junction can change during joint development, resulting in a rotation of the column axes.

(5) Continual termination of joints results in a systematic increase in joint spacing, and hence column diameter, on moving towards the centre of the flow.

In addition Long and Wood (1986) describe an "entablature" structure which commonly occurs in the central portions of basalt flows. The outer "colonnade" zones show regular columnar jointing as described above, whilst the inner zone is much less regular, both in joint spacing and orientation. This has been variously attributed to more rapid cooling by water incursion into the cooling rock (Long and Wood, 1986) or chemical variations through the flow (Philpotts and Burkett, 1987).

14.3 Jointing at study sites

As jointing is quite variable, and the jointing observed can depend strongly upon the orientation of the joints with respect to the exposure (Pollard

and Aydin, 1988), the joint patterns seen in the field were examined in context of the overall profile rather than simply site-specific observations.

Assessment of sensible parameters to describe the jointing was difficult for these sites. As most of the joints were essentially vertical, and true columnar joints display an almost random distribution of dip-directions, orientation data was virtually meaningless. For regular columnar jointing, the mean (or modal) joint spacing is the most useful parameter, but for the complex jointing patterns seen in these ignimbrites, the measured joint spacing was entirely dependent upon the orientation of the exposure. Consequently, the quantitative data which was collected proved valueless in describing and distinguishing the sites. All sites had a preponderance of vertical joints, with a wide variety of orientations. The measured joint spacing varied with outcrop direction to the extent that the data were not reproducible between outcrops a short distance apart. The data presented in the site descriptions in table 2.1 proved to give the best description of the jointing.

14.3.1 Whakamaru Ignimbrite

The profile exposed at Maraetai shows a wide variety of jointing, ranging from very complex, curved joints at the base (plate 14.1a), through a zone of blocky jointing with approximately equally-spaced horizontal and vertical joints (plate 14.1b), to wide, columnar joints (plate 14.1c), and finally an essentially unjointed material (plate 14.1d) at the top of the profile.

The complex jointing is the most interesting in this profile: an essentially vertical jointing pattern exists, but the joints are curved along both horizontal and vertical axes. The joints are also more closely spaced (moderate spacing) than their columnar counterparts higher in the profile.

The change to a widely spaced, blocky pattern occurs quite suddenly on moving up the profile; in the past this has been interpreted as representing the boundary between two separate flows (Maloy and Lowe, 1945), though no modelling of the mechanisms for producing a blocky zone at such a boundary have been undertaken.

Above the blocky zone, complex jointing continues, though the joint patterns tend to become more regular on moving up through the profile. This is evidenced by the curvature of the joints decreasing and the jointing becoming more consistently vertical.

The columnar jointed zone is only very poorly exposed, due to heavy vegetation, but can be assumed to make up a significant portion of the profile.

(a) unjointed zone (top)

At the top of the profile is a zone of unjointed material. Some joints do occur in this zone; they are generally approximately vertical, and show some curvature. In general they occur in groups with several joints spaced 2 - 3 m apart, separating truly unjointed zones of 10 - 15 m width. The joints are highlighted on the overlay. Note that the horizontal grooves on the cutting are machinery scrape marks.

The wall at the base of this view is approximately 2 m high.

(b) columnar jointed zone (bottom)

Outcrops consisting of two or three isolated columns make up the columnar jointing zone. They are inaccessible in all cases. These occur at the same level as the unjointed zone, and it is believed that these are the remnants left after weathering of the softest material. The columns tend to occur in groups which form rounded, domed features.

The columns in this view are approximately 5 m wide.

Plate 14.1: Jointing in the Whakamaru Ignimbrite profile at Maraetai.

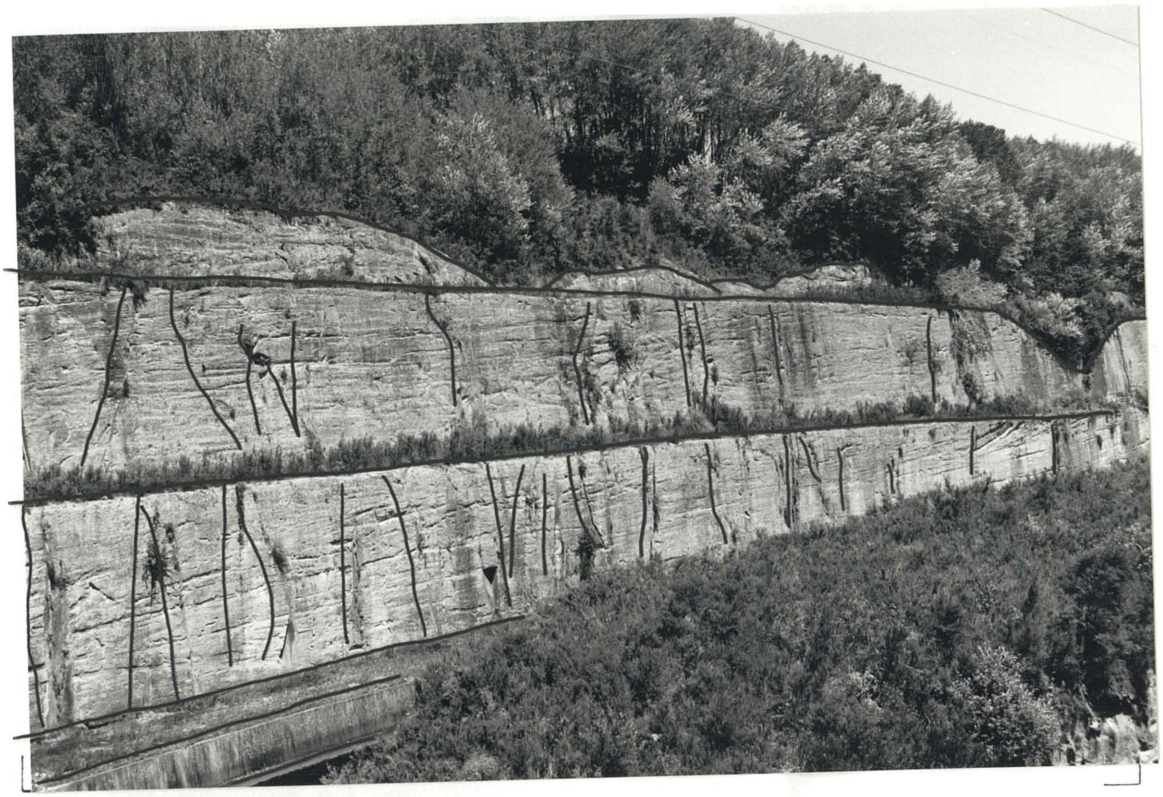

(c) blocky zone (top)

In the blocky zone, persistent horizontal joints with a spacing similar to the vertical joint spacing split the rock mass into approximately equidimensional blocks. This zone is of only limited vertical extent (approximately 10 m), and the change from the under- and over-lying complex jointing is sudden.

(d) complex zone (bottom)

The zone of complex jointing makes up by far the bulk of the profile. Essentially vertical joints dominate, but these are extensively curved along both vertical and horizontal axes. The joint spacing is moderate (approximately 0.5 m) in the direction perpendicular to the face, but extremely wide in the direction parallel to the face, splitting the rock mass into a series of large, curved plates.

Plate 14.1 (cont.): Jointing in the Whakamaru Ignimbrite profile at Maraetai.

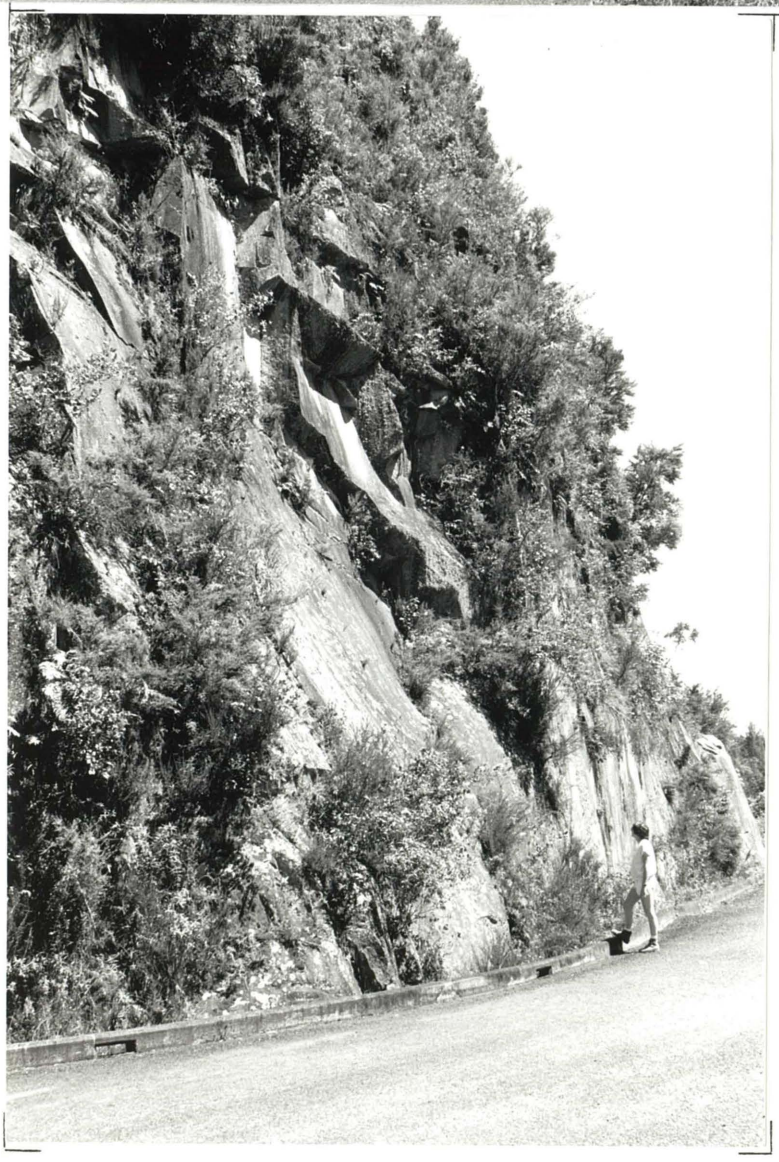

The exposures which do exist consist of two or three very widely spaced columns together left as individual outcrops (plate 14.1c); they are inaccessible in all cases.

The unjointed zone is exposed only in artificially-cut sections of ignimbrite. This zone does actually contain joints, mostly they are approximately vertical, but occasionally they show significant curvature. In general these joints occur in groups spaced approximately 2-3 m apart, and separated by completely unjointed zones of up to 10-15 m (plate 14.1d).

The unjointed zone occurs at the same true elevation as the columnar jointed zone in many places. As all other evidence suggests a horizontal mode of deposition for the ignimbrite, they are thus inferred to represent the same stratigraphic level, though no samples could be obtained to confirm this. As the unjointed material occurs only in artificial exposures, and the columnar material occurs only in natural exposures, it is assumed that the columnar appearance is the result of weathering and erosion accentuating the joint pattern by removing the unjointed material and leaving the columns standing proud.

Of interest within the Whakamaru Ignimbrite is that some variants on these patterns exist. At Waihaha, near Lake Taupo (grid reference NZMS 260 T18 494723), no unjointed zone exists at the top of the profile, and the entire thickness shows fairly regular columnar jointing. In contrast, near Waipapa (grid reference NZMS 260 T16 445194), a much more complicated profile exists, with exceptionally complex jointing at the base, and isolated zones of well-developed, truly columnar joints occurring within the profile.

14.3.2 Ongatiti Ignimbrite

The jointing in the Ongatiti Ignimbrite is much simpler than that in the Whakamaru Ignimbrite; it provides an essentially classical example of very widely spaced columnar jointing in ignimbrite (plate 14.2), with only slight variations in the jointing in the profile. Like the Whakamaru Ignimbrite, the columns are comprised of large, curved faces rather than straight planes intersecting at sharp junctions as described by Aydin and DeGraff (1988). A distinctive, horizontal break occurs approximately half-way down the profile (plate 14.2).

The Ongatiti Ignimbrite shows a "classical" columnar jointing pattern. Large, widely spaced, curved joints define very large, curved columns. These extend through the entire exposed profile. A distinctive horizontal break occurs approximately half-way down the profile.

Plate 14.2: Jointing in the Ongaititi Ignimbrite.

The lower site of the Owharoa Ignimbrite shows a moderately spaced columnar jointing pattern. The joints show less curvature than those in the Ongatiti Ignimbrite, and meet at sharp angles of intersection. Column orientation is relatively uniform over small areas, as shown in this plate, but varies markedly around the site, making the total jointing pattern approach a complex form.

Plate 14.3: Jointing in the Owharoa Ignimbrite.

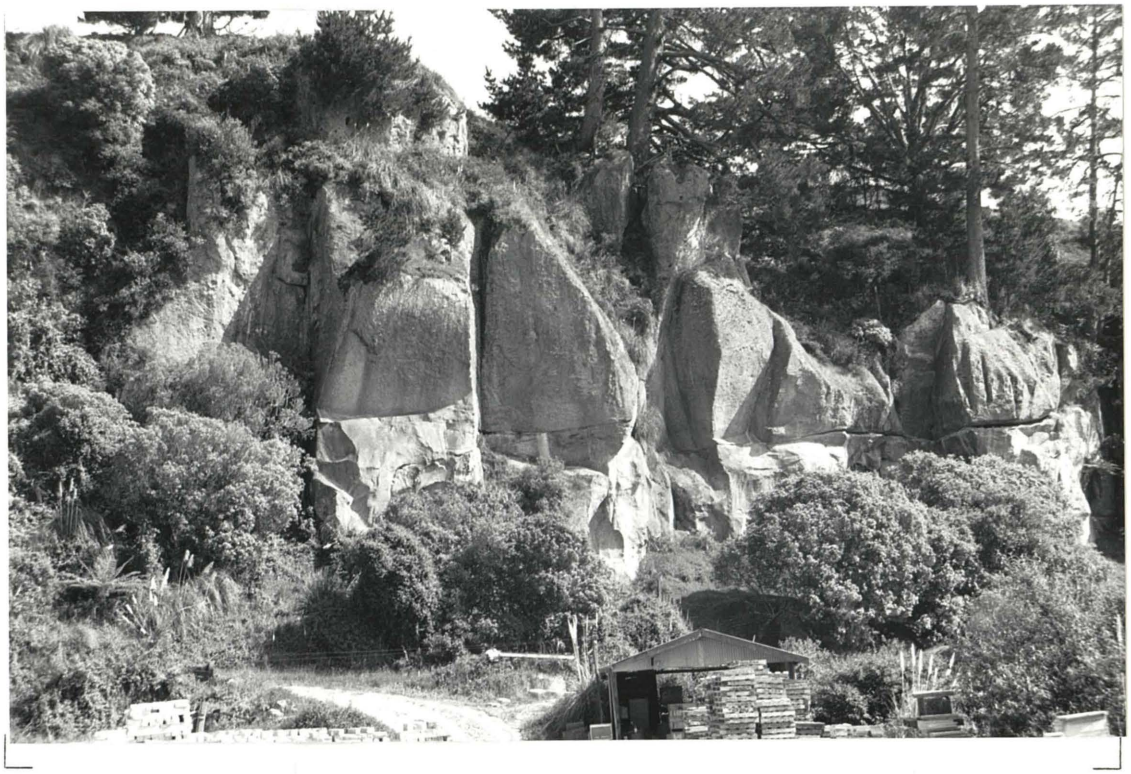

14.3.3 Owharoa Ignimbrite

Little exposure exists of the Owharoa Ignimbrite. From the sites studied, the lower one shows a moderately spaced columnar jointing pattern (plate 14.3), in which the joint faces are very straight compared with those of the Ongatiti Ignimbrite. The upper site has both vertical and horizontal joints, suggesting that it is similar to the blocky zone of the profile at Maraetai. Exposure is insufficient to properly describe the jointing at this upper site.

14.4 Summary

Jointing in ignimbrites is much more complex than the simple columnar jointing pattern which is often quoted as characteristic. This does occur in limited areas, but is accompanied by regions of complex, curved jointing with variable joint spacing, zones of blocky jointing, and regions of essentially unjointed material. These variations may all exist in one profile (Whakamaru Ignimbrite), or a subset of them may exist (Ongatiti and Owharoa Ignimbrites).

The dominance of vertical jointing, and the extreme dependence of data on the orientation of the face makes quantitative data irreproducible, and thus virtually meaningless. Classification of joint block shape and size using the terms defined in section 2.3.3.1 proved the most appropriate means of describing the jointing patterns.

PART 4 - MODELS FOR STRENGTH, JOINTING, AND GEOMORPHIC DEVELOPMENT

CHAPTER 15 - RELATIONSHIPS BETWEEN PETROGRAPHIC AND GEOMECHANICAL PROPERTIES

15.1 Introduction

Regression analysis of the relationships between the petrographic parameters measured in chapters 10 to 13, and the geomechanical properties, established in chapter 4, was undertaken in order to identify those parameters which are responsible for the strength of ignimbrite. From such analysis, intuitive models of the nature and development of strength have been developed.

15.2 Methods

15.2.1 Regression

Linear regression analysis was used, in the same manner as in chapter 8, to seek relationships between the petrographic and geomechanical properties. Initially, regressions were restricted to linear regression on two variables, with the geomechanical property as the dependent variable, and the petrographic property as the independent variable. Regression coefficients adjusted for the degrees of freedom (r^2_{adj}) of greater than 0.50 were considered to indicate a possible relationship (note that an r^2_{adj} value of 0.50 corresponds to an original r value of approximately 0.80 for the sample size used).

Regressions for each mechanical property were carried out using all of the petrographic parameters measured in chapters 10 to 13 (texture, fabric, post-depositional alteration, chemistry, proportions of groundmass, crystals, pumice, and lithics, and proportion of various mineral species making up the crystal component). For the textural parameters, the measured mean value was used in all cases; for the fabric and post-depositional alteration, rankings were developed to quantify the descriptions given in chapter 12 and 13. These rankings are described below.

Further regression analyses were carried out on derived hardness values to investigate further the controls on strength noted in section 8.4.2. The derived hardness values were obtained by multiplying the measured Shore scleroscope hardness by the proportion (%) of the appropriate component. For the crystal component, an overall crystal hardness for each

	1	2	3	4
FABRIC:				
shard form	platy	curved	cuspate	complex
shard alignment	random	partial	general	parallel
shard contacts	none	point	tangential	complete
pore shape	rounded	slightly elongated	elongated	strongly elongated
pore filling	vapour phase	open	partial	dense
crystal form	whole	slight breakage	shattered	fragments
cry / gm contact	plucked	loose	non-welded	welded
pumice form	spherulitic,	open, glassy	fragmented, glassy	dense, glassy
pum / gm contact	lapping	non-welded, random	non-welded, parallel	welded
ALTERATION:				
shard welding	none	dust	tips	glass
devitrification	none	slight	considerable	extensive
vapour phase alteration	none	slight	considerable	extensive

Table 15.1: Ranking classifications for fabric and alteration parameters.
cry = crystal, pum = pumice, gm = groundmass

ignimbrite was obtained by summing the product of the mineral hardness (table 6.3) and the proportion of that mineral in the ignimbrite (table 10.2). For this calculation, all amphiboles were grouped together, as were pyroxenes, as the crystal hardness values were established on representative crystals from these groups.

15.2.2 Ranking

The fabric parameters could only be determined qualitatively; ranking scales were developed in order to analyse these numerically. Each parameter was divided into a four-fold classification (based on the definitions given in tables 12.1 and 13.2), and ranking numbers of 1 - 4 applied to these classifications; regression analyses were performed using these ranking numbers. In all cases, the low numbers were assigned to the end which intuitively was expected to correspond to a low strength, and the high numbers to the opposite extreme. This was merely a convention designed to produce positive slopes, the order of assignment should have no influence upon the resulting regression coefficient. The ranking classifications are defined in table 15.1, and the numbers assigned to each ignimbrite are given in table 15.2.

15.2.3 Control data

With the exception of the chemistry, no control data were available for this analysis. The data of Hind (1986) include the bulk rock chemistry of his specimens, but do not include the other petrographic properties as examined here. No other suitable published geomechanical or petrographic data were available.

15.2.4 Multiple regression

After identifying possible relationships from simple linear regression on two variables, multiple regression was attempted with the aim of developing mathematical models of strength, and assigning weighting ratios to each significant petrographic property. Unfortunately, this technique proved unsuitable, as in many cases the independent variables used in the analysis were strongly correlated with each other. This reduced the number of possible predictors, and, in the worst cases, resulted in singular matrices. Under these

	shard form	shard alignment	shard contacts	pore shape	pore filling
WHAKA/up	1	1	2	1	1
WHAKA/low	4	3	3	1	4
ONG /1	1	1	2	1	2
ONG /2	2	2	3	2	3
ONG /3	3	3	3	2	4
OWH/up	4	3	3	3	4
OWH/low	4	4	3	4	4

	crystals	cry / gm contact	pumice	pum / gm contact
WHAKA/up	1	1	1	1
WHAKA/low	1	1	1	1
ONG /1	3	3	2	1
ONG /2	3	3	2	1
ONG /3	3	3	2	1
OWH/up	4	3	2	1
OWH/low	4	3	4	1

	shard welding	devitrification	vapour phase alteration
WHAKA/up	1	4	4
WHAKA/low	4	3	3
ONG /1	2	2	2
ONG /2	2	2	2
ONG /3	3	2	2
OWH/up	4	2	2
OWH/low	4	2	2

Table 15.2: Assignment of ranking numbers to each ignimbrite. cry = crystal, pum = pumice, gm = groundmass

circumstances, computation of the regression equations was impossible (Younger, 1979). Consequently, detailed mathematical relationships could not be determined using this technique.

Methods of examining the correlation between the petrographic parameters (factor analysis) could be used to identify the internal relationships between the parameters, and define hypothetical factors which account for these relationships. These hypothetical factors could then be used as the independent variables within a regression analysis (Lawley and Maxwell, 1971; Joreskog, 1976). However, it is not surprising that apparent relationships exist between the petrographic parameters, as they are merely rankings based on descriptions of the rock, and the described parameters are not completely independent (shard alignment and pore shape, for example, are strongly related). To carry out detailed statistical analysis on these parameters, with only seven original data points, is unwarranted, as over-interpretation of small variations is likely.

Therefore, qualitative models of the petrographic control on strength were developed based upon the initial linear regression on two variables. If more detailed statistical analysis is required, then further research, using the techniques developed here, and based upon the parameters identified as significant, should be undertaken with a greater number of ignimbrite blocks studied.

15.3 Petrographic controls on strength

15.3.1 Compressive strength

Table 15.3 presents the regression coefficients for compressive strength; only those parameters for which regression coefficients greater than 0.50 are included in the table. Some high regression coefficients can be seen for the textural parameters, with possible relationships existing between compressive strength and the crystal and pumice areas. These may be expected to be related mechanically, in that the size of the crystals and pumice clasts will influence the concentration of stresses around these components (section 4.8.3).

Many high regression coefficients are apparent between compressive strength and fabric parameters, suggesting that these have a major influence over the development of strength in these materials. In particular, the shard form and alignment, and the pore filling, are all strongly related to the

	$\sigma_{c,tot}$	$\sigma_{c,sat}$	$\sigma_{c,dry}$	$\sigma_{c,soft}$
TEXTURE:				
crystal area		0.54	0.54	
pumice area		0.60		0.66
FABRIC:				
shard form	0.63	0.77	0.74	0.68
shard alignment	0.71	0.86	0.87	0.61
shard contact			0.55	
pore filling	0.59	0.63	0.75	
ALTERATION:				
shard welding	0.59	0.73	0.69	
CHEMISTRY:				
Al_2O_3	0.56			0.53
PROPORTIONS:				
% groundmass				0.77
DERIVED HARDNESS:				
$S_{gm,tot} \cdot \%_{gm}$	0.76			
$S_{gm,sat} \cdot \%_{gm}$		0.71	0.62	
$S_{gm,dry} \cdot \%_{gm}$		0.87	0.76	
$S_{pum,sat} \cdot \%_{pum}$		0.58		
$S_{pum,dry} \cdot \%_{pum}$		0.52		
$S_{pum,soft} \cdot \%_{pum}$				0.51
$S_{lith,tot} \cdot \%_{lith}$	0.60			
$S_{lith,dry} \cdot \%_{lith}$			0.62	
$S_{lith,soft} \cdot \%_{lith}$				0.69

Table 15.3: Regression coefficients for compressive strength.

compressive strength. These three fabric parameters together describe the nature of the packing of the material (whether it is densely packed, or has an open structure). This packing appears to be the prime control on the compressive strength of the ignimbrites, which seems intuitively reasonable, as the closeness of the packing will influence the initiation and propagation of microfractures.

The other parameter to which the compressive strength is strongly related is the nature of the welding between the shards. This is also expected intuitively, as glassy welding will produce much stronger bonds than non-welded contacts, or dust welding. Interestingly, the compressive strength appears to bear little relationship to the other contacts within the material (shard contacts; crystal / groundmass contacts, or pumice / groundmass contacts).

Devitrification and vapour phase alteration processes appear to have no influence upon the compressive strength, nor does the chemistry. Two comparatively low regression coefficients are apparent for the chemistry against compressive strength, but the control data of Hind (1986) do not reflect these relationships. Likewise, the proportions of minerals within the crystal population do not appear to significantly affect the compressive strength, and, surprisingly, nor do the component proportions. However, the relationship apparent between the groundmass proportion and the softening factor is probably physically based, as the groundmass will provide most of the pore space for fluid absorption, and hence control the capacity for softening.

Derived hardness parameters are quite strongly related to the compressive strength, which is a reflection of the relationship between component hardness and compressive strength noted in section 8.4.2.1. In this case, the derived hardnesses, which take the proportion of each component into account, generally show higher regression coefficients than the original measured hardnesses for the groundmass, but lower coefficients for the pumice clasts.

15.3.2 Cohesion

In table 15.4 the regression coefficients for cohesion against petrographic parameters are presented. From this table it is apparent that very few high regression coefficients exist between these parameters, suggesting that the petrographic properties measured in this study are not the main controls over the cohesion of the material. Cohesion is a largely empirical

	c_{tot}	c'	c	c_{soft}
TEXTURE:				
crystal area	0.50	0.50	0.55	
pumice perimeter			0.65	
pumice form-factor		0.63		
CHEMISTRY:				
MgO			0.53	
LOI	0.68	0.78	0.74	
PROPORTIONS:				
% groundmass				0.55
DERIVED HARDNESS:				
$S_{gm,sat} \cdot \%_{gm}$		0.56		
$S_{lith,sat} \cdot \%_{lith}$				0.71

Table 15.4: Regression coefficients for cohesion.

parameter. It is derived in the same manner as for soils (as the intercept of a shear stress versus normal stress graph), and as such incorporates components of true cohesion and frictional resistance[1]. Chemical or molecular interactions are generally considered responsible for cohesion in soils (Terzaghi and Peck, 1948); in sedimentary rocks, cohesion is often attributed to chemical cementation during diagenesis (Attewell and Farmer, 1976).

From table 15.4, textural parameters may be seen to have a small influence on the cohesion of the ignimbrites studied. Weak regressions exist between the mean crystal area and cohesion, and slightly stronger relationships exist between the pumice perimeter length and form-factor (negative slope), and the cohesion of oven-dry and saturated specimens respectively. The perimeter relationship seems to be reflecting a dependence upon the area of contact between the groundmass and the clasts contained within it. The relationships between area, form-factor and cohesion are assumed to be reflecting this same effect, as the shape will indirectly influence the length of contact. The fact that these regression coefficients are not very high, and that the direct perimeter measurement does not have a high regression in all cases, suggests that this relationship is not a strong one.

Fabric and alteration parameters show no relationships with cohesion. This seems to confirm the assumption that cohesion is not strongly influenced by the physical packing, or the contacts between components.

---

[1] Shear strength is usually described by a failure envelope on a shear stress versus normal stress graph; the slope of the line gives the angle of internal friction, and the intercept gives the cohesion. Two different approaches to defining the failure envelope can be taken (see attached figure). A curvilinear relationship can be drawn for which the intercept is very small (or passes through the origin), implying that little or no strength is derived from cohesion. For this curve, the frictional strength varies with normal stress, particularly in the region of low normal stress. Often however, this curved relationship is approximated by a straight line. In this case the frictional strength is constant, and the cohesion has a relatively large, finite value. This latter approach was used in this study. The value of cohesion derived in this manner therefore incorporates any true cohesion which may be derived from molecular interactions and cementation, plus a frictional component derived from the graphical approximation with a straight line.

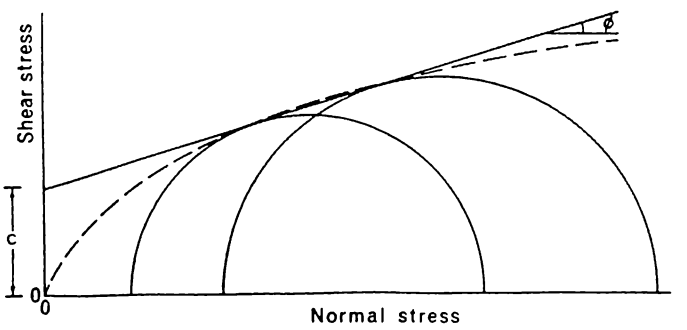

	ϕ_{tot}	ϕ'	ϕ
TEXTURE:			
crystal length			0.71
crystal perimeter			0.62
FABRIC:			
shard contact		0.63	
crystal form			0.53
crystal / groundmass contact			0.50
ALTERATION:			
devitrification			0.76
vapour-phase alteration			0.76
PROPORTIONS:			
biotite			0.52
DERIVED HARDNESS:			
$S_{lith,sat} \cdot \%_{lith}$		0.80	
$S_{lith,soft} \cdot \%_{lith}$		0.84	

Table 15.5: Regression coefficients for angle of internal friction.

The highest regression coefficients are found in a series of values relating the cohesion to the loss on ignition for the chemical analysis (negative slope). This value is a measure of the amount of volatiles (predominantly water) contained within the materials making up the ignimbrite. This would appear to be the most significant control on cohesion of all of the parameters measured, and suggests a molecular basis for the development of cohesion. However, the interpretation of this relationship is difficult, as the loss on ignition could include a variety of volatile components, or could simply be reflecting a change in the degree of crystallinity of the material (devitrification of glass will result in a loss of water from the structure).

As for the compressive strength, the relationship between groundmass proportion and softening factor for cohesion is thought to be realistic, as the groundmass will control the capacity for moisture to influence the strength, either chemically or through pore water pressures.

The derived hardness values, as for the original measured Shore scleroscope hardnesses, are not related to the cohesion; the two relationships apparent are believed to be coincidental.

15.3.3 Angle of internal friction

Table 15.5 presents regression coefficients for angle of internal friction against petrographic parameters. Most high regression coefficients exist for the texture, fabric, and alteration parameters, with no significant regressions for the chemistry, or component proportions. This confirms that, unlike cohesion, friction is based upon physical relationships between components, rather than chemical interactions.

Crystal length and perimeter each appear to bear some relationship to the angle of internal friction, as do the fabric parameters of the shard contact relationships, the crystal form, and the crystal / groundmass contact. Each of these effects can be explained on a physical basis, with the perimeter length and groundmass contact relationships all defining the areas over which contact between the components occurs, and hence over which friction is developed.

However, the slopes of the regression lines are negative in all cases. This goes against intuitive reasoning, which suggests that an increased

	$\sigma_{t,tot}$	$\sigma_{t,sat}$	$\sigma_{t,dry}$	$\sigma_{t,soft}$
FABRIC:				
shard form				0.73
shard alignment	0.65	0.74	0.77	0.74
shard contact				0.95
pore shape	0.63	0.70	0.77	
pore filling				0.89
pumice form		0.54		
CHEMISTRY:				
TiO_2		0.59		
Al_2O_3		0.54		
CaO		0.50		
PROPORTIONS:				
% groundmass		0.52	0.57	0.58
DERIVED HARDNESS:				
$S_{pum,tot} \cdot \%_{pum}$	0.71			
$S_{pum,sat} \cdot \%_{pum}$		0.88	0.66	
$S_{pum,dry} \cdot \%_{pum}$		0.85	0.63	
$S_{lith,sat} \cdot \%_{lith}$				0.69
$S_{lith,soft} \cdot \%_{lith}$				0.50

Table 15.6: Regression coefficients for tensile strength.

contact area will increase the total friction in the specimen. These relationships are, therefore, not believed to be realistic, and certainly do not provide sensible predictors of the friction angle. The reason for this lies in the very small variation in the measured friction angle values, which implies that the overall structure of ignimbrite determines its relatively high friction angle compared with other rocks, but that differences in the structure between specimens are insignificant. The slopes for the regressions discussed above are very low, hence the precise equations and the direction of the slopes are meaningless. However, the fabric and textural parameters are believed to be the main features which influence the development of friction.

Devitrification and vapour phase alteration are quite strongly related to the dry tensile strength. These are believed to influence tensile strength by increasing the area of contact between groundmass components, as well as the roughness of these components (roughness will increase as the glass shards crystallise).

One high regression exists between the amount of biotite in the specimen and the oven-dry angle of internal friction, and two high regression coefficients are seen for the derived lithic hardness against the saturated angle of internal friction. No physical basis can be seen for these relationships (as the areal proportion of biotite crystals and lithic clasts is so small) and they are assumed to be coincidental.

15.3.4 Tensile strength

Table 15.6 presents the regression coefficients for tensile strength against petrographic parameters. Textural parameters are unimportant in controlling the tensile strength.

Fabric parameters appear to be of considerable significance; shard alignment and pore shape, in particular, are highly correlated with the tensile strength. These indicate a slightly different control on tensile strength than on compressive strength. Under compressive stresses the material tends to compact, and hence it is the density of the packing which controls the ability of the rock to withstand these stresses. For tensile stresses, the reliance appears to be more on the alignment of the shards, with aligned shards and the resulting elliptical pores apparently resulting in high tensile stresses (see section 15.4.5 for further discussion).

The softening factor under tensile stress is highly correlated with a number of the parameters describing the packing of the groundmass (the

shard form, alignment, and contacts, and the pore filling). This can be attributed to the greater accessibility of the groundmass to water in a loose, open fabric (compared with a dense, tightly packed fabric), which will allow higher pore water pressures to develop. This is also reflected by a relationship between the proportion of groundmass and the softening factor.

The form of the pumice clasts also shows a relationship with tensile strength, though the regression coefficient is not particularly high. From section 8.4.2.2, strong relationships exist between pumice hardness and tensile strength. This is also seen in the derived hardness values in table 15.6, with the regression coefficients generally (but not in all cases) increased by taking the proportion of the ignimbrite comprised of pumice into account. Consequently, the hardness of the pumice clasts is a very important control on the tensile strength. This is believed to be due primarily to the influence of elasticity on the rebound hardness (section 6.2), as the elasticity, or ability of the pumice clasts to deform, will influence the stress distribution around these clasts, and therefore the strength of the rock. It is assumed that the form (glassiness and vesicularity) of the pumice clasts will influence their hardness, hence the relationship between pumice form and tensile strength. The dependence upon the pumice is also believed to be indirectly reflected by the weak regressions apparent between the proportion of groundmass and the tensile strength.

Several possible relationships exist between the chemistry and the saturated tensile strength. These may be coincidental, or they may reflect some chemical changes in the material upon saturation which result in increased tensile strength; they are difficult to interpret in physical terms.

The only other possible relationships are between the derived saturated lithic hardness, the lithic softening factor, and the softening factor under tensile stresses. These reflect exactly the high regression coefficients between lithic hardness, softening, and tensile softening (table 8.4). The areal insignificance of the lithic clasts is taken to imply that these are not causal relationships. However, they may be reflecting the fact that similar parameters control the softening of the lithic clasts as control the softening of the ignimbrites as a whole.

15.3.5 Index properties

The same analysis was undertaken for the index properties of density, porosity, ultrasonic wave velocity, and slake durability index. Shore

scleroscope hardness was not considered, as it was included in the derived hardness values, and it has been noted that the same trends exist between direct hardness and the derived hardness. Regression coefficients are not presented for these index properties, as they do not assist in further interpretation.

Bulk density and porosity are related to the same fabric parameters as the compressive strength. This is to be expected, as these parameters, particularly those describing the fabric, are merely measures of the packing, which is, in turn, an indication of the density and porosity. Likewise, these relationships reflect the strong predictive relationships between density, porosity, and compressive strength which were established in section 8.3.

Grain density is related to a variety of mineral proportions, and the total percentage of crystals. These relationships are believed to be realistic, as it is the minerals which make up the ignimbrite which determine the average grain density.

The proportion of unconnected pore space ($\Delta\eta$) does not show any direct relationships with the fabric, which is rather surprising. However, it has a number of high regression coefficients relating it to the crystal texture, the chemical composition, and the mineral proportions. These seem to have no real physical basis, as this parameter can only feasibly be interpreted in terms of the fabric of the material. It is thought that the high errors involved in determining this parameter are the cause of this apparent inconsistency, and that the measured values are inaccurate.

The Schmidt hammer rebound, ultrasonic wave velocity, and slake durability are all related to the same groundmass fabric parameters as the density, porosity, and compressive strength, reflecting the influence of the same controls on each of these properties. The L-type hammer rebound is also related to the percentage of the material comprised of groundmass, and the mean size of the pumice clasts. This suggests that the different hardnesses of the components are significant in determining the overall hardness of the intact rock.

In the case of the ultrasonic wave velocity, the pore shape is as significant as the packing parameters, which agrees with the observations made in section 7.5.2. Crystal and pumice fabrics, together with the amount of devitrification and vapour-phase alteration, also influence the velocity of wave propagation. This is the result of the waves having to travel through all of the components of the ignimbrite, and hence the fabric of all components will influence their propagation. Many of the other geomechanical and index

σ_c	c	ϕ	σ_t	l_{d2}
TEXTURE:				
crystal area pumice area	crystal area pumice perimeter pumice form-factor	crystal length crystal perimeter		crystal area crystal length crystal perimeter
FABRIC:				
shard form shard alignment pore filling		shard contacts crystal form crystal / groundmass contact	shard alignment pore shape pumice form	shard form shard alignment shard contact pore filling
ALTERATION:				
shard welding		devitrification vapour phase alteration		shard welding
CHEMISTRY:				
	loss on ignition			
PROPORTIONS:				
			% groundmass	

Table 15.7: Parameters which show relationships with strength.

properties simply reflect the fabric of the groundmass, which is volumetrically the most significant component.

Some relationships also exist between the slake durability index and the crystal size. These may simply be caused by the large crystals being unable to pass through the mesh of the durability apparatus, and thus being included in the retained component despite being completely separated from the rock. This was commonly observed during slake durability testing.

15.4 Models for strength

15.4.1 Summary of significant parameters

Table 15.7 summarises the petrographic parameters which regression analysis suggests have some relationship with strength. Due to its engineering significance for soft rocks, the slake durability index has been included as a strength property in this list.

It is apparent that textural and fabric parameters are the most frequently related to strength, and that these are the parameters which primarily control the development of strength within ignimbrites. However, it is also apparent that different parameters are responsible for the different types of strength (compressive, shear, and tensile). Hence, the different variations of these strengths between the specimens noted in chapter 4.

15.4.2 Compressive strength

The compressive strength is believed to be primarily a result of the groundmass fabric. In particular, it is the alignment of the shards, the amount of shattered, fragmentary material infilling the pores, and the nature of the welding at the contacts between shards, which control the compressive strength (note that welding is defined as the actual coalescence of the glassy components). These factors describe the degree of packing of the ignimbrite, and the tightness of the bonding between the shards; dense packing and welded contacts result in a high compressive strength and low softening factor, and an open packing with non-welded contacts results in a low compressive strength and high softening factor. Dense packing arises from close, parallel shards and pores densely infilled with fragmentary material.

These parameters will influence the distribution of of stress within the material, its capacity to compact prior to failure, and the ability of microfractures

to propagate. A dense material will not be capable of undergoing significant further compaction, whereas an ignimbrite with an open structure will be able to do so. Welded contacts will support high stresses, and distribute these across the groundmass framework; much of the stress within an open structure will be transmitted to fragmentary material within the pore spaces. Microfractures will readily propagate through non-welded contacts which are weak, whereas much higher stresses will be required to break welded contacts. These features describe the geomechanical behaviour of ignimbrites under compressive stresses.

An additional, but less significant, influence upon the compressive strength is the mean size of the crystals and pumice clasts within the material. These sizes appear to control the concentration of stress around these components, which is responsible for the initiation of microfractures. Such microfractures must be initiated at these inhomogeneities before the factors described above which influence their propagation can become important. The crystal and pumice clast sizes are inversely related to compressive strength: large crystals and clasts result in a low strength, and small crystals and clasts result in a high strength. The actual percentage of the area occupied by these components is, surprisingly, not significant, it is merely their mean size which is important.

The final parameter which is believed to be significant is the hardness of the pumice clasts; as well as the size of the pumice clasts, their hardness, and hence ability to deform, may also influence the concentration of stresses around the clasts. The derived hardness gives lower regression coefficients than the direct hardness, hence the proportion of the material occupied by pumice clasts is again shown to be insignificant. For both pumice clasts and crystals, this insignificance of the proportion is attributed to a threshold proportion which is low. As long as there are enough inhomogeneities to allow stresses to concentrate sufficiently for microfractures to initiate, the actual proportion above this threshold is irrelevant.

These are the only significant controls on compressive strength noted in this study. An ignimbrite of high compressive strength in both saturated and oven-dry conditions, and with a relatively low softening factor in compression, may therefore be expected to have the following features: shards which are close together, aligned so as to be approximately parallel, and welded to their neighbours; pores which are densely infilled with fragmentary material; crystals and pumice clasts which are small on average; and hard (rebound hardness) pumice clasts. This ignimbrite will also show only minimal

(compared with other ignimbrites) compaction and plastic deformation on compression, and the final rupture will be brittle. Conversely, an ignimbrite which is weak in compression, and shows considerable softening on saturation, may be expected to have the following characteristics: randomly arranged, non-welded shards; open pore spaces; large crystals and pumice clasts; and soft pumice clasts. This ignimbrite will also show considerable compaction and deformation in compression, and the final failure will not be a discrete event.

The bulk density and, especially, porosity of the ignimbrites were noted in chapter 8 to provide good surrogate measures of the compressive strength. These are obviously just bulk measures of the packing of the material which, from the above discussion, is the primary control on the compressive strength. Hence such a relationship is expected. Likewise, the groundmass hardness (both direct and derived) is related to compressive strength. This parameter is an intermediate measure of strength, in this case it is believed that the same packing factors described above which control compressive strength also influence the groundmass hardness in the same way.

15.4.3 Cohesion

Cohesion is not well modeled by the petrographic parameters examined in this study. The primary control on cohesion is believed to exist on a molecular scale, and is best reflected by the amount of volatiles contained within the structure of the glass and minerals making up the ignimbrite. The glass, in particular, will be hydrated.

Lesser influences upon the cohesion are the mean crystal area, and the mean pumice perimeter and form-factor. These are merely believed to influence cohesion by controlling the length of contact between the components, and hence influencing the area over which chemical effects can operate.

Cohesion is a poorly understood parameter, and the results of this study have done little to elucidate the nature of cohesion, except to suggest that the development of cohesion appears to occur on a molecular scale. This points the way for future research into this parameter, which should concentrate upon chemical influences on the cohesion.

15.4.4 Angle of internal friction

As for the compressive strength, it is the textural and fabric properties which control the angle of internal friction. However, the variations between ignimbrites are small, so a definitive model is difficult to develop. However, from the relationships seen in the preceding analysis, the following model is postulated.

It is the area of contact between individual components of the ignimbrite which is most significant, as it is this contact area along which frictional resistance is developed as the components move with respect to each other. Crystals appear to be the most important component in developing this frictional resistance, with both their perimeter length and roughness having an influence. This is reflected in the form of the crystals, in that a population of large, whole crystals has a shorter, and smoother, total perimeter, and thus lesser friction, than one of small, shattered crystals. Added to this is the nature of the contacts between the crystals and the groundmass - plucked contacts, as seen in the Whakamaru Ignimbrite, result in lower frictional resistance than the lapping-type contacts seen in each of the other ignimbrites.

The nature of the shard contacts is also important. Ignimbrites in which the shards contact over a large area (tangential to complete contacts, table 15.1) have higher angles of internal friction than those in which the shards contact at points only. Again, this is believed to be a purely mechanical effect related to the area over which the components are in contact.

Therefore, ignimbrites for which small, fractured crystals which are in close, firm contact with the groundmass are common, will have a high angle of internal friction. High friction angles will also result from shards which contact tangentially, or over relatively large areas. Conversely, ignimbrites characterised by large, whole crystals will have low angles of internal friction, as will ignimbrites in which the shards are in point contact only. Increased devitrification or vapour phase alteration may increase the friction angle by increasing the area and roughness of these contacts.

15.4.5 Tensile strength

Much of the control on the tensile strength comes from the fabric of the rock, and from the degree of shard alignment in particular (density and porosity, and hence packing, were seen to be relatively unimportant in section 8.3). Ignimbrites with close, parallel shards and elliptical pore spaces are

those with the high tensile strengths. This is believed to reflect the distribution of stresses within the ignimbrites. When the shards are aligned, the stresses are acting along the faces of shards, which will tend to compact against parallel shards. Such compaction will inhibit tensile failure. Conversely, when the shards are randomly arranged, the shards will be able to move in response to the stress by twisting around fulcrums provided by the neighbouring shards. In this way the structure will be disrupted, and failure will result. Consequently, ignimbrites with randomly arranged shards will undergo considerable plastic deformation prior to tensile failure, and the strength will be low; ignimbrites with aligned shards will exhibit a brittle failure, and a high tensile strength. In this model, the direction of shard alignment with respect to the principal stress is relatively insignificant, as reflected by the relatively small anisotropy for tensile strength in the Owharoa Ignimbrite specimens.

A second, very important, control upon the tensile strength of ignimbrite is the nature of the pumice clasts, their hardness in particular. Pumice hardness, which is assumed to be related to the form of the pumice clasts, is strongly related to tensile strength; ignimbrites with soft, spherulitic pumice clasts have relatively low tensile strengths compared with ignimbrites which contain dense, glassy pumice clasts. The proportion of pumice clasts has some influence on this, as the derived hardness values are generally slightly better predictors of tensile strength than the direct hardness measurements. Soft pumice clasts will deform more readily than the surrounding groundmass. They thus provide weak zones around which stresses can concentrate, and hence, as for the compressive strength, control the initiation of microfractures.

This model accounts for the relatively weak tensile strength of the lower Whakamaru Ignimbrite specimen compared with the lower Owharoa Ignimbrite specimen. Despite exhibiting the properties required for high compressive strength, the alignment of the shards is not as well developed in the Whakamaru Ignimbrite, and the pumice clasts are very soft due to devitrification; its tensile strength is consequently low.

15.4.6 Slake durability

It is the nature of the packing, and the shard welding, which control the resistance of the material to slaking. Ignimbrites with closely aligned shards, pores which are densely infilled with fragmentary material, and welded shards, will allow only small amounts of water into their structure, and the relatively

weak forces involved in wetting and drying or mechanical abrasion will be unable to disrupt the tightly packed structure, or break the welded bonds. In contrast, ignimbrites for which the shards are randomly arranged and non-welded, and the pores are open, will admit considerable quantities of water into their structure. The forces involved in wetting and drying will be much greater, and the resulting tendency to break down will be enhanced by the loose, non-welded structure. Mechanical abrasion will also readily exploit this weakness.

15.5 Volcanological context

Using simplified, ideal situations, these models for strength development in ignimbrites can be placed into a context which takes established volcanological variations into account to derive predictions for the variations in strength within an ignimbrite sheet. These are, of necessity, ideal models, as detailed spatial variations in the petrographic parameters examined in this study have not been investigated.

15.5.1 Variations in eruption conditions

The eruption conditions, in terms of the heat and energy of the eruption, will exert the main control over the nature of the ignimbrite which is produced. In particular, a highly energetic eruption, such as described in model A, section A1.4.3.1, will result in a high eruption column in which significant cooling of the pyroclasts can occur, a highly fluidised and expanded pyroclastic flow, and a relatively thin, cool deposit. In contrast, a less energetic, but more voluminous, eruption as described in model B, section A1.4.3.2, will produce a low eruption column in which very little cooling of the pyroclasts can occur, a poorly fluidised pyroclastic flow, and a relatively thick, hot deposit.

In model A, the highly fluidised pyroclastic flow will result in the shards being widely separated, and they will be deposited in a loose, random arrangement, with point contacts and open pore spaces. The energy of the eruption and flow might also be expected to fragment the crystals, producing small crystals with rough outlines. These characteristics will lead to ignimbrites with:

(1) low bulk density and high porosity,

(2) low compressive strength,

(3) relatively high angle of internal friction,
(4) low tensile strength, and
(5) low slake durability.

In contrast, the poorly fluidised pyroclastic flows of model B eruptions will result in closely packed glass shards on deposition. The thickness and heat of the deposit will allow compaction after deposition which will enhance this dense packing, increasing the alignment of the shards and the denseness of the pore filling. Crystals will tend to be relatively large and unbroken. These characteristics will result in the opposite strength properties to those above:

(1) high bulk density and low porosity,
(2) high compressive strength,
(3) low angle of internal friction,
(4) high tensile strength, and
(5) high slake durability.

Devitrification and vapour-phase alteration occurring after deposition will tend to increase the angle of internal friction, and decrease the tensile strength by softening the pumice clasts.

However, these are very general trends, and within ignimbrites there are many textural variations resulting from vertical and lateral variations in the deposit. These are discussed below.

15.5.2 Vertical variations

Significant sorting may occur during transport in the pyroclastic flow. This results in two main trends: the large pumice clasts rise to the top (reverse grading), and the large crystals and lithic clasts concentrate at the base of the deposit (normal grading) (Sparks *et al.*, 1973). This sorting is particularly active in the highly fluidised model A type pyroclastic flows (Walker *et al.*, 1980), but is also reported for the voluminous ignimbrites of model B type eruptions (Lipman, 1986). From section 15.4, a concentration of large pumice clasts at the top of the deposit will reduce the compressive strength somewhat, and will considerably reduce the tensile strength in this zone, as this parameter is sensitive to the presence of soft pumice clasts. Likewise, a normal grading of crystals will result in a lowered compressive strength and angle of internal friction, and increased cohesion at the base of the flow relative to its upper portions.

In the voluminous ignimbrites of model B, the temperature and thickness of the deposits will result in compaction and shard welding after deposition; this will be particularly marked where the material has infilled valleys in the pre-existing topography (Smith, 1960a,b; Ragan and Sheridan, 1972). This compaction will be greatest at depth within the deposit, due to high overburden stress and heat retention, and will cause the groundmass fabric to become more densely packed, with aligned shards and densely filled pore spaces (Riehle, 1973). From section 15.4, this will result in an increase in compressive strength, tensile strength, and slake durability with depth in the flow. These effects, as they influence the groundmass fabric, will generally outweigh the influences of sorting noted above. These same variations may be enhanced by variations in the pyroclastic flow with depth; the base of the flow is believed to be denser and less fluidised than the upper portions (Wilson and Walker, 1982). Hence the deposit will have a denser groundmass fabric at the base than at the top.

15.5.3 Lateral variations

Sorting will also occur with distance from source; large, heavy material will be deposited close to source, while light, smaller material will be transported greater distances (Wilson and Walker, 1982; Walker and Wilson, 1983; Walker, 1985). The head of the flow will also be more fluidised than the rear portions, due to entrapment of air by the front of the flow (Wilson and Walker, 1982). Cooling will also occur during transport. Consequently, with distance from source the ignimbrite may be expected to become finer, though large pumice clasts will be transported great distances; it may be expected to have a more open, less dense groundmass fabric; and will be cooler on deposition. These features will lead to the ignimbrites at distance from source being less compacted, and hence having lower compressive strengths, tensile strengths, angles of internal friction, and slake durabilities than their counterparts closer to source.

15.6 Summary

The groundmass fabric has the greatest influence over the geomechanical behaviour of ignimbrite. This is true for the compressive and tensile strengths, and a variety of index properties. The influence of the groundmass fabric is modified by the texture and fabric of the crystals and

clasts included within the ignimbrite, but these effects assume lesser significance.

However, the same properties of the groundmass fabric do not control each form of strength; compressive strength and slake durability are controlled by the packing and welding of the shards, whereas the tensile strength is most influenced by the alignment of shards and the resulting pore shapes. These variations are attributed to differences in the stress distributions, and resulting deformation and fracture patterns, of the materials under different types of stress.

Shear stress is not readily described by petrographic parameters; cohesion appears to bear a relationship to the chemical composition of the materials, but the relationship could not be well defined by the parameters measured in this study. The overall shard fabric is believed to control the angle of internal friction, but little variation in the angle of internal friction exists between the ignimbrites studied, so the influence of the parameters measured in this study is relatively minor.

CHAPTER 16 - MODELS FOR JOINTING AND GEOMORPHIC DEVELOPMENT

16.1 Introduction

Based upon the models for ignimbrite strength developed in chapter 15, together with the measurements presented in parts 2 and 3 of this thesis, idealised models for the patterns and development of jointing within a profile, and the geomorphic evolution of an ignimbrite sheet have been developed. These models are presented in this chapter.

16.2 Model for jointing

16.2.1 Summary of main features

The following is a list of the main features associated with the jointing observed at the study sites.

(1) The Whakamaru Ignimbrite exposed at Maraetai shows a profile exhibiting the entire range of ignimbrite jointing patterns observed, ranging from complex jointing at the base, through a zone of columnar jointing, to essentially unjointed material near the top. The Owharoa and Ongatiti Ignimbrites each show only a portion of the total profile - the central columnar zone. Therefore, the Maraetai profile will be used as the basis for the model.

(2) Each ignimbrite has been emplaced upon a very different pre-existing topography; the Ongatiti Ignimbrite appears to have filled a very wide, flat-floored valley at the study area (Olissoff, 1981), and the Whakamaru Ignimbrite at Maraetai has infilled a deep, narrow river gorge (Briggs, 1973), making it an example of the model B type ignimbrites discussed in section A1.4.3.2. The pre-existing topography beneath the Owharoa Ignimbrite cannot be determined.

(3) Moving downwards through the Maraetai profile the following notable physical changes occur:

(a) a large decrease in porosity (42 % to 16.6 %),

(b) a large increase in compressive strength (0.23 MPa to 26 MPa saturated), and

(c) a huge increase in the resistance to slaking (30 % to 98.8 % slake durability index).

Also, although the tensile strength of the upper material could not be measured, from the model discussed in section 15.4.5 it can be assumed to be much lower than that measured for the lower specimen, based on the fabric of the rock.

All of these variations can be attributed primarily to changes in the groundmass fabric, which is open and porous, with randomly arranged and non-welded shards in the upper specimen, and densely packed, with aligned, welded shards in the lower specimen.

16.2.2 Controls on joint development

The primary process by which joints develop in ignimbrite appears to be the release of the tensile stress which develops during cooling and compaction of the mass. Intuitively, the degree to which stress builds up must depend upon:

(1) the initial heat of the material upon emplacement,
(2) the rate at which this heat can be lost,
(3) the degree to which the material can deform without undergoing brittle fracture, and
(4) the tensile strength of the material at the time of joint formation (the tensile strength will vary with time as the mass cools).

The first of these factors, the emplacement temperature, will be controlled by the temperature of the magma body, and the energy of the eruption and resulting pyroclastic flow. The energy of the eruption will control the height to which the eruption column reaches, and the energetics of the flow, thereby dictating the capacity for air entrainment, and hence pyroclast cooling, before emplacement.

The rate of heat loss will depend upon the thermal conductivity of the material, and the rate at which volatiles can be lost through fluid escape. For any given point within the mass, the rate at which cooling can occur will depend upon its distance from the cooling surface. As DeGraff and Aydin (1987), and Long and Wood (1986) have shown for basalts, cooling to the upper surface (in contact with the atmosphere) is much more efficient than cooling to the lower surface (underlying rocks). Thus, for simplicity, in this model the effects of the lower cooling surface will be ignored, and therefore the rate at which a point can cool will be dependent upon its depth in the profile; a point near the surface will cool much faster than one deep in the profile.

These two factors, emplacement temperature and rate of heat loss, will dictate the amount of welding of the glass shards which can occur. True welding of glass requires temperatures in excess of 650 °C (Cas and Wright, 1987). Consequently, a point near the top of a flow may be expected to undergo less welding than one much lower in the flow where higher temperatures are reached, and are maintained for longer. Obviously, significant variations in the emplacement temperature with time during the eruption may override this pattern, but for this idealised model these effects will be ignored.

Also, for significant compaction of the mass to occur, a sufficient overburden stress is required. This induces physical compaction of the groundmass, and enhances compaction by encouraging plastic deformation of the shards. Again, a point at the top of the profile will undergo considerably less compaction than one lower in the flow, due both to a simple increase in overburden stress with depth, and to the increased plasticity of the shards due to higher temperatures.

As seen in chapter 15, the amount of compaction and welding of the groundmass provides the major control on the strength of the ignimbrite, in particular, on the compressive strength, tensile strength, and, by implication, the elasticity (or deformability) of the material, and thus its tendency to undergo either brittle or plastic failure. An ignimbrite with a loose, open, non-welded fabric will readily deform under a weak stress. Hence, most of the cooling stresses will be accommodated by plastic deformation rather than brittle failure, and consequently only a very few, widely-spaced joints may be expected. In contrast, an ignimbrite for which the shards are close together and have welded contacts will be considerably less deformable, and will need to release stresses by brittle fracture, thus producing more closely-spaced joints. The tensile strength will also be greater, allowing higher stresses to develop, and hence requiring more joints for their release.

16.2.3 The model

Figure 16.1 summarises an idealised profile through an ignimbrite sheet based on the jointing seen at Maraetai. Four main stages are represented as described below. At all levels the changes between these stages are gradational.

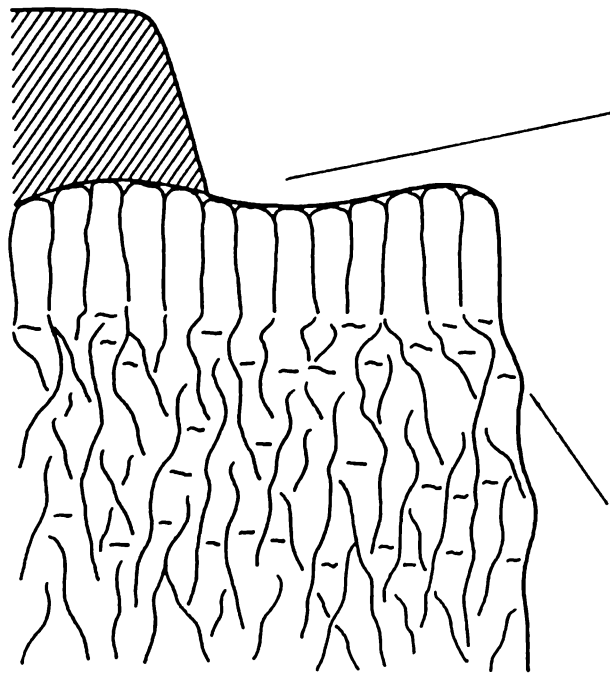

Upper Zone:

minimal overburden stress, rapid heat loss;
little compaction, no welding;
low strength, high deformability;
very widely spaced, vertical jointing

increase in compaction and welding;
increase in strength, reduction in deformability;
regular, widely spaced vertical jointing, occasional horizontal breaks;
vertical and horizontal joint spacing reduces

Lower Zone:

high overburden stress, high heat retention;
considerable compaction, glass welding;
high strength, brittle fracture;
complex, curved joints due to complex cooling surface

Figure 16.1: Development of joints in the Whakamaru Ignimbrite exposed at Maraetai.

(1) At the top the material cools most rapidly, it is very deformable and of low strength; hence the material has few joints and is classified as unjointed.

(2) On moving downwards the rate of heat loss slows, the material becomes less deformable, and shows widely-spaced vertical joints. Weathering and erosion will result in these being expressed as wide, arcuate columns with large aspect ratios. These joints are invariably curved to some extent, especially on their vertical faces. This is in contrast to the columnar joints described by Aydin and DeGraff (1987) for basalts, in which the joint faces are essentially straight-line segments meeting at sharp intersections. The curvature is thought to be the result of the much less brittle nature of ignimbrite (when compared with basalt) resulting in the stresses being released along long, curved planes rather than short, straight planes. The degree to which these columns are developed increases gradually down the profile, with the joint spacing decreasing and becoming more regular.

As the material at this stage is still very deformable, each vertical increment of joint growth (section 14.2.2) is large. These vertical growth increments result in horizontal breaks in the profile. Hence, horizontal breaks are infrequent in this columnar jointed zone. They do exist however, as seen in the Ongatiti Ignimbrite profile (section 14.3.2).

(3) Further down however, the vertical joint spacing becomes much closer, and the distance between horizontal breaks in the profile is concomitantly reduced, breaking the material into a blocky structure in its most extreme form of development. In effect, just as the distance over which stresses can be distributed (as reflected by the spacing of vertical joints) decreases, so too does the distance to which each joint will propagate in a single increment; hence there will be horizontal discontinuities.

(4) At the lowest level the jointing becomes much more closely spaced, the joints develop extreme curvature, and the distinction between the vertical and horizontal joint sets becomes less apparent, however a dominance of essentially vertical joints still exists. This is the complex jointing zone.

The close spacing in this zone is due to high overburden stresses, high temperatures, and slow cooling. The material becomes competent through compaction and welding, and exhibits a brittle fracture mode. This results in the development of numerous, closely spaced joints. However, in a simple situation, these joints would be expected to assume the same columnar form as their counterparts higher in the profile. Basalts, which are an extreme

example of a competent, brittle rock, develop very clear columnar joints, and these ignimbrites should follow the same pattern. Possible reasons for the development of complex jointing are

(a) large-scale plastic deformation during cooling, and/or
(b) a complex cooling surface resulting from the pre-existing topography upon which the ignimbrite was deposited.

Large-scale plastic deformation of the material during cooling and compaction of the mass, and following joint development, has clearly occurred at Maraetai, as the joint faces can be seen to form large vertical sags. Thus the material has compacted and welded sufficiently to deform as a coherent fluid, rather than as individual pyroclasts as in its original emplacement, yet has sufficient strength to undergo brittle fracture. The slow deformation of a pane of glass is seen as an analogy to this.

Probably a more common cause of complex jointing is the existence of a complex cooling surface caused by the ignimbrite being deposited in a valley. The model above has assumed that cooling occurs towards a flat upper surface. In such a situation, cooling, and hence stress distribution, is even and predictable, and regular vertical jointing patterns result. However, it was noted above that cooling will also occur towards the underlying ground surface, albeit at a much slower rate. If this ground surface is horizontal, then the cooling in this direction will also be even and predictable. If however, the ground is not horizontal, then the cooling surface will be very complex, with cooling occurring towards each side of the pre-existing valley at rates dependent upon the precise shape of the valley walls (the same will be true over pre-existing ridges). As the joints will propagate in the direction perpendicular to the cooling surface at each point (section 14.2.1), the complexity of the cooling surface will be reflected in a complex jointing pattern. The precise pattern will, therefore, be strongly dependent upon the local conditions at the time of joint development. This effect can be assumed to be greatest at some distance (depth) from the contact with the atmosphere, as the cooling at this upper surface will be so much faster than that towards the ground that its influence will dominate the upper regions.

16.2.4 Ongatiti and Owharoa Ignimbrites

The Ongatiti and Owharoa Ignimbrites each only show a portion of the profile described for Maraetai. In the case of the Owharoa Ignimbrite, this can

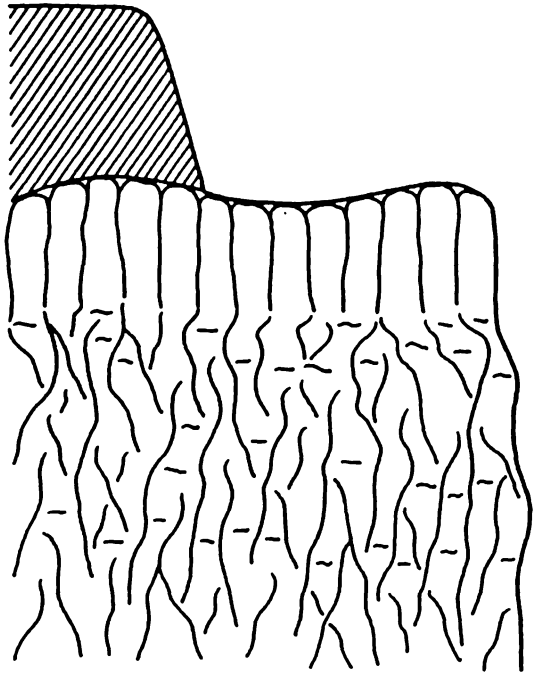

steep faces controlled by high shear strength of material; jointing insignificant due to very wide spacing

columnar jointing; erosion along weak, closely-spaced joints between columns leaves resistant columns exposed

steep, precipitous cliff faces reflect the complex jointing and high intact strength; cliff retreat is by joint block failure

Figure 16.2: Model for hillslope development.

be attributed simply to the minimal exposure available, and possible erosion of much of the profile.

The Ongatiti Ignimbrite exhibits only the columnar jointed zone. The deposition on a horizontal surface means that a zone of complex jointing would not be expected, as discussed above. However, the absence of a non-welded, unjointed upper zone may be surprising. In this case it is the dust welding (section 12.4.1) which is believed to have resulted in a reduction in the temperature required for welding, and therefore allowed the welding to extend to the upper surface. Thus, although cooling would be rapid at this upper surface, and compaction insignificant, the material would still develop some strength through welding, and hence exhibit columnar jointing.

16.3 Model for geomorphic development

A model for the geomorphic development of ignimbrites can be derived using the jointing model discussed above and the strength parameters measured in part 2. As for the jointing model, the profile at Maraetai will be used as a conceptual base, as it presents the most complete section. Other ignimbrites may display only portions of this profile, and their landforms will reflect those portions only. The following discussion is in two sections, initially an idealised hillslope profile is developed, and this is then used to derive a model for overall landscape evolution.

16.3.1 Hillslope development

The following model for hillslope development is summarised in figure 16.2. At the base, the high intact strength and durability of the ignimbrite cause the jointing to exert the greatest control upon the hillslope development, with erosion and cliff retreat occurring primarily through the failure of joint blocks. As the jointing is predominantly vertical, this results in steep, precipitous cliff faces. However, the complex nature of the jointing is reflected in curved faces, which frequently retreat by exfoliation of platy joint blocks. The boundary between this zone and the overlying columnar jointed zone is gradational, with many joints extending through the boundary.

In the central zone the columnar jointing of the ignimbrite becomes apparent. The material is still of relatively high strength and high durability, and is consequently resistant to failure of the intact rock; the jointing patterns again exert the major influence on hillslope development. The widely spaced

columnar joints are frequently separated by zones of closely spaced joints. These zones represent areas of weakness, and are preferentially eroded. This leaves the relatively strong columns standing as isolated outcrops, often in groups of several joints forming a single exposure. The boundary between this and the upper zone is sharp, but wavy. The columnar joints appear to coalesce into dome forms at their upper surface. Such domes may be from less than 30 m to greater than 100 m across, with areas of soft material surrounding them.

At the top of the profile is a soft zone, which is characterised by very few joints, low strength, and extremely low durability. The intact rock of this zone is therefore prone to physical weathering by means of wetting and drying, and mechanical abrasion. This, accompanied by the paucity of joints, means that the intact strength of the rock is a more important control over the hillslope development than the jointing patterns.

What is remarkable about this material is its ability to maintain very steep slopes for long periods of time (almost vertical artificial cuttings of greater than 40 years age still maintain their initial form with no apparent failure). With the low compressive strength, and lack of joints, the material is best analysed as a soil rather than a hard rock. Under these conditions the shear strength has a major influence in determining the stable slope angle. The relatively high cohesion (compared with soils) of this material, and the very high angles of internal friction (note that the friction angles are the same for this material as for the other ignimbrites) means that this material is able to maintain very steep slopes. A simple infinite slope analysis (Lambe and Whitman, 1979) for the soft, upper Whakamaru Ignimbrite suggests that the dry material is able to maintain approximately vertical slopes (calculated as 89 °) of 14 m, whilst the saturated ignimbrite can support approximately 7 m high vertical cliffs. Although this is a very crude analysis, it highlights the ability of the material to maintain very steep slopes.

16.3.2 Landform development

From this idealised hillslope profile, a model of landform development on an ignimbrite sheet can be derived. Initially the upper, soft material is exposed; the low durability of this material makes it susceptible to rapid stream incision, resulting in dissection of the surface of the deposit (figure 16.3a). This produces steep, narrow gullies, due to the ability of the material to remain stable at relatively high angles.

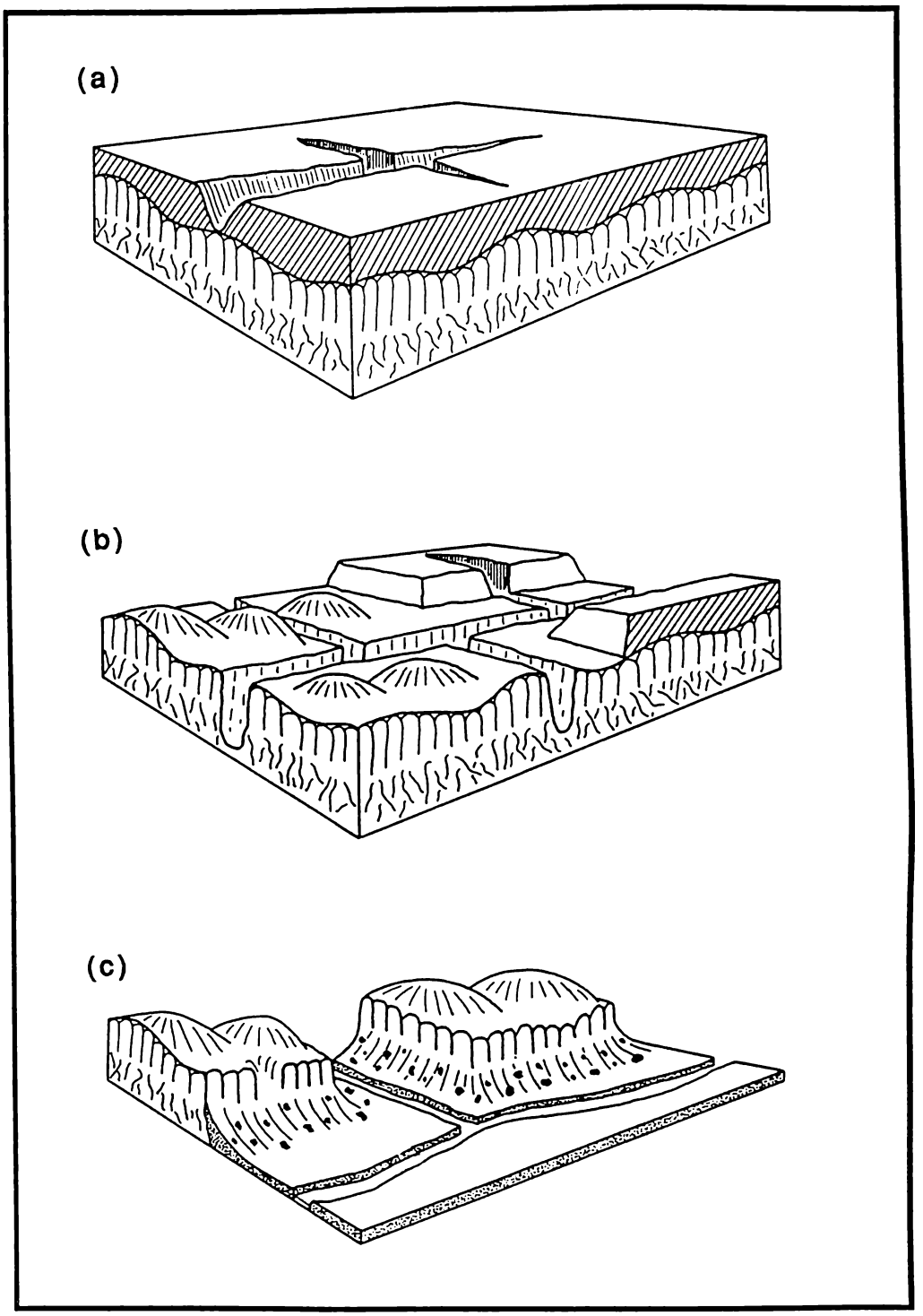

Figure 16.3: Stages in landscape development on an ignimbrite sheet. (a) Rapid erosion of steep gullies in the upper, unjointed zone. (b) Stripping of poorly welded material exhumes a rounded topography on the columnar jointed zone. Narrow gorges develop in the underlying ignimbrite. (c) Valley widening leaves rounded hills, steep, jointed faces and blocky talus slopes.

As this material is stripped away, an erosional bench representing the boundary between the hard, columnar jointed ignimbrite and the soft, upper material is exposed (figure 16.3b). This bench has an uneven surface reflecting the waviness of the boundary between the two zones, and the tendency for the columnar joints to coalesce into dome forms at their upper surface. Below this surface, the high strength and predominantly vertical jointing of the ignimbrite lead to very steep, precipitous cliffs and narrow gorges. These features can be seen in plate 16.1.

Further retreat of these cliffs occurs through the collapse of joint blocks, so vertical faces are maintained as the valleys widen. Talus slopes develop at the base of these cliffs, and the resulting three landform units are: an upper, rounded, eroded surface; a vertical, jointed face; and a blocky lower slope (figure 16.3c, plate 16.2a). Continued degradation of these slopes leads to increased masking of the jointed rock faces by talus deposits (plate 16.2b) Eventually the ignimbrite is almost completely buried, with resistant columns exposed above the ground surface (plate 16.3a); and the final stage is a very typical, rounded ignimbrite topography (plate 16.3b). This topography is characterised by drainage systems with no outlets, as the jointing of the underlying ignimbrite is sufficient to provide drainage.

The above discussion applies to the voluminous model B type eruptions of section A1.4.3.2. The high-energy model A type eruptions will produce ignimbrites with the characteristics of the soft, upper material described above. The resulting landforms will reflect these characteristics, with the development of steep, narrow valleys, and rapid erosion of the material.

16.4 Summary

Idealised models of joint development, hillslope form, and geomorphic development based upon the geomechanical and petrographic measurements made in this study have been derived. These all rely upon predictable variations in the primary petrographic features recognised as influencing the strength of the ignimbrites - the groundmass fabric and the nature of shard welding. Variations in these properties caused by emplacement conditions result in predictable strength variations, and in characteristic jointing patterns associated with each strength zone. It is these strength and jointing patterns which dictate the means by which erosion can affect an ignimbrite, and hence the resulting landform patterns.

(a) general view (top)

A general view of the Whakamaru Ignimbrite near Waipapa is seen. At the level of the camera, and to the extreme right front of the photograph, is the soft, upper material. This appears to be at the same elevation as the skyline at the rear of the photograph, suggesting an original flat depositional surface for the ignimbrite sheet. This upper material falls steeply to a lower bench at the level of the bridge. This steep drop represents the edge of the retreating soft material as it is stripped away. The erosional bench below this material is not flat, but has numerous subdued domes over it; these are believed to represent the coalescence of the underlying jointing into such domes, and is the form of the boundary between the levels of different degrees of induration and jointing. The bridge visible in the centre of the photograph spans a narrow gorge of 30 m across by 60 m depth. The walls of this gorge are near vertical, reflecting the influence of the vertical jointing and relatively high intact rock strength. This stream is a tributary of the Waikato River which flows from right to left across the photograph.

(b) Waikato River Valley (bottom)

In this photograph the Waikato River valley itself is seen, somewhat further upstream at Maraetai. The narrowness of the gorge is evident, with nearly vertical cliffs bounding the river on each side. The cliff to the left front of the photograph is 100 m high from the road to the skyline. The form of these cliffs is controlled by the predominantly vertical jointing pattern of the ignimbrite. Large, curved joint faces can be seen on the left of the photograph. At this point little or no soft material is present at the top of the profile, due to erosion. It thickens some distance back from the valley.

Plate 16.1: Early stages of landform development in ignimbrite.

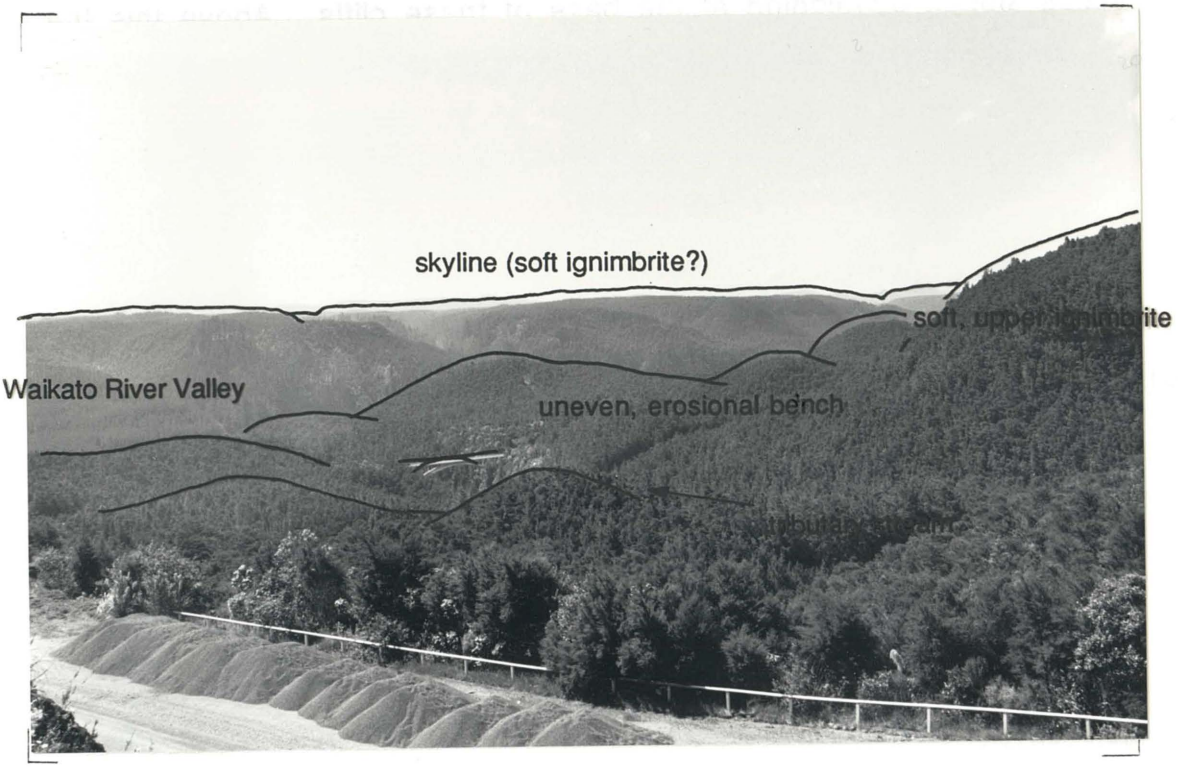
skyline (soft ignimbrite?)
Waikato River Valley
uneven, erosional bench


terrace

(a) (top)

The collapse of joint blocks from the columnar jointed zone results in talus slopes developing at the base of these cliffs. Above this the columns remain standing vertically, with a rounded upper surface to the outcrop. Frequently these features may be expressed as part of an isolated outcrop, as shown in this example, or the same landform units may develop along the walls of valleys.

(b) (bottom)

With continued erosion the talus slopes enlarge, and begin to mask the vertical slopes, leaving only isolated rocky outcrops at the top of the slopes. Large, fallen boulders at the base of the slopes are typical.

Plate 16.2: Middle stages of landform development in ignimbrite.

(a) (top)

With continued landscape development, the vertical outcrops become completely masked. Occasionally, single, resistant columns remain exposed.

(b) (bottom)

The final stage of development is the complete masking of all of the ignimbrite, leaving a very typical, low, rounded topography. This topography is characterised by a lack of drainage channels, and the presence of springs, as the hydrology is dominated by the jointing of the ignimbrite, which allows considerable groundwater movement.

Plate 16.3: Final stages of landform development in ignimbrite.

CHAPTER 17 - CONCLUSIONS

17.1 Geomechanical variability of ignimbrite

17.1.1 Measured strengths

Ignimbrites are weak rocks; compressive strengths measured in this study show values spanning the ranges of low (44 MPa) to very low (0.23 MPa) strength rocks in the classification of Deere and Miller (1966). Likewise, their cohesion is weak (0.06 - 13 MPa) in comparison with other rocks, generally being comparable with soft sedimentary rocks, but their angle of internal friction is relatively high, and relatively uniform between the ignimbrites (~33 ± 2 °). The tensile strength of ignimbrites is low (0.12 - 7.1 MPa), but not as low as might be expected compared with sedimentary rocks of low compressive strength. Saturation leads to considerable softening of the materials for compressive strength, tensile strength, and cohesion, with softening factors of 3 to 5 being common, and values as high as 10 being reached occasionally. Saturation has little influence upon the angle of internal friction.

Available measurements suggest that ignimbrites are highly deformable rocks, with low values of Young's modulus, and high values of Poisson's ratio. This is reflected in the nature of the failure in mechanical testing; all of the specimens showed considerable plastic deformation prior to failure. This was most pronounced in the weak and saturated specimens, with the strong, oven-dry specimens showing the most brittle fracture mechanism. However, even in these rocks, the failure was not a discrete event.

Associated with these strength variations are comparable variations in the bulk density (1212 - 2124 kg m^{-3}, oven-dry) and porosity (14 - 42 % effective porosity) of the materials. Ignimbrites also span a wide range of slake durabilities, with indices ranging from 30 % mass retained after two slaking cycles, to 99 % retained.

Although weak, the strength of ignimbrites is highly variable, and ranges over at least two orders of magnitude in terms of the compressive strength and cohesion, and at least one order of magnitude for the tensile strength. These variations occur between ignimbrites, but can also exist within one ignimbrite deposit. In fact, the materials are characterised by very rapid vertical and lateral variations in strength, which can lead to two orders of magnitude change in the above strength properties within one vertical section.

17.1.2 Wider variation

These values represent the range of materials measured in this study. One case exists in the literature (Hind, 1986) of an ignimbrite for which the compressive strength is above the range measured here, reaching a value of 79 MPa (medium strength, Deere and Miller (1966)) for an oven-dry specimen. All other reported cases lie within the range above.

However, geomechanical testing such as undertaken in this study, and other reported studies, relies upon the ability to extract a coherent block of material from which to prepare test specimens, as well as on the ability of these specimens to remain intact during preparation and testing. Many ignimbrites do not satisfy these requirements; in the field they are incoherent deposits which do not contain joints. They vary from relatively fine, sand sized material, to deposits of large, clast-supported pumice clasts. Obviously they can not be tested by rock mechanics methods; they must be treated as soils, and tested using appropriate soil mechanical means. From the petrographic correlations established in this study it can be assumed that these materials will be very weak in compression and tension, and exhibit low cohesion values. However, they can be expected to have relatively high angles of internal friction, and should thus be best modeled as a loose, well graded sand. These materials are volumetrically significant portions of ignimbrites, as many high-energy eruptions produce deposits which are entirely of this nature, and similar materials may be found at the top of the profile in more voluminous ignimbrites.

17.1.3 Value of "ignimbrite" as an engineering term

The term "ignimbrite" is defined genetically, and hence incorporates all of the variability discussed above. It becomes apparent therefore, that the identification of material as ignimbrite does little to indicate the engineering properties of the material, except to imply that it will be relatively weak compared with many rocks. Without close examination of the materials in the field, no engineering development on ignimbrite should be contemplated, as the material may be essentially an engineering soil, or it may be a weak, yet competent, rock. If it is of soil consistency, it should be treated in the same way as an unconsolidated sand. If it is a rock, then some index properties are useful as predictors of the ignimbrite strength. Simple petrographic properties can also be used as indicators of the geomechanical properties.

17.2 Strength indices

17.2.1 Bulk density and porosity

The porosity (true and effective) is an excellent predictor of compressive strength of oven-dry ignimbrites; predictive equations derived from the data in this study adequately predict the strength of control data. Dry bulk density is also a good predictor of compressive strength (both oven-dry and saturated), and the saturated bulk density also predicts compressive strength, but less precisely. Any of these properties could, using the predictive equations presented in chapter 8, be used to obtain estimates of the compressive strength from small specimens for which geomechanical testing is impossible. These properties do not successfully predict the other types of strength examined in this study.

17.2.2 Schmidt hammer rebound

The Schmidt hammer rebound provides a good indication of the compressive and tensile strengths of ignimbrite for the range of materials tested in this study; predictive equations relating Schmidt hammer rebound values to the compressive and tensile strengths have been presented in chapter 8. However, despite the Schmidt hammer rebound and the strength being related, there is a large error involved in the predictive equations. Hence, Schmidt hammers are not sensitive to small changes in the strength. They are good for identifying and quantifying major strength variations, and for predicting general values of compressive and tensile strength, but they will not predict subtle changes, nor give precise predictions of the strength properties.

17.2.3 Ultrasonic wave velocity

Ultrasonic wave velocity does not predict the compressive or shear strength of ignimbrites at all. It does, however, appear to provide a good index of the tensile strength, and predictive equations were presented in chapter 8. Different equations exist for oven-dry and saturated tensile strengths, yet the wave velocity terms are not dependent upon the moisture content. Hence, it is possible to predict the range of tensile strengths at the moisture extremes from measurements of the wave velocity at any moisture content. This means that these relationships, which were derived under laboratory conditions, should

readily transfer to field conditions where the moisture content cannot be controlled.

17.3 Relationships between petrography and geomechanics

The groundmass fabric has the greatest influence over the geomechanical behaviour of ignimbrite. This is true for compressive and tensile strengths, and a variety of index properties. The influence of groundmass fabric is modified by the texture of the crystals and clasts included within the ignimbrite, but these effects assume lesser significance. Shear strength is not readily described by petrographic parameters.

17.3.1 Compressive strength

The compressive strength of ignimbrites is primarily a result of the alignment of the glass shards, the amount of fragmentary material infilling the pores, and the nature of the welding at the contacts between the shards. These parameters describe the packing of the groundmass, and thus the capacity of the material to undergo plastic deformation prior to failure; they also control the ability of microfractures to propagate through the groundmass, as microfractures must disrupt the structure, and break the bonds between individual shards.

An additional, but less significant, control on compressive strength is the mean size of the crystals and pumice clasts within the material. These factors are important in controlling the concentration of stresses around such components, and hence the initiation of microfractures. The hardness of the pumice clasts is also related to the compressive strength of the rocks in the same way - the extent to which clasts deform influences the concentration of stresses within the rock, and hence the initiation of microfractures.

An ignimbrite of high compressive strength, low deformability, and a relatively small loss of compressive strength on saturation, may therefore be recognised by the following characteristics:

(1) shards which are close together, and aligned so as to be almost parallel to one another,
(2) pores which are largely infilled with fragmentary material,
(3) welded contacts between individual shards,
(4) crystals and pumice clasts which are small on average, and
(5) hard pumice clasts.

The first two of these indicative parameters may be replaced by porosity (or bulk density as a less accurate surrogate) if detailed examination is not undertaken, as these are bulk measures of the packing of the ignimbrite. A low porosity (or high bulk density) is characteristic of an ignimbrite with high compressive strength.

Conversely, an ignimbrite with petrographic parameters at the opposite extremes to those described above will characteristically have a low compressive strength, will undergo large amounts of plastic deformation, and will suffer a marked loss of strength on saturation.

17.3.2 Tensile strength

The degree of alignment of the shards is the primary control on the tensile strength of ignimbrites. Ignimbrites with randomly arranged shards undergo considerable plastic deformation prior to tensile failure, and the strength is low; ignimbrites with aligned shards exhibit a brittle failure, and a high tensile strength. The direction of testing with respect to the shard alignment creates only a small anisotropy.

The hardness and proportion of pumice clasts is also an important influence upon tensile strength; ignimbrites with soft, devitrified pumice clasts have relatively low tensile strengths compared with ignimbrites containing dense, glassy pumice clasts. Soft pumice clasts deform more readily than the surrounding groundmass, and thus provide regions of stress concentration and microfracture development.

The following characteristics (in order of importance) are thus typical of an ignimbrite with a high tensile strength and a brittle failure mechanism:

(1) shards aligned so as to be almost parallel,
(2) dense, glassy pumice clasts, and
(3) a relatively low proportion of pumice clasts.

A hand specimen surrogate measure for the alignment of shards is the shape of the pumice clasts; lenticular pumice clasts which have undergone considerable compaction are generally associated with aligned shards.

Ignimbrites with the opposite characteristics to those listed above can be expected to have low tensile strengths, and to undergo considerable plastic deformation.

17.3.3 Shear strength

Cohesion is not well described by the petrographic parameters examined in this study. Possible relationships with the loss on ignition during geochemical analysis suggest that cohesion may exist on a molecular scale, but the relationships could not be well defined by the parameters measured in this study.

The texture and fabric of the ignimbrites are the main controls on the angle of internal friction, with the length of contact between the various components, and the roughness of these contacts being the most important factors. However, there is little variation in the internal friction angles measured, so it is apparent that the overall shard fabric of ignimbrites is responsible for the high friction angles measured, but the friction is insensitive to variations in the fabric parameters measured.

17.4 Models for jointing and geomorphic development

Idealised models of joint development and geomorphic evolution have been presented. These are based upon the geomechanical and petrographic parameters measured in this study, and make use of predictable variations in the primary petrographic features recognised as influencing the strength of ignimbrites - the groundmass fabric and the nature of the shard welding. Variations in these properties are caused by the conditions of eruption, transport, and deposition, and can be predicted using models derived from the volcanological literature. They result in predictable strength variations, and in characteristic jointing patterns associated with each strength zone. It is these strength and jointing patterns which dictate the means by which erosion can affect an ignimbrite, and hence the resulting landform patterns.

17.5 Further research

Ignimbrites are very complex rocks for which minimal geotechnical research has been undertaken. This means that there is considerable scope for further research following on from the present study.

Large volumes of ignimbrite are essentially soils in an engineering sense, and can not be tested by rock mechanics methods. Considerably more research is required to quantify and understand the strength of these materials. This work should concentrate on treating the material as a soil, and should thus look in detail at the controls on shear strength, and particularly the frictional resistance, of the material. Triaxial testing with controlled moisture contents should provide the greatest amount of information, but large specimens will be required to account for the coarse grain size of many of the materials.

In terms of the petrographic control over the strength of ignimbrite, the compressive and tensile strengths, the angle of internal friction, and the slake durability of the materials have been well explained by physical relationships between the components making up the materials. However, the cohesion has not. The nature of this form of strength deserves more investigation, with the suggestion of a chemical basis providing a starting point for such research.

Jointing is a property of ignimbrites which requires considerably more investigation. In this study, only qualitative jointing descriptions were obtained. Careful field measurement, and the establishment of a series of meaningful measurements for describing the joints is essential for geotechnical purposes. Simple joint spacing and orientation are not sufficient. Following this, an examination of the development of jointing in these materials is necessary. Such work would preferably take the form of numerical modeling of the joint development in a cooling mass, from which the extent to which the cooling surface controls the development of complex jointing could be assessed. For this to be successful however, the actual jointing needs to be carefully described, and the conditions for joint development, in terms of temperature, tensile strength, and magnitude of cooling stresses, need to be defined.

A final area of important research is to refine the models for strength in terms of the vertical and lateral variations within an ignimbrite, in order to develop good predictive models of strength variation through an ignimbrite sheet. A first step in such research would be to investigate the detailed variations through an ignimbrite profile, in order to relate the strength

variations to the inferred volcanological conditions of transport, deposition, and post-depositional alteration of the material. The Hinuera Stone Quarry, for which some volcanological investigation has been undertaken, and from which cut blocks can be obtained, would be a realistic place to undertake such work. If the strength can be closely related to vertical variations in volcanological conditions, then lateral inferences can be drawn. This will then point the way for detailed examination of lateral variations.

REFERENCES

REFERENCES

Anon., 1983; *Pundit manual for use with the portable ultrasonic non-destructive digital indicating tester, mark IV.* C.N.S. Electronics Ltd.

Al-Jassar, S.H., and Hawkins, A.B., 1979; Geotechnical properties of the Carboniferous limestone of the Bristol area; the influence of petrography and chemistry. *Proceedings of the Fourth Congress of the International Society for Rock Mechanics* 1: 3-13.

Alonso, M., and Finn, E.J., 1975; *Physics.* Addison-Wesley, Massachusetts.

Armstrong, R.A., Bristow, J.W., and Allsopp, H.L., 1986; High temperature ash-flows of the Jozini Formation, Southern Africa. Volcanology and Petrogenesis. *International Volcanological Congress, New Zealand, 1-9 February 1986. Abstracts*: 27.

Attewell, P.B., and Farmer, I.W., 1976; *Principles of Engineering Geology.* Chapman and Hall.

Aydin, A., and DeGraff, J.M. 1988; Evolution of Polygonal Fracture Patterns in Lava Flows. *Science* 239: 471-475.

Barberi, F., Innocenti, F., Lirer, L., Munno, R., Pescatore, T., and Santacore, R., 1978; The Campanian Ignimbrite: a Major Prehistoric Eruption in the Neopolitan Area (Italy). *Bulletin Volcanologique* 41: 10-31.

Beavis, F.C., 1985; *Engineering Geology.* Blackwell, Melbourne.

Bennett, F.D., 1974; On Volcanic Ash Formation. *American Journal of Science* 274: 648-661.

Blank, H.R., 1965; Ash-flow deposits of the Central King Country, New Zealand. *New Zealand Journal of Geology and Geophysics* 8: 588-607.

Bieniawski, Z.T., 1976; Rock mass classification in rock engineering. *Proceedings of the Symposium on Exploration for Rock Engineering,* Johannesburg, November 1976: 97-106.

Bieniawski, Z.T., 1988; The Rock Mass Rating (RMR) System (Geomechanics Classification. *In* Kirkaldie, L. (ed), *Rock Classification Systems for Engineering Purposes.* American Society for Testing and Materials, Philadelphia:17-34.

Biot, M.A., 1956a; Theory of Propagation of Elastic Waves in a Fluid-Saturated Porous Solid. I. Low-Frequency Range. *The Journal of the Acoustical Society of America,* 28(2): 168-178.

Biot, M.A., 1956b; Theory of Propagation of Elastic Waves in a Fluid-Saturated Porous Solid. II. Higher Frequency Range. *The Journal of the Acoustical Society of America,* 28(2): 179-191.

Briggs, N.D., 1973; *Investigations of New Zealand pyroclastic-flow deposits.* Unpublished Ph.D. thesis in Geology, Victoria University of Wellington.

Briggs, N.D., 1975; Determination of the cause of thickness variation in ignimbrites (Note). *New Zealand Journal of Geology and Geophysics* 18: 501-506

Briggs, N.D., 1976a; Recognition and Correlation of Subdivisions within the Whakamaru Ignimbrite, Central North Island, New Zealand. *New Zealand Journal of Geology and Geophysics* 19: 463-501.

Briggs, N.D., 1976b; Welding and Crystallization Zonation in Whakamaru Ignimbrite, Central North Island, New Zealand. *New Zealand Journal of Geology and Geophysics* 19: 189-212.

Brown, E.T. (ed), 1981; *Rock Characterization, Testing and Monitoring. ISRM Suggested Methods.* Pergamon Press.

Caress, M.E. ,and Walker, G.P.L., 1986; The youngest Toba Tuff, Sumatra: study of a large-scale, high aspect ratio ignimbrite. *International Volcanological Congress, New Zealand, 1-9 February 1986. Abstracts*: 35.

Carmichael, R.S. (ed), 1984; *Handbook of the physical properties of rocks, Volume 3.* CRC Press, Inc., Boca Raton, Florida.

Carr, R.G., 1981; A scanning electron microscope study of post-depostional changes in the Matahina Ignimbrite, North Island, New Zealand. *New Zealand Journal of Geology and Geophysics* 24: 429-434.

Cas, R.A.F., and Wright, J.V., 1987; *Volcanic successions modern and ancient.* Allen and Unwin, London.

Challis, G.A., 1978; Upper Quaternary Volcanism. *In* Suggate, R.P., Stevens, G.R., and Te Punga, M.T. (eds), *The Geology of New Zealand.* Government Printer, Wellington: 651-663.

Cox, K.G., Bell, J.D., and Pankhurst, R.J., 1979; *The Interpretation of Igneous Rocks.* George Allen and Unwin, London.

Dapple, 1986; *Imageplus+ Manual.*

Day, M.J., and Goudie, A.S., 1977; Field assessment of rock hardness using the Schmidt test hammer. *British Geomorphological Research Group Technical Bulletin* 18: 19-29.

Dearman, W.R., 1974; Weathering classification in the characterisation of rock for engineering purposes in British practice. *Bulletin of the International Association of Engineering Geology* 9: 33-42.

Deere, D.U., and Miller, R.P., 1966; Engineering Classification and Index Properties for Intact Rock. *Technical Report No. AFWL-TR-65-116, Air Force Weapons Base,* Kirkland Air Force Base, New Mexico.

De Graff, J.M., and Aydin, A., 1987; Surface morphology of columnar joints and its significance to mechanics and direction of joint growth. *Geological Society of America Bulletin* 99: 605-617.

Druitt, T.H., and Sparks, R.S.J. ,1982; A proximal ignimbrite breccia facies on Santorini, Greece. *Journal of Volcanology and Geothermal Research* 13: 147-171.

Durgunoglu, H.T., and Mitchell, J.K., 1975a; Static Penetration Resistance of Soils. I - Analysis. *In* American Society for Testing and Materials, *Proceedings of the conference on in situ measurement of soil properties.* June 1-4, 1975: 151-171.

Durgunoglu, H.T., and Mitchell, J.K., 1975b; Static Penetration Resistance of Soils. II - Evaluation of theory and implications for practice. *In* American Society for Testing and Materials, *Proceedings of the conference on in situ measurement of soil properties.* June 1-4, 1975: 172-189.

Edgington, E.S., 1980; *Randomization Tests.* Marcel Dekker, New York.

Evison, F.F., 1956; The seismic determination of Young's Modulus and Poisson's Ratio for rocks *in situ. Geotechnique* 6(3): 118-123.

Ewart, A., and Healy, J., 1966; Ignimbrites of the Waihi District. *In* Thompson, B.N., Kermode, L.O., and Ewart, A. (eds), *New Zealand Volcanology. Central Volcanic Region.* NZDSIR, Information Series, no 50: 139-147.

Farmer, I.W., 1968; *Engineering properties of rocks.* Spon.

Farmer, I.W., 1983; *Engineering Behaviour of Rocks, 2nd edition.* Spon.

Farmer, I.W., Hignett, H.J., and Hudson, J.A., 1979; The role of geotechnical factors in the cutting performance of tunnelling machines in rocks. *Proceedings of the Fourth Congress of the International Society for Rock Mechanics* 1: 371-377.

Fieldes, M., 1968; Mineral Weathering. *In* New Zealand Soil Bureau, Soils of New Zealand. Part 2. *New Zealand Soil Bureau Bulletin* 26(2).

Fisher, R.V., and Schmincke, H-U., 1984; *Pyroclastic Rocks.* Springer-Verlag.

Fisher, R.V., Schmincke, H-U., and van Bogaard, P., 1983; Origin and emplacement of a pyroclastic flow and surge unit at Laacher See, Germany. *Journal of Volcanology and Geothermal Research* 17: 375-392.

Frisillo, A.L., and Stewart, T.J., 1980; Effect of Partial Gas/Brine Saturation on Ultrasonic Absorption in Sandstone. *Journal of Geophysical Research* 85(B10),:5209-5211.

Froggatt, P.C. ,1981; Stratigraphy and nature of Taupo Pumice Formation. *New Zealand Journal of Geology and Geophysics* 24: 231-248.

Furkert, W.F., 1935; Remedial measures on the Arapuni hydro-electric scheme of power development on the Waikato River, New Zealand. *Minutes of the Proceedings of the Institution of Civil Engineers* 240: 1-55.

Geological Society Engineering Group Working Party, 1977; Working Party Report: The description of rock masses for engineering purposes. *Quarterly Journal of Engineering Geology* 10: 355-388.

Geological Society Engineering Group Working Party, 1988; Engineering geophysics: Report by the Geological Society Engineering Group Working Party. *Quarterly Journal of Engineering Geology* 21: 207-271.

Goodman, R.E., 1980; *Introduction to Rock Mechanics.* John Wiley and Sons.

Hatherton, T., 1954; The Magnetic Properties of the Whakamaru Ignimbrites. *New Zealand Journal of Science and Technology* 35: 421-432.

Hawkes, I., and Mellor, M.,1970; Uniaxial testing in rock mechanics laboratories. *Engineering Geology* 4(3): 177-286.

Healy, J., 1959; Whakamaru Ignimbrites (Series). *In* Fleming, C.A. (ed.), *Lexique Stratigraphique International. Volume VI Oceanie:* 476.

Heiken, G., 1972; Morphology and Petrography of Volcanic Ashes. *Geological Society of America Bulletin* 83: 1961-1988.

Heiken, G., and Wohletz, K., 1985; *Volcanic Ash.* University of California Press.

Hildreth, W., and Mahood, G.A., 1986; Ring-fracture eruption of the Bishop Tuff. *Geological Society of America Bulletin* 97: 396-403.

Hind, K.J. ,1986; *A Geotechnical Investigation of Ignimbrite in the Ruahihi Area, Tauranga.* Unpublished M.Sc. thesis, University of Waikato.

Hornell, P.G., and Werner, P.N.,1930; Report on Arapuni hydro-electric power-station. *Report presented to both houses of the General Assembly, New Zealand* D-1c.

Huppert, F., 1986; *Petrology of soft tertiary sedimentary rocks and its relationship to geomechanical behaviour, Central North Island, New Zealand.* Unpublished Ph.D. thesis, University of Auckland.

Huppert, F., 1988; Influence of microfabric on geomechanical behaviour of Tertiary fine-grained sedimentary rocks, from Central North Island, New Zealand. *Bulletin of the International Association of Engineering Geology* 38: 83-94.

Idral, A., 1986; *Geotechnical Poroperties of Owharoa Ignimbrite.* Unpublished Dip. App. Sci. report, University of Waikato.

Informix Software, 1988; *Wingz Reference Manual.*

Inoue, M., and Ohomi, M., 1981; Relation between uniaxial compressive strength and elastic wave velocity of soft rock. *Proceedings of the International Symposium on Weak Rock, Tokyo, 21-24 September 1981*: 9-13.

Irfan, T.Y., and Dearman, W.R., 1978; Engineering classification and index properties of a weathered granite. *Bulletin of the International Association of Engineering Geology* 17: 79-90.

Izett, G.A., 1981; Volcanic Ash Beds: Recorders of Upper Cenozoic Silicic Volcanism in the Western United States. *Journal of Geophysical Research* 86B: 10200-10222.

James, L.S., 1955; Stresses and deflections: Maraetai Dam. *International Congress on Large Dams, 5th, Paris, Transactions* 3: 273-291.

Janach, W., and Merminod, A., 1982; Rock Abrasivity Test with a Modified Schmidt Hammer. *International Journal of Rock Mechanics and Mining Sciences and Geomechanics Abstracts* 19: 43-45.

Jenni, J.P., and Balissat, M., 1979; Rock testing methods performed to predict the utilization possibilities of a tunnel boring machine. *Proceedings of the Fourth Congress of the International Society for Rock Mechanics* 2: 267-273.

Johnston, D.H., and Toksoz, M.N., 1980; Ultrasonic P and S Wave Attenuation in Dry and Saturated Rocks Under Pressure. *Journal of Geophysical Research* 85(B2), 925-936.

Joreskog, K.G., Klovan, J.E., and Reyment, R.A., 1976; *Methods in Geomathematics, 1. Geological Factor Analysis.* Elsevier.

Jumikis, A.R., 1979; Rock Mechanics. *Series on Rock and Soil Mechanics* 3(5). Trans Tech Publications.

Kidybinski, A., 1979; Experience with hard rock penetrometers used for mine rock stability predictions. *Proceedings of the Fourth Congress of the International Society for Rock Mechanics* 2: 293-301.

King, M.S., 1983; Static and Dynamic Elastic Properties of Rocks from the Canadian Shield. *International Journal of Rock Mechanics and Mining Sciences, and Geomechanics Abstracts* 20(5): 237-241.

Kirkaldie, L., Williamson, D.A., and Patterson, P.V., 1987; Rock Material Field Classification Procedure, 2nd edition. *Reprinted in* Kirkaldie, L. (ed.), Rock Classification Systems for Engineering Purposes. *ASTM Special technical publication* (STP): 984.

Kylander, B.R., and Dean, S.L., 1985; Hackle plume geometry and joint propagation dynamics. *Proceedings of the International Symposium on Fundamentals of Rock Joints, Bjorkliden, 15-20 September 1985*: 85-94.

Lambe, T.W., and Whitman, R.V., 1979; *Soil Mechanics, SI Version.* John Wiley and Sons.

Lawley, D.N., and Maxwell, A.E., 1971; *Factor Analysis as a Statistical Method. Second edition.* Butterworths, London.

Lipman, P.W., 1986; Emplacement of large ash-flow sheets and relation to caldera collapse. *International Volcanological Congress, New Zealand, 1-9 February 1986. Abstracts*: 58.

Long, P.E., and Wood, B.J., 1986; Structures, textures, and cooling histories of Colombia River basalt flows. *Geological Society of America Bulletin* 97: 1144-1155.

Maloy, C.L., and Lowe, A.D., 1945; Physical properties of the foundation rock at the proposed dam site at Maraetai, on the Waikato River. *New Zealand Journal of Science and Technology. Section B* 27(2): 77-111.

Marshall, P.,1930; Report on Rocks at Arapuni. *Report presented to both houses of the General Assembly, New Zealand* D-1.

Marshall, P., 1935; Acid Rocks of the Taupo-Rotorua Volcanic District. *Transactions of the Royal Society of New Zealand* 64: 323-375.

Martin, R.C., 1965; Lithology and Eruptive History of the Whakamaru Ignimbrites in the Maraetai Area of the Taupo Volcanic Zone, New Zealand. *New Zealand Journal of Geology and Geophysics* 8: 680-701.

Martin, R.P., 1986; Use of index tests for engineering assessment of weathered rocks. *Proceedings 5th International Congress IAEG, Buenos Aires*: 433-450.

Matula, M., 1981; Recommended symbols for engineering geological mapping. Report by the IAEG Commission on Engineering Geological Mapping. *Bulletin of the International Association of Engineering Geology* 24: 227-234.

McBirney, A.R., and Murase, T., 1970; Factors Governing the Formation of Pyroclastic Rocks. *Bulletin Volcanologique* 34: 372-384.

McCarroll, D., 1987; The Schmidt hammer in geomorphology: five sources of instrument error. *British Geomorphological Research Group Technical Bulletin* 36: 16-27.

McPhie, J., 1986; Eruption and emplacement of voluminous, very high aspect ratio ignimbrite: a late Permian example, northeastern NSW. *International Volcanological Congress, New Zealand, 1-9 February 1986. Abstracts*: 59.

Mining Research and Development Establishment, 1977; NCB Cone Indenter. *MRDE Handbook 5.*

Murase, T., and McBirney, A.R., 1973; Properties of Some Common Igneous Rocks and Their Melts at High Temperatures.*Geological Society of America Bulletin* 84: 3563-3592.

Murphy, W.F., 1982; Effects of partial water saturation on attenuation in Massilon sandstone and Vycor porous glass.*Journal of the Acoustical Society of America* 71(6): 1458-1468.

Nappi, G. ,and Ottaviani, M., 1986; Geological and geotechnical characteristics of volcanic tuffs of Central and Southern Italy. *Proceedings of the Fifth International IAEG Congress, Buenos Aires, 1986* 2: 455-464.

Nur, A., and Simmons, G., 1969; The effect of saturation on velocity in low porosity rocks. *Earth and Planetary Science Letters* 7: 183-193.

O'Connell, R.J., and Budiansky, B., 1974; Seismic Velocities in Dry and Saturated Cracked Solids. *Journal of Geophysical Research* 79(35): 5412-5425.

O'Connell, R.J., and Budiansky, B., 1977; Viscoelastic Properties of Fluid-Saturated Cracked Solids. *Journal of Geophysical Research* 82(36): 5719-5735.

Olissoff, E.S., 1981; *Quaternary stratigraphy and ignimbrites of the Karapiro-Arapuni region.* Unpublished M.Sc. thesis, University of Waikato.

Orsi, G., and Sheridan, M.F., 1986; The Green Tuff of Pantelleria: an example of rheoignimbrite. *International Volcanological Congress, New Zealand, 1-9 February 1986. Abstracts*: 67.

Pain, H.J., 1983; *The Physics of Vibrations and Waves. Third edition.* John Wiley and Sons.

Pasamehmetoglu, A.G., Karpuz, C., and Irfan, T.Y., 1981; The weathering characteristics of ankara andesites from the rock mechanics point of view. *Proceedings of the International Symposium on Weak Rock, Tokyo, 21-24 September 1981*: 185-189.

Paulsson, B.N., and King, M.S., 1980; Between-hole Acoustic Surveying and Monitoring of a Granitic Rock Mass. *International Journal of Rock Mechanics and Mining Sciences, and Geomechanics Abstracts* 17: 371-376.

Petersen, D.W., 1979; Significance of the flattening of pumice fragments in ash-flow tuffs. *In* Chapin, C.E., and Elston, W.E., Ash-Flow Tuffs. *Geological Society of America Special Paper* 180: 195-204.

Philpotts, A.R., and Burkett, A.R., 1987; Structures, textures, and cooling histories of Colombia River basalt flows: Discussion and reply. *Geological Society of America Bulletin* 99: 886-888.

Pollard, D.D., and Aydin, A., 1988; Progress in understanding jointing over the past century. *Geological Society of America Bulletin* 100: 1181-1204.

Poole, R.W., and Farmer, I.W., 1980; Consistency and Repeatability of Schmidt Hammer Rebound Data During Field Testing. *International Journal of Rock Mechanics and Mining Sciences and Geomechanics Abstracts* 17: 167-171.

Price, R.H., 1983; Analysis of Rock Mechanics Properties of Volcanic Tuff Units from Yucca Mountain, Nevada Test Site. *SAND82-1315, Sandia National Laboratories,* Albuquerque, New Mexico.

Price, R.H., Nimick, F.B., Connolly, J.R., Keil, K., Schwarz, B.M., and Spence, S.J., 1985; Preliminary Characterization of the Petrologic, Bulk, and Mechanical Properties of a Lithophysal Zone Within the Topopah Spring Member of the Paintbrush Tuff. *SAND84-0860, Sandia National Laboratories,* Albuquerque, New Mexico.

Proceq S.A., 1960; *Building Material Test Hammer Type P. Operating Instructions.*

Proceq S.A., 1977; *Building Material Test Hammer Types N and NR. Operating Instructions.*

Protod'yakanov, M.M., Koifman, M.I., and others, 1969; *Mechanical properties of rocks.* Israel Program for Scientific Translations, Jerusalem.

Ragan, D.M., and Sheridan, M.F., 1972; Compaction of the Bishop Tuff, California. *Geological Society of America Bulletin* 83: 95-106.

Report of the Committee to Inquire into the Failure of the Ruahihi Canal, Ministry of Works and Development, Wellington, 1982.

Report of the Committee to Inquire into the Canal Failure on the Whaeo Power Scheme, Ministry of Works and Development, Wellington, 1983.

Rippa, F., and Vinale, F., 1983; Structure and mechanical behaviour of a volcanic tuff. *ISRM Proceedings* 1: B33-B40.

Rogan, A.M., 1982; A geophysical study of the Taupo Volcanic Zone, New Zealand. *Journal of Geophysical Research* 87: 4073-4088.

Ross, C.S., and Smith, R.L., 1961; Ash-flow tuffs: Their origin, geologic relations, and identification. *United States Geological Survey, Professional Paper* 366.

Ryan, T.A., Joiner, B.L., and Ryan, B.F., 1982; *Minitab Reference Manual.*

Sanglerat, G., 1972; The penetrometer and soil exploration. Interpretation of penetration diagrams - theory and practice. *Developments in Geotechnical Engineering 1.* Elsevier.

Schofield, J.C., 1967; Sheet 3, Auckland (1st ed). *Geological Map of New Zealand 1 : 250 000.* DSIR, Wellington.

Selby, M.J., 1982; *Hillslope materials and processes.* Oxford University Press.

Sheorey, P.R., Barat, D., Das, M.N., Mukherjee, K.P., and Singh, B., 1984; Schmidt Hammer Rebound Data for Estimation of Large Scale *In Situ* Coal Strength. *International Journal of Rock Mechanics and Mining Sciences and Geomechanics Abstracts* 21: 39-42.

Sheridan, M.F., 1970; Fumerolic Mounds and Ridges of the Bishop Tuff, California. *Geological Society of America Bulletin* 81: 851-868.

Singh, D.P., 1981; Determination of some engineering properties of weak rocks. *Proceedings of the International Symposium on Weak Rock, Tokyo, 21-24 September 1981*: 315-320.

Skinner, D.N.B., 1986; Neogene Volcanism of the Hauraki Region. *In* Smith, I.E.M. (ed), *Late Cenozoic Volcanism in New Zealand.* Royal Society of New Zealand, Bulletin 23: 21-47.

Smith, P.J., 1977; *Topics in Geophysics.* Open University Press.

Smith, R.L., 1960a; Ash Flows. *Bulletin of the Geological Society of America* 71: 795-842.

Smith, R.L., 1960b; Zones and zonal variations in welded ash flows. *United States Geological Survey Professional Paper* 354-F.

Smith, R.L. 1979; Introduction. *In* Chapin, C.E., and Elston, W.E., Ash-Flow Tuffs. *Geological Society of America Special Paper* 180:

Sparks, R.S.J., 1976; Grain size variations in ignimbrites and implications for the transport of pyroclastic flows. *Sedimentology* 23: 147-188.

Sparks, R.S.J., 1978a; The dynamics of bubble formation and growth in magmas: a review and analysis. *Journal of Volcanology and Geothermal Research* 3: 1-37.

Sparks, R.S.J., 1978b; Gas release rates from pyroclastic flows: an assessment of the role of fluidization in their emplacement. *Bulletin Volcanologique* 41: 1-9.

Sparks, R.S.J., Francis, P.W., Hamer, R.D., Pankhurst, R.J., O'Callaghan, L.O., Thorpe, R.S., and Page, R., 1985; Ignimbrites of the Cerro Galan Caldera, NW Argentina. *Journal of Volcanology and Geothermal Research* 24: 205-248.

Sparks, R.S.J., and Wilson, L., 1976; A model for the formation of ignimbrite by gravitational column collapse. *Journal of the Geological Society of London* 132: 441-451.

Sparks, R.S.J., Wilson, L., and Hulme, G., 1978; Theoretical modelling of the generation, movement and emplacement of pyroclastic flows by column collapse. *Journal of Geophysical Research* 83: 1727-1739.

Stern, T.A., 1979; Regional and residual gravity fields, Central North Island, New Zealand. *New Zealand Journal of Geology and Geophysics* 22: 479-485.

Taylor, R.K., and Spears, D.A., 1981; Laboratory investigation of mudrocks. *Quarterly Journal of Engineering Geology* 14: 291-309.

Terzaghi, K., and Peck, R.B., 1948; *Soil Mechanics in Engineering Practice.* John Wiley and Sons.

Toksoz, M.N., Cheng, C.H., and Timur, A., 1976; Velocities of seismic waves in porous rocks. *Geophysics* 41(4): 621-645.

Vickers, B., 1983; *Laboratory Work in Civil Engineering. Soil Mechanics. Second edition*, Granada.

Vutukuri, V.S., Lama, R.D., and Saluja, S.S., 1974; Handbook on Mechanical Properties of Rocks. Volume I - Testing Techniques and Results. *Series on Rock and Soil Mechanics* 2(1). Trans Tech Publications.

Walker, G.P.L., 1981; Plinian Eruptions and Their Products. *Bulletin Volcanologique* 44: 223-240.

Walker, G.P.L., 1983; Ignimbrite Types and Ignimbrite Problems. *Journal of Volcanology and Geothermal Research* 17: 65-88.

Walker, G.P.L., 1985; Origin of coarse lithic breccias near ignimbrite source vents. *Journal of Volcanology and Geothermal Research* 25: 157-171.

Walker, G.P.L., Self, S., and Froggatt, P.C., 1981a; The ground layer of the Taupo Ignimbrite: a striking example of sedimentation from a pyroclastic flow. *Journal of Volcanology and Geothermal Research* 10: 1-11.

Walker, G.P.L., and Wilson, C.J.N., 1983; Lateral variations in the Taupo Ignimbrite. *Journal of Volcanology and Geothermal Research* 18: 117-133.

Walker, G.P.L., Wilson, C.J.N., and Froggatt, P.C., 1980; Fines-depleted ignimbrite in New Zealand - The product of a turbulent pyroclastic flow. *Geology* 8: 245-249.

Walker, G.P.L., Wilson, C.J.N., and Froggatt, P.C., 1981b; An ignimbrite veneer deposit: the trail-marker of a pyroclastic flow. *Journal of Volcanology and Geothermal Research* 9: 409-421.

Wedepohl, 1969; *Handbook of geochemistry.* Springer-Verlag.

Wilkins, R.H., Simmons, G., Wissler, T.M., and Caruso, L. ,1986; The Physical Properties of a Set of Sandstones - Part III. The Effects of Fine-grained Pore-filling Material on Compressional Wave Velocity. *International Journal of Rock Mechanics and Mining Sciences, and Geomechanics Abstracts* 23(4): 313-325.

Williams, H., and McBirney, A., 1979; *Volcanology.* Freeman, Cooper and Co., San Francisco.

Williams, R.B.G. ,and Robinson, D.A., 1983; The effect of surface texture on the determination of the surface hardness of rock using the Schmidt hammer. *Earth Surface Processes and Landforms* 8: 289-292.

Wilson, C.J.N., 1980; The role of fluidization in the emplacement of pyroclastic flows: an experimental approach. *Journal of Volcanology and Geothermal Research* 8: 231-249.

Wilson, C.J.N., 1984; The role of fluidization in the emplacement of pyroclastic flows, 2: experimental results and their interpretation. *Journal of Volcanology and Geothermal Research* 20: 55-84.

Wilson, C.J.N., 1985; The Taupo Eruption, New Zealand II. The Taupo Ignimbrite. *Philosophical Transactions of the Royal Society of London* 314: 229-310.

Wilson, C.J.N., 1986; Reconnaissance Stratigraphy and Volcanology of Ignimbrites from Mangakino Volcano. *In* Smith, I.E.M. (ed), *Late Cenozoic Volcanism in New Zealand.* Royal Society of New Zealand, Bulletin 23: 179-193.

Wilson, C.J.N., Houghton, B.F., and Lloyd, E.F., 1986; Volcanic History and Evolution of the Maroa-Taupo Area, Central North Island. *In* Smith, I.E.M. (ed), *Late Cenozoic Volcanism in New Zealand.* Royal Society of New Zealand, Bulletin 23: 194-223.

Wilson, C.J.N., Rogan, A.M., Smith, I.E.M., Northey, D.J., Nairn, I.A., and Houghton, B.F., 1984; Caldera Volcanoes of the Taupo Volcanic Zone, New Zealand. *Journal of Geophysical Research* 89: 8463-8484.

Wilson, C.J.N., and Walker, G.P.L., 1982; Ignimbrite depositional facies: the anatomy of a pyroclastic flow. *Journal of the Geological Society of London* 139: 581-592.

Wilson, C.J.N., and Walker, G.P.L., 1985; The Taupo Eruption, New Zealand I. General Aspects. *Philosophical Transactions of the Royal Society of London* 314: 199-228.

Wilson, L., 1976; Explosive Volcanic Eruptions - III. Plinian Eruption Columns. *Geophysical Journal of the Royal Astronomical Society* 45: 543-556.

Wilson, L., Sparks, R.S.J., Huang, T.C., and Watkins, N.D., 1978; The control of volcanic column heigths by eruption energetics and dynamics. *Journal of Geophysical Research* 83: 1829-1836.

Wilson, L., Sparks, R.S.J., and Walker, G.P.L., 1980; Explosive volcanic eruptions - IV. The control of magma properties and conduit geometry on eruption column behaviour. *Geophysical Journal of the Royal Astronomical Society* 63: 117-148.

Winkler, K.W., 1983; Frequency Dependent Ultrasonic Properties of High-Porosity Sandstones. *Journal of Geophysical Research* 88(B11): 9493-9499.

Winkler, K.W., 1985; Dispersion Analysis of Velocity and Attenuation in Berea Sandstone. *Journal of Geophysical Research* 90(B8): 6793-6800.

Wolff, J.A., and Wright, J.V., 1981; Rheomorphism of welded tuffs. *Journal of Volcanology and Geothermal Research* 10: 13-34.

Wright, J.V., 1981; The Rio Caliente Ignimbrite: Analysis of a Compound Intraplinian Ignimbrite from a Major Late Quarternary Mexican Eruption. *Bulletin Volcanologique* 44: 189-221.

Wright, J.V., and Walker, G.P.L., 1981; Eruption, transport and deposition of ignimbrite: a case study from Mexico. *Journal of Volcanology and Geothermal Research* 9: 111-131.

Yamanouchi, T., Gotoh, K., and Murata, H., 1981; Design of cut slopes preventing tensile failure in a pyroclastic flow deposit "Shirasu". *Proceedings of the International Symposium on Weak Rock, Tokyo, 21-24 September, 1981*: 867-872.

Yang, H.J.P., and King, M.S., 1986; A Study of Elastic Wave Velocities in Dry and Water-saturated, Regularly-jointed Rock Masses. *International Journal of Rock Mechanics and Mining Sciences, and Geomechanics Abstracts* 23(3): 277-280.

Younger, M.S., 1979; *Handbook for Linear Regression.* Duxbury Press.

APPENDICES

APPENDIX 1 - FORMATION OF IGNIMBRITE

A1.1 Introduction

The definition of ignimbrite used in this study follows that of Walker (1983). This defines ignimbrite as:

> "a pyroclastic deposit or rock body, made predominantly from pumiceous material which shows evidence of having been emplaced as a concentrated and hot particulate flow."

The "ash-flow tuffs" commonly referred to in American literature are comparable with ignimbrites in this sense.

Ignimbrites have commanded considerable attention from physical volcanologists over the past decade, resulting in a much more complete understanding of their mode of formation. The following sections briefly review the presently accepted models for ignimbrite eruption, deposition and post-depositional alteration. In later sections the mode of formation of the ignimbrites studied will be interpreted in terms of these models.

A1.2 Vesiculation and fragmentation of the magma

The pumiceous material which forms an ignimbrite develops from a highly evolved, usually rhyolitic or dacitic magma. Such a magma is rich in silica, has a high volatile content, low water content and is characterised by a relatively low temperature and very high values of viscosity (10^2 to 10^5 N s m^{-2}). The pyroclasts formed in these silicic magmas have shapes which are controlled by the geometry of the vesicles formed within the highly viscous liquid (Heiken and Wohletz, 1985).

A number of authors have discussed the theoretical aspects of the development of gas bubbles within a rhyolitic magma chamber, for example, McBirney and Murase (1970), Murase and McBirney (1973), Bennett (1974) and Sparks (1978a). These have been reviewed by Williams and McBirney (1979), Fisher and Schmincke (1984) and Heiken and Wohletz (1985). These studies have not agreed on a single mechanism for vesicle development and growth, although several basic ideas are held in common.

A1.2.1 Magma vesiculation

Degassing of the magma by bubble formation is believed to occur very readily under low pressures due to the high volatile levels in the magma. The development and rise of bubbles can be modelled numerically, assuming ideal, spherical bubbles, rising in an infinite fluid (Sparks, 1978a). At an initial stage their growth is uninhibited by neighbouring bubbles. However, as bubble nucleation continues, the growth of the bubbles is retarded by the presence of others surrounding them. Given the high viscosity of the liquid, coalescence of the bubbles by disruption of the intervening walls is not significant (McBirney and Murase, 1970); thus a stage is reached at which bubble growth ceases due to interference from their neighbours. At this stage the bubble population covers its maximum range of sizes, which Sparks (1978a) has calculated as being from ~1 mm to ~10 mm.

This modelling is based on ideal, spherical bubbles. However, distortion and stretching of the bubbles may occur during vesiculation and extrusion. This results in a variety of vesicle forms ranging from spherical to tubular, subparallel vesicles (Fisher and Schmincke, 1984). This elongation is thought to be the result of bubbles forming as the erupting magma moves upwards in the magma chamber; bubble rise itself is too slow to produce such forms in a viscous melt (McBirney and Murase, 1970).

A1.2.2 Magma fragmentation

Magma froth becomes a brittle substance which is too viscous to flow through the vent and must first be fragmented. In the theory of Heiken and Wohletz (1985) this fragmentation is the result of an expansion wave which develops at the magma/atmosphere interface at the start of an eruption. This propagates down into the essentially solid froth at the same time as a shock wave propagates into the atmosphere. Bubble walls are disrupted by the wave which breaks the magma into coherent clasts and accelerates them out of the vent. Sparks (1978a) suggests that gas pressures within bubbles continue to increase even after bubble growth ceases. These high pressures will result in the bursting of large bubbles which are near the fragmentation surface, as their internal pressure is greater than that surrounding them.

In either case, as the vesiculated and broken material is erupted from the chamber, the underlying magma in turn moves up into the void, vesiculates, is disrupted and erupted. Therefore, as the eruption proceeds

hotter, and less viscous, melt moves in. This results in less vesicular, higher density pumice being erupted later in the eruption.

A1.3 Pyroclastic fragments

Pyroclastic ejecta from a vesiculated magma chamber, as described above, will contain a number of components; pumice, glass shards, crystals and lithic fragments. These are erupted along with copious quantities of gases released from the magma.

A1.3.1 Pumice

Pumice is a white or pale grey to brown, highly vesicular glass foam with thin bubble walls composed of translucent glass (Fisher and Schmincke, 1984). The shape of the clasts produced by fragmentation of the magma froth is entirely dependent on the shape of the vesicles in the magma before disintegration; elongated clast shapes are controlled by elongated vesicles and equant clast shapes by spherical, undeformed vesicles. The surfaces of the pumice clasts are very rough due to broken vesicle walls (Heiken, 1972).

A1.3.2 Glass shards

Glass shards are formed from shattered vesicle walls. Fisher and Schmincke (1984) describe three end-member types:

(1) cuspate or lunate-shaped fragments which are commonly Y-shaped in cross section and represent the remnants of three bubble junctions,

(2) flat plates from the glass walls separating large, flattened vesicles, and

(3) small pumice fragments (pumice shards) composed of intact vesicles enclosed by glass walls.

Izett (1981) suggests that pumice shards tend to develop from relatively high viscosity rhyolitic magmas with temperatures <850 °C, whereas bubble junctions (type 1) and bubble wall (type 2) shards tend to develop from lower viscosity rhyolitic magmas at temperatures >850 °C.

A1.3.3 Crystals

Within the magma chamber euhedral crystals will develop if allowed relatively free growth. Characteristic minerals of a silicic magma include bipyramidal quartz, euhedral biotite, high temperature (disordered) forms of plagioclase and sanidine, and euhedral pyroxene and amphibole (Fisher and Schmincke, 1984). Resorption of these crystals within the magma chamber often produces rounded outlines, deep embayments along the margin, and zoning of the crystals (Cox, Bell and Pankhurst, 1979). Breakage of the crystals frequently occurs during eruption and transport (Fisher and Schmincke, 1984).

A1.3.4 Lithic fragments

Lithic fragments include cognate clasts, which are fragments of co-magmatic volcanic rocks from previous eruptions of the same volcano, and accidental fragments derived from surrounding basement rocks (Fisher and Schmincke, 1984). They may be picked up as wall rock from the magma chamber prior to the eruption, or from the vent and surrounding rocks during eruption and transport.

A1.4 Eruption and deposition

A1.4.1 Plinian eruption columns

The eruption of a fragmented magma chamber typically results in the production of a Plinian eruption column. Plinian eruptions are amongst the most powerful of explosive volcanic events (Walker, 1981) and are characterised by a vertical eruption column consisting of a turbulent stream of pyroclastic fragments, magmatic gases and entrained air. Such eruption columns have been modelled by Sparks and Wilson (1976), Wilson (1976), Wilson *et al.* (1978) and Wilson *et al.* (1980). They are believed to occur in two stages; a lower gas-thrust phase in which the energy of the eruption lifts the pyroclasts to heights of 1.5 to 4.5 km, and an upper convective phase which can transport the material to heights of up to 55 km.

Expansion of the magmatic gases due to pressure release imparts high velocities, of 400 to 600 m s^{-1}, to the pyroclasts as they leave the vent. Atmospheric drag plus conservation of energy reduces their velocity to zero,

which marks the end of the gas-thrust phase. During this initial rise of the column, air is entrained into the turbulent jet, resulting in a decrease in the bulk density and temperature of the mass, together with an increase in the column radius. The density decrease is enhanced by the fall-out of large clasts from the column.

If the column density has fallen to less than atmospheric at this point then the buoyancy of the clasts will dominate the system and the grains will rise in a convective plume (the convective phase). If however, the density of the column has not fallen below that of the atmosphere then convection cannot begin and the column will collapse under the influence of gravity. The great height of the eruption column provides the energy for rapid radial dispersion as a pyroclastic flow.

A1.4.2 Pyroclastic flows

At the base of the collapsing column the mixture is envisaged as forming a dilute, highly turbulent, high velocity flow. Sparks *et al.* (1978) model this as a turbulent fluid. Within such a fluid the larger (heavier) particles will settle through the flow and be concentrated at the base. This will occur rapidly at first, resulting in a rapid thinning of the flow and the formation of a basal zone of high particle concentration within a few kilometres of the vent. The flow is thus believed to segregate into a dense, concentrated lower zone (the pyroclastic flow proper) and a dilute upper part consisting of all those particles small enough to be carried away above the flow by gas turbulence. These two phases are believed to exist as separate entities.

Fluidisation is believed to play an important role in the movement of the pyroclastic flow (Sparks, 1976, 1978b). When fluidised, individual particles become supported by the rising gas and the bed of particles behaves as a fluid rather than a coherent body. Such a flow can travel very readily over large distances as its movement is virtually frictionless. Fluidisation experiments by Wilson (1980, 1984) suggest that a pyroclastic flow travels primarily as a laminar flow, which may be more or less fluidised depending on the initial eruption conditions. A poorly fluidised flow will result in a relatively homogeneous deposit, and increased fluidisation will lead to greater sorting with the development of vertical gas-flow channels and the separation of coarse (heavy) and fine (light) particles (Wilson, 1980). The energy and heat of such a pyroclastic flow is the result of the initial eruption conditions (the gas

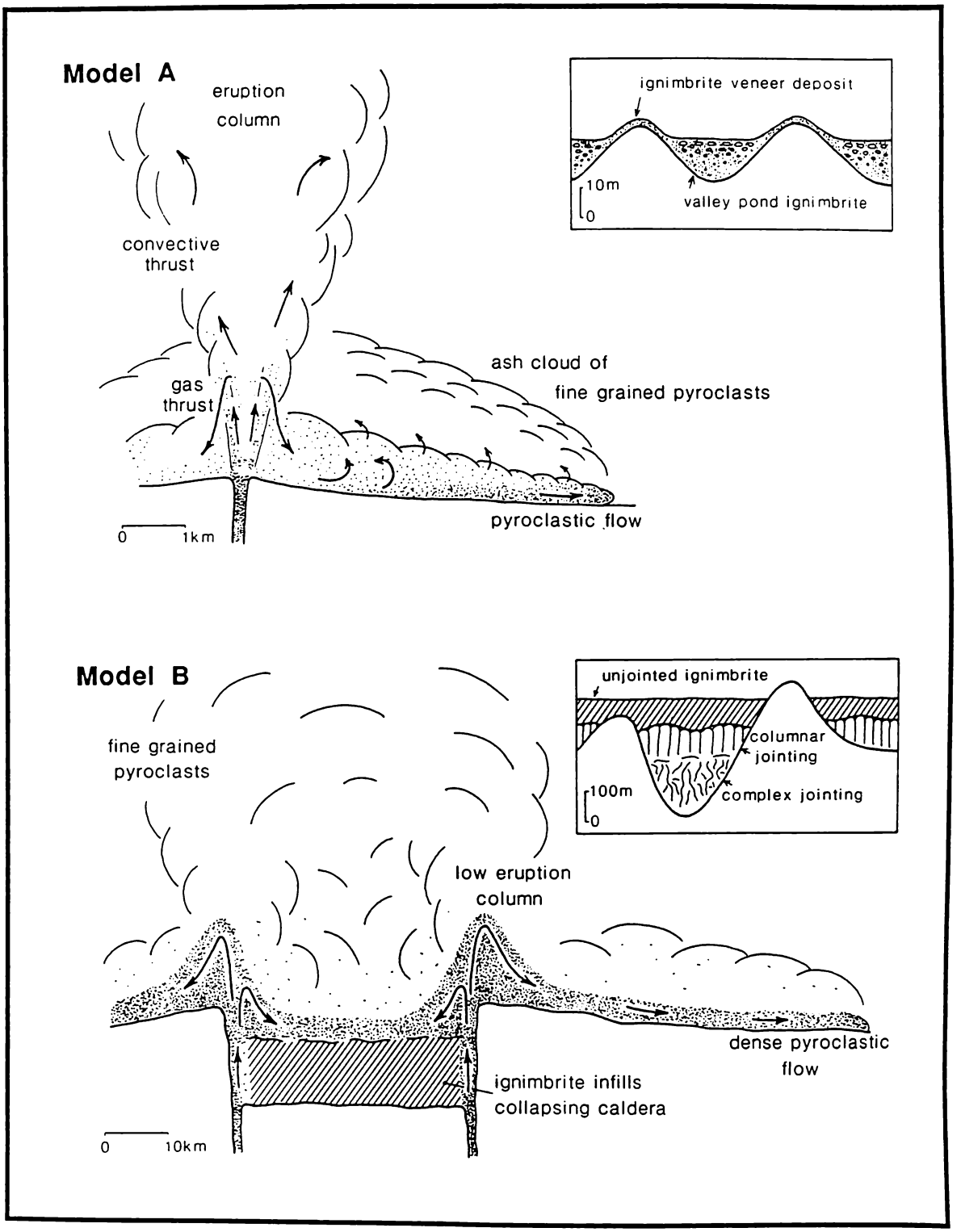

Figure A1.1: Models for the initiation of pyroclastic flows. In model A the collapse of a Plinian column produces a fast moving, highly fluidised pyroclastic flow and a relatively thin, soft ignimbrite. In model B low, continuously collapsing eruption columns produce hot, poorly fluidised pyroclastic flows, and thick, hard ignimbrites.

content and velocity) as these control the height to which the column reaches and hence the time for cooling as the mass collapses back to the ground.

A1.4.3 End-member models

Figure A1.1 shows, schematically, two end-member models of the initiation of a pyroclastic flow. Model A is essentially the, now standard, Plinian eruption scenario, described above, in which a very high eruptive energy is present. Model B involves the same essential model for a much lower energy eruption. These models represent end-members in a whole spectrum of eruptive types, and each produces quite distinctive ignimbrite deposits. The two models will be discussed in turn.

A1.4.3.1 Model A

Model A follows the entire scenario of a Plinian eruption column with convective dispersal leading later to column collapse. Such a collapse will result in the development of a very high energy, highly fluidised pyroclastic flow capable of covering vast areas and largely unconstrained by the topography. The product of such a flow will be a relatively thin, non-welded deposit which is thickest in the valleys and thinnest on the ridges. The Taupo Ignimbrite of New Zealand is an example of such a deposit. This ignimbrite is spread over a roughly circular area of ~80 km radius with thicknesses ranging from <10 cm to >100 m (Froggatt, 1981). It consists almost entirely of non-welded pumice clasts and glass shards and shows considerable sorting throughout the deposit. The Taupo Ignimbrite has been described in detail by a number of authors (Walker *et al.,* 1980, 1981a,b; Froggatt, 1981; Wilson and Walker, 1982, 1985; Walker and Wilson, 1983; Wilson, 1985) who have defined a variety of facies and their depositional mechanisms.

A1.4.3.2 Model B

Model B applies to much more voluminous ignimbrites. This model is essentially similar to model A, but an eruption of much lower energy and greater rate of material discharge may prevent the development of an initial Plinian eruption column (Lipman, 1986). The eruption will involve a relatively low, continuously collapsing pyroclastic fountain (McPhie, 1986). Such eruptions are frequently associated with caldera development and, therefore,

may not have a unique vent, but may form along a series of vents or arcuate fissures marking the caldera ring faults (Hildreth and Mahood, 1986).

The pyroclastic flows produced will be relatively poorly fluidised and slow moving. They will thus be controlled by the topography and will conserve heat much more efficiently than the flows of model A (Walker, 1983; McPhie, 1986). Although these hot, poorly fluidised pyroclastic flows are largely restricted to the valleys, the quantity of material produced is such that they inundate the land surface, leaving a plateau which covers all but the highest peaks.

In this case the large volumes involved and poor fluidisation result in a much more homogeneous deposit which commonly shows very thick layers of unsorted ignimbrite. Some sorting features, such as pumice concentrations, do occur (Lipman, 1986), and predictable variations in pumice, lithic and crystal size and proportion, with distance from source, have been described; for example by Briggs (1976a,b). Sorting by the pyroclastic flow occurs, but the variations are not as significant as in model A.

A1.4.3.3 Spectrum of ignimbrite types

In practice these two models are not separate mechanisms, they are end-members of a spectrum of ignimbrite types. Many ignimbrites have been described which show properties ranging between these two end-members, for example by Barberi *et al.* (1978), Wright (1981), Wright and Walker (1981), Druitt and Sparks (1982), Fisher *et al.* (1983) and Sparks *et al.* (1985). Each of these ignimbrites has been described in detail and their eruptive and depositional history interpreted in terms of differing levels of energy, heat and fluidisation of the pyroclastic flows. The eruption and flow conditions, and hence the resulting ignimbrite properties, vary over a wide range which is dependent upon the initial magmatic and vent conditions.

Walker (1983) uses the dimensions of the deposits to distinguish these types. Measuring a vertical dimension (average thickness) and horizontal dimension (diameter of a circle covering the same area as the deposit) allows an aspect ratio to be calculated. Model A will fall into the Low Aspect Ratio field and model B produces High Aspect Ratio ignimbrites. Again, these are the end-members of a continuous spectrum. It is mainly the high aspect ratio end of this spectrum which is of concern in this study, as these ignimbrites form the thick, extensive deposits which are likely to be of engineering significance.

A1.5 Post-depositional alteration

The processes by which a newly deposited ignimbrite becomes altered and indurated are reviewed in detail by Ross and Smith (1961) and Smith (1960a). Three major stages are recognised; welding, crystallisation and compaction. Associated with these changes is the development of jointing within the mass. Not every ignimbrite undergoes all, or even any, of these processes, as they are each dependent on the temperature, volatile content and chemical composition of the original deposit.

A1.5.1 Welding

Welding involves the cohesion of glassy fragments in a viscous state. This may range from an incipient stage in which the glass shards adhere only at their points of contact to the complete welding of the surfaces of glassy fragments. As welding progresses, there is usually a darkening of the glass to a dense black glass as the end product (Smith, 1960a).

A1.5.2 Crystallisation

In many ignimbrites mineralogical changes occur during cooling. Two distinct phases are recognised; devitrification and vapour phase alteration (Ross and Smith, 1961).

Devitrification is the development of crystals from glass. Devitrification is therefore confined within the margins of glass shards, pumice vesicle walls or massive glass fragments (Smith, 1960b). In thin section devitrification can be recognised by axiolitic or spherulitic textures (Smith, 1960b). An axiolitic structure consists of crystals which grow at right angles to the shard surfaces; sometimes this is confined to the margins of the shards, but often it extends right through the shard and leaves a dark 'suture' line down the centre. Spherulitic textures consist of small aggregates of crystals which show an outwardly radiating structure. The crystals formed by devitrification are too small to be identified under an optical microscope. However, X-Ray Diffraction suggests that cristobalite and alkalic feldspar are the characteristic minerals (Smith, 1960a).

Vapour phase crystallisation is defined as the growth of crystals from a vapour in pore spaces. It generally forms much coarser crystals than devitrification and is most common in the upper, porous regions of ignimbrites

(Smith, 1960b). Typical vapour phase minerals are tridymite and feldspars with, more rarely, biotite, amphiboles, and zeolites (Ross and Smith, 1961).

A1.5.3 Compaction

Compaction frequently accompanies the welding and crystallisation of the material. Two types of compaction are identified: mechanical compaction which is the result of simple loading and involves no significant change in particle shape; and welding compaction which results from viscous deformation of glassy components (Fisher and Schmincke, 1984).

With mechanical compaction very little alteration in the depositional texture is observed, except that elongated particles tend to be rotated so that their long axes are parallel to the horizontal plane. This may result in a significant loss of porosity in the rock mass (Fisher and Schmincke, 1984).

Welding compaction is evidenced in thin-section by alignment and distortion of the glass shards. As seen in hand-specimen, this form of compaction produces a eutaxitic texture (Ross and Smith, 1961) in which the components align perpendicular to the loading axis and hence give the rock a streaky appearance. This is most notable in the pumice clasts, which frequently lose all of their pore space (Ragan and Sheridan, 1972), become very dark, elongated, and develop a ragged edge in cross section. These are referred to as fiamme (Ross and Smith, 1961).

In many cases the distortion of the glassy components becomes so significant that the ignimbrite takes on the appearance of a flow rock. Where evidence of this exists, these rocks are referred to as rheoignimbrites (Wolff and Wright, 1981; Armstrong *et al.,* 1986).

A1.5.4 Controls on alteration processes

Ross and Smith (1961) discuss three components which, they consider, control the alteration of ignimbrites. These are:

(1) the chemical composition of the magma from which they were formed,

(2) the proportion and character of the volatiles originally dissolved in the magma, and

(3) the temperature at the time of eruption and at successively later stages.

These factors control the viscosity and the welding temperature of the glass, the amount and temperature of gases available for vapour phase crystallisation and the ability of the shards to devitrify. Their importance is, in turn, modified by such physical relationships as the thickness of the deposit, the lithostatic pressures developed in the system, the total volume of the deposit, and the texture of the ignimbrite. These factors control the rate at which heat and volatiles are able to escape from the system (Ross and Smith, 1961).

A1.5.5 Effects of alteration processes

The nature and effects of the alteration processes are complex and interrelated. It is very common for all processes to occur together, producing a compact, densely welded and extensively crystallised deposit; or conversely, for none of the processes to occur, producing a loose, non-welded deposit. Frequently however, one or more of the processes may occur without the others. Ross and Smith (1961) cite examples of very porous, non-welded ignimbrites which have undergone extreme devitrification and vapour phase alteration due to a high volatile content. At the opposite extreme they discuss ignimbrites which may be entirely welded, yet still remain in a glassy state.

In general, it may be assumed that flows from model A, discussed earlier, will be relatively cool by the time of their emplacement, and will therefore produce ignimbrites in which only minimal post-depositional alteration occurs. Thus the ignimbrite will be a loose, non-welded deposit in which has undergone only minimal devitrification and vapour phase alteration. The Taupo Ignimbrite fits this description well; overall there has been insufficient heat for welding of the glassy components, and little chemical alteration has occurred.

At the other extreme, the very hot flows of model B will produce a densely welded deposit in which devitrification and vapour phase alteration is intense, especially where the deposit is very thick in the valleys. The Bishop Tuff, described by Sheridan (1970), and Ragan and Sheridan (1972), fits this model well. Thick sections of the Bishop Tuff usually have zones of dense welding, extreme compaction and considerable devitrification in the central part of the sheet, and a zone of devitrification and vapour phase alteration in the overlying, non-welded ignimbrite. In many places above the most devitrified ignimbrite, are vertical zones of intense vapour phase alteration

which form indurated pipes and mounds; these represent fossil fumeroles, or gas release pipes (Sheridan, 1970).

However, beyond these extremes are a number of ignimbrites which do not fit the general rule. The Green Tuff of Pantelleria, for example, is a very thin ignimbrite which is spread over a wide area, yet it is densely welded, even where less than 1 m thick (Orsi and Sheridan, 1986). In this case the chemistry of the material (trachytic) may have controlled the temperature, and hence degree of welding. Conversely, the Toba Tuff of Sumatra forms very thick deposits which remain non-welded, and do not show significant alteration (Caress and Walker, 1986). In this case the pyroclastic flow(s) were presumably relatively cool, yet they were controlled by the topography and produced thick deposits in the valleys.

A1.6 Summary

An ignimbrite is formed from a vesiculated magma which is fragmented on eruption to produce a mixture of pumice clasts, glass shards, and crystals. During eruption lithic clasts may be incorporated into the mixture. There may be a very wide range of clast sizes erupted.

A pyroclastic flow is the means of transporting these clasts. It consists of a high energy stream of separate particles, which moves as a partially fluidised mass and is thus capable of travelling over vast distances. The nature of the pyroclastic flow is dependent upon the initial magmatic and eruption conditions. A very energetic eruption will produce a cool, highly fluidised flow, whereas a volumetrically larger, but less energetic, eruption will produce a hot, poorly fluidised, pyroclastic flow.

Ignimbrite shows variable amounts of sorting depending upon the nature of the pyroclastic flow. A highly fluidised flow will result in a well sorted deposit, but a poorly fluidised flow will produce a homogeneous deposit. However, ignimbrite is characteristically a chaotic, relatively homogeneous material which may range in thickness from <10 cm to several hundreds of metres.

After deposition a number of alteration processes may occur. These include welding and devitrification of the glassy material, deposition of crystals from escaping gases and compaction of the mass. These serve to indurate the material.